Inverse model systems to investigate metal-support interactions in Fischer-Tropsch catalysis

Lebohang Macheli

Thesis submitted to the University of Cape Town in fulfilment of the academic requirements for the degree of **Doctor of Philosophy**

Catalysis Institute

Department of Chemical Engineering

2019

Declaration

I, **Lebohang Macheli** certify that this submission is my own, unaided work, except for the information obtained from literature sources and my prescribed supervisors. All sources of information have been adequately acknowledged and referenced. I have not received assistance from any other source in completing this submission.

Signed by candidate

Signature:..... Date:02/08/2019

Acknowledgements

Gratitude goes to my supervisor Prof. Eric van Steen for his endless support, guidance and throughout the entire study. Being supervised by Professor Eric has shaped my critical thinking ability and helped unleashed my potentials. Thank you very much.

I also acknowledge all the support from colleagues and student who supported through the endeavors of studying. My sincere gratitude goes to Professor Amitava Roy for X-ray helping with X-ray absorption spectroscopy experiments. I highly appreciate the contribution made by Dr. Bryan Doyle and Dr. Emanuela Carleschi on XPS experiments. I appreciate efforts made by Prof. Patricia Kooyman for helping with electron microscope experiments. I appreciate

Studying endeavors require both moral and emotional support. I appreciate Dr. Gerard Leteba, Dr. Molefi Matsutsu, Mr. Motlokoa Khasu, Mr. Shaine Raseale, Miss Avela Kunene and Ms. Victoria Damane for their continuous support. You have been pillars on my strength and motivation when I needed it.

I appreciate the DST-NRF centre for excellence in catalysts (C*change) for funding the work. It is through the funds that this work became possible. I would also like to thank my family for the support, through my entire study. Words of encouragement and motivation always kept me through.

Presentations and Publications

Oral Presentations

2019	*Nano-Korea2019, Kintex, Korea*
2018	Annual Conference of the Catalysis Society South Africa (CATSA), Limpopo, South Africa
2018	DST-NRF Centre of Excellence in Catalysis (c*change) Workshop, Limpopo, South Africa
2017	DST-NRF Centre of Excellence in Catalysis (c*change) Workshop, North-West, South Africa
2017	Annual Conference of the Catalysis Society South Africa (CATSA), North-West, South Africa
2016	DST-NRF Centre of Excellence in Catalysis (c*change) Workshop, Drakensberg, South Africa
2015	DST-NRF Centre of Excellence in Catalysis (c*change) Workshop, Stellenbosch, South Africa

Poster Presentations

2019	*26th North American Catalysis Society Meeting, Chicago,* Illinois
2018	*Syngas Conversion,* Cape Town South Africa
2017	*Faraday Discussions*, Cape Town, South Africa

Publications

L. Macheli, A. Roy, E. Carleschi, B. P. D. Doyle and E. van Steen, *Catal. Today*,(in press), DOI:https://doi.org/10.1016/j.cattod.2018.10.018)

L. Macheli, E. Carleschi, B. P. D. Doyle, G. Leteba, Kooyman, P and E. van Steen, “tuning catalytic performance in Fischer-Tropsch synthesis by metal-support interactions” (in preparation).

L. Macheli, E. Carleschi, B. P. D. Doyle, G. Leteba and E. van Steen, “Introducing silane ligands on cobalt oxides,to investigate metal-suport interactions” (in Preparation)

Abstract

This thesis aims to gain insight into the effects of metal-support interaction in Co/SiO_2 catalysts using an inverse model system by modifying Co_3O_4 nanocrystallites with silanes (i.e. tetraethoxysilane, trimethyl chlorosilane, triphenyl ethoxysilane). It is postulated that the formation of Co-O-Si will alter the catalytic properties of the cobalt site to which silane is bonded and the adjacent ligand-free sites. The desire is to understand the effects of metal support interactions obtained after reduction of the model system on its performance in Fischer-Tropsch synthesis, which was used as a test reaction, taking into account the change in the reducibility and metal surface area. Cobalt oxide was synthesize using sodium dodecylsulphate assisted oxidative precipitation or cobalt carbonyl decomposition and was contacted with the respective silanes in different solvents. The presence of silanes on the surface of cobalt oxide both prior and after reduction was confirmed using infrared spectroscopy. Modification of cobalt oxide with the silanes does not affect the morphology of cobalt oxide nano-crystallite and may have formed silicate islands on the surface of cobalt oxide. The presence of the silane retards the reduction process by changing the activation energy required for the reduction process. The presence of this material on the surface of cobalt decrease the surface area. However, the catalytic activity increased drastically.

The interaction of Co_3O_4 with tetraethoxysilane was manipulated by using different solvents (mixtures) (i.e. anhydrous environment vs acid/base hydrolysing environment). For the modification in anhydrous environment, the formation of silica on the surface of Co_3O_4 is facilitated by heat treatment. However, in hydrous environment, the formation of silica on the surface of Co_3O_4 is initiated by the hydrolysis of tetraethoxysilane. The effects of modification using different solvent was tested in the Fischer-Tropsch synthesis. The modification under acid catalysed hydrolysis facilitate the formation of Co-O-Si contact points followed by increase catalytic activity compared to catalysts modified in other solvents.

An insight about the effects of calcination on the interaction of silica and cobalt was obtained by calcining a modified sample at different temperatures. Low temperature (573 K) calcination facilitate stronger interactions. The interaction becomes weaker in increasing temperature up

to 873 K. Calcination at temperature from 973 K-1173 K result in very strong interaction that leads to the formation of Co_2SiO_4.

To further obtain an enlightenment regarding the electronic effects caused by the modification of cobalt oxide with silane, silanes of different electronic behaviour were used. In addition to electron withdrawing tetraethoxysilane, electron donor silane (triphenyl ethoxysilane and trimethyl chlorosilane) were used to modify the surface of cobalt oxide. While the activity was increased, the product selectivity was altered differently by the different silanes used.

Contents

List of figures

List of Tables

Abbreviations

AAS	Atomic absorption spectrometry
EDS	Energy-dispersive X-ray spectroscopy
FID	Flame ionization detector
FT	Fischer-Tropsch
FTIR	Fourier Transform infrared
FWHM	Full width at half maximum
GC	Gas chromatography
MMSI	Medium metal-support interaction
NTP	Normal temperature and pressure (298.15 K, 1 bar)
SMSI	Strong metal-support interaction
STP	Standard temperature and pressure (273.15 K, 1 bar)
TCD	Thermal conductivity detector
TEM	Transmission electron microscopy
TEOS	Tetraethoxysilane
TMCS	Trimethyl chlorosilane
TPD	Temperature-programmed desorption
TPES	Triphenyl ethoxysilane
TPR	Temperature-programmed reduction
WMSI	Weak metal-support interaction
XANES	X-ray absorption near edge spectroscopy
XRD	X-ray diffraction
XPS	X-ray photoemission spectroscopy

1. **Introduction**

Heterogeneous catalysts contain nano-particles to maximize the utilization of the catalytically active material. To minimize deterioration of the catalyst performance due to sintering, improved heat flow from and to the catalytically active sites, and minimize pressure drop, the catalytically active nano-sized particles are put on a support material. This carrier is usually an oxidic material such as silica or alumina or carbon derived materials such as silicon carbide or carbon nanotubes. The support is often thought to be inert but is known to affect via so-called strong metal support interactions e.g. the chemisorptive properties of the catalytically active materials and may thus affect their performance. It is argued that model systems are required to obtain a better understanding of strong-metal support interactions.

1.1. Background metal-support interaction

Heterogeneous catalysts are pillars, on which processes in the chemical industry have evolved. They are being used in several industrial processes such as pharmaceutical industry[1], chemical industry[2], environmental application and green energy generation[3]. The primary advantage of heterogenous catalyst systems arises from their ability to provide an alternative pathway thereby enhancing the rate of reaction and lowering the activation barrier for the conversion of the reactants. A molecular-level understanding of the heterogeneous catalyst and the role played by each component in a heterogeneous catalyst may result in faster improvement and optimization of the catalyst system performance than using the classical trial and error method.

Heterogeneous catalysts come in various forms ranging from resins and zeolites, to metal oxides/sulphides and metals. The use of these materials in nano-particle form may be advantages, if the nano-particles are desired (to maximize the amount of catalytically active material exposed to reactants in the fluid phase). Nanoparticles are of have attracted attention in science as they bridge a gap between bulk materials and atomic or molecular structures. They offer higher mass specific activity over a range of chemical reaction such as the energy conversion reactions e.g. methanol oxidation, selective hydrogenation reactions, electrochemical reactions or Fischer-Tropsch synthesis. For structure insensitive catalytic reactions such as hydrogenolysis, methanol synthesis and Fischer-Tropsch synthesis, the turnover frequency (TOF) has been shown not to be a function of crystallite size of the active material. Thus, the mass-specific activity of the catalytically active phase is maximized by utilizing a catalytic active phase with a high surface-to-volume ratio typically provided by small nano-sized particles[4]. On the other hand, some catalysed chemical reactions are structure-sensitive with the turnover frequency decreasing or increasing with increasing particle size. If turnover frequency decrease with increasing particles as observed for CO oxidation[5] or hydrogenation of hydrocarbons[6], the mass specific activity is still enhanced by reducing the particle sizes. However, if the turnover frequency increases with particles size as shown for Fischer-Tropsch synthesis[7], or oxidation reduction reactions[8], there is an optimum size at which the mass specific activity is highest (*See Fig. 1-1*) [9–11]

.

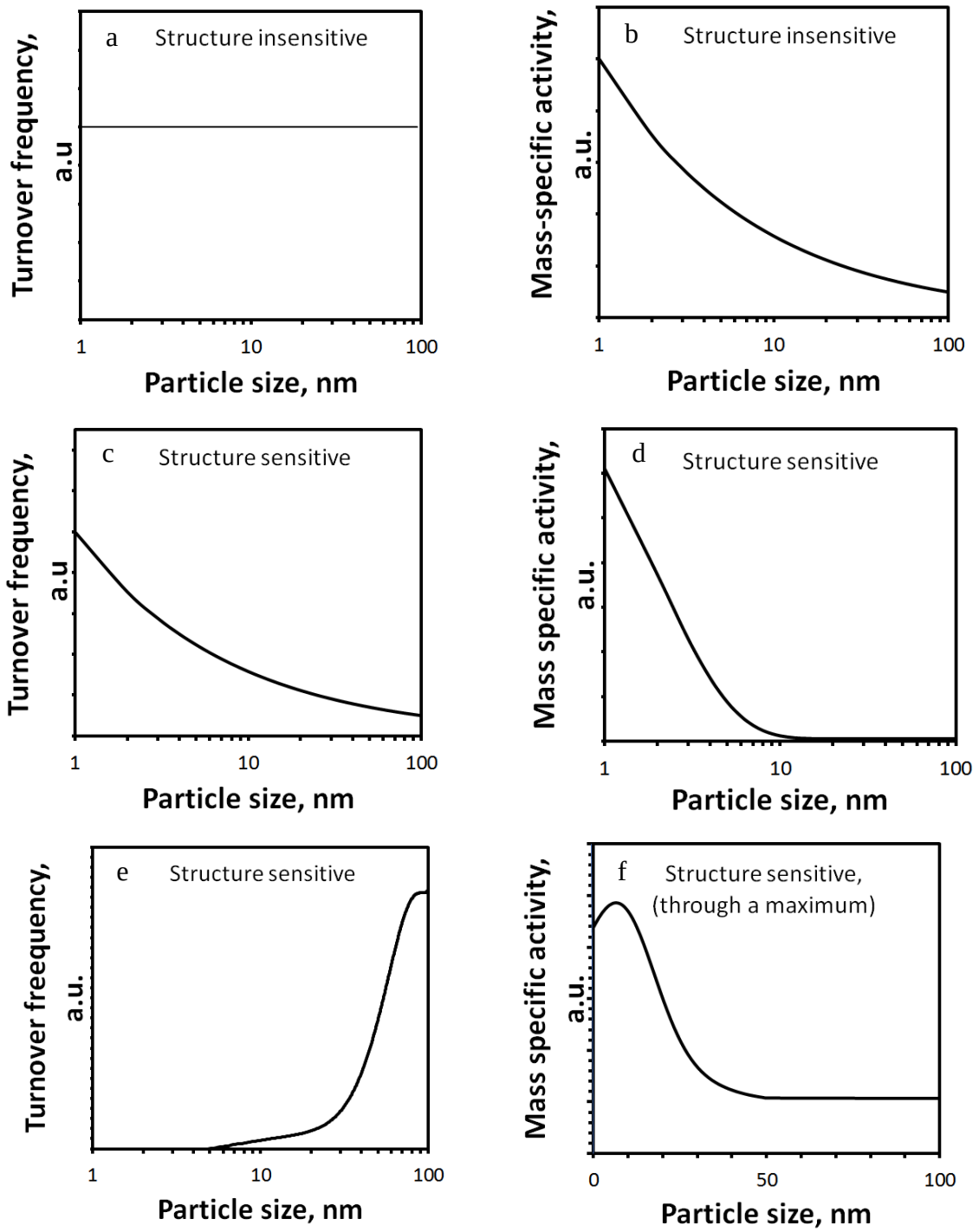

Figure 1-1: Illustration of the difference in terms of activity dependence on particle size for structure sensitive and structure insensitive catalytic reactions **(**Redrawn from data generated by Liu et al.[9],Taghavi et al.[10] and Somrajai et al.[11])

The long-term stability of nanoparticles in catalysis is compromised by their tendency to undergo the thermodynamically favoured sintering process. This can be kinetically inhibited by dispersing the nano-sized, catalytically active phase (or its precursor) on a support, if it may be assumed that sintering is controlled by particle coalescence or that diffusion of the adatom is

the rate controlling step in Ostwald ripening[12]. Well-dispersed nanoparticles on a support may result in well-distributed active sites and hence reduce the rate of conversion per unit volume of the catalyst. This may thus also reduce the competition between the product and the reactants for the active site thus reducing the probability of mass-/heat transfer limitations.

Support material may also reduce the risk of deactivation and catalyst failure due to particle size reduction or particle break up. This process may result in the formation very small particle, which will result in an increase in the pressure drop in a fixed bed reactor and may result in particle loss by carry-over in other types of reactors. Support particles may minimize 1) abrasion of particle through particle-particle interaction or collision of particles with reactor wall for fluidized or slurry reactors if the support is mechanically strong or 2) break-up due to thermal stresses (induced by rapid heating/cooling) if the support has a low thermal expansion. Furthermore, attrition due to chemical stress e.g. during the reaction process may be minimized,

The support is not only supplying thermal and mechanical stability to the catalyst particles, but may also play an active role in the reaction (e.g. hydrogenation of benzene[13], water-gas shift[14], oxidation of methane[15,16], CO_2 Conversion[17], naphtha reforming over Pt/Al_2O_3 catalyst[18]). This indicates that even though support materials have often been regarded to be catalytically inert materials that only supply platform for the dispersion of the active phase, the support may not always be inert. A support may directly or indirectly affect the catalyst activity and selectivity[19–22]. Supports may influence the behavior of a catalyst both through physical properties or chemical properties they have.

The support may, for a given preparation method, determine the obtained crystallite size of the catalytically active material[23]. Nanoparticles of sizes less than 6-8 nm show a decreased catalytic activity for some chemical reactions e.g. Fischer-Tropsch synthesis[24]. This is because small particles particles have a higher fraction of low coordination sites available[25,26]. Low coordination sites will have stronger bonding to adsorbates, thus affecting the overall reactivity. Recent theoretical studies have shown that sites responsible for the dissociation of CO on a f*ace*-centred cubic (f.c.c) cobalt crystal surface decrease with decreasing crystallite size[26] resulting in lower reactivity. Adsorption strength of adsorbates seems to be particle size

dependent. Small gold particles adsorb CO more strongly[27] than relatively large particles. Preferential adsorption of adsorbates has been reported with varying particle size. Smaller cobalt particles seem to preferentially adsorb hydrogen over CO and this may explain the changes in the selectivity with changing crystallite sizes for some reactions[28].

The support may influence the strength of adsorption of specific molecules, not only by changing the metal crystallite size, but also by a phenomenon called metal-support interactions. These metal-support interaction may alter the electronic properties of the catalytically active material thus changing the heats of adsorption of the adsorbates[4,15]. Tauster and co-workers[29] showed that the chemisorption properties of the group VIII metals were drastically altered by the interaction with titania after catalyst preparation through incipient wetness impregnation. Similarly, different heats of adsorption have been observed by Vannice *et al.*[30,31] when platinum of various crystallite sizes was dispersed on various support material after activation in hydrogen at high temperature (>770 K). The adsorption strength of CO was higher for Pt/SiO_2 catalyst and minimum for the Pt/TiO_2 catalysts[30]. *Figure 1-2* summarizes the heats of adsorption of both platinum catalysts disperse on various supports from the data generated by Vannice[30]. This data clearly indicates that heat of CO adsorption is a function of both support material used as well as particle size.

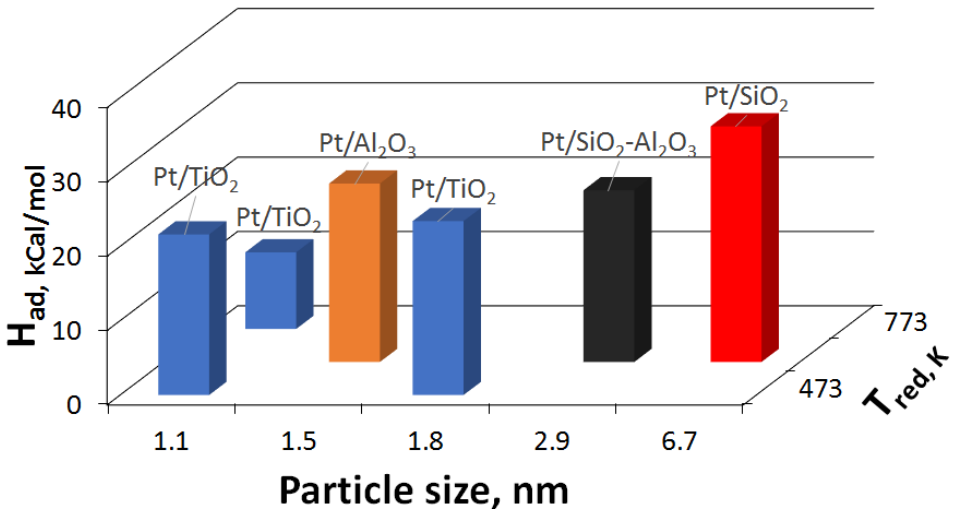

Figure 1-2: A bar graph indicating the dependence of CO adsorption heat on the particle size and reduction temperature for platinum catalyst supported of various support material

This change in the chemisorption properties is not observed upon activation of the catalyst at low temperatures (<473 K)[29]. This dramatic subdual in the hydrogen and CO chemisorption abilities of the titania supported group VIII metals is not due to sintering of the particle as this high temperature reduction did not induce particle growth as confirmed using TEM. It was ascribed to a phenomenon named strong metal support interaction (SMSI)[29]. The strong-metal support interactions observed through a change in the strength of chemisorption could be reversed upon oxidation and re-reduction of the catalyst. This further signifies that collapse of the catalyst support had not taken place and thus could not explain the change in chemisorption properties of H_2 and CO on Pt catalyst supported on titania.

The strong metal-support interaction may originate from a modification of the electronic configuration of the metal due to the support in close proximity of the metal (through polarization)[32] or bonding of the metal and the support (ligand effect) [33,34] . The idea that the metal-oxide interface may play a role in catalytic reactions is commonly acknowledged[35–38], but an understanding of the properties of the interface at a molecular level is still at its infancy. In fact, while past research has shown the existence of metal-oxide interactions[39–42], none have been able to control the extent or degree of metal-oxide interface generated.

An in-depth understanding of metal-oxide interface requires that the interface be exposed either to reactants or be exposed to perform direct spectroscopic analysis. However, in a conventional catalyst configuration whereby the metal nanoparticles are incorporated on the support, the interface is concealed between the metal and the support. A better model of the oxide supported metal catalyst exposing the metal-oxide interface to reactants is required. A number of approaches to create such a model includes usage of model systems such as thin layer deposition[43], single atom catalysis[39], imaging nanoparticles on a model support[44,45], or inverse systems where a support is rather dotted onto the surface of the metal[46–50].

1.2. Brief Background on Fischer-Tropsch synthesis

Synthesis gas conversion to high quality transportation fuel via the Fischer-Tropsch synthesis is of interest today. Fischer-Tropsch synthesis produce a wide range of chemicals which include olefins and paraffin and thus becomes a promising option for fuel synthesis. The feed to the

Fischer-Tropsch synthesis reactor is a mixture containing carbon monoxide and hydrogen. The reaction occurs over a catalyst surface and can be formally represented by:

$$nCO + 2nH_2 \rightarrow C_nH_{2n} + nH_2O$$ ..... Equation 1-1

Fischer-Tropsch synthesis requires a catalytically active surface to initial activate CO prior to hydrogenation. The metals active for the Fischer-Tropsch synthesis include, but not limited to, iron, cobalt, ruthenium and nickel. When used as catalysts, these metals are usually supported on a support material (e.g. silica, alumina, titania) to enable maximum use of the metal by increasing the dispersion, mechanical and thermal stability. These support materials seem to interact differently with the catalytically active material and as such affect their catalytic performance in chemical reactions e.g. Fischer-Tropsch synthesis. As such, Fischer-Tropsch synthesis may be manipulated by using metal-support interactions.

1.3. Surface modification of oxides with silanes

Catalysis is a surface phenomenon and surface properties play an important role in the ultimate catalytic activity of the exposed surface facets. Chemical arrangement of a catalyst surface may be transubstantiated via surface modification by introducing organic or organometallic moieties on a catalyst surface to alter their properties such as acidity/basicity[51] hydrophobicity [52–57] mechanical stability [58], thermal stability [58–60] or the electronic properties of the site to which these moieties are bonded [61]. These surface moieties can be regarded as a ligand to the catalytic active surface and thus modifying the catalytically active site.

Tethering a modifying agent/ligand to the surface can be achieved via strong adsorption, ion-exchange, or by chemically reacting of the reactive part of the modifying agent with a reactive part of the surface[48,61–65]. The modification of a catalytically active surface by functionalization requires a stable ligand and a stable attachment point of the ligand to the surface under the applied reaction conditions. For instance, surface hydroxyl groups on the surface may act as an anchoring point for modifying agents[59,62–65].

The commonly used coupling agents are organofunctional silanes of the form $RSiX_n$, where n can be a halide, alkoxy group or and alkyl group and R represents the organofunctional group.

Silanes undergo a hydrolysis reaction with water creating silanol species (Si-OH) which in the present of metal hydrate (M-OH) surface groups may undergo a condensation reaction creating M-O-Si bonds[66]. Moreover, the silanol groups are also subject to undergo condensation reaction resulting in Si-O-Si.[67] In dry solvents, the alkoxysilanes may undergo alcohol condensation the metal hydrate resulting in the formation of monodentate M-O-Si surface species[48,62].

1.4. References

1 H. Liang, J. M. Raitano, L. Zhang and S.-W. Chan, *Chem. Commun. (Camb).*, 2009, **2009**, 7569–7571.

2 M. A. Khodagholi and M. Irani, *J. Chem.*, 2013, **2013**, 1–7.

3 N. Toshima, *Pure Appl. Chem.*, 2013, **85**, 437–451.

4 C. T. Campbell and J. R. V. Sellers, *Faraday Discuss.*, 2013, **162**, 9.

5 M. Haruta, *Catal. Today*, 1997, **36**, 153–166.

6 C. R. Henry, *Surf. Sci. Rep.*, 1998, **31**, 231–233.

7 N. Fischer, B. Clapham, T. Feltes, E. van Steen and M. Claeys, *Angew. Chemie - Int. Ed.*, 2014, **53**, 1342–1345.

8 H. Yano, J. Inukai, H. Uchida, M. Watanabe, P. K. Babu, T. Kobayashi, J. H. Chung, E. Oldfield and A. Wieckowski, *Phys. Chem. Chem. Phys.*, 2006, **8**, 4932–4939.

9 J. X. Liu, P. Wang, W. Xu and E. J. M. Hensen, *Engineering*, 2017, **3**, 467–476.

10 M. B. Taghavi, G. M. Pajonk and S. J. Teichner, *J. Colloid Interface Sci.*, 1979, **71**, 451–465.

11 G. A. Somorjal and J. Carrarza, *Ind. Eng. Chem. Fundumentals*, 1986, **25**, 63–69.

12 V. M. Kaganer, W. Braun and K. K. Sabelfeld, *Phys. Rev. B - Condens. Matter Mater. Phys.*, 2007, **76**, 1–11.

13 V. Mazzieri, N. Figoli, F. Pascual and P. L'Argentine, *Catal. Letters*, 2005, **102**, 79–82.

14 Y. Sun, M. Grigore, S. S. Hla, L. D. Morpeth and J. H. Edwards, *Int. J. Hydrogen Energy*, 2016, **41**, 10335–10345.

15 T. H. Nguyen, A. Łamacz, A. Krztoń, A. Ura, K. Chałupka, M. Nowosielska, J. Rynkowski and G. Djéga-Mariadassou, *Appl. Catal. B Environ.*, 2015, **165**, 389–398.

16 D. Wang, O. Dewaele, A. M. De Groote and G. F. Froment, *J. Catal.*, 1996, **159**, 418–426.

17 D. Ma, B. Li, K. Liu, X. Zhang, W. Zou, Y. Yang, G. Li, Z. Shi and S. Feng, *J. Mater. Chem. A*, 2015, **3**, 23136–23142.

18 M. A. Sánchez, V. A. Mazzieri, J. M. Grau, J. C. Yori and C. L. Pieck, *J. Chem. Technol.*

Biotechnol., 2011, **86**, 1198–1204.

19 H. J. Wan, B. S. Wu, Z. C. Tao, T. Z. Li, X. An, H. W. Xiang and Y. W. Li, *J. Mol. Catal. A Chem.*, 2006, **260**, 255–263.

20 M. Qing, Y. Yang, B. Wu, J. Xu, C. Zhang, P. Gao and Y. Li, *J. Catal.*, 2011, **279**, 111–122.

21 Y. Yang, H. W. Xiang, L. Tian, H. Wang, C. H. Zhang, Z. C. Tao, Y. Y. Xu, B. Zhong and Y. W. Li, *Appl. Catal. A Gen.*, 2005, **284**, 105–122.

22 X. D. Hou, Y. Z. Wang and Y. X. Zhao, *Catal. Letters*, 2008, **123**, 321–326.

23 R. Geyer, J. Hunold, M. Keck, P. Kraak, A. Pachulski and R. Schödel, *Chemie-Ingenieur-Technik*, 2012, **84**, 160–164.

24 D. Barkhuizen, I. Mabaso, E. Viljoen, C. Welker, M. Claeys, E. van Steen and J. C. Q. Fletcher, *Adv. Mater.*, 2006, **78**, 1759–1769.

25 L. M. Falicov and G. A. Somorjai, *Proc. Natl. Acad. Sci. U. S. A.*, 1985, **82**, 2207–2211.

26 P. van Helden, I. M. Ciobîcə and R. L. J. Coetzer, *Catal. Today*, 2016, **261**, 48–59.

27 S. Shaikhutdinov, R. Meyer, C. Lemire and H. J. Freund, *Catal. Letters*, 2003, **86**, 211–219.

28 J.-Y. Park, Y.-J. Lee, P. R. Karandikar, K.-W. Jun, K.-S. Ha and H.-G. Park, *Appl. Catal. A Gen.*, 2012, **411–412**, 15–23.

29 S. J. Tauster, S. C. Fung and R. L. Garten, *J. Am. Chem. Soc.*, 1978, **100**, 170–175.

30 M. A. Vannice, L. C. Hasselbring and B. Sen, *J. Chem. Phys.*, 1985, **89**, 2972–2973.

31 M. A. Vannice and C. Sudhakar, *J. Chem. Phys.*, 1984, **88**, 2429–2432.

32 I. J. Adadurov, *J. Phys. Chem. USSR*, 1935, **6**, 206–220.

33 T. Bligaard and J. K. Nørskov, *Electrochim. Acta*, 2007, **52**, 5512–5516.

34 T. Bligaard and J. K. Nørskov, *Electrochim. Acta*, 2007, **52**, 5512–5516.

35 H. Idriss, M. Scott, J. Llorca, S. C. Chan, W. Chiu, P. Sheng and A. Yee, *ChemSusChem*, 2008, **1**, 905–910.

36 C. Xu, G. Chen, Y. Zhao, P. Liu, X. Duan, L. Gu, G. Fu, Y. Yuan and N. Zheng, *Nat. Commun.*, 2018, **9**, 3367.

37 K. Mudiyanselage, S. D. Senanayake, L. Feria, S. Kundu, A. E. Baber, J. Graciani, A. B. Vidal, S. Agnoli, J. Evans, R. Chang, S. Axnanda, Z. Liu, J. F. Sanz, P. Liu, J. A. Rodriguez and D. J. Stacchiola, *Angew. Chemie Int. Ed.*, 2013, **52**, 5101–5105.

38 G. Chen, C. Xu, X. Huang, J. Ye, L. Gu, G. Li, Z. Tang, B. Wu, H. Yang, Z. Zhao, Z. Zhou, G. Fu and N. Zheng, *Nat. Mater.*, 2016, **15**, 564–569.

39 L. Wang, H. Li, W. Zhang, X. Zhao, J. Qiu, A. Li, X. Zheng, Z. Hu, R. Si and J. Zeng, *Angew.*

Chemie - Int. Ed., 2017, **56**, 4712–4718.

40 J. C. Matsubu, S. Zhang, L. Derita, N. S. Marinkovic, J. G. Chen, G. W. Graham, X. Pan and P. Christopher, *Nat. Chem.*, 2017, **9**, 120–127.

41 H. Tang, J. Wei, F. Liu, B. Qiao, X. Pan, L. Li, J. Liu, J. Wang and T. Zhang, *J. Am. Chem. Soc.*, 2016, **138**, 56–59.

42 A. M. Abdel-Mageed, D. Widmann, S. E. Olesen, I. Chorkendorff, J. Biskupek and R. J. Behm, *ACS Catal.*, , DOI:10.1021/acscatal.5b01520.

43 D. W. Kim, K. D. Kim, H. O. Seo, N. K. Dey, M. J. Kim, Y. D. Kim, D. C. Lim and K. H. Lee, *Catal. Letters*, 2011, **141**, 854–859.

44 M. Bowker, P. Stone, P. Morrall, R. Smith, R. Bennett, N. Perkins, R. Kvon, C. Pang, E. Fourre and M. Hall, *J. Catal.*, 2005, **234**, 172–181.

45 O. Dulub, W. Hebenstreit and U. Diebold, *Phys. Rev. Lett.*, 2000, **84**, 3646–3649.

46 S. D. Senanayake, D. Stacchiola and J. A. Rodriguez, *Acc. Chem. Res.*, 2013, **46**, 1702–1711.

47 E. van Steen, M. Claeys, K. P. Möller and D. Nabaho, *Appl. Catal. A Gen.*, 2018, **549**, 51–59.

48 R. P. Mogorosi, N. Fischer, M. Claeys and E. van Steen, *J. Catal.*, 2012, **289**, 140–150.

49 R. P. Mogorosi, M. Claeys and E. van Steen, *Top. Catal.*, 2014, **57**, 572–581.

50 A. P. Petersen, R. P. Forbes, S. Govender, P. J. Kooyman and E. van Steen, *Catal. Letters*, 2018, **148**, 1215–1227.

51 M. A. Markowitz, P. E. Schoen, P. Kust and B. P. Gaber, *Colloids Surfaces A Physicochem. Eng. Asp.*, 1999, **150**, 85–94.

52 A. Parvathy Rao and A. Venkateswara Rao, *J. Mater. Sci.*, 2010, **45**, 51–63.

53 R. A. Sperling and W. J. Parak, *Philos. Trans. R. Soc.*, 2010, **368**, 1333–1383.

54 R. Xie, D. Li, B. Hou, J. Wang, L. Jia and Y. Sun, *CATCOM*, 2011, **12**, 589–592.

55 A. Zola, L. . da Silva, L. . Moretti, C. Fraga, E. F. Sousa-Arguiar and A. P. Arroyo, *Top. Catal.*, 2016, 219–229.

56 L. Shi, J. Chen, K. Fang and Y. Sun, *Fuel*, 2008, **87**, 521–526.

57 Y. Kirmanidou, M. Sidira, M. Drosou, V. Bennani, A. Bakopoulou, A. Tsouknidas, N. Michailidis and K. Michalakis, *Biomed Res. Int.*, 2016, **2016**, 1–21.

58 C. S. Pauly, A.-C. Genix, J. G. Alauzun, M. Sztucki, J. Oberdisse and P. Hubert Mutin, *Phys. Chem. Chem. Phys.*, 2015, **17**, 19173–82.

59 M. Ojeda, F. Jose, P. Terreros, S. Rojas, T. Herranz and L. G. Fierro, *Langmuir*, 2006, **22**,

3131–3137.

60 E. Ukaji, T. Furusawa, M. Sato and N. Suzuki, *Appl. Surf. Sci.*, 2007, **254**, 563–569.

61 N. Gurbuz, I. Ozdemir, T. Seckin and B. Cetinkaya, *J. Inorg. Organomet. Polym.*, 2004, **14**, 149–159.

62 D. W. Sindorf and G. E. Maciel, *J. Am. Chem. Soc.*, 1983, **105**, 3767–3776.

63 H. . Baney, M. Itoh, A. Sakakibara and T. Suzuki, *Chem. Rev.*, 1995, **95**, 1409–1430.

64 A. V. Rao and R. R. Kalesh, *Sci. Technol. Adv. Mater.*, 2003, **4**, 509–515.

65 R. M. Pasternack, S. R. Amy and Y. J. Chaba, *Langmuir*, 2008, **24**, 12963–12971.

66 M. Longhi, S. R. Kunsta, L. Vanessa, R. Beltrami, E. K. Kerstner, V. Hugo, V. Sarmento and P. Alegre, *Mater. Res.*, 2015, **18**, 1140–1155.

67 J. J. Brinker and G. Scherer, *Sol-Gel Science: The Physics and Chemistry of Sol-Gel Processing*, Academia Press, Inc., New York, 1990.

2. **Metal-Support Interactions**

The role of a support material in catalysis is not restricted to offering a platform for dispersing the catalytically active material only. The support material may interact with the catalytically active material in a way that my alter the intrinsic activity of the catalyst. The function of the support other than dispersing the catalytically active metal is reviewed in this section. The development of the metal-support interactions, their role in catalysis and the different ways in which they can be studied for better insight have been discussed, in this chapter.

2.1. Technical aspects of metal-support interactions

Heterogeneous catalysts are the workhorse of the chemical industry providing a catalytically active surface for chemical transformations to take place. They have typically undergone a long developmental route gradually improving its performance. Hence, catalysts nowadays are complex mixtures containing the catalytically active material (often as nano-sized materials) and other materials such as support, binder, and promoters. The interaction between the constituents in the catalysts are often not well explored and not well understood. The advent of the field of nano-materials synthesis has opened the field of catalysis to gain more control over the catalytic properties, in cases in which the crystallite size affects the catalytic activity,[1] to synthesize model systems[2] to investigate properties pertinent to nano-sized systems,[3] or to investigate interactions present in industrial catalysts[4]. The interest of the dissertation is in the interaction between the metal (and its precursor) to the support.

Metals may interact differently with different support materials. Metal-support interactions may be classified into weak metal-support interactions (WMSI) with interactions due to van der Waals forces, medium metal support interactions (MMSI) typically observed with metals clusters in zeolite channels and strong metal-support interactions (SMSI), which is observed with metals supported on oxides as previous done by Burch[5]. The concept of strong metal-support interactions was further developed by Vannice *et al.*[6] when explaining the increase in the heats of adsorption of CO and H_2 on Group VIII metals supported on TiO_2. Strong metal-support interaction is known to alter the kinetic parameters, and as such intrinsic activity of these materials[7], and catalyst lifetime. This has broadly been ascribed to metal-support interactions and may arise from **electronic interaction**,[4,8] or **polarization effect**[9]**, strain effects**[10,11] or **creeping of the support**[12]. Metal-support interaction may also arise from the, **ligand effect** due to coordination of metal by the oxide[13,14] or even interfacial reactivity[15]**.** The bond formation between metals and supports may result also in the formation of irreducible metal-support compounds[16].

Electronic effect

Metal-support interaction may occur through charge transfer from the oxide support to the catalytically active metal or from the metal to the oxide support. The driving force for the charge transfer is the difference in the work functions of both the support and the catalytically active

metal. An electron transfer from an oxide to a metal can readily occur, when they are put into contact, by the spontaneous alignment of their Fermi levels, provided the work function of the metal is greater than that of the oxide[17]. If the charge transferred is only localized at the interface, a Schottky contact (*see Fig. 2-1)* and is characterized by charge polarization at the metal-support interface is formed.

The concept of polarization was first postulated in 1935 by Adadurov[18] when he proposed that oxides surfaces with high cation charge can polarize the respective supported metals. This polarization occurs because of electron transfer from the oxide support to the catalytically active metal or from the metal to the oxide support. The driving force for the charge transfer is the difference in the work functions of both the support and the catalytically active metal in a thermodynamic equilibrium. The polarization hypothesis was experimentally evidenced using X-ray crystallography and UV photoemission[19,20] with Pt nanoparticles supported on ceria. The Pt $4f^{7/2}$ core level binding energy of supported Pt nanoparticle were higher that of the bulk because of electron transfer from platinum to ceria upon contact[22].

The gradient of electrochemical potential governs the direction of electron flow[17]. An electron transfer from an oxide to a metal can readily occur, when they are put into contact, by the spontaneous alignment of their Fermi levels, if the work function of the metal is greater than that of the oxide[17]. In this case, the carrier shall be partially positive while the metal surface shall have an induced negative charge. The interface may thus be considered to have a polarized charge. The contact potential is retained at the interface as an interfacial dipole. As such, the polarization effect in catalytic reactions may be observed only at the metal-support Schottky interface[21].

Polarization of the metal may thus alter the catalytic behavior of the metal, since it changes the electronic structure of the metal. This could indirectly impact the chemisorption energy of the adsorbates. This has been verified electrochemical stripping of CO from bimetallic platinum catalyst[22] and by vibrational spectroscopic techniques of CO adsorbed of Pt[23], or competitive hydrogenation of aromatic compounds[24]. For instance, it was thought that the suppression in the amount of H_2 on platinum catalyst supported on TiO_2 was due to electronic modification[25]. It was perceived that the electronic properties of platinum (on which H_2 adsorbs) adapted the

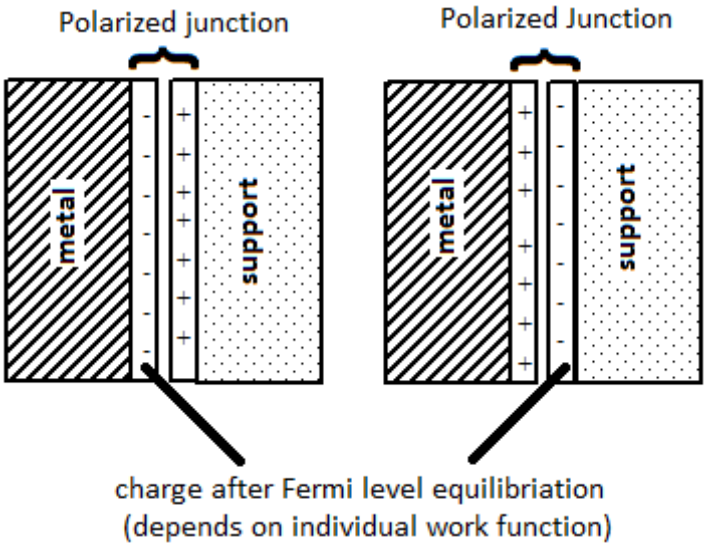

Figure 2-1: Polarization effect at the interface between the metal and the support (left) electrons are transferred from support to metal (right) electrons are transferred from metal to support during Fermi level equilibration

electron configuration of gold (on which H_2 does not adsorb)[25]. This was corroborated with insitu electrical conductivity measurements which showed that platinum on TiO_2 with strong metal support interaction has excess d-electrons originating from the reduced support adapting the d-electronic configuration of gold[17]. This was done by comparing the conductivity of titania deposited active metal against the conductivity of bare support.

Charge transfer can also be explained in terms of metal support interactions as due to a localized strong bonding between a support and a noble metal[26]. Artificial electronic type of metal-support interaction has been induced by use of alkaline promoters. For example, an electron donor effect of potassium oxide/hydroxide on Fe catalyst was used as an explanation for a change in catalytic performance of a potassium doped iron-based catalyst in the Fischer-Tropsch synthesis[27,28]. A similar effect has been observed by Barber *et al.*[29] where Pt was modified with either carbon by coking or sulfur by contacting with H_2S in hydrogen for the competitive hydrogenation reactions of benzene and toluene. The electronic modification resulted in a changed the product selectivity of the hydrogenation reactions[29].

However, electron transfer may be less important, for large particles (> 2 nm) due to high electron densities in metals as compared to the counterpart electron densities of the semiconductors[30,31]. As Ponec[31] argued a transfer of an electron from the support in the order of one electron into a sea of a thousand electrons should not have a large effect on catalysis.

Conversely, Santos and Dumesic[32] have posed a substantial argument for charge transfer from the catalytically active metal to the support. i.e. from Fe to TiO_2 based on ammonia synthesis activity after a high temperature reduction. Presuming that an electron transfer between metal particle and TiO_2 does occur, the crucial point to be clarified is whether it is a cooperative electronic interaction or a localized interaction or, indeed, whether the electron transfer directly affects catalysis[33].

Electronic effects may be initiated by high temperature reduction of catalyst system. Reduction of TiO_2 supported Pt catalyst at high temperatures (>770 K), for instance, may result in oxygen vacancies and Ti^{3+} cations according to the following the reaction equations[25];

$$\boldsymbol{Ti^{4+} + 2O^{-} + H_2 \rightarrow Ti^{3+} + H_2O + O^{-} + anion\ vacancy} \quad \text{Equation 2-1}$$

The partial reduction of titania has been confirmed using EPR spectroscopy[34] and XPS[35]. The latter showed the presence of Ti^{3+} species characterized by a binding energy of 457.3 eV corresponding to the 2p level in Ti^{3+} appearing as a shoulder on the lower binding energy side of the Ti2p photoemission peak. Comparably, a peak corresponding to Pt with a valence less than zero is observed on the higher binding energy side of Pt 4f photoemission peak at 71.1 eV. It is thus though the that Pt and Ti^{3+} interact through metal-metal interaction resulting in $Pt^{-}Ti^{4+}$. A metal atom situated at an oxide ion vacancy could interact sufficiently strongly with a Ti^{3+} cation, why may result in electron transfer to the metal[25,36]. However, this bond is not observed when calcination is performed in oxidizing atmosphere[37].

Ligand effects

During catalyst synthesis, the catalyst is exposed to hydrothermal conditions which may induce a chemical interaction between metal precursor and support as they are in close proximity. This interaction may result in the formation of a chemical bond between the active metal and the support. The support anchors on to the active metal through an oxo (Metal-O-Support) bridge *(*see *Fig.2-2).* The support may then be considered as a supra-molecular ligand attached to the catalytically active phase. The important role of metal-oxide interfaces has been pointed out in numerous studies. As an example, Pt/FeOx[38]and Pt/CeOx[39]interface are vastly active for primary alcohol oxidation; Cu/SiOx facilitates the of hydrogenation of dimethyl oxalate to ethylene glycol[40].

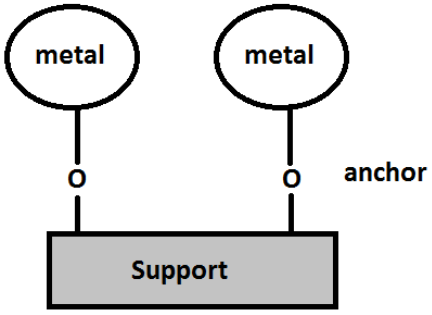

Figure 2-2: Support material as a supra-molecular ligand to the metal particle

Supra-molecular ligands bonded to catalytically active metal precursor may act as anchoring points of catalytically active metal precursor to the support. The ligand attached to the active metal may affect the properties on the metal. The introduced ligands does not only change physical properties, but the electronic properties of the site to which the ligand is bonded may also be modified resulting into entirely different catalyst activity or selectivity[4]. This electronic influence may not be restricted to the surface atom to which the ligand/support is bonded but may also alter atoms surrounding the ligand-blocked site. The affected atoms that surround the ligand-blocked site may be referred to as special contact zone (see *Fig. 2-3*). Consequently, the catalytic properties of such adjacent, ligand-free surface atoms (special contact zone) may be changed, too.

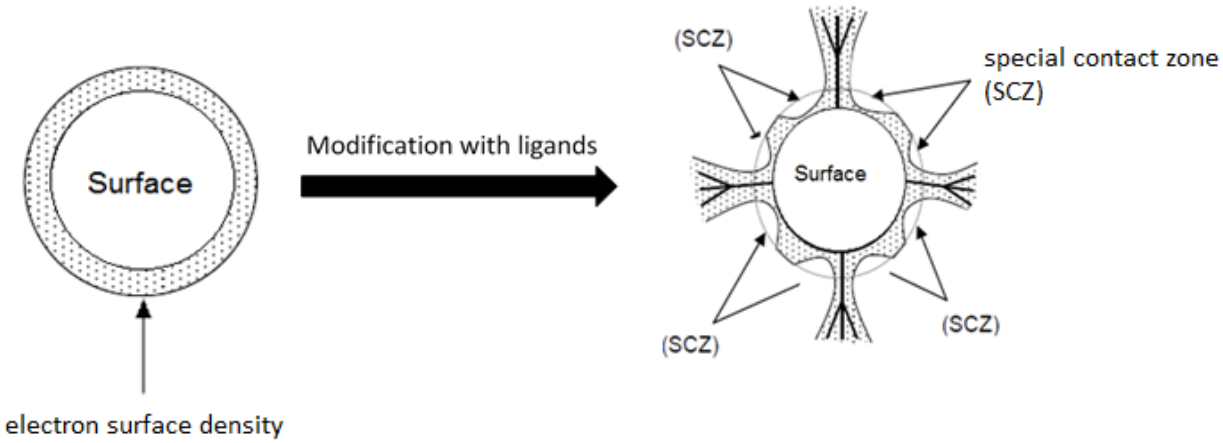

Figure 2-3: Special contact zones due to modification of nano-particles with ligands[41]

These special contact zones can be regions of high electron density or highly electron deficient regions. This is due to electron redistribution occurring because of the ligand attached. In fact,

by varying the ligand, the electronic density at the special contact zones of a metal might be tuned. Electron redistribution could be achieved by either introducing an electron donor or an electron withdrawing ligand onto the surface of the metal[42]. Electron withdrawing ligands are expected to increase the electron deficiency of the metal whereas electron donating ligands are expected to favour electron rich special contact regions.

The special contact sites may be responsible for the difference in activity and selectivity observed for a certain catalytically active metal supported on different support. Pt/TiO_2 contacts sites are believed to be conducive to hydrogen dissociation, resulting in higher methane selectivity and lower olefin selectivity in the CO hydrogenation reactions [43,44]. Such special contact sites were also reported to be the active sites for the hydrogenolysis of methyl cyclopentane producing n-hexane by Zuegg and Kramer[45]. This effect highlights the significance of adjusting the electronic properties of the metal surface atoms for better selectivity and catalytic activity.

Formation of overlayer/creeping of the support

It is usually acknowledged that high temperature reduction of catalyst supported on reducible oxides results in the formation of an overlayer of a support on the surface of the catalytically active material (see *Fig. 2-4*). The resulting metallic core decorated by a thin layer of a metal oxide allows the development of (partial) core-shell systems. At high temperatures, reducible support oxide can be partially reduced leading to the formation (sub)oxide species that readily migrate onto the surface of the active metal precursor during pre-reduction[15] or even at the reducing conditions present within certain chemical reactors. For instance, in the presence of hydrogen adsorbing metals (e.g cobalt, ruthenium), TiO_2 reduction is enhanced due to a greater diffusion of hydrogen surface species from the metal sites by spillover, since the hydrogen dissociation is favored over hydrogen adsorbing metal clusters[46]. This mechanism gives rise to the growth of new support layers around metal particles[47].

The driving force for this decoration process is provided by the high surface energies of the metal relative to the surface energy of the (sub)oxide[48,49]. The metal-support system minimizes its energy, resulting in the formation of a support-overlayer on the active material. For instance, in the case of TiO_2 support, the adsorbed TiO_x may start moving in the direction that leads to a

decrease the system energy thus resulting in the formation of a support-overlayer on the active material as reported for Ru/TiO_2 systems[50]. While it may be thought that the mobility of TiO_2 increases with increasing temperature, it seems the driving force is more of the partial reduction of TiO_2 than the mobility. This is because calcination of TiO_2 supported catalyst in oxidizing atmosphere does not form overlayers[37].

Figure 2-4: Illustration of support creeping upon high temperature reduction

Although, the formation of these overlayers is regarded as unfavorable as they may block the active site of the catalytically active metal, the contact sites are thought to be responsible for the improved activity observed for the TiO_2 supported catalyst[5,44,51]. As an added benefit, the formation of overlayers on the catalytically active metal surface may hinder sintering. Zhang *et al.*[37] calcined a Pt/TiO_2 catalyst both in a reducing and oxidizing atmosphere. The formation of the overlayer only takes place in a reducing atmosphere. This can be explained in two possible ways: either in the oxidizing atmosphere Pt attains a higher oxidation state and diffuses into the matrix of titania[52] and forms Pt-titanium compounds or the mobility of Ti^{n+} cations on platinum oxide may be limited. While it was initially thought that the suppression in the CO chemisorption undergoing strong metal support interaction was only due to the coverage of the active metal by the support[53,5455], other studies with the aid of vibrational and Auger spectroscopy have shown that at low coverages of Pt by titania, more than one CO adsorption site was deactivated by on Ti atom[52]. Therefore, the explanation that the suppression of CO chemisorption is only due to physical coverage of adsorption sites by the support layer can be ruled out.

Strain effects

For supported catalyst, the metal lattice in direct contact with the support may adapt a lattice parameter to approach that of the support. It usually occurs in two different ways: (i) the lattice of the support and that of the metal match during the relaxation process and (ii) the mismatch of the lattice of the support and that of the metal resulting in defect sites (see *Fig. 2-5)*. This

may cause a strain in the exposed surface leading to changes in the lattice constants of the metal. An increase in the lattice constant may increase or decrease the strength of adsorbates depending on the position of thee d-band [11,56]. A compressed lattice lowers the d-band centre, whereas an expanded lattice raises the d-band center[57]. With a compressed strain occurring, the d-band overlap increases resulting in a downshift of the d-band centre eventually resulting in weaker metal-adsorbate bonding strength[57]. A change in the strength of the metal–adsorbate bonding[11,58] may thus change the catalytic performance in terms of activity and selectivity.

The strain effect due to different support materials may cause a certain metal to adapt different geometric shapes or crystal phases (e.g. hcp or fcc) on different support materials[59,60]. The support effects on shape and size were studied by Baker *et al.*[61]. Annealing platinum supported on titania, alumina, silica and carbon under hydrogen atmosphere resulted in platinum particles of different shapes and sizes. This in turn affects the catalytic performance of Pt over various supports.

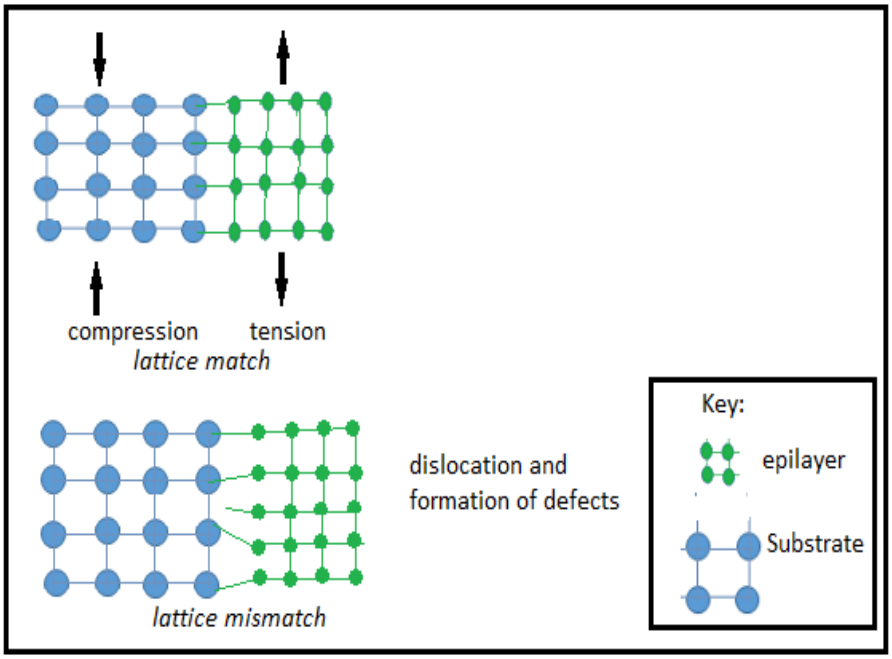

Figure 2-5: Lattice reconstruction during the contact of a substrate and an epilayer due to contact effect (top) the lattice of the epilayer and substrate matches (bottom) lattices do not match

Interaction of support substrates with adsorbate

Tauster and co-workers[26] showed that at elevated temperatures under hydrogen atmosphere, TiO_2 may be partially reduced to TiO_{2-x} (where x<2). Partial reduction of titania support may result on formation of the oxygen vacancies and Ti^{3+} cations. This Ti^{3+} cations may enhance the rate of CO dissociation in the CO hydrogenation reaction as the vacancy on the support interacts with CO adsorbed on the catalytically active metal (see *Fig. 2-6)*[44]. In addition to the M/TiO_2 systems, the contact effect has been also observed in other oxide substrates, such as CeO_2, Nb_2O_5, La_2O_3[62,63] while on irreducible support, as alumina, the sintering effect seems to be more important than the contact effect[64].

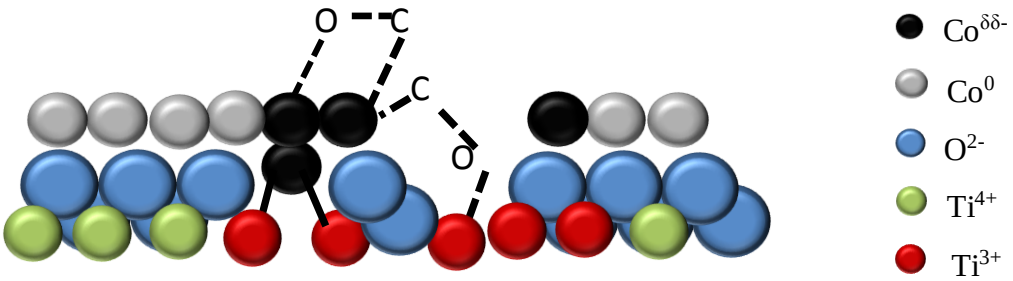

Figure 2-6: Interactions of CO at the interface of Co/TiO_2 (adapted from Burch and Flambard[5])

Rieck and Bell[65] proposed a mechanism, by which the support facilitates CO disproportionation on titania supported palladium catalysts. They postulated that reduced titania species may interact with the adsorbed CO to form the adsorbed carbon species on the metal surface (see *Fig. 2-8)*. They ascribed the higher specific activity of titania supported palladium catalyst over silica supported palladium catalyst to this effect.

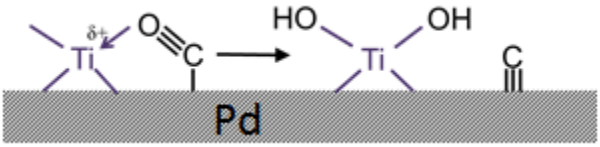

Figure 2-7: Proposed mechanism for CO dissociation on titania supported palladium catalyst following partial reduction of Ti^{4+} (adapted from Rieck and Bell[65])

The other role that partially reducible oxide support plays is to transfer oxygen to or from the metal. This requires contact between the catalytically active metal or its precursor and the support material be maximized[30]. The importance of the partial transfer of oxygen between the support to the metal may be to increase the stability of the catalytically active site either by keeping the active oxide phase or by maintaining the reduced active phase depending on direction of the oxygen transfer. For instance, partial transfer of oxygen was found to be

important in the methane oxidation over Pd/CeO_2 catalyst, where PdO is the active phase for methane oxidation[66].

On the contrary, for the Co/Ga_2O_3 system, the partially reduced oxide support may enhance the reduction process by extracting an oxygen atom from the catalytically active metal oxide precursor thereby making the reduction process occur at relatively lower temperatures[67]. A clear example has been reported by Huber *et al*.[67] During reduction of the Gd_2O_3 supported cobalt catalyst. GdO_x species migrate to the cobalt metal surface and are thought to assist the reduction process by extracting oxygen atoms from the cobalt oxide surface. This mechanism may also account for the observed reduction behaviour for ceria supported systems with reduction peaks of a ceria supported Co_3O_4 catalyst appearing at relatively low temperatures compared to that of unsupported Co_3O_4[68].

Formation of irreducible metal-support compounds

Catalytically active metals are typically supported on an inorganic oxide to increase their dispersion. During the catalyst preparation metal-support compounds, such as silicates, titanate or aluminates may be formed. However, the chemistry and stage at which cobalt silicate is formed.is still being debated For instance, Kogelbauer et al.[16] reported that cobalt silicate are formed starting from metallic cobalt. Van Steen et al.[69] on the other hand proposed the formation of an intermediate cobalt silicate surface phase during the initial decomposition of the cobalt nitrate precursor or by a reaction between the aqueous cobalt complexes and surface silanol groups. Ernst et al.[70] attributed the formation of cobalt silicate to the reaction of unreduced CoO present during the reduction of the catalyst with silica to form high surface area cobalt orthosilicate.

These metal-support compounds are highly irreducible in nature and therefore undesirable since the represent a loss in the catalytically active material. For instance, temperature programmed reduction studies shows that cobalt silicate only reduces at temperatures higher than 800 K when using diluted hydrogen gas[69]. The energy intensive reduction at high temperatures may result in sintering of the catalytically active materials, thus reducing the catalytically active metal surface area. However, some of these metal-support compounds may be necessary for improved dispersion of the catalytically active metal on the support[71].

2.2. Models for studying metal-support interactions

Metal-support interactions have been studied using real catalysts by varying the catalyst pre-treatment conditions[26] or the physical properties of the support[72,73]. Metal-support interactions can also be studied using model systems. This may involve the deposition of a thin, catalytically active film on a substrate[74], imaging nanoparticles on a model support[75,76], using core-shell systems or creating a reverse system[77,78], in which the support is deposited as nanoparticles on the catalytically active material.

Conventional approach[30]

Metal-support interactions may be explored using a conventional approach, core-shell approach or an inverse approach. The conventional approach is whereby a catalytically active substrate is dotted over a support material (see *Fig. 2-8).* Attempts to understand metal-support interactions using this model have been pursued by varying oxide supports for a specific reaction[79]. Metal-support interactions in this regard were followed by changing metal precursors, and preparation conditions and followed with different characterizations techniques such as temperature programmed reduction[69].

Metal-support support interaction are not purely structural effects. They may also give rise to electronic effects upon coordination of the metal and the support or even polarization. Hence, the interface between the metal and the support is of great interest. However, with the conventional approach, the metal-support interface is usually concealed between the metal and the support making it difficult to follow the effects of metal-support support interaction at the interface. With the addition of chemical promoters, understanding metal-support interaction using the conventional approach becomes even more complex as the interaction of promoters may also affect the catalyst performance[80].

Changing the support has been often applied as a method to get insights in metal support interactions. However, other support characteristics may also affect the performance of the catalyst. Depending on the pore size, the size of the resulting nanoparticle (synthesized by impregnation) may differ. Some of these size and morphological differences may be avoided by synthesizing mono-dispersed nanoparticles that are to be dispersed on a support material. However, changes in the porosity may affect transport of adsorbates to the metal surface. The

transport to a metal entrapped into a pore may be different from the transport to a metal nanoparticle found just on the outside of the support. These effects that make it difficult to be separated from the exclusive view changes brought about by metal-support interactions.

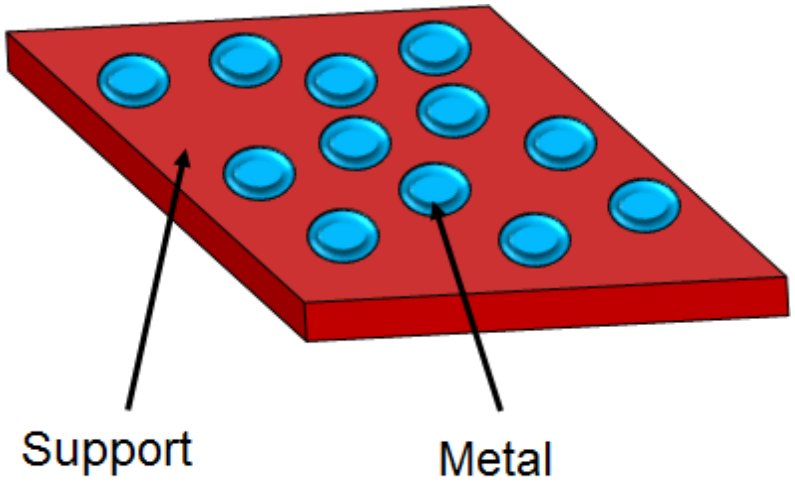

Figure 2-8: Representation of a conventional catalyst

The conventional approach may also be manipulated by using supported single crystal approach[74] or supported single atom catalysis[81] (see *Fig. 2-9*). It has been shown, using X-ray photoemission spectroscopy, that for the single copper crystal supported on silica, copper exist in a different oxidation state at interface the between the copper crystal and the silica support[74]. This may result in different catalytic properties at the interface.

In the single atom catalysis, single atoms are dispersed over a support material. This system has been applied in various catalytic reactions such as glucose oxidation[82], and styrene hydrogenation[83]. Single atoms have been observed to interact in different ways with the support material. They may anchor onto the support material through the formation of an oxo bridge between the atom and the support[83,84]. Alternatively, the metal atom may occupy the position of the metal in the support structure as has been observed in the atomic deposition of platinum on FeO_x using high resolution high-angle annular dark field scanning microscopy[84].

The formation of a metal-oxygen-support interfaces may result in charge transfer between the metal and support material thus altering the charge on the metal atom. This charge may affect the catalytic activity. Single atoms may have single or identical active site and this may enhance

their selectivity[85]. Any change in the interaction of the metal-atom with the support can then be correlated to changes in the selectivity[81].

Figure 2-9: Illustration of single crystal on a thin layer (left) and single atoms on a support (right)

Core-shell[86]

Core-shell system are made such that either the support makes and the catalytically active material makes a s shell or vice versa. Where the calatylically actictive material material is the shell, the core is aimed to modify the electronic properties of the active shell metal. Attempts have been made to make a core-shell system using porous oxide supports as shells while the active material make a core[38,40,87]. In this regard, the shell must be porous enogh to allow diffusion of adsorbates on to the surface of the active core. An additional advantage of this system hinges from the enhance abitility to resist sintering. The core-shell approach may allow control of the extent of metal-support interactions depending on the method used. They catalyst can be made into an egg-yolk form, where the core is *floating* inside a void shell[30]. This type is characterized with minimal metal-support interaction. On the hand, the synthesis procedure may lead to the a core-shell system where the metal is encompassed inside the oxide with maximum interaction[40].

Inverse approach

In the inverse approach, a support or support-like material is deposited in small quantities as nanoparticles on surface of the catalytically active material[88](see *Fig. 2-9*). This system will result in a loss in the number of catalytically active sites. However, the inverse catalysts could be catalytically more active than the conventional catalyst composed of the same compound[30]. However, if the support material is deposited in small quantities, this approach eliminates the contributions of support porosity to the activity of the catalyst and may help to obtain a better

understanding of the ligand effect compared to the conventional approach. A direct link between the catalyst properties and the catalytic activity may be established from the inverse system, as the reactants can have a direct interaction with the catalytically active sites and the interface between the catalytically active material and the support-like material can be studied eliminating other support effects[77,89].

Deposition of small quantities of the support material on the active material may mimic the effect of metal-support interaction at the interface generated through the creeping of support materials as observed for partially reducible oxidic support materials after catalyst activation in hydrogen. The presence of the supported suboxides may be enhanced by successive reduction-oxidation-reduction. The metal-support interaction that resulted from the successive reduction-oxidation-reduction process resulted in an increased surface area and as such an enhanced activity in the Fischer-Tropsch synthesis[12]. This metal-support interfaces seem to be responsible for the enhance activity.

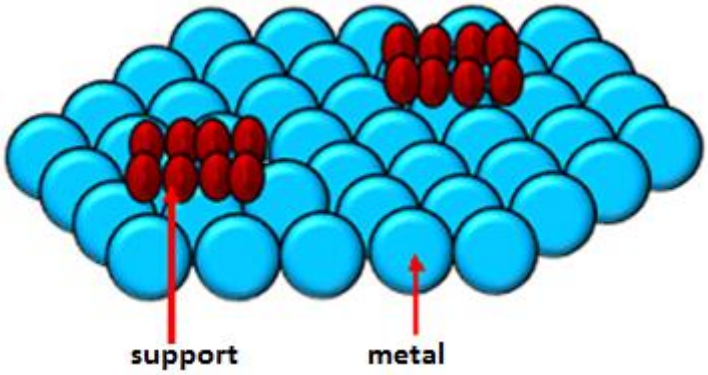

Figure 2-10: Illustration of an inverse model system to investigate metal-support interactions

2.3. Generation of metal-support interactions

The generation of metal-support interaction may be affected by various factors that include catalyst preparation methods (e.g. heat treatment), support properties or even the chemical reaction they catalyze[90]. The formation irreducible metal-support compounds is influenced by changing parameters such as metal precursors, silica precursors, solvents, pH or calcination atmosphere and temperature[69,91]. High temperature calcination studies show that results in a formation of metal-support compounds from a solid state reaction of metal (oxide) and the support[69]. The effects of pH on the formation of cobalt silicate in cobalt-silica catalyst have been reported by Ming and Baker[91] from the perspective of varying reducibility of catalysts prepared

from different pH. Reactions that involve water are also prone to catalyst deactivation due to formation of silicate compounds[16].

Metal-support interactions may be influence by the reaction conditions of the catalyzed reaction. For instance, at high CO-conversions in the cobalt-based Fischer-Tropsch synthesis, the water partial pressures are high and may result in the oxidation of metallic cobalt to the CoO phase. The CoO phase may act as a requisite for the formation of irreducible metal-support compounds[16]. Matsubu et al.[90] reported an adsorbate facilitated metal-support interaction during the CO_2 hydrogenation over a ruthenium catalyst supported over reducible support. During the hydrogenation process, HCO_x species that bind strongly on the reducible support were identified. This strongly bound adsorbate induced oxygen vacancies in the support and facilitated the creeping effect of the support over ruthenium[90].

This ligand-type of interaction may be generated through a condensation reaction involving surface hydroxyl groups of the support and hydroxyl groups adsorbed on the metal or present on a metal oxide. This could happen during a as the solid-state interactions between the metal and the support oxides[4,41,92]. The metal-support bond via the oxo bridge may also be formed during the preparation of the catalysts involving solvents or using other reactive catalyst or support precursors. For instance, Fe_3O_4 nanoparticles were contacted with alkoxides of titania and silica (i.e. titanium butoxide and tetraethoxysilane) and this resulted in Fe-O-Ti and Fe-O-Si bridges respectively[4,93]. The formation of this bonds of bridges was confirmed using infrared spectroscopy.

2.4. Characterization for metal support interactions

Catalyst characterization is fundamental to catalysis science. It can help gain a better understanding of catalyst performance or deactivation at a molecular level and it is thus anticipated to obtain improved control over the catalyst by correlating the catalyst performance (i.e. activity or selectivity) to its physical, chemical, or electronic properties. Knowledge on the dominant factors affecting catalyst performance may lead to design of improved catalysts.

However, it is difficult to utilize a single characterization technique to describe the nature of supported metal catalyst systems. This is because of the complexity of the systems themselves

thus requiring usage of complementary characterization techniques to improve understanding of the principal processes that occur on the atomic/molecular level. The understanding of the processes occurring at the molecular level may help to tune the parameters that significantly influence the selectivity and activity of the catalytic system. The different parameters that need to be well understood include interaction of the catalytically active metal and/or support, and adsorbates. Catalyst formulation process may also require more insight to enable the design of a catalyst of desired properties thus making it crucial to understand every step of the catalyst formulation. The catalyst formulation steps comprise of synthesis => calcination => activation => catalytic reaction => deactivation and regeneration.

Earlier characteristic studies of supported catalysts using electron microscopy were able to reveal the creeping of the support onto the catalytically active material which occurs during high temperature reduction[94]. The advent of high-resolution transmission electron microscopes has given information about the shape and size of the catalyst. However, electron microscopy fails to give information about the local composition at the catalyst surface. The most often used techniques that attempt to give a molecular level understanding of the supported heterogeneous catalyst includes but not limited to X-ray absorption near-edge structures (XANES),[95–98] extended x-ray absorption fine structures (EXAFS),[48,98–100] infrared or Raman spectroscopy (which uses vibrational modes of the chemical bonds between bonded atoms),[101,102] solid state NMR,[103–105] X-ray photoelectron spectroscopy (XPS). These techniques give information on the composition and valency of the elements in the catalyst before and after reaction test[37,106–108]The added advantage of vibrational spectroscopy is that it can be used to characterize both the catalyst and the molecules adsorbed on the surface of the catalyst (e.g. to determine CO adsorbed onto a metal catalyst surface[100,109,110]). Nevertheless, vibrational spectroscopy requires additional characterization techniques to unveil the surface the effects of metal-support interaction that occur in the case of supported catalyst systems[4].

Efforts have been made to use X-ray absorption spectroscopy to understand metal-support interactions[15,99,110–113]. Tsakoumis and colleagues[113] reported the formation of irreducible cobalt aluminates from the XANE experiments. The existence of metal-oxygen-support bonds has been demonstrated also via the use of Extended X-ray absorption fine structure (EXAFS) [85,99,114]. However, it is not always easy to confirm the metal-support bond in other systems as

the metal-support bonds may contribute less to the overall signal due to weak backscattering amplitude in the EXAFS signal[99].

2.5. References

1 M. Haruta, *Catal. Today*, 1997, **36**, 153–166.

2 D. Barkhuizen, I. Mabaso, E. Viljoen, C. Welker, M. Claeys, E. van Steen and J. C. Q. Fletcher, *Adv. Mater.*, 2006, **78**, 1759–1769.

3 N. Fischer, B. Clapham, T. Feltes, E. van Steen and M. Claeys, *Angew. Chemie - Int. Ed.*, 2014, **53**, 1342–1345.

4 R. P. Mogorosi, N. Fischer, M. Claeys and E. van Steen, *J. Catal.*, 2012, **289**, 140–150.

5 R. Burch and A. . Flambard, *J. Catal.*, 1982, **78**, 389–405.

6 M. A. Vannice, L. C. Hasselbring and B. Sen, *J. Chem. Phys.*, 1985, **89**, 2972–2973.

7 M. Vannice and R. . Garten, *J. Catal.*, 1979, **56**, 236–248.

8 G. . Schwab and K. Koller, *J. Am. Chem. Soc.*, 1968, **90**, 3078–3080.

9 T. Kittel and E. Roduner, *J. Phys. Chem. C*, 2016, **120**, 8917−8926.

10 A. Nilsson and L. G. M. Pettersson, in *Chemical Bonding at Surface and Interfaces*, eds. A. Nilsson, L. G. M. Pettersson and J. K. Noskov, Elsevier B.V., 1st edn., 2001.

11 M. Mavrikakis, B. Hammer and J. K. Nørskov, *Phys. Rev. Lett.*, 1998, **81**, 2819–2822.

12 C. H. Mejia, T. W. van Deelen and K. P. De Jong, *Nat. Commun.*, 2018, **9**, 4459–4465.

13 T. Bligaard and J. K. Nørskov, *Electrochim. Acta*, 2007, **52**, 5512–5516.

14 T. Bligaard and J. K. Nørskov, *Electrochim. Acta*, 2007, **52**, 5512–5516.

15 K. Hayek, R. Kramer and Z. Paál, *Appl. Catal. A Gen.*, 1997, **162**, 1–15.

16 A. Kogelbauer, J. C. Weber and J. G. Goodwin, *Catal. Letters*, 1995, **34**, 259–267.

17 J. M. Herrmann, *J. Catal.*, 1984, **89**, 404–412.

18 I. J. Adadurov, *J. Phys. Chem. USSR*, 1935, **6**, 206–220.

19 A. Bruix, J. A. Rodriguez, P. J. Ramírez, S. D. Senanayake, J. Evans, J. B. Park, D. Stacchiola, P. Liu, J. Hrbek and F. Illas, *J. Am. Chem. Soc.*, 2012, **134**, 8968–8974.

20 W. E. Kaden, T. Wu, W. A. Kunkel and S. L. Anderson, *Science*, 2009, 826–828.

21 P. Peljo, J. A. Manzanares and H. H. Girault, *Langmuir*, 2016, **32**, 5765–5775.

22 M. P. Mercer, D. Plana, D. J. Fermín, D. Morgan and N. Vasiljevic, *Langmuir*, 2015, **31**, 10904–10912.

23 a Rodriguez, C. M. Truong and D. W. Goodmanb, *J.Chem.Phys*, 1992, **96**, 7814–7825.
24 A. K. Aboul-gheit, *J. Appl. Chem. Biotechnol.*, 1977, **27**, 121–124.
25 J. A. Horsley, *Am. Chem. Soc.*, 1979, **101**, 2870–2879.
26 S. J. Tauster, S. C. Fung and R. L. Garten, *J. Am. Chem. Soc.*, 1978, **100**, 170–175.
27 M. E. Dry, T. Shingles, L. J. Boshoff and G. J. Oosthuizen, *J. Catal.*, 1969, **15**, 190–199.
28 M. A. Petersen, M. J. Cariem, M. Claeys and E. van Steen, *Appl. Catal. A Gen.*, 2015, **496**, 64–72.
29 J. Barbier, P. Marecot and L. Tifouti, *React. Kinet. catal. lett.*, 1986, **32**, 269–274.
30 M. Cargnello, P. Fornasiero and M. J. Gorte, *Catal. Letters*, 2012, **142**, 1043–1048.
31 V. Ponec, *Stud. Surf. Sci. Catal.*, 1982, **11**, 63–75.
32 J. Santos and J. A. Dumesic, *Stud. Surf. Sci. Catal.*, 1982, **11**, 43–51.
33 G. L. Haller and D. E. Resasco, *Adv. Catal.*, 1989, **36**, 173–235.
34 H. Liu, H. T. Ma, X. Z. Li, W. Z. Li, M. Wu and X. H. Bao, *Chemosphere*, 2003, **50**, 39–46.
35 J. Zhang, M. Zhang, Z. Jin, J. Wang and Z. Zhang, *Appl. Surf. Sci.*, 2012, **258**, 3991–3999.
36 C. M. Greenlief and J. M. White, *J. Phys. Chem.*, 1985, **89**, 5025–5028.
37 M. Zhang, Z. Jin, Z. Zhang and H. Dang, *Appl. Surf. Sci.*, 2005, **250**, 29–34.
38 G. Zhao, F. Yang, Z. Chen, Q. Liu, Y. Ji, Y. Zhang, Z. Niu, J. Mao, X. Bao, P. Hu and Y. Li, *Nat. Commun.*, 2017, **8**, 1–8.
39 A. Ostroverkh, V. Joha, P. Kús, S. Romana and V. Matolin, *Langmuir*, 2016, **32**, 6297–6309.
40 C. Xu, G. Chen, Y. Zhao, P. Liu, X. Duan, L. Gu, G. Fu, Y. Yuan and N. Zheng, *Nat. Commun.*, 2018, **9**, 3367.
41 R. P. Mogorosi, University of Cape Town, 2012.
42 P. F. da Silva, J. L. Fiorio and L. M. Rossi, *ACS Omega*, 2017, **2**, 6014–6022.
43 S. J. Tauster, *J. Catal.*, 1978, **55**, 29–35.
44 M. A. Vannice and C. Sudhakar, *J. Chem. Phys.*, 1984, **88**, 2429–2432.
45 H. Zuegg and R. Kramer, *ACS Symp. Ser.*, 1986, **298**, 145–151.
46 R. T. K. Baker, E. B. Prestridge and L. L. Murrell, *J. Catal.*, 1983, **79**, 348–358.
47 V. A. de la Peña O'Shea, M. C. Á. Galván, A. E. P. Prats, J. M. Campos-Martin and J. L. G. Fierro, *Chem. Commun. (Camb).*, 2011, **47**, 7131–7133.
48 Q. Fu and T. Wagner, *Surf. Sci. Rep.*, 2007, **62**, 431–498.
49 E. Ruckenstein, *ACS Symp. Ser.*, 1986, **298**, 152–168.
50 A. T. Bell, *Science*, 2003, **299**, 1688–1691.

51 S. J. Tauster, *ACS Symp. Ser.*, 1986, **298**, 1–9.

52 C. S. Ko and R. J. Gorte, *J. Catal.*, 1984, **90**, 59–64.

53 S. Takatani and Y. W. Chung, *Appl. Surf. Sci.*, 1984, **19**, 341–347.

54 S. Takatani and Y. Chung, *J. Catal.*, 1984, **90**, 75–83.

55 H. Tang, J. Wei, F. Liu, B. Qiao, X. Pan, L. Li, J. Liu, J. Wang and T. Zhang, *J. Am. Chem. Soc.*, 2016, **138**, 56–59.

56 J. K. Norskov, T. Bligaard, J. Rossmeisl and C. H. Christensen, *Nat Chem*, 2009, **1**, 37–46.

57 A. Nilsson, L. G. M. Pettersson, B. Hammer, T. Bligaard, C. H. Christensen and J. K. Nørskov, *Catal. Letters*, 2005, **100**, 111–114.

58 P. Strasser, S. Koh, T. Anniyev, J. Greeley, K. More, C. Yu, Z. Liu, S. Kaya, D. Nordlund, H. Ogasawara, M. F. Toney and A. Nilsson, *Nat. Chem.*, 2010, **2**, 454–460.

59 J. Y. Li, W. Li, M. J. Jin and X. J. Jin, *Mater. Res. Lett.*, 2015, **3831**, 107–113.

60 M. L. Benson, P. K. Liaw, H. Choo, D. W. Brown, M. R. Daymond and D. L. Klarstrom, *Mater. Sci. Eng. A*, 2011, **528**, 6051–6058.

61 R. T. K. Baker, E. Prestridge and R. Garten, *J. Catal.*, 1979, **56**, 390–406.

62 Z. L. Wang, C. Colliex, V. Paul-Boncour, A. Percheron-Guegan, J. C. Achard and J. Barrault, *J. Catal.*, 1987, **105**, 120–143.

63 F. B. Noronha, C. A. Perez, M. Schmal and R. Frety, *Phys. Chem. Chem. Phys.*, 1999, **1**, 2861–2867.

64 P. L. L. Gai, *Curr. Opin. Solid State Mater. Sci.*, 1999, **4**, 63–73.

65 J. S. Rieck and A. T. Bell, *J. Catal.*, 1986, **99**, 262–277.

66 W. R. Schwartz and L. D. Pfe, *J. Phys. Chem. C*, 2012, **116**, 8571–8578.

67 G. W. Huber, S. J. M. Butala, M. L. Lee and C. H. Bartholomew, *Catal. Letters*, 2001, **74**, 45–48.

68 X. Wang, S. Zhao, Y. Zhang, Z. Wang, J. Feng, S. Song and H. Zhang, *Chem. Sci.*, 2016, **7**, 1109–1114.

69 E. van Steen, G. S. Sewell, R. a. Makhothe, C. Micklethwaite, H. Manstein, M. de Lange and C. T. O'Connor, *J. Catal.*, 1996, **229**, 220–229.

70 B. Ernst, S. Libs, P. Chaumette and A. Kiennemann, *Appl. Catal. A Gen.*, 1999, **186**, 145–168.

71 K. E. Coulter and A. G. Sault, *J. Catal.*, 1995, 154, 56–64.

72 A. Y. Khodakov, R. Bechara and A. Griboval-Constant, *Appl. Catal. A Gen.*, 2003, **254**, 273–

288.

73 A. M. Saib, M. Claeys and E. van Steen, *Catal. Today*, 2002, **71**, 395–402.

74 X. Xu, J. He and D. W. Goodman, *J. Chem. Physics,* 1993, **284**, 103–108.

75 M. Bowker, P. Stone, P. Morrall, R. Smith, R. Bennett, N. Perkins, R. Kvon, C. Pang, E. Fourre and M. Hall, *J. Catal.*, 2005, **234**, 172–181.

76 O. Dulub, W. Hebenstreit and U. Diebold, *Phys. Rev. Lett.*, 2000, **84**, 3646–3649.

77 J. A. Rodríguez and J. Hrbek, *Surf. Sci.*, 2010, **604**, 241–244.

78 S. D. Senanayake, D. Stacchiola and J. A. Rodriguez, *Acc. Chem. Res.*, 2013, **46**, 1702–1711.

79 V. Mazzieri, N. Figoli, F. Pascual and P. L'Argentine, *Catal. Letters*, 2005, **102**, 79–82.

80 X. D. Hou, Y. Z. Wang and Y. X. Zhao, *Catal. Letters*, 2008, **123**, 321–326.

81 X.-F. Yang, A. Wang, B. Qiao, J. Li, J. Liu and T. Zhang, *Acc. Chem. Res.*, 2013, **46**, 1740–1748.

82 H. Zhang, T. Watanabe, M. Okumura, M. Haruta and N. Toshima, *Nat. Mater.*, 2011, **11**, 49–52.

83 G. Kyriakou, G. Kyriakou, M. B. Boucher, A. D. Jewell, E. A. Lewis, T. J. Lawton, A. E. Baber, H. L. Tierney, M. Flytzani-stephanopoulos and E. C. H. Sykes, *Science (80-.).*, 2012, **335**, 1209–1212.

84 B. Qiao, A. Wang, X. Yang, L. F. Allard, Z. Jiang, Y. Cui, J. Liu, J. Li and T. Zhang, *Nat. Chem.*, 2011, **3**, 634–641.

85 C. H. Choi, M. Kim, H. C. Kwon, S. J. Cho, S. Yun, H. T. Kim, K. J. J. Mayrhofer, H. Kim and M. Choi, *Nat. Commun.*, 2016, **7**, 1–9.

86 A. Govender, W. Barnard, E. J. Olivier, R. P. Forbes, E. van Steen and J. H. Neethling, *Mater. Charact.*, 2016, **121**, 93–102.

87 S. Y. Moon, B. Naik, C. H. Jung, K. Qadir and J. Y. Park, *Catal. Today*, 2016, **265**, 245–253.

88 A. P. Petersen, R. P. Forbes, S. Govender, P. J. Kooyman and E. van Steen, *Catal. Letters*, 2018, **148**, 1215–1227.

89 J. a. Rodriguez, J. Graciani, J. Evans, J. B. Park, F. Yang, D. Stacchiola, S. D. Senanayake, S. Ma, M. Perez, P. Liu, J. F. Sanz and J. Hrbek, *Angew. Chemie - Int. Ed.*, 2009, **48**, 8047–8050.

90 J. C. Matsubu, S. Zhang, L. Derita, N. S. Marinkovic, J. G. Chen, G. W. Graham, X. Pan and P. Christopher, *Nat. Chem.*, 2017, **9**, 120–127.

91 H. Ming and B. G. Baker, *Appl. Catal. A, Gen.*, 1995, **123**, 23–36.

92 J.-Y. Park, Y.-J. Lee, P. R. Karandikar, K.-W. Jun, K.-S. Ha and H.-G. Park, *Appl. Catal. A Gen.*, 2012, **411–412**, 15–23.

93 R. P. Mogorosi, M. Claeys and E. van Steen, *Top. Catal.*, 2014, **57**, 572–581.

94 T. Koyama, A. T. Bell, Z. Weng-Sieh, R. Gronsky, F. Engelke, T. S. King and M. Pruski, *J. Catal.*, 1994, **149**, 142–148.

95 B. L. Mojet, J. T. Miller, D. E. Ramaker and D. C. Koningsberger, *J. Catal.*, 1999, **186**, 373–386.

96 S.-J. Jong and S. Cheng, *Appl. Catal. A Gen.*, 1997, **104**, 120–135.

97 M. Fernández-García, A. Martínez-Arias, J. C. Hanson and J. A. Rodriguez, *Chem. Rev.*, 2004, **104**, 4063–4104.

98 P. Hu, Z. Huang, Z. Amghouz, M. Makkee, F. Xu, F. Kapteijn, A. Dikhtiarenko, Y. Chen, X. Gu and X. Tang, *Angew. Chemie - Int. Ed.*, 2014, **53**, 3418–3421.

99 X. Carrier, E. Marceau, H. Carabineiro, M. Che and X. Carrier, *Phys. Chem. Chem. Phys.*, 2009, **11**, 7527–7539.

100 O. S. Alexeev, S. Y. Chin, M. H. Engelhard, L. Ortiz-Soto and M. D. Amiridis, *J. Phys. Chem. B*, 2005, **109**, 23430–23443.

101 N. Fischer, M. Minnermann, M. Baeumer, E. van Steen and M. Claeys, *Catal. Letters*, 2012, **142**, 830–837.

102 D. W. Kim, K. D. Kim, H. O. Seo, N. K. Dey, M. J. Kim, Y. D. Kim, D. C. Lim and K. H. Lee, *Catal. Letters*, 2011, **141**, 854–859.

103 E. W. Zhao, H. Zheng, K. Ludden, Y. Xin, H. E. Hagelin-Weaver and R. Bowers, *Catal. Letters*, 2016, **6**, 974–978.

104 A. Zola, L. . da Silva, L. . Moretti, C. Fraga, E. F. Sousa-Arguiar and A. P. Arroyo, *Top. Catal.*, 2016, 219–229.

105 M. Pudukudy and Z. Yaakob, *Chem. Pap.*, 2014, **68**, 1087–1096.

106 D. E. Ramaker, G. E. van Dorssen, B. L. Mojet and D. C. Koningsberger, *Top. Catal.*, 2000, **10**, 157–165.

107 T. Herranz, X. Deng, A. Cabot, J. Guo and M. Salmeron, *Exch. Organ. Behav. Teach. J.*, 2009, **2**, 10721–10727.

108 R. Riva, H. Miessner, R. Vitali and G. Del Piero, *Appl. Catal. A Gen.*, 2000, **196**, 111–123.

109 J. M. González Carballo, E. Finocchio, S. García, S. Rojas, M. Ojeda, G. Busca and J. L. G. Fierro, *Catal. Sci. Technol.*, 2011, **1**, 1013.

110 D. C. Koningsberger, J. de Graaf, B. L. Mojet, D. E. Ramaker and J. T. Miller, *Appl. Catal. A Gen.*, 2000, **191**, 205–220.

111 V. M. Gonzalez-DelaCruz, J. P. Holgado, R. Pereñíguez and A. Caballero, *J. Catal.*, 2008, **257**, 307–314.

112 X. Carrier, E. Marceau and M. Che, *Pure Appl. Chem.*, 2006, **78**, 1039–1055.

113 N. E. Tsakoumis, R. E. Johnsen, W. Van Beek, M. Rønning and E. Rytter, *ChemComm*, 2016, **52**, 20–22.

114 D. E. Ramaker, J. de Graaf, J. a. R. van Veen and D. C. Koningsberger, *J. Catal.*, 2001, **203**, 7–17.

3. **Scope of the thesis**

3.1 The purpose of the study

Catalytically active metals supported on different inorganic oxide support material may show different behaviour in various processes. The difference in their activity is usually attributed to the role played by the support, also known as metal-support interactions. It is important that these metal-support interactions are understood better, in particular on how they may affect the catalytic activity and selectivity in the specific catalytic reactions. This could determine the way in which the support material for a specific catalytically active metal for a certain industrial process is selected.

In real catalysts, where the catalytically active metal is dispersed over a support material, the contact point between the metal and the support is usually concealed by between the metal and the support. This makes it difficult to characterize this interaction or even understand their effects at molecular level. A model system that can isolate and control the extent of metal-support interaction is thus needed. Inverse catalyst systems might be an appropriate model system. They are prepared by introducing a small amount of the support (or its precursor) on to the surface of the catalytically active metal or its precursor. From this point of view, the support material can be regarded as a supra-molecular ligand attached on the surface of the metal.

This thesis aims to gain insight into the effects of metal-support interaction in Co/SiO_2 catalysts using an inverse model system by modifying Co_3O_4 nanocrystallites with silanes (i.e. tetraethoxysilane, trimethyl chlorosilane, triphenyl ethoxysilane). It is postulated that the formation of Co-O-Si will alter the catalytic properties of the cobalt site to which silane is bonded and the adjacent ligand-free. sites The desire is to understand the effects of metal support interactions obtained after reduction of the model system on its performance in Fischer-Tropsch synthesis, which will be used as a test reaction., taking into account the change in the reducibility and metal surface area.

3.2 Thesis lay out

This work thesis investigated metal-support interactions using SiO_2/Co inverse catalyst in the context of Fischer-Tropsch synthesis. **Chapters 1 and 2** are introductory chapters giving a background to the topic as well as giving a critical review of the previous work done on metal-

support interactions, how they may be generated and characterized and their effects in catalytic reactions. **Chapter 3** give the scope and the lay out of the thesis. **Chapter 4** highlights the effects of increase SiO_2 on the surface of Co_3O_4. The Si/Co ratio was varied by varying the initial TEOS concentration. With increasing Si/CO ratio upto 63 mmol/mol the catalytic activity of Co is increased indicating that the SiO_2/Co interface may be responsible for the enhanced activity. The effects of solvent type during the modification of process are discussed in **Chapter 5.** Modification was performed in either n-hexane, ethanol/water misxture (with or without acid or base). Since the succeeding step after contacting cobalt oxide and TEOS is the calcination step, the effects of calcination temperature were studied and the results are discussed in **Chapter 6.** To further understand the ligand effects, monodentate silane ligands were used and the result are discussed in **Chapter 7**. These ligands can decompose during high temperature heat treatments. As such, CoO was opted over Co_3O_4 since the reduction of CoO occur at relatively low temperatures (temperatures below silane decomposition temperature). **Chapter 8** of this thesis gives a summary and conclusions taken from the presented results.

4. **Metal-support interactions in SiO2/Co inverse catalyst for Fischer-Tropsch synthesis: effects of silane (TEOS) concentration during the modification**[a]

The surface of Co_3O_4 nano-cubes has been modified by adsorption of small amounts of tetraethoxysilane from a solution in n-hexane. The resulting silicate species on and near the Co_3O_4 surface have been characterized using XPS, FTIR and XANES, and may have formed neso or island silicates. The presence of these silicate species hinders the reduction of these materials. IR-visible bonds of some of the adsorbed species remain intact after reduction in hydrogen at elevated temperatures. The intrinsic catalytic activity of the modified, reduced modified Co_3O_4 nano-cubes have been tested for their activity and selectivity in the Fischer-Tropsch synthesis under industrially relevant conditions. It is observed that the cobalt time yield increases more than 7-fold by the presence of the silicate species on the surface. The increase in activity does not seem to correlate with a change in the resulting metal surface area Implying an increase in the intrinsic activity.

[a] This chapter is based on a published article

(L. Macheli, A. Roy, E. Carleschi, B. P. D. Doyle and E. van Steen, *Catal. Today*,(in press), DOI:https://doi.org/10.1016/j.cattod.2018.10.018)

4.1. Introduction

Complex mixtures of nanosized materials find a key role in various aspects of technology. For, example, supported metal nanoparticles are applied as catalytic materials in chemical industry. The optimum use of the catalysts relies on their interlinked physical and chemical attributes such as metal crystallite size and structure, mechanical strength, or electronic configuration. Recent research has also shown that catalyst performance can be tuned by controlling the interaction between the metal and the support[1]. Metal-support interactions can be optimized by varying support materials, manipulating the metal crystallite size and structure, or by tuning the catalyst activation conditions.

Metal-support interactions were initially identified through a decrease in the ability of metal to adsorb reactants. Tauster et al.[2–4] showed that the capacity for CO adsorption of metals varies depending on the support material and the activation temperature used. The catalytic activity of such catalysts is expected to decrease for materials that shows a suppression in the ability to adsorb reactants. However, metal-support interactions, today, can be manipulated in a way that may enhance their catalytic performance. Cargnello et al.[5] made use of inverse catalyst prepared by deposition of reducible oxides on the surface the active material. The performance of these material is reported to be more active than their conventional counterparts. Recently, De Jong's group[1] manipulated metal-support interactions by performing successive reductions-oxidation-reduction steps a catalyst supported on reducible supports. These successive steps optimize the interaction of the support islands formed during the creeping process (that occurs during reduction) with the active metal and as such enhance the catalytic performance.

Studies by van Steen's group[6–9] has focussed on the modification of catalyst precursors using alkoxides to gain a better understanding on the role of metal-support interactions in supported catalyst. The idea is to create a reverse model catalyst, where the surface modification may mimic interactions present in supported metal catalysts and the support can be regarded as a supramolecular ligand to the catalytically active material. The focus is on the modification of the oxidic precursor of the catalytically active phase, which may provide anchoring points for the modifying agent. The presence of the modifying agent in the oxidic precursor does affect the catalyst activation[6,7,9]. Van Heerden and van Steen[8] have shown theoretically that the presence of this type of ligands on the surface may also change the reactivity in the Fischer-Tropsch

synthesis by providing an alternative pathway for CO-activation. This chapter discusses the modification of Co_3O_4 with tetraethoxysilane and its effect on the activity and selectivity in the Fischer-Tropsch synthesis after reduction in hydrogen.

4.2. Experimental

Synthesis of Co_3O_4

Co_3O_4-nanocubes with an average size of 23.8 ± 4.5 nm (as determined using TEM) were synthesized using a hydrothermal oxidative precipitation method[10,11]. A solution containing 5.3 g $Co(NO_3)_2 \cdot 6H_2O$ (20 mmol, Merck, >99.0 %) in 20.0 mL deionized water was added to a solution containing 1.8 g of NaOH (45 mmol) and 5.4 g sodium dodecylsulphate (20 mmol) in 180 mL deionized water at 368 K with an addition rate of 10 mL/min. Air was purged through the solution for 5 hours, after which the solid was recovered by centrifugation. The crystals were purified by multiple washing steps with a 1.0 M aqueous HCl-solution and distilled water. Residual chlorine present in the sample was shown to be removed after calcination at 473 K for 2 hours in a static oven.

Modification of Co_3O_4 nanoparticles with TEOS

The obtained, calcined cobalt oxide was re-suspended in n-hexane yielding a suspension with a solid concentration of 1.4 g/L. The Co_3O_4-nanocubes were contacted with solutions of tetraethoxysilane in n-hexane with concentrations varying 0.13 and 6.4 mM (0.003 – 0.143 vol.-%) for a period of 5 hours. After contacting the solid with the solution, the solid was recovered by centrifugation and washed 5 times with 50 mL with n-hexane. The samples were subsequently dried at 393 K for 2 hours and calcined at 573 K for 2 hours in a static oven. The sample were obtained with Si/Co ratio of 3 mmol/mol, 9 mmol/mol, 28 mmol/mol and 63 mmol/mol and were named NC-Hex-TEOS-03-573K, NC-Hex-TEOS-09-573K, NC-Hex-TEOS-28-573K, NC-Hex-TEOS-63-573K respectively. The unmodified sample calcined at 573 K was named NC-Hex-573K.

Synthesis of Co_2SiO_4

Co_2SiO_4 was synthesized through the cobalt hydroxide-silica intermediate which was subsequently calcined. The intermediate was formed by dropwise addition of ammonia into aqueous solution silicic acid, cobalt nitrate and sulphuric acid (Co:Si=2) until the pH of the

mother liquor was 7.5. The resulting precipitate was washed with distilled water, dried at 393 K for 12 hours and calcined at 1273 K for 30 min at heating ramp of 5 K/min. The phase purity of Co_2SiO_4, was determine using X-ray diffractometry.

Synthesis of SiO_2 Stöber's *spheres*

Silica spheres were synthesized using the Stöber's method[12]. A solution containing tetraethoxysilane in ethanol was added to a known amount of water and refluxed at 348 K for 10 hours in the presence of ammonium hydroxide which acted as a hydrolysis catalyst. The resulting silica particles were washed with ethanol and distilled water and calcined at 573 K for 2 hours.

Characterization

Elemental analysis and the silicon loading of the calcined sampled was determined using energy dispersive X-ray analysis (EDX) on a scanning electron microscope (LEO S444 SEM) equipped with a Four Quadrant Back Scatter Detector and an energy dispersive Fissons Kevex X-ray spectrometer. The samples were prepared by sprinkling them on an aluminium stub covered with a carbon tape. Si loading was expressed as the atomic ratio of Si:Co . The error associated with this measurement was ascertained by computing an average of 5 line-scans for each sample.

The phase structure of the model catalysts was determined using a Bruker AXS D8 Advance X-ray laboratory diffractometer operated at 40 kV and 40 mA utilizing a Co source ($\lambda_{Co\text{-}K\alpha}$ = 0.178897 nm) and a VÅNTEC position-sensitive detector. The morphology of the samples was analysed by a transmission electron miscrope using JEM200CX (JEOL, JAPAN) operating at 120 kV. The FTIR-spectra of the calcined samples diluted in KBr (dilution ratio: 1:400) was recorded on a Nicolet 5700 operating in the transmission mode.

X-ray photoemission spectroscopy (XPS) spectra were acquired at room temperature and with an overall energy resolution of 0.6 eV, using a SPECS PHOIBOS 150 hemispherical electron energy analyser and a mono- chromatic Al Kα photon source (hν = 1486.71 eV). Charging of the sample surface was counteracted by means of a low-energy flood gun (electron energy = 2 eV, electron flux = 20 μA).

Si K edge X-ray absorption near edge structure (XANES) spectroscopic measurement was performed at Louisiana State University's electron storage ring, the J. Bennett Johnston, Sr., Center for Advanced Microstructures and Devices (CAMD), USA. CAMD operates the ring at 1.3 GeV. The measurement was conducted at the "windowless" Low Energy X-Ray Absorption Spectroscopy (Lexas) beamline, which has a resolution of ~1 eV at these energies. A 13 µm thick Kapton™ window separated the ring from the experimental chamber. The monochromator is Lemonnier-type with design modifications made at Bonn University, Germany. InSb (111) crystals were used in the monochromator. The monochromator was calibrated with Si white line peak of quartz at 1846.1 eV[13]. The scans were from 1800 eV to 1830 eV, from 1830 eV to 1870 eV, from 1870 eV to 1910 eV, with steps of 0.5 eV, 0.1 eV and 0.3 eV, respectively. The samples were prepared by smearing a very thin layer on a silicon- and sulphur-free Kapton™ tape and then covering it with a Mylar™ film. Since the Si concentration was low, no dilution was necessary to reduce self-absorption. All samples were measured in the fluorescence mode, with integration time varying between 1 and 5 seconds depending on the concentration and several runs were averaged. The spectra were reproducible within ±0.03 eV. A Ketek™ silicon drift detector with an effective area of 80 mm^2 was used for fluorescence X-ray measurements. The full width half maximum (FWHM) of the detector at 5.9 keV is 135 eV. Data analysis was performed with Athena[14].

The reducibility of the samples was characterized using H_2-temperature programmed reduction (H_2-TPR), which was carried out in an AutoChem2950 (Micromeritics Instrument Corp., USA). The sample (ca. 0.03 g) was degassed at 393 K under 50 mL (NTP)/min argon for 1 hr. The temperature was subsequently decreased to 340 K followed by the change in gas composition to 5 vol-% H_2/Ar keeping the flow rate at 50 mL (NTP)/min. The temperature was linearly increased from 340 K to 1173 K (heating rate: 10 K/min). The quantity of hydrogen consumed was determined by first calibrating the TPR instrument against the temperature programmed reduction of a known mass of silver oxide (Ag_2O) with 5 % hydrogen in argon (vol/vol) at 50 mL (NTP)/min. The peak area was obtained by integrating the measured TCD signal against time and related to the amount of H_2 by a calibration factor.

$$\dot{n}_{H_2,consumed} = f_{TPR,i} \cdot A_i \quad \text{..... Equation 4-1}$$

Where A_i is the area under the curve of species i, and $f_{TPR,i}$ is the calibration factor of species i given by:

$$f_{TPR,i} = \frac{n_{H_2\ for\ reduction\ Ag_2O}}{Area_{Ag_2O}} \quad \text{.....Equation 4-2}$$

Where $n_{H_2\ for\ reduction\ Ag_2O}$ is the number of moles of hydrogen required for the reduction of a known mass of Ag_2O and $Area_{Ag_2O}$ is the integrated area under the curve for of TCD signal against time during the reduction of Ag_2O.

Degree of reduction of cobalt oxide to metallic cobalt is of great importance in the performance of the catalyst. The degree of reduction of the catalyst were determined for Co_3O_4 and the sample with the Si/Co-ratio of 63 mmol/mol by reducing the catalyst at 673 K for 16 hours, succeeded by cooling in argon. Temperature programmed reduction of the reduced samples by ramping the temperature by 10 K/min in a gas mixture of 5% H_2 in argon. The degree of reduction was computed from the relative hydrogen consumption of the reduced catalyst to that required for complete reduction of Co_3O_4.

Supporting the nanocubes

The samples were dispersed on to β-SiC microspheres (SiCAT, $d_{particle}$= 100 µm, S_{BET} = 25 m^2/g, V_{pore} = 0.30 cm^3/g) by sonicating 0.1 g of the (modified) Co_3O_4-nanocubes together with 0.9 g of β-SiC microspheres in a mixture of 10 vol.-% oleic acid in n-hexane for 1 hour. The solvent was dried off at 393 K for 2 hr. The solid was subsequently calcined at 573 K for 3 hr in an oven (heating ramp: 3 K/min). The actual cobalt loading was determined using atomic absorption spectroscopy. The samples were digested 50 mL of 3 M hydrofluoric acid. The samples were diluted 50 times with water and the concentration of cobalt was determined. The supported catalysts were named with Si/Co ratio of 3 mmol/mol, 9 mmol/mol, 28 mmol/mol and 63 mmol/mol and were named Cat-Hex-TEOS-03-573K, Cat-Hex-TEOS-09-573K, Cat-Hex-TEOS-28-573K, Cat-Hex-TEOS-63-573K respectively. The unmodified supported catalyst was named Cat-Hex-573K.

Fischer-Tropsch synthesis

The Fischer-Tropsch synthesis was performed in a fixed bed reactor. The catalyst (0.1 g (modified) Co_3O_4-nanocubes/0.9 g β-SiC, $d_{particle}$ = 100 µm) was further diluted with 2.0 g silicon

carbide ($d_{particle}$=200-250 µm) and loaded into the isothermal zone of the reactor. The catalyst was reduced in hydrogen (40 mL(NTP)/min) at 1 bar and 623 K (heating rate: 5 K/min) for 16 hrs. After the reduction, the catalyst is cooled down to 493 K in argon. The Fischer-Tropsch synthesis is performed at 493K, 20 bar, $(H_2/CO)_{inlet}$ = 2 and $F_{CO,0}/W$ = 5.56 mmol/(min·g_{Co}). The Fischer-Tropsch synthesis was performed for 72 hr. Subsequently, that catalyst bed was flushed with argon for 1 hr and cooled down to room temperature in argon. The spent catalyst was passivated by flowing CO_2 over the catalyst bed at 20 mL(NTP)/min for 2 hours at room temperature. The catalyst was removed by first removing the SiC placed on top of the catalyst bed. The catalyst was then separated from the silicon carbide diluent using a 150 µm sieve. There were no visible signs of wax adhered to the spent catalyst and no attempts were made to remove wax from the spent catalyst.

Characterization of spent catalyst

Dispersion of cobalt in the spent catalyst was determined using static H_2 chemisorption at 398 K in a Micromeritics ASAP 2020 analyzer. The sample (0.5 g) was dried at 383 K overnight to remove any adsorbed moisture and subsequently reduced in-situ for 12 hours at 493 K with hydrogen. Following the reduction, the system was purged using helium prior to evacuation. The H_2-chemisorption was conducted at 398 K. To determine the actual amount cobalt in the spent catalyst, all the sample used was quantitatively transferred to a polypropylene bottle containing 50 mL of 3 M hydrofluoric acid. The concentration of cobalt in solution was determined using atomic absorption spectrometry (AAS).

4.3. Results and discussion

Characterization of Co_3O_4

The morphology of the Co_3O_4 -nanocubes synthesized using oxidative deposition were imaged using transmission electron microscope. The crystallite size distribution was modelled using a log-normal distribution (*see Figure 4-1)*. The obtained material attains a cubic shape with an average size of 23.8 ± 4.5 nm. The particle size distribution is a wide and with the smallest particle being 15 nm in diameter and the largest particle being 30 nm. More than 80 % of the nanoparticles have a diameter ranging between 18 nm to 25 nm. There is no visible effect on the morphology that arises due to the modification process as the shape and size of the Co_3O_4 nanocubes remain unaffected after the modification as shown using TEM. This can be observed

from comparing the obtain values of μ and δ obtained from the best fit of the log-normal distribution curves (see *Fig 4-2*).

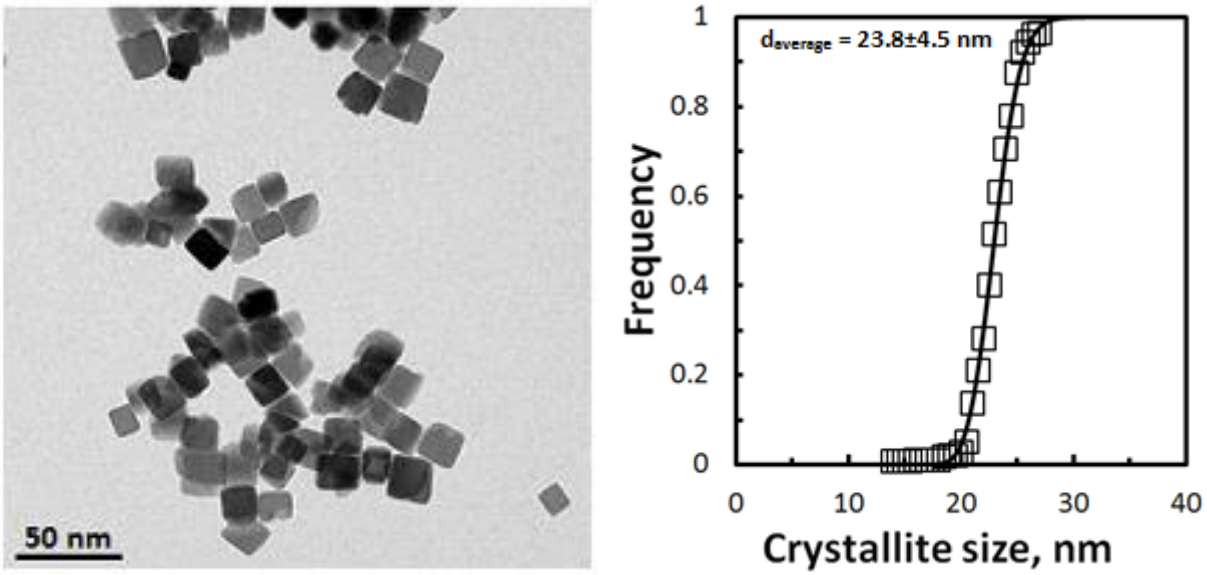

Figure 4-1: Co_3O_4 nano-crystallites obtained using oxidative precipitation[10,11] (left) and their cumulative size distribution (right) modelled as a log-normal distribution (μ = 3.15; σ = 0.19)

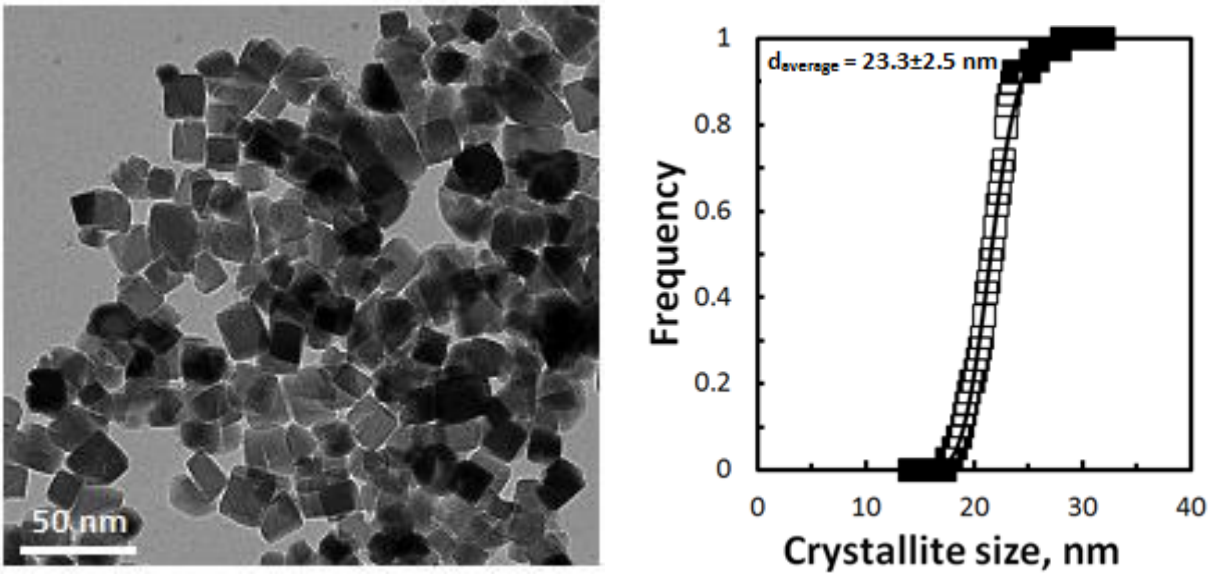

Figure 4-2: Co_3O_4 nano-crystallites after silylation (63 mmol/mol Si/Co) (left) and their cumulative size distribution (right) modelled as a log-normal distribution (μ = 3.14; σ = 0.11) ±

The expected molar ratio of cobalt to oxygen in Co_3O_4 is 42.8:52.7. However, elemental analysis of the un-calcined synthesized material with electron dispersive x-ray spectroscopy shows the presence of cobalt, oxygen and chlorine. Chlorine is expected to be in the form of HCl that adsorbed during the washing step. Upon calcination at 473 K in a static oven, HCl desorbs

completely from the samples. The atomic compositions of the samples prior and after calcination are shown in *Table 4-1*. The cobalt content is 40.9±5.5% and the oxygen content is 59.1±7.1% as expected for Co_3O_4 with some excess oxygen. The slight excess oxygen (expected value 57.1%) may be ascribed to the presence of adsorbed oxygen containing species (e.g. in the form of hydroxyl species), but may also indicate that Co_3O_4 is not stoichiometric with excess oxygen[15,16]. On the other hand this difference may be associated with the error range of EDX.

Table 4-1: Composition of the prepared Co_3O_4 nanocubes as determined by SEM/EDX

	% atomic composition	
Element	**before calcination**	**after calcination at 473 K**
Co	39.5 ± 6.0	40.9 ± 5.5
O	57.1 ± 5.1	59.1 ± 7.1
Cl	3.4 ± 0.9	0

The phase structure of the synthesized Co_3O_4 nanocubes was determined using X-ray diffraction (*see Fig. 4-3*). The only observed diffraction lines for all the samples are at 2θ angles of 21.98, 36.35, 43.05, 43.83, 52.39, 64.39, 70.04 and 77.40 which are characteristic diffraction lines of spinel Co_3O_4[17] using a Co-K_α source (Eva software, CCD). This indicates that the synthesized Co_3O_4 nanocubes are XRD pure[17,18]. There is no non-crystalline matter observed both TEM and XRD indicating that the wash with HCl after the synthesis was successful. The lattice parameter the calcined Co_3O_4 (473 K) was determined by fitting the X-ray diffraction pattern to be 0.809 nm using the (311) reflection.

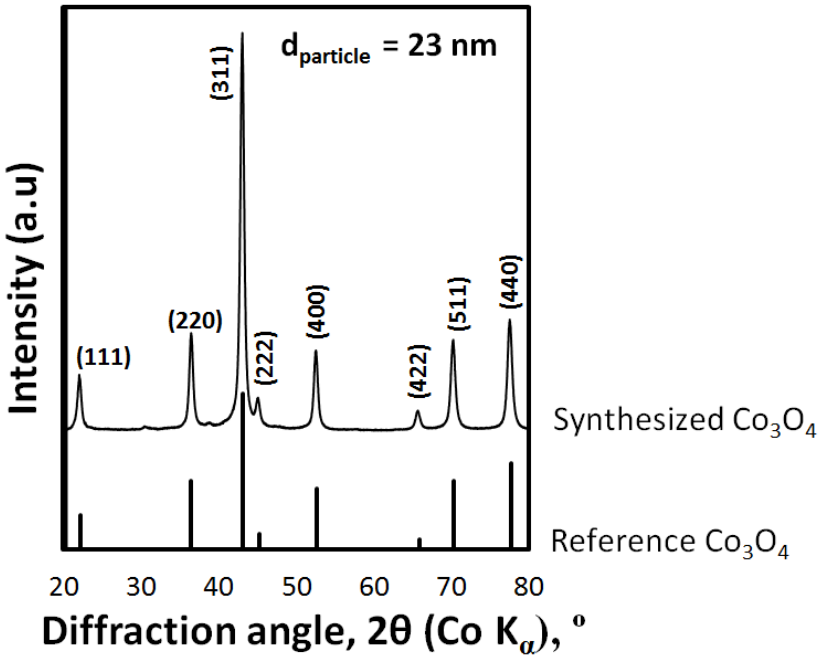

Figure 4-3: Bulk Co_3O_4 crystallites obtained via high temperature calcination (1173 K) of a cobalt-hydroxide-silica intermediate

Characteristics of Co_2SiO_4

The morphology of the Co_2SiO_4 synthesized via high temperature calcination of cobalt based precursor in the presence of silicic acid were imaged using transmission electron microscope (*see Fig. 4-4)*. The obtained Co_2SiO_4 forms lumpy structures with an average size greater than 400 nm in diameter.

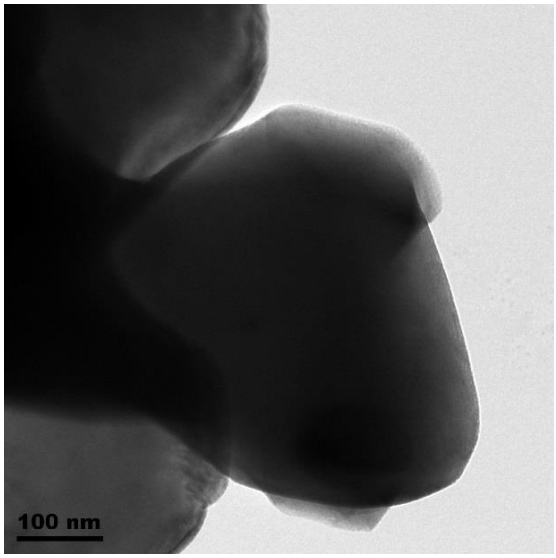

Figure 4-4: Co_2SiO_4 synthesized by high temperature calcination of cobalt based precursor in the presence of silicic acid (T_{cal} = 1173 K)

The synthesized *Co_2SiO_4 was* characterized using x-ray diffractometry. The X-ray diffraction pattern of the samples has diffractions lines which are characteristic diffraction lines of bulk *Co_2SiO_4*[17] using a Co-K_α source (Eva software, CCD) (*see Fig. 4-5*). The sample showed also diffraction lines due to presence of amorphous silica[17] although no diffraction lines due to the presence of Co_3O_4[17,18] were observed. This indicates that the synthesized Co_2SiO_4 was not XRD pure. The lattice constant for Co_2SiO_4 was determined to be: a = 0.478 nm, b = 1.03 nm and c = 0.6006 nm.

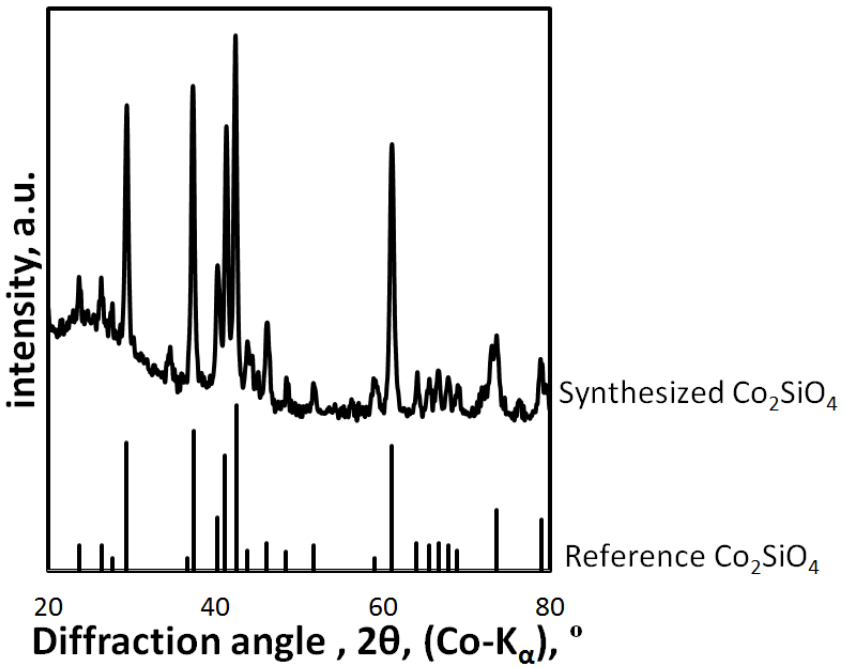

Figure 4-5: X-ray diffractogram of Co_2SiO_4 synthesized by high temperature calcination of cobalt hydroxide-silica mixture at 1273 K

Similarly, silica Stöber's spheres were viewed under transmission electron microscope (*see Fig. 4-6 (left)).* The obtained silica attains a spherical shape with an average size of 250 ± 3 nm. The particle size distribution is wide and with the smallest particle being 50 nm in diameter and the largest particle being 110 nm. Characterization of silica spheres with X-ray diffraction indicates that silica spheres attain an amorphous phase showing a broad diffraction line at 2θ angles between 20° and 22°[17] (*see Fig. 4-6 (right)).*

The anticipated molar ratio of cobalt: silico: oxygen in Co_2SiO_4 is 2:1:4. Indeed, elemental analysis of the synthesized cobalt silicate with electron dispersive x-ray spectroscopy shows the presence of cobalt, silicon and oxygen in the ratio of 2.1:1:4.3 showing that bulk cobalt silicate

synthesized was in the expected atomic ratio (*see Table 4-2*). However, while the stoichiometric ratio of Si to O in silica may be expected to be 1:2, the atomic compositions of the silica and after calcination at 573 K is 1:2.5 (*see Table 4-2)*. The silicon content is 28.6±3.6% and the oxygen content is 71.4±2.1% as expected for silica with some excess oxygen. The slight excess oxygen (expected value 67%) may be ascribed to the presence of adsorbed oxygen containing species (e.g. in the form of hydroxyl species).

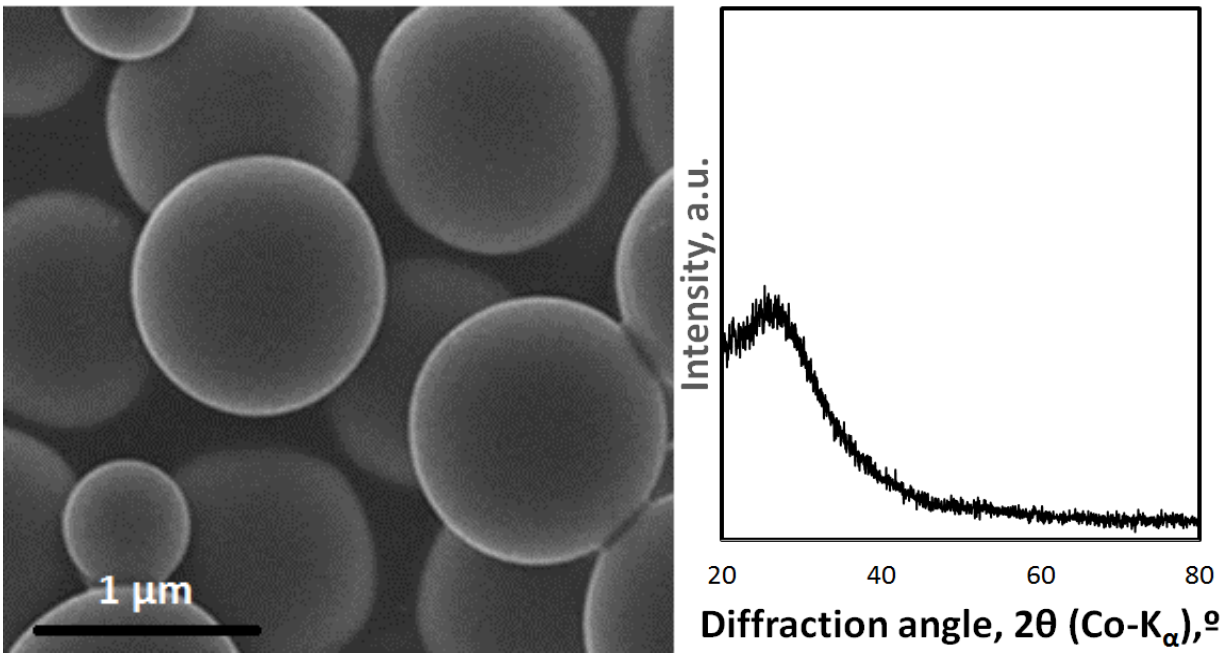

Figure 4-6: StÖber's silica hydrolysis of tetraethoxysilane in ethanol and ammonia calcined at 573 K(left) and their X-ray diffraction pattern (right)

Table 4-2: Composition of the prepared Co_2SiO_4 and SiO_2as determined by SEM/EDX

Element	***% atomic composition***	
	Co_2SiO_4	SiO_2
Co	28.4 ± 1.0	-
O	58.1 ± 1.3	25.6±1.1
Si	13.5 ± 0.6	74.4±1.6

The Co_3O_4-nanocubes were contacted with solutions of tetraethoxysilane in n-hexane with concentrations varying 0.13 and 6.4 mM (0.003 – 0.143 vol.-%) for a period of 5 hours to obtain samples with different silicon loadings (*see Table 4-3*). The extent of silylation as a function of time of exposure was monitored using SEM-EDX. The content of the tetraethoxysilane adsorbed

on the surface of Co_3O_4 was expressed as a molar ratio of $\left(\frac{Si}{Co}\right)$. The $\left(\frac{Si}{Co}\right)$ molar ratio was plotted as a function of exposure time (see *Fig. 4-7*). The resulting uptake ranges from 3 to 63 mmol Si per mol of Co (*Fig. 4-7*). This correspond to a surface coverage of ca. 5 to 130 molecules of tetraethoxysilane per nm^2 assuming an average size of the Co_3O_4 nano-cubes of 23.8 nm. The high uptake of tetraethoxysilane clearly indicates the formation of oligomers on the surface[19].

Table 4-3: Effect of initial concentration of TEOS on the final uptake on the surface of Co_3O_4

$[TEOS]_{initial}$, (mM)	**$[TEOS]_{final}$[1], (mM)**	**Si loading (mmol Si/mol Co)**
6.4	5.8	63
1.6	1.4	28
0.64	0.58	9.0
0.22	0.23	6.0
0.13	0.12	3.0

[1] The final concentration of TEOS in the suspension was calculated using the initial concentration of TEOS, the uptake of TEOS and the initial mass of Co_3O_4 added: $[TEOS]_{final} = \frac{V(350ml)\cdot[TEOS]_{initial} - 3\cdot\frac{m_{Co_3O_4}}{M_{Co_3O_4}\left(240.8\frac{g}{mol}\right)}\left(\frac{Si}{Co}\right)_{sample}}{V(350ml)}$

The uptake of tetraethoxysilane by Co_3O_4-nanocubes is slow (see *Fig. 4-6*) and can be modelled using an Avrami growth model[20]. This model takes care of the formation of silicate islands on the surface of Co_3O_4 nanocubes during. It relates the silicon uptake to the formation of silicate islands in terms of dimensionality of the growth, m, and a time constant, τ as shown in *Equation 4-3:*

$$\left(\frac{Si}{Co}\right) = \left(\frac{Si}{Co}\right)_{eq} \cdot \left(1 - e^{\left(\frac{-t}{\tau}\right)^m}\right) \quad \text{.....Equation 4-3}$$

Where $\left(\frac{Si}{Co}\right)$ is the silicon to cobalt ratio at a particular time t, $\left(\frac{Si}{Co}\right)_{eq}$ is the equilibrium silicon to cobalt ratio, τ is the time constant of the nucleation process and m is the dimensionality of the growth process[20]. The specific values of m and τ are governed by the rate of constant and the number of nuclei. The value of m is 1 for growth of one-dimensional shape such as rods, 2 for flat disc shapes and 3 for spherical shapes. Non-integer dimensionality can be obtained for

irregular shaped particles that may be formed if nucleation and growth of particles happens at the same time. The best fits are obtained with the parameters shown in *Table 4-4.*

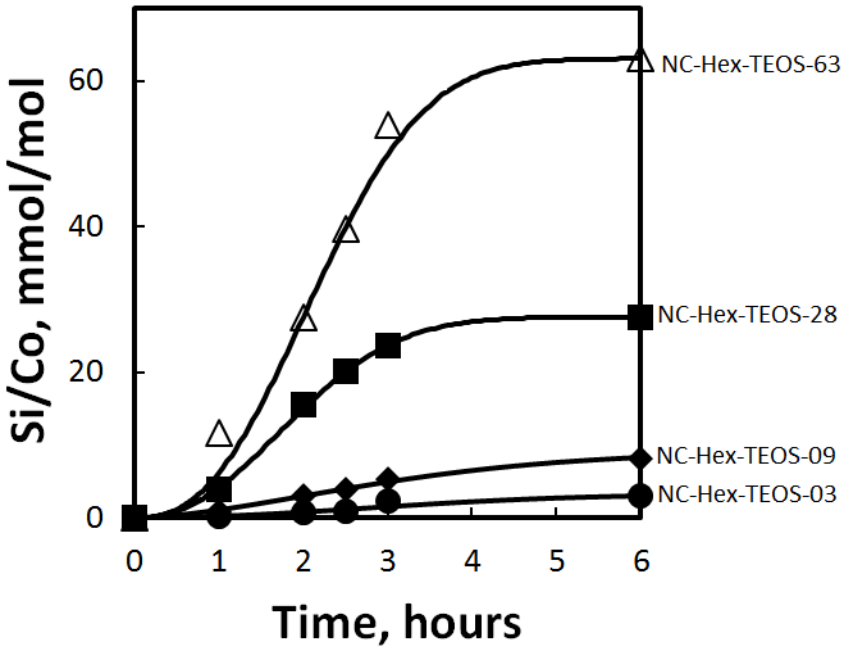

Figure 4-7: Tetraethoxysilane uptake by Co_3O_4 nano-cubes in dry n-hexane as a function of time to produce modified samples with Si/Co ratio of 3,9,28, and 63 mmol/mol using $[TEOS]_{initial}$ = 0.13 mM, 0.64 mM, 1.60 mM and 6.4 mM respectively and calcined at 573 K

Table 4-4: Modelling the rate uptake of tetraethoxysilane uptake in n-hexane using the generic Johnson-Mehl-Avrami-Kolmogorov model[20]

$[TEOS]_{initial}$ (mM)	**0.13**	**0.64**	**1.60**	**6.4**
M	2.05±0.71	1.99±0.53	2.16±0.24	2.51±0.59
τ, hours	3.75±0.54	3.48±0.33	2.51±0.	2.22±0.93
$\left(\frac{Si}{Co}\right)_{max}, \frac{mmol}{mol}$、	3.24±0.99	9.11±1.30	27.6±1.41	63.1±9.6
R^2	0.9899	0.9971	0.9994	0.9988

The rate of tetraethoxysilane uptake increases during the first 3 hours of the process and reached a maximum. The adsorption of tetraethoxysilane on a hydroxylated surface, such as the surface of Co_3O_4 nano-cubes as visualized by an absorption band at 3380 cm^{-1} in the FTIR spectrum of calcined Co_3O_4 nanocubes[21] may proceed via a condensation reaction[22,23] yielding ethanol and monodentate surface species, similar to the adsorption of dimethyl

diethoxy silane on silica under anhydrous or near anhydrous conditions[24] and the adsorption of 3-aminopropyltriethoxysilane on aluminium oxide[19]. The auto-catalytic nature of the process might be ascribed to the slow generation of reactive silanol via hydrolysis under near anhydrous conditions resulting in an acceleration of the silicon deposition. Auto-condensation of silanol groups may result in the formation of siloxane oligomers, which may condense/deposit on the surface[23]. The deposited oligomers may result in a 2-dimensioal thin layer of silica over Co_3O_4 or silica islands grown on the surface. The idea about the dimensionality of such silica oligomers may be obtained from the value of **m,** in the Avrami model. The obtained values of **m** are 2.05 ± 0.71, 1.99 ± 0.53, 2.16 ± 0.24 and 2.47 ± 0.59 for the samples having a $\left(\frac{Si}{Co}\right)$ ratio of 3 mmol/mol, 9 mmol/mol, 28 mmol/mol and 64 mmol/mol respectively. The values of **m,** suggest that may have grown into 2 dimensional silica surface species growing from a layers into 3D shapes[25].

The value of $\boldsymbol{\tau}$ is inversely proportional to the number of nuclei of particles to be grown per unit volume and the rate of grow of such particle [20,25]. Thus, the value of $\boldsymbol{\tau}$ may give some information of the size of the silica islands.

$$\boldsymbol{\tau} \propto \left(\frac{\mathbf{1}}{\boldsymbol{number\ of\ nuclei\ per\ unit\ volume}}\right), \left(\frac{\mathbf{1}}{\boldsymbol{rate\ of\ growth}}\right) \text{ … … … … … ……. ……Equation 4-4}$$

For particles to grow, a significant number of nuclei enough to initiate growth is required. If the rate of nucleation is higher than the rate of growth smaller particles may be expected. However, if the rate of grow is larger than the rate of nucleation then larger particles may be formed. The obtained time constant, $\boldsymbol{\tau}$, for the growth of silica on the surface of Co_3O_4 nanocubes in n-hexane is 3.75 ± 0.14, 3.48 ± 0.17, 2.51 ± 0.34, 2.22 ± 0.32 hours for the samples having a $\left(\frac{Si}{Co}\right)$ ratio of 3 mmol/mol, 9 mmol/mol, 28 mmol/mol and 64 mmol/mol respectively. Clearly, there is a gradual decrease in the value of $\boldsymbol{\tau}$ as the silica loading is increased. The decrease suggests there is a difference in either the rate of growth of the surface silicate species or the number of nuclei on the surface of Co_3O_4 nanocubes or both.

The silylation process does not affect the phase structure of the samples visibly as monitored using XRD (see *Fig. 4-8).* The only observed diffraction lines for all the samples are at 2θ angles

of 21.98, 36.35, 43.05, 43.83, 52.39, 64.39, 70.04 and 77.40 which are characteristic diffraction lines of spinel Co_3O_4[17] using a Co-K_α source (Eva software, CCD). The presence of amorphous silica on the surface of Co_3O_4 would be identified by a broad diffuse band at ca. $2\theta = 22^{\circ}$[17]. The absence of the diffraction may be due to low loading of silica on the surface Co_3O_4 (< 4.5 wt.-%). In addition, silica phase may be sufficiently crystalline to diffract X-rays due to its homogeneous distribution over Co_3O_4 as small clusters (*see Fig. 4-9*) as has been observed for alumina modified cobalt oxide[9].

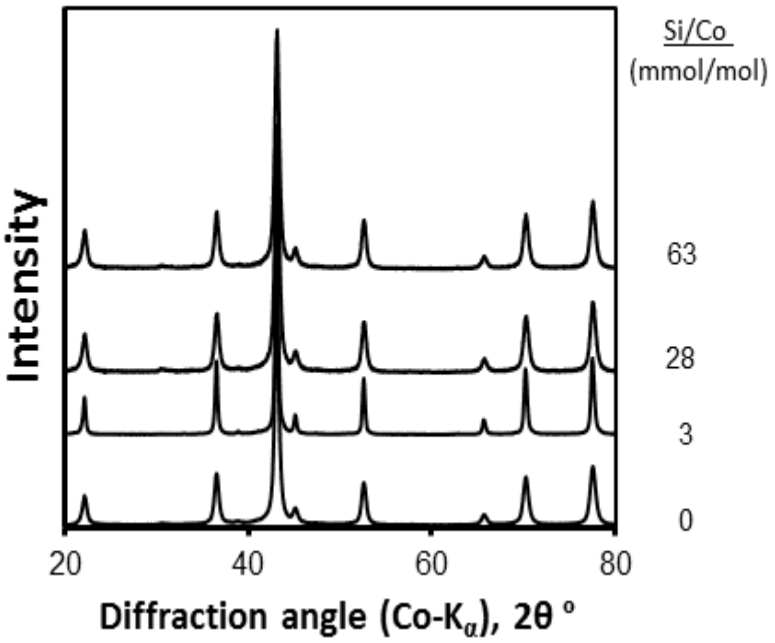

Figure 4-8: X-ray diffractogram of the model catalysts of different silicon loading synthesized by contacting Co_3O_4 with tetraethoxysilane in n-hexane

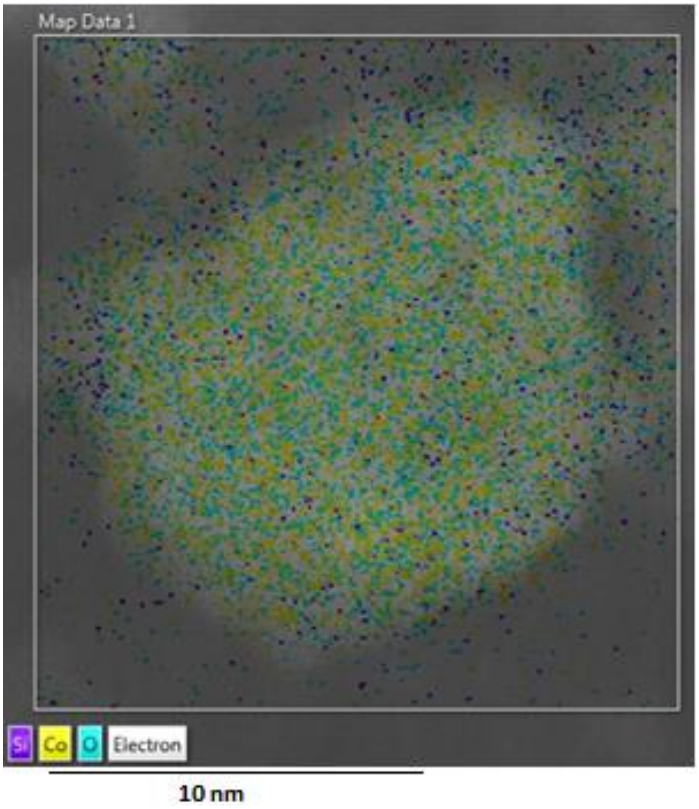

Figure 4-9: Si, Co an O EDS mapping for a sample NC-Hex-TEOS-63-573K showing Si is homogeneously distributed as small clusters over the Co_3O_4

Fourier transform infrared spectroscopy was used to investigate the nature of interaction between Co_3O_4 nanocubes and the modifying silica on the surface of the model catalyst after calcination at 573 K. *Figure 4-10* shows the FTIR spectra of (un)modified Co_3O_4 in the region 525-700 cm^{-1}. All the samples show absorption bands at 550 cm^{-1} and 658 cm^{-1}. The band at 550 cm^{-1} is ascribed to the vibration of the Co-O stretch while the latter can be ascribed to the stretch vibration of the Co (III)-O bond in the Co_3O_4 lattice[21]. A side band appear at 659 cm^{-1} upon modification for the modified samples. This absorption band can been attributed to the bending modes of the Co-O-Si bonds as reported by Yin *et al*.[22] for Co/SiO_2 core-shell structures reduced in hydrogen at 973 K . It may be difficult to recognize this absorption band as it intersects with the absorption bands due to Co (III)-O stretch in the Co_3O_4 lattice occurring at 658 cm^{-1} [21].

Additional absorption bands can be seen in the FTIR-spectra of all the samples contacted with solution of tetraethoxysilane in the range of 1200-700 cm^{-1} (see *Fig. 4-11*) with strong bands appearing at 800 cm^{-1}, 1020 cm^{-1} and 1100 cm^{-1}. These bands are characteristic for the presence

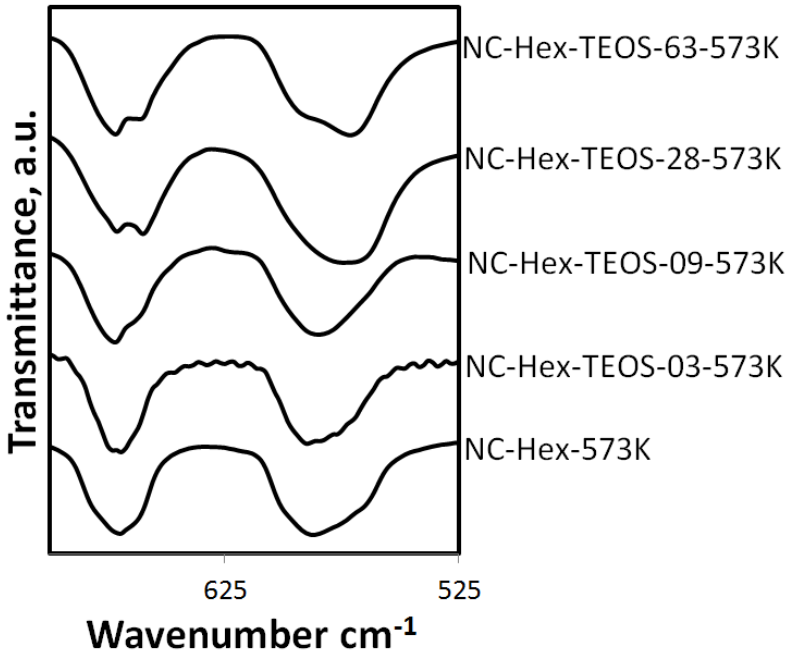

Figure 4-10: TIR-spectra of Co_3O_4 nanocubes modified by contacting with solutions of tetraethoxysilane in n-hexane with different initial concentrations in the range 700-1200 cm^{-1}

of extraneous silica in the modified samples. The band at 800 cm^{-1} can be attributed to the in-plane Si- O-Si bending vibration[26]. The band at 1020 cm^{-1} has been attributed to Co-O-Si vibration[27,28], but may also be attributed to the presence of oligomeric silicate species[19,29]. The simultaneous increase in the absorption band at 1020 cm^{-1} and the absorption band at 800 cm^{-1} may indicate that the band at 1020 cm^{-1} is more likely to be attributed to oligomeric silicate species[29] than Co-O-Si vibrations. The band at 1100 cm^{-1} is characteristic of the asymmetric stretching of the Si-O-Si of amorphous SiO_4 tetrahedra[19,30]. The intensity of these bands increases with increasing silicon to cobalt ratio. It is interesting to note that the intensity of the adsorption band at 1100 cm^{-1} decreases relatively to the intensity of the absorption bands at 1020 cm^{-1} and 800 cm^{-1} possibly indicating an increase in the extent of auto-condensation with increasing silicon to cobalt ratio. The FTIR-spectra of the modified samples also show the presence of a minor band at ca. 870 cm^{-1}. This band is not due to the presence of bulk cobalt orthosilicate, which would show major bands at 900 cm^{-1} and 935 cm^{-1} [31]. The presence of this band may indicate the presence of monodentate Co-O-Si species as observed in the adsorption

of dimethyl diethoxy silane on silica[24] and similar to those identified in the analogous iron-silica species[6].

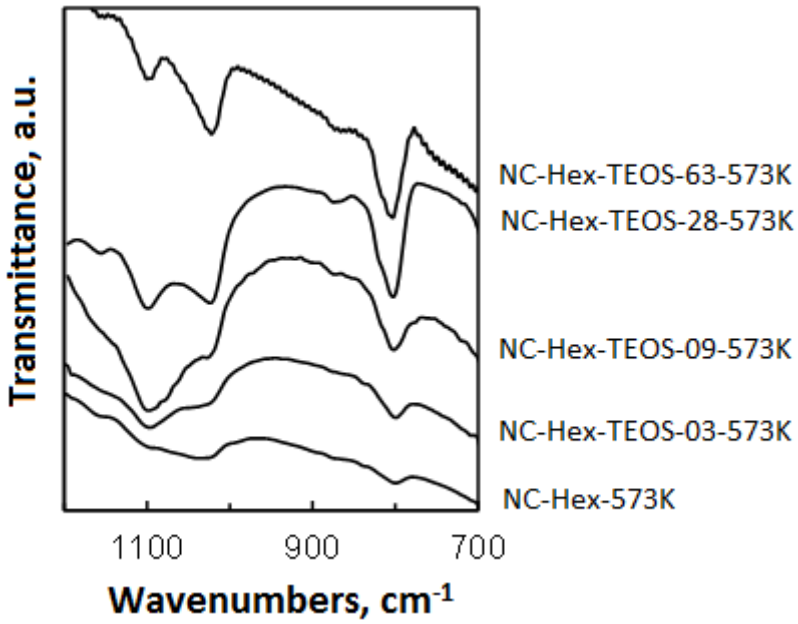

Figure 4-11: FTIR-spectra of Co_3O_4 nanocubes modified by contacting with solutions of tetraethoxysilane in n-hexane with different initial concentrations in the range 700-1200 cm^{-1}

An in-situ reduction study exposing the sample containing 28 mmol silicon per mol of cobalt to hydrogen at 673 K for 16 hrs showed that all the characteristic absorption band of silica remain intact, i.e. the major absorption bands at 800 cm^{-1}, 1020 cm^{-1} and 1100 cm^{-1} and the weaker absorption band at ca. 870 cm^{-1} (*see Fig. 4-12*). This implies that these species are not reducible under the applied reduction conditions.

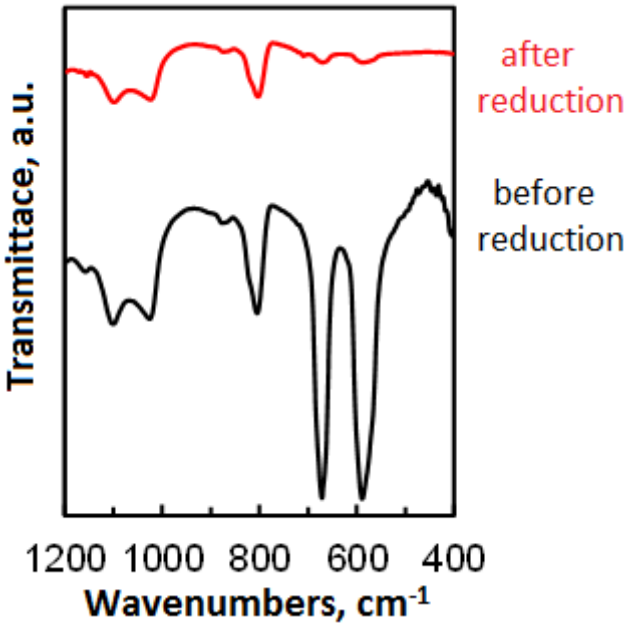

Figure 4-12: In-situ reduction of Co_3O_4 nanocubes exposed to a solution of tetraethoxysilane in n-hexane for 5 hrs (resulting Si/Co = 28 mmol/mol) in hydrogen at 623K for 16 hrs (spectra recorded at room temperature).

Electronic modification of cobalt atoms by Si was suggested by XPS. *Figure 4-13 (left)* shows a distinctive photoemission characteristic of Co 2p of pure Co_3O_4 (bottom spectrum) with spin-orbit peaks at ~780 eV and ~796 eV being ascribed to Co $2p_{3/2}$ and Co $2p_{1/2}$ respectively. The Co^{3+} and Co^{2+} components are clearly indicated as well as the satellite structure. Taking the ratios of the areas of the 3+ and 2+ peaks, we obtain an average valence of +2.7. This concurs with the theoretical value of +2.67. The Co 2p spectrum for the Co_3O_4 nanocubes modified with tetraethoxysilane and containing 63 mmol Si/mol Co sample has a similar spectrum to the spectrum of the unmodified Co_3O_4 nanocubes. Deconvoluting the Co^{3+} and Co^{2+} contribution resulted in a slightly lower average valence of +2.6. The higher intensity of the satellite in this spectrum agrees with previous work which shows a proportionality between the intensity of the 2+ component and the satellite structure[32]. The lower average valence of cobalt in the near surface region after exposing the sample to a solution of tetraethoxysilane in n-hexane may indicate some reduction of surface cobalt due to the presence of decomposition products of tetraethoxysilane or the solvent, n-hexane.

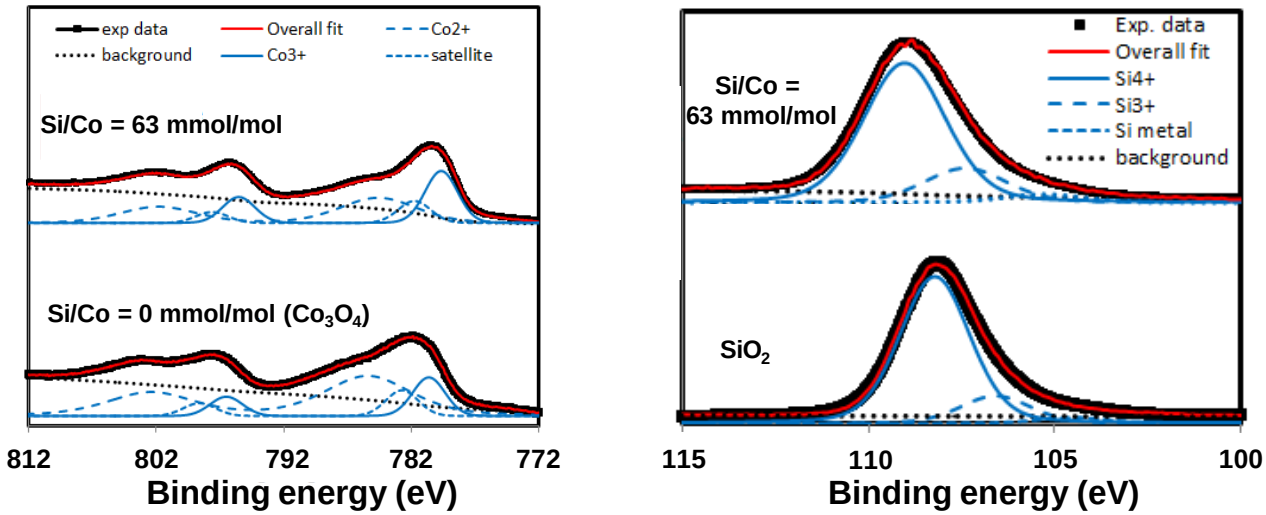

Figure 4-13: X-ray photoemission spectra of Co 2p of unmodified Co_3O_4-nanocubes and Co_3O_4 nanocubes modified with tetraethoxysilane containing 63 mmol Si/mol Co (left) and Si 2p for SiO_2 (Stöber spheres[12]) used as reference and Co_3O_4 nanocubes modified with tetraethoxysilane containing 63 mmol Si/mol Co (right)

The Si 2p spectrum of the modified Co_3O_4 sample is compared to the reference of the as-synthesized SiO_2 Stöber-spheres[12] (*se Fig. 4-13 (right)*). The Si 2p photoemission peaks of the reference silica is characterized by two convoluted peaks that are ascribed to SiO_2 (108.21 eV) and Si-O suboxides (107.23 eV). The ratio of the Si 2p photoemission peak attributed to SiO_2 and the Si 2p photoemission attributed to the Si-O suboxides is 4. The Si 2p photoemission peaks for the sample modified with tetraethoxysilane is similar to that of reference silica. However, the ratio of the peak ascribed to the Si 2p of SiO_2 (Si^{4+}) to that of the Si-O suboxide decreases drastically to 2.5. This indicates a significant increase in the relative quantity of suboxide. This may be ascribed to the difference in the structure of the silica islands on the surface of cobalt and the amorphous silica used as a reference. Furthermore, as expected a shift to the lower binding energy by 0.6 eV is observed in the Si 2p peak of the sample modified with tetraethoxysilane. This may confirm that electron density goes towards Si atoms from the cobalt atom.

Si K edge XANES was further used to disentangle the generation metal-support interaction. Si K edge XANES can provide information about the near neighbours, coordination and bond distances. *Figure 4-14* shows the Si K edge spectra for the modified Co_3O_4 nanocubes (Si/Co= 63 mmol/mol) along with those of as-synthesized Co_2SiO_4, amorphous Stöber SiO_2, and a reference commercial crystalline (quartz). The shift in peak location of the Si K edge white line has been

correlated to the degree of polymerization of the silicate[33]. The white line peaks for Co_2SiO_4 and for the modified Co_3O_4 nanocubes (Si/Co = 63 mmol/mol) are at 1846.96 eV and 1845.63 eV, respectively, suggesting a lower degree of polymerization than that of quartz or α-SiO_2, typical of neso- or island silicates. A comparison of the XANES spectrum of the modified Co_3O_4 nanocubes (Si/Co = 63 mmol/mol) with that of quartz and α SiO_2 also suggests a lower degree of crystallinity. Co_2SiO_4 shows a minor peak (B) at 1852.90 eV while the modified Co_3O_4 nanocubes (Si/Co = 63 mmol/mol) shows a similar peak at 1850.19 eV (B). Based on theoretical simulations[34], this peak has been assigned to second shell neighbour (Si-O-M, where M is a metal), while the peak (C) at ca. 1865 eV is from the first Si-O shell. The location of peak B in the modified Co_3O_4 nanocubes (Si/Co = 63 mmol/mol) suggests structural difference from Co_2SiO_4.

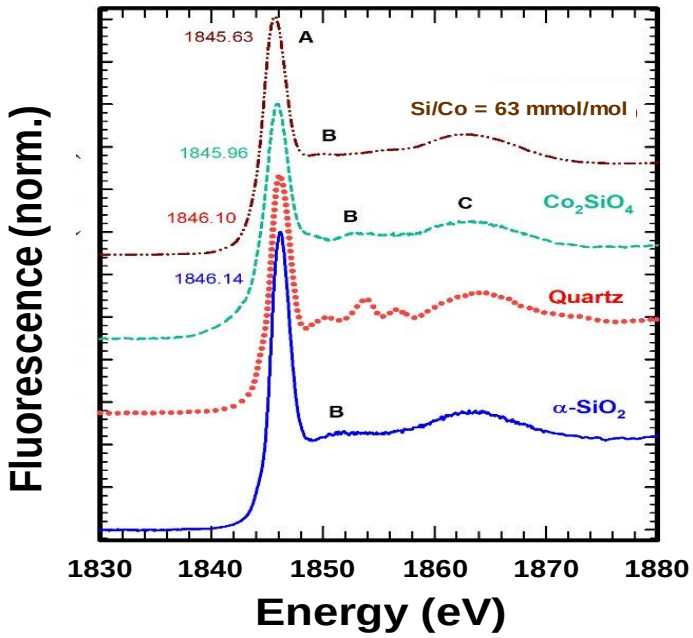

Figure 4-14: Si K-edge XANES spectra for the sample containing 63 mmol Si/mol Co and the reference samples SiO_2 and Co_2SiO_4

The spectroscopic data indicate, but do not unequivocally prove, the presence of a chemical bond between cobalt/cobalt (II,III)oxide and extraneous silica. Cobalt in Co_3O_4 chemically bonded to silica is expected to be more difficult to reduce than pure Co_3O_4[35] or a physical mixture of silica and Co_3O_4[36]. Hence, the reduction process of these samples was further investigated using temperature programmed reduction (TPR; see *Fig. 4-15*). The total amount of hydrogen consumed in this experiment indicates that Co_3O_4-nanocubes are completely reduced. The first reduction peak maximum for the unmodified Co_3O_4 nanocubes occurs at 530 K and the second peak maxima occurs at 700 K. This is typically ascribed to the two-step

reduction process of Co_3O_4 → CoO → Co[9,35–38]. The ratio of hydrogen consumption attributed to the two reduction peaks is much smaller than the required ratio of 1:3 for this reduction process. This may imply a more complex reduction process, when involving relatively large, well-crystalline Co_3O_4 nanocubes and the first reduction step may involve only surface reduction[39]. The rate of reduction of a solid with hydrogen at a given temperature T can be described by:

$$\frac{d\alpha}{dT} = \mathrm{k(T)f(\alpha)} \quad \text{Equation 4-5}$$

Where α is the degree of reduction, k (T) is the temperature-dependent rate constant. The function f(α) varies based on various gas-solid reaction models derived from different kinetic studies (*see Table 4-5*). The rate constant can be describe as a function of temperature, T using the Arrhenius equation:

$$k(T) = \mathrm{A}e^{\frac{-E_a}{RT}} \quad \text{Equation 4-6}$$

Where A is the pre-exponential factor, E_a is the activation energy of nucleation and R is the idea gas constant. Thus, the rate of reduction can be described as a function of temperature as:

$$\frac{\boldsymbol{d\alpha}}{\boldsymbol{dT}} = \mathbf{A}\boldsymbol{e}^{\frac{-E_a}{RT}}\mathbf{f(\alpha)} \quad \text{Equation 4-7}$$

Table 4-4: f(α) of different reduction models adapted for Lin *et al.*[38]

Reduction model	$f(\alpha)$
3-dimensional nucleation model according to Avrami-Erofeev	$(1-\alpha)\left(-3\ln(1-\alpha)^{\frac{2}{3}}\right)$
2-dimensional nucleation model according to Avrami-Erofeev	$(1-\alpha)\left(-2\ln(1-\alpha)^{\frac{1}{2}}\right)$
Unimolecular decay	$(1-\alpha)$
Three-dimensional diffusion according to Jander	$\frac{3}{2}(1-\alpha)^{\frac{1}{3}}\left((1-\alpha)^{\frac{1}{3}}-1\right)^{-1}$

For the obtained temperature programmed reduction data (TPR; see *Fig. 4-15)*, the first reduction step is thought to be best described using a two-dimensional nucleation model according to Avrami-Erofeev model, whereas the subsequent reduction process is thought to be best described according to a uni-molecular decay model[38]. The newly developed high temperature peak was best fitted using a unimolecular decay model. The TPR-profiles were deconvoluted accordingly by fitting the whole TPR profile to these two models. The activation energy for the 1st reduction step in the reduction of Co_3O_4 nanocubes assuming the two-

dimensional nucleation model was determined to be 34±3 kJ/mol (A = $10^{0.7\pm0.4}$ s^{-1}), whereas the activation energy for the 2nd reduction step assuming a uni-molecular decay model was determined to be 127±21 kJ/mol (A = $10^{7.2\pm1.5}$ s^{-1}) (*see Table 4-5*).

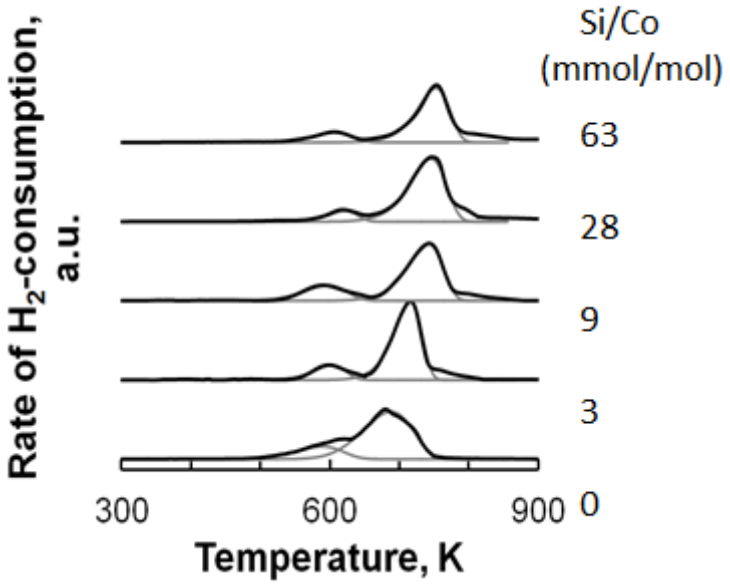

Figure 4-15: Temperature programmed reduction (TPR) profiles of silica-modified Co_3O_4-nanocubes (heating rate 10 K/min; 5% H_2 in Ar; grey lines: fit of consecutive two-dimensional nucleation model followed by a uni-molecular decay)

The modification of Co_3O_4 nanocubes with tetraethoxysilane retards both reduction steps. The reduction temperature for the two reduction processes has shifted to 623 K and 798 K respectively, for the sample with a Si/Co-ratio of 63 mmol/mol (NC-Hex-TEOS-63-573K). It can be further noted that a high temperature shoulder starts appearing in the TPR-profiles of the Co_3O_4 nanocubes after exposure to solutions of tetraethoxysilane in n-hexane. This has been attributed to a strong interaction between Co_3O_4 and surface silicate[35,37,40] e.g. in the form of cobalt silicate or surface silicate. The hydrogen consumption peaks in the TPR-profiles of the modified Co_3O_4-nanocubes were also fitted to a two-dimensional nucleation model according to Avrami-Erofeev[20,38] followed by a uni-molecular decay for both the second reduction step and the reduction of the strongly bound cobalt. With increasing TEOS loading, the activation required for reduction increases (*See Table 4-6)*. This therefore explains the shift towards higher reduction temperatures upon addition of TEOS to the Co_3O_4 nanocubes. The pre-exponential factor, A, does not seem to vary upon modification. Therefore, the delay in the reduction process of Co_3O_4 is due to an increase in the activation energy but not any changes in the pre-exponential factor. For the sample containing 63 mmol/mol (Si/Co) (NC-Hex-TEOS-63-473K),

the activation energy for the two-dimensional nucleation increased to 57±11 kJ/mol (A = $10^{2.6\pm0.9}$ s^{-1}) implying that the presence of silicon in the sample retards the reduction of Co_3O_4 to CoO. The consecutive uni-molecular decay of CoO to metallic cobalt is also retarded and an activation energy of 195±34 kJ/mol (A = $10^{11.6\pm2.6}$ s^{-1}) was determined. The increase in the activation energy of the 2nd reduction peak indicates that the silicate species do not only affect the reduction process of Co_3O_4 → CoO, but also have a remarkable influence on the consecutive reduction process. The change in the observed activation energy strongly suggests that silicate is bonded to the surface of the nanocubes, since it hinders the reduction of ionic cobalt in these materials. It is accepted that reducibility of a supported oxides is a function of the metal-support bond strength and hence activation energy.

Table 4-5: Kinetic parameter for the reduction of tetraethoxysilane modified Co_3O_4 nanocubes

$\left(\frac{Si}{Co}\right)$ $ratio$,	Activation energy, kJ/mol			A, s^{-1}			R^2,[a]		
mmol/mol	Peak 1	Peak 2	Peak 3	Peak 1	Peak 2	Peak 3	Peak1	Peak2	Peak3
0	34 ± 3	127±21		$10^{0.7\pm0.4}$	$10^{7.2\pm1.5}$	-	0.97	0.99	-
3	38 ± 7	135±14	47 ±11	$10^{1.7\pm1.3}$	$10^{6.6\pm3.5}$	$10^{3.4\pm1.1}$	0.93	0.98	0.99
9	45 ± 15	176±23	54 ± 9	$10^{-1.3\pm0.8}$	$10^{-8.3\pm1.3}$	$10^{3.6\pm0.7}$	0.99	0.99	0.97
28	52 ± 9	170±28	87 ± 13	$10^{1.9\pm1.1}$	$10^{-9.9\pm3.7}$	$10^{3.4\pm0.9}$	0.97	0.98	0.98
63	57 ± 11	195±34	93 ± 25	$10^{2.6\pm0.9}$	$10^{11.6\pm2.6}$	$10^{3.5\pm1.4}$	0.99	0.99	0.99

[a] Coefficient of regression obtained by fitting the TRP profiles to the respective reduction models

The samples were supported on β-SiC to test their activity in the Fischer-Tropsch synthesis. The nanocubes were well dispersed onto the support (see *Fig. 4-16).* The actual cobalt loading in the supported catalysts was determined using ICP-AAS. The expected Co loading from a 10 wt-% Co_3O_4 was 7.3 wt-%. The actual loading of cobalt loading from the samples was determined using ICP-AAS both before and after Fischer-Tropsch synthesis (*see Table 4-7)*. The actual loading of cobalt in the samples is slightly lower than the expected Co loading. This may arise from the non-stoichiometric nature of the synthesized Co_3O_4 showing that the ratio of Co:O in the sample is less than ¾. The cobalt loading does not seem to change even after the Fischer-Tropsch synthesis for all samples. This suggest that the metal is not removed from the support even during the Fischer-Tropsch synthesis.

Table 4-6: Actual cobalt loading in the supported fresh and spent catalyst determined from AAS

Sample ID	Cobalt loading, % w/w Fresh catalyst	Cobalt loading, % w/w Spent catalyst
Co_3O_4	6.9 ± 0.4	5.8 ± 0.3
0.003 mol Si/mol Co	5.9 ± 0.6	6.0 ± 0.4
0.009 mol Si/mol Co	6.6 ± 0.9	6.3 ± 0.7
0.03 mol Si/mol Co	5.8 ± 0.8	5.9 ± 0.2
0.06 mol Si/mol Co	6.0 ± 0.2	6.3 ± 0.6

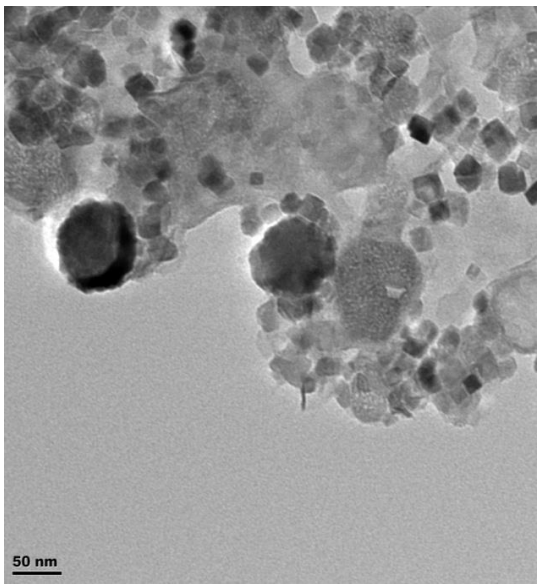

Figure 4-16: TEM images for Co_3O_4–nanocubes ($d_{Co_3O_4}$ = 25 nm) supported on β-SiC microspheres after re-suspending the nanocubes in a solution of 10% vol/vol oleic acid in n- hexane.

Degree of reduction of cobalt oxide to metallic cobalt is of great importance in the performance of the catalyst. The degree of reduction of the catalyst were determined for Co_3O_4 and the sample with the Si/Co-ratio of 63 mmol/mol by reducing the catalyst at 673 K for 16 hours, succeeded by cooling in argon. Temperature programmed reduction of the reduced samples by ramping the temperature by 10 K/min in a gas mixture of 5% H_2 in argon. The degree of reduction was computed from the relative hydrogen consumption of the reduced catalyst to that required for complete reduction of Co_3O_4. The degree of reduction of the catalyst is only slightly reduced upon introducing the silicon modification (see *Table 4-7).*

The activity was monitored as a function of time on line (see *Fig. 4-17*) and the initial activity was recoded after 20 hours which is the time where pseudo-steady state was reached (variation in conversion is less than 4 %). These values of the initial conversion may have been affected by

any changes in the catalyst that may take place during the 20 hours (e.g. sintering). A CO conversion of 0.5 % was obtained over the unmodified, reduced Co_3O_4 nanocubes supported on β-SiC after 72 hours on line. An increase in the CO-conversion with increasing silicon content was obtained, and the catalytic activity remained relatively constant as a function of time on line. The activity of the catalyst can also be expressed as an integral rate in the form of the cobalt time yield. The cobalt time yield after 44 hrs on line increases by a factor of 20 upon increasing the Si/Co ratio from 0 to 63 mmol/mol (from 0.7 X 10^{-4} s^{-1} in the Fischer-Tropsch synthesis over the unmodified Co_3O_4 dispersed over β-SiC to 14 X 10^{-4} s^{-1} over modified Co_3O_4 with Si/Co=63 mmol/mol).

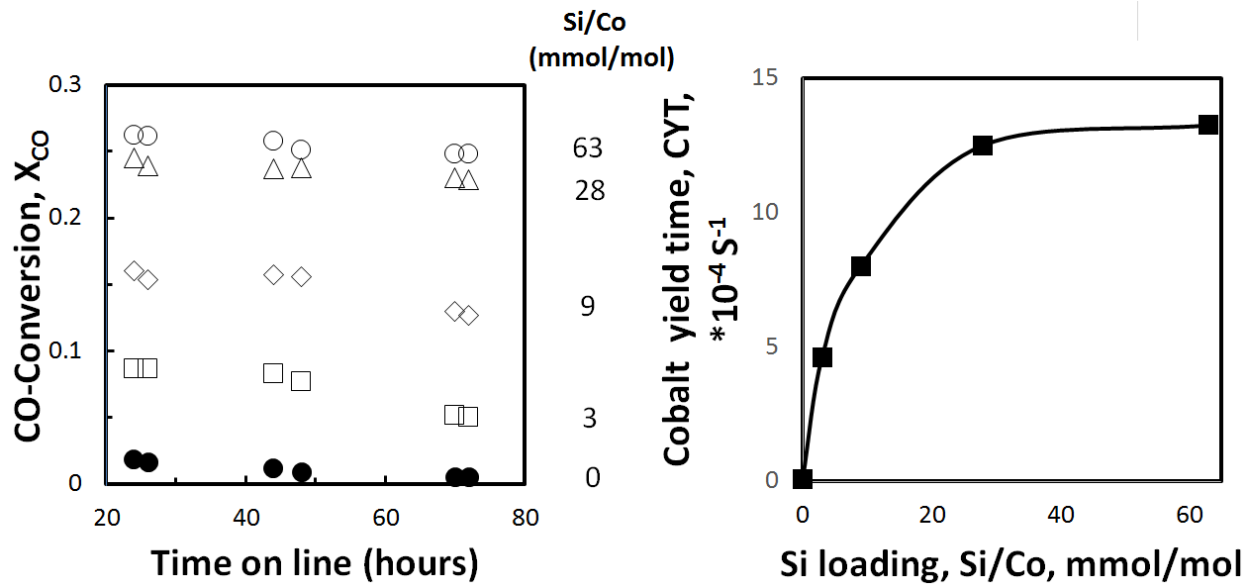

Figure 4-17: Effect of modifying Co_3O_4 with tetraethoxysilane in dry hexane on the activity in the Fischer-Tropsch synthesis (498K, 20 bar) after reduction in H_2 at 673K for 16 hrs
Left: CO conversion as a function of time on stream
Right: Cobalt-time-yield as a function of silicon loading

The catalyst activity can be expressed as an integral rate of CO -conversion per unit mass of the active metal (see *Fig. 4-18*), as determined in the spent catalyst. When the cobalt surface is modified with tetraethoxysilane, the specific rate of CO-conversion increases rapidly. For the unmodified sample the rate of CO conversion is 0.13 mmol CO/(min.g_{co}). The rate of CO conversion increased to 1.7 mmol CO/(min.g_{co}).

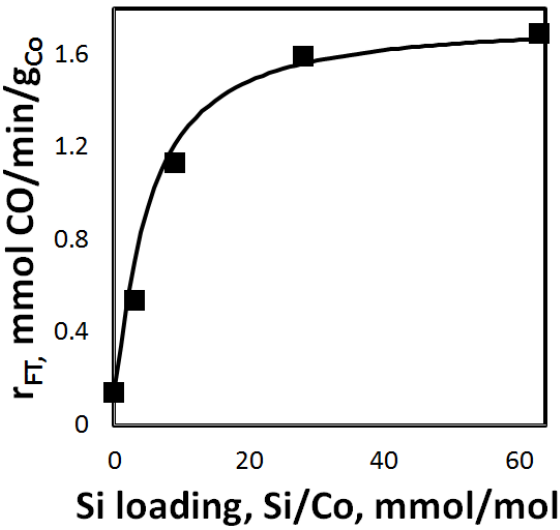

Figure 4-18: Rate of Fischer-Tropsch reaction per unit mass of cobalt after 44 hours times on stream.

Catalytic activity can be expressed by in terms of turnover frequency. The turnover frequency also shows a strong improvement from 0.01 s^{-1} for the unmodified sample to 0.1-0.5 s^{-1} for the modified samples (see *Table 4-6*) implying that the reactivity of the surface atoms has changed upon modification of Co_3O_4 with tetraethoxysilane. The rate of CO-hydrogenation on extended surfaces is thought to be low due to the high activation barrier for CO-dissociation[8,41,42].The hydroxyl groups attached to the promoter could interact with adsorbed CO in its vicinity on the less active terrace sites. The interaction between hydroxyl groups and adsorbed CO may result in a lowering of the activation barrier for CO-dissociation not too dissimilar to the proposed route for hydrogen assisted CO-dissociation on terrace sites[41] as shown for the presence of hydroxyl groups on an alumina ligand on Co(111)[8].

It would be expected that the catalytic activity of the modified samples be lower due to the reduced degree of reduction following the modification process. However, the conversion increases upon modification, suggesting the effects of modification may rather be chemical or may offer different chemical mechanism for the CO hydrogenation. It may be hypothesized that the change in the activity can be attributed to a change in the metal surface area under reaction conditions. The spent catalyst was passivated and recovered, after which the hydrogen uptake on the re-reduced spent catalyst was determined (*see Table 4-7*). The hydrogen uptake on the re-reduced, spent catalyst does not change much. The measured uptake corresponds to a dispersion of 2.8-5.8% implying metal particle sizes between 16 and 34 nm. This would indicate

minimal sintering/particle break-up upon catalyst activation and Fischer-Tropsch synthesis thus a change in the metal surface area cannot account for the difference in the activity.

Methane is an undesired, but inevitable product of the Fischer–Tropsch synthesis. Hence, the methane selectivity is of great industrial interest. The obtained methane selectivity over these materials is acceptable and seems to decrease with increasing silicon content (see *Table 4-4*). When CO dissociates on the surface of a catalyst, it may form surface C_1-species. The amount of C_1-species depends on the rate of CO dissociation. An enhancement in the rate of CO-dissociation could lead to an increase in the surface coverage of cobalt with the C_1-species and this may increase the chances of chain growth and hence a reduction in the methane selectivity[39] However, the observed decrease in the methane selectivity cannot be unequivocally attributed to a promotional effect of silicon, since methane selectivity is also affected by the levels of CO-conversion[43–45].

To deconvolute the promotional effect of silicon on cobalt from CO-conversion levels on methane selectivity, the catalyst with a Si/Co ratio of 63 mmol/mol and unmodified Co_3O_4 were studied at 15% CO-conversion. The selectivity to methane remains almost constant for all catalyst over a period of 44 hours. The methane selectivity for the unmodified catalyst (Co_3O_4) is 9.4% and upon modification reduces to 8.6%. Thus, the modification of Co_3O_4 nanocubes results in a decrease in the methane selectivity.

The decrease in the methane selectivity is accompanied by an increase in the chain growth probability in the range C_3-C_{10} (see *Table 4-6*). This indicates that the treatment of Co_3O_4-nanocubes yields a catalyst with a higher selectivity towards the desired long chain products. The formation of long chain products may be favoured by the enhanced dissociation of CO on the surface yielding more ‘monomeric’ species on the surface thus enhancing the rate of chain growth over desorption.

Table 4-7: Activity and selectivity of reduced Co_3O_4-nanocubes modified by exposure to solutions of tetraethoxysilane in hexane in the Fischer-Tropsch synthesis (reduction in H_2, T_{red} = 673 K, t_{red} = 16 hrs; Fischer-Tropsch synthesis: T = 493 K, p = 20 bar, $F_{CO,0}/W$ = 0.09 mmol/(g_{Co}.s), $(H_2/CO)_{inlet}$ = 2)

Si/Co, mmol/mol	H_2-uptake of reduced catalyst, $cm^3(STP)/g_{Co}$	Degree of reduction, %	X_{CO}[a], %	TOF[b], s^{-1}	S_{CH_4}, C-%	Chain growth probability, α
0	6.1 ± 0. 0	88	0.5	0.001	10.2	0.68
3	5.3 ± 1.3	n.d.[c]	5.1	0.008	10.0	0.71
9	11.0 ± 6.4	n.d.[c]	12.9	0.021	8.9	0.73
28	6.5 ± 1.4	n.d.[c]	23.0	0.038	8.2	0.76
63	5.4 ± 1.7	82	24.8	0.041	7.0	0.77

[a] Activity 72 hrs on stream; [b] turnover-frequency based on a cobalt dispersion of 3.2%;

4.4. Conclusions

In this study the effect of modifying the precursor of a catalytic active material for the Fischer-Tropsch synthesis with an alkoxide to give some insight in the effect of metal-support interaction on the catalytic activity was investigated. The modification of Co_3O_4 nanocubes with small amounts of tetraethoxysilane yields, besides silicate oligomers around the particles, to attachment of silicate species to the Co_3O_4 nano-particle as indicated by FTIR and XANES. The presence of neso- or island silicates may mimic aspects of the interaction of cobalt oxide with the support as indicted by the retarded reduction of Co_3O_4 particles. The presence of these silicate species in close proximity to the catalytically active surface results in an increase of the turnover frequency in the Fischer-Tropsch synthesis. This enhancement in activity is tentatively attributed to the presence of an alternative reaction pathway for CO-dissociation due to the presence of the silicate structures.

4.5. References

1 C. H. Mejia, T. W. van Deelen and K. P. De Jong, *Nat. Commun.*, 2018, **9**, 4459–4465.

2 S. J. Tauster, *ACS Symp. Ser.*, 1986, **298**, 1–9.

3 S. J. Tauster, S. C. Fung, R. T. K. Baker and J. A. Horsley, *Science*, 1981, **211**, 1121–1125.

4 S. J. Tauster, S. C. Fung and R. L. Garten, *J. Am. Chem. Soc.*, 1978, **100**, 170–175.

5 M. Cargnello, P. Fornasiero and M. J. Gorte, *Catal. Letters*, 2012, **142**, 1043–1048.

6 R. P. Mogorosi, N. Fischer, M. Claeys and E. van Steen, *J. Catal.*, 2012, **289**, 140–150.

7 R. P. Mogorosi, M. Claeys and E. van Steen, *Top. Catal.*, 2014, **57**, 572–581.

8 T. van Heerden and E. van Steen, *Faraday Discuss.*, 2017, **197**, 87–99.

9 A. P. Petersen, R. P. Forbes, S. Govender, P. J. Kooyman and E. van Steen, *Catal. Letters*, 2018, **148**, 1215–1227.

10 J. Feng and H. C. Zeng, *Chem. Mater.*, 2003, **15**, 2829–2835.

11 X. Liu, G. Qiu and X. Li, *Nanotechnology*, 2005, **16**, 3035–3040.

12 W. Stober and A. Fink, *J. Colloid Interface Sci.*, 1968, **26**, 62–69.

13 C. Real, M. D. Alcalá, A. Muñoz-Páez and J. M. Criado, *Nucl. Instruments Methods Phys. Res. Sect. B Beam Interact. with Mater. Atoms*, 1997, **133**, 68–72.

14 B. Ravel and M. Newville, *J. Synchrot. Radiat.*, 2005, **12**, 537–541.

15 P. N. Shelke, Y. B. Khollam, P. N. Pabrekar, P. S. More, A. M. Datir, S. D. Chakane, K. C. Mohite and P. Koinkar, *Int. J. Mod. Phys. Conf. Ser.*, 2012, **06**, 197–202.

16 Z. Grzesik, A. Kaczmarska and S. Mrowec, *Solid State Phenom.*, 2015, **227**, 421–424.

17 R. Xie, C. Wang, L. Xia, H. Wang, T. Zhao and Y. Sun, *Catal. Letters*, 2014, **144**, 516–523.

18 X. D. Hou, Y. Z. Wang and Y. X. Zhao, *Catal. Letters*, 2008, **123**, 321–326.

19 D. G. Kurth and T. Bein, *Langmuir*, 1995, **11**, 3061–3067.

20 M. Avrami, *J. Chem. Phys.*, 1939, **7**, 1103–1112.

21 R. Xu and H. C. Zeng, *Langmuir*, 2004, **20**, 9780–90.

22 L. L. Tedder, G. Lu and J. E. Crowell, *J. Appl. Phys.*, 1991, **69**, 7037–7049.

23 J. J. Brinker and G. Scherer, *Sol-Gel Science: The Physics and Chemistry of Sol-Gel Processing*, Academia Press, Inc., New York, 1990.

24 D. W. Sindorf and G. E. Maciel, *J. Am. Chem. Soc.*, 1983, **105**, 3767–3776.

25 M. Avrami, *J. Chem. Phys.*, 1942, **9**, 177–184.

26 X. J. Yin, K. Peng, A. P. Hu, L. P. Zhou, J. H. Chen and Y. W. Du, *J. Alloys Compd.*, 2009, **479**, 372–375.

27 I. Puskas, T. H. Fleisch, J. B. Hall, B. L. Meyers and R. T. Roginski, *J. Catal.*, 1992, **134**, 615–628.

28 A. H. Kababji, B. Joseph and J. T. Wolan, *Catal. Letters*, 2009, **130**, 72–78.

29 X. Yang, P. Roonasi and A. Holmgren, *J. Colloid Interface Sci.*, 2008, **328**, 41–47.

30 X. Huang and Z. Chen, *J. Cryst. Growth*, 2004, **271**, 287–293.

31 S.-J. Jong and S. Cheng, *Appl. Catal. A Gen.*, 1995, **126**, 51–66.

32 T. J. Chuang, C. R. Brundle and D. W. Rice, *Surf. Sci.*, 1976, **59**, 413–429.

33 D. Li, G. M. Bancroft, M. E. Fleet and X. H. Feng, *Phys. Chem. Mater.*, 1995, **222**, 115–122.

34 I. Davoli, E. Paris, S. Stizza, M. Benfatto, M. Fanfoni, A. Gargano, A. Bianconi and F. Seifert, *Phys. Chem. Miner.*, 1992, **19**, 171–175.

35 E. van Steen, G. S. Sewell, R. a. Makhothe, C. Micklethwaite, H. Manstein, M. de Lange and C. T. O'Connor, *J. Catal.*, 1996, **229**, 220–229.

36 H. Ming and B. G. Baker, *Appl. Catal. A, Gen.*, 1995, **123**, 23–36.

37 M. P. Rosynek and C. A. Polansky, *Appl. Catal.*, 1991, **73**, 97–112.

38 H. Y. Lin and Y. W. Chen, *Mater. Chem. Phys.*, 2004, **85**, 171–175.

39 L. Hu, K. Sun, Q. Peng, B. Xu and Y. Li, *Nano Res.*, 2010, **3**, 363–368.

40 R. Xie, D. Li, B. Hou, J. Wang, L. Jia and Y. Sun, *CATCOM*, 2011, **12**, 589–592.

41 M. Ojeda, F. Jose, P. Terreros, S. Rojas, T. Herranz and L. G. Fierro, *Langmuir*, 2006, **22**, 3131–3137.

42 R. A. van Santen, I. M. Ciobîcâ, E. van Steen and M. M. Ghouri, *Adv. Catal.*, 2011, **54**, 127–187.

43 D. B. Bukur, Z. Pan, W. Ma, G. Jacobs and B. H. Davis, *Catal. Letters*, 2012, **142**, 1382–1387.

44 E. van Steen, M. Claeys, K. P. Möller and D. Nabaho, *Appl. Catal. A Gen.*, 2018, **549**, 51–59.

45 W. Ma, G. Jacobs, Y. Ji, T. Bhatelia, D. B. Bukur, S. Khalid and B. H. Davis, *Top. Catal.*, 2011, **54**, 757–767.

5. **Metal-support interactions in SiO_2/Co inverse catalyst for Fischer-Tropsch synthesis: effects of solvent type during the modification**

The effectiveness of method of deposition of tetraethoxysilane on the surface of Co_3O_4 was tested by varying solvent/solvent mixtures with or without ammonia or glyoxylic acid. Deposition of tetraethoxysilane of Co_3O_4 nanocubes in n-hexane yield ethoxylated surface species which when calcined at 573 K result in silica oligomers interacting strongly with cobalt(II,III)oxide. While temperature seems important in the interaction of silica and cobalt oxide, modification of Co_3O_4 nanocubes with tetraethoxysilane in a hydrolyzing environment results in a stronger interaction due to the formation of surface cobalt silicate formed through hydrolysis and condensation of tetraethoxysilane. The presence of silicate species reduces the metal dispersion and the reducibility of Co_3O_4 nanocubes. The intrinsic catalytic activity of the modified, reduced modified Co_3O_4 nano-cubes have been tested for their activity and selectivity in the Fischer-Tropsch synthesis under industrially relevant conditions. The catalyst modified in the presence of glyoxylic acid has the highest activity that can be correlated to the formation of surface cobalt silicate (Co-O-Si interface).

5.1. Introduction

The use of catalyst model systems in heterogeneous catalysis can bring insight in the chemical interactions at the surfaces at a molecular level. Inverse catalyst can be used as a model system, a discussed by Schwab[1]; they consist of the catalytically active metal dotted with small quantities of and oxide support material. The inverse catalyst model systems have found application in oxidative catalysis[2], CO hydrogenation reactions[3], or hydrogen generation reactions[4]. The added advantage of this model system is that reactants can have access to the metal-support interface. This explains why inverse catalyst may show a better catalytic activity than their conventional counterpart. For instance, the inverse ZnO/Cu(111) catalyst show an improved catalytic activity compared to the conventional Cu/ZnO catalyst in the methanol synthesis[5]. The interaction of the oxide overlayers with the catalytically active material can be manipulated in a way that can enhance the activity. As an example, the decoration of cobalt with TiO_2 or Nb_2O_5 resulted in loss of surface area due to blockage by the suboxides overlayers formed during the reduction process thus reducing their performance[6]. However, when the catalyst was treated using sequential reduction-oxidation-reduction steps, the catalytic activity increased. [6]

Inverse catalyst can be prepared using various techniques, usually resulting in island of oxide dotted on the active metal[7–9]. Recently, the oxide nanoparticles were dotted onto the metal using alkoxide precursors of the oxide[7,10]. Co_3O_4 nanoparticle were modified with alumina using aluminium iso-propoxide and through high resolution electron microscopy, alumina islands were spotted on the surface of Co_3O_4 after calcination[7].

Tetraethoxysilane has been used as a precursor for the synthesis of silica nanoparticles following Stöber's method[11]. This method involves a base catalysed hydrolysis of tetraethoxysilane in presence of short chain alcohols[12,13] and condensation reactions involving the hydrolysed species. The method has been manipulated to give silica particles of various characteristics by: 1) using acids as catalysts for the hydrolysis reaction[14], 2) controlling the reaction temperature[15] and 3) the ratio of tetraethoxysilane to water and solvent[12]. This chapter describes the effect on solution used during the deposition of tetraethoxysilane on Co_3O_4.

5.2. Experimental

Synthesis of Co_3O_4

Co_3O_4-nanocubes were synthesized as described in chapter 4. To obtain Co_3O_4 nanocubes with an average size of 23.8 ± 4.5 nm (as determined using TEM) were synthesized using a hydrothermal oxidative precipitation method[16,17]. A solution containing 5.3 g Co(NO3)2.6H2O (20 mmol, Merck, >99.0 %) in 20.0 mL deionized water was added to a solution containing 1.8 g of NaOH (45 mmol) and 5.4 g sodium dodecylsulphate (20 mmol) in 180 mL deionized water at 368 K with an addition rate of 10 mL/min. Air was purged through the solution for 5 hours, after which the solid was recovered by centrifugation. The crystals were purified by multiple washing steps with a 1.0 M aqueous HCl-solution and distilled water. Residual chlorine present in the sample was shown to be removed after calcination at 473 K for 2 hours in a static oven.

Modification of Co_3O_4 nanoparticles with TEOS

The obtained, calcined cobalt oxide was re-suspended in different solvent mixtures. Sample NC-Hex-TEOS was synthesized by re-suspending the Co_3O_4 nanocubes in hexane. The Co_3O_4-nanocubes were contacted with tetraethoxysilane dissolved in n-hexane yielding a suspension with a solid concentration of 1.4 g/L and tetraethoxysilane with an initial concentration of 6.4 mM (0.143 vol.-%) for a period of 5 hours. After contacting the solid with the solution, the solid was recovered by centrifugation and washed 5 times with n-hexane. The samples were subsequently dried at 393 K for 2 hours and calcined at 573 K for 2 hours in a static oven.

Samples NC-Eth-TEOS, NC-Acid-TEOS and NC-Base-TEOS were synthesized through hydrolysis. A control sample (NC-Eth-TEOS) was synthesized by re-suspending Co_3O_4 nanocubes in a mixture containing 280 mL of absolute ethanol (Sigma-Aldrich), and 20 mL distilled and contacting them for 5 hours with tetraethoxysilane solution in 50 mL absolute ethanol to yield a solid solution of 1.4 g/L and tetraethoxysilane concentration 6.4 mM (0.143 vol.-%). Sample NC-Acid-TEOS was prepared by re-suspending Co_3O_4 nanocubes in a mixture containing 280 mL of absolute ethanol (Sigma-Aldrich), and 20 mL distilled water (pH=7.0) to which 7 mmol glyoxylic acid (Sigma-Aldrich) was added. A solution of tetraethoxysilane in absolute ethanol (50 mL) was added to the suspension and the reaction was monitored over 5 hours. For the synthesis of the modified nanocubes in the presence of a base (NC-Base-TEOS), Co_3O_4 nanocubes were resuspended in a mixture containing 280 mL of absolute ethanol (Sigma-

Aldrich), and 18 mL distilled water (pH=6.9) to which 4 mL of 35% ammonia solution (7 mmol, NH_3) was added. The suspension was mixed for 5 hours with a solution containing tetraethoxysilane in absolute ethanol to produce a solid concentration of 1.4 g/L and tetraethoxysilane concentration of 6.4 mM (0.143 vol).

To monitor the rate of uptake of tetraethoxysilane on Co_3O_4 surface, a 50 µL solution was drawn from the mother solution and solvent was decanted from the solid which was washed several times with ethanol. The Si uptake was monitored using SEM/EDX on the obtained powder. To obtain the deposition of a similar amount of tetraethoxysilane the contact time was varied (vide verde) and the contact time to obtain ca. 63 mmol Si per mol of cobalt for the samples NC-Hex-TEOS, NC-Eth-TEOS, NC-Acid-TEOS and NC-Base-TEOS was 300 minutes, 90 minutes, 35 minutes and 50 minutes respectively (*see Table 5-1*). Gelation due to rapid formation of silica gel upon contacting the solutions was not observed. This could be due to the low concentrations of tetraethoxysilane. The modified materials were subsequently washed with absolute ethanol, dried at 393 K for 2 hours and calcined at 573 K for 2 hours in a static oven and the respective materials were named NC-Hex-TEOS-63-573K, NC-Eth-TEOS-63-573K, NC-Acid-TEOS-63-573K and NC-Base-TEOS-573K.

Table 5-1: Reaction times taken to produce a specified $\left(\frac{Si}{Co}\right)$ ratio for the samples modified in different solvents

Sample ID	$\left(\frac{Si}{Co}\right)$, mmol/mol	Reaction time, min
NC-Hex-TEOS-63-573K	63.4 ± 2.1	300
NC-Eth-TEOS-63-573K	61.7 ± 1.7	90
NC-Acid-TEOS-63-573K	64.6 ± 1.4	35
NC-Base-TEOS-63-573K	65.3 ± 1.9	50

Supporting the nanocubes

The modified Co_3O_4 nanoparticles were deposited on β-SiC microspheres (SiCAT, $d_{particle}$= 100 µm, S_{BET} = 25 m^2/g, V_{pore} = 0.30 cm^3/g) by sonicating 0.1 g of the (modified) nanocubes together with 0.9 g of β-SiC microspheres in a mixture of 10 vol.-% oleic acid in n-hexane for 1hr as described in chapter 4. The solvent was dried at 393K for 2 hr in a static oven. The solid was

subsequently calcined at 573K for 3hr in an oven (heating ramp: 3K/min) to decompose any residual oleic acid. The supported catalysts were labelled Cat-Hex-TEOS-63-573K, Cat-Eth-TEOS-63-573K, Cat-Acid-TEOS-63-573K and Cat-Base-TEOS-63-573K for the Co_3O_4 nanocubes modified with tetraethoxysilane in n-hexane, hydrolysis without acid or base, hydrolysis with acid and hydrolysis with a base respectively.

Characterization

The silicon loading of the calcined samples was determined using energy dispersive X-ray analysis (EDX) on a scanning electron microscope (LEO S444 SEM) equipped with a Four Quadrant Back Scatter Detector and an energy dispersive Fissons Kevex X-ray spectrometer. The morphology of the samples was studied with a JEM200CX (JEOL, JAPAN) transmission electron microscope (TEM) operating at 120kV. The samples were prepared by re-suspending the sample powders in chloroform. The phase structure of the model catalysts was determined using a Bruker AXS D8 Advance X-ray laboratory diffractometer operated at 40 kV and 40 mA utilizing a Co source (λ_{Co}-Kα = 0.178897 nm) and a VÅNTEC position-sensitive detector.

The presence of the modifying ligands on the cobalt oxide surface prior to reduction was analysed using an FTIR spectrometer (Nicolet 5700). The sample was prepared by diluting 1.0 mg of the model catalyst with 0.2 g of KBr and then pressed into pellets. A total of 32 scans were taken in the range between 400 and 4000 cm^{-1} for each sample after a background scan of KBr was taken in the transmission mode at the resolution of 8 cm^{-1}.

X-ray photoemission spectroscopy (XPS) spectra of the samples were acquired at room temperature and with an overall energy resolution of 0.6 eV, using a SPECS PHOIBOS 150 hemispherical electron energy analyser and a monochromatized Al Kα photon source (hν = 1486.71 eV). Charging of the sample surface was counteracted by means of a low-energy flood gun (electron energy = 2 eV, electron flux = 20 μA).

Temperature programmed reduction analysis was carried out in Micromeritics AutoChem2950 (Micromeritics Instrument Corp., USA) equipped with a thermal conductivity detector. The samples were prepared by diluting ca. 30 mg Co_3O_4 (modified with silica or unmodified) with 1.0 g SiC to minimize the likelihood of sintering and improve heat transfer to and from the catalyst

particle. The (modified) nanocubes were diluted with SiC by suspending the nanocubes in ethanol (10 mL) and adding the required amount of SiC followed by drying at 333 K for 2 hours. The SiC diluted samples were placed into a quartz reactor in the Micromeritics AutoChem2950 and were dried and degassed at 393K under 50 mL (NTP) /min argon for 1 hour to ensure complete removal of excess moisture and other contaminants. The temperature was successively decreased to 340 K followed by the change in gas composition to 5 % H_2/Ar (vol/vol) keeping the flow rate at 50 mL (NTP)/min. The temperature was linearly increased from 340 K to 1223 K using a constant heating rate of 10 K/min. The quantity of hydrogen consumed was determined as described in chapter 4.

Temperature programmed desorption of CO was performed in Micromeritics AutoChem2920 (Micromeritics Instrument Corp., USA) equipped with a thermal conductivity detector. The supported catalyst (1.0 g) was loaded into the quartz reactor and reduced at 673 K for 1 hour under with (20 mL/min). The gas was switched to helium (50 mL/min) to remove all hydrogen and the temperature was subsequently reduced and held at 393 K for 1 hour. The temperature was further reduced at to 383 K, and CO was dosed into the system for 15 times (0.012 mmol CO per dose per gram of Co). Adsorbed CO was thermally desorbed by ramping the temperature at 10 K/min to 1223 K.

The dispersion of fresh and spent cobalt in the supported catalyst was determined using H_2 chemisorption. This was performed on a Micromeritics ASAP 2020 using the static volume method. The sample holder was loaded with 0.5 g of sample sandwiched between two layers of glass wool. The sample holder was degassed at 383 K overnight to remove any adsorbed moisture. The catalyst was reduced *in situ* for 12 hours at 493 K with hydrogen. Following the reduction, hydrogen was removed from the system using helium as a purge gas prior to evacuation. The H_2-chemisorption was conducted at 398 K.

Fischer-Tropsch synthesis

The Fischer-Tropsch synthesis was performed in a fixed bed reactor system. The catalyst (0.1g (modified) Co_3O_4-nanocubes/0.9 g β-SiC, $d_{particle}$=100 µm) was further diluted with 2.0 g silicon carbide ($d_{particle}$=200-250µm) and loaded into the isothermal zone of a fixed-bed reactor. The catalyst was reduced in hydrogen (40 mL (NTP)/min) at 1 bar and 623 K (heating rate: 5 K/min)

for 16 hours. After the reduction, the catalyst is cooled down to 493 K in argon. The Fischer-Tropsch synthesis is performed at 493 K, 20bar, $(H_2/CO)_{inlet}$=2 and $F_{CO,0}/W$ = 0.28 mmol/(min·g_{co}) for unmodified Co_3O_4 nanocubes and 6.15-9.29 mmol/(min·g_{Co}) for the modified catalyst. Different space velocities were used to achieve a similar conversion levels (ca. X_{CO} = 15 %) for all the catalysts. The Fischer-Tropsch synthesis was performed for 44 hours.

Subsequently, the catalyst bed was flushed with argon for 1 hr and cooled down in argon to room temperature. The spent catalyst was passivated by flowing CO_2 over the catalyst bed at 20 mL (NTP)/min for 2 hours at room temperature. The catalyst was removed by first removing the SiC placed on top of the catalyst bed. The catalyst was then separated from the silicon carbide diluent using a 150 µm sieve. The metal surface area of the spent catalyst sample was determined as described above using static hydrogen chemisorption. This requires accurate knowledge on the cobalt content in the spent sample used for the determination of the metal surface area. To determine the actual amount cobalt in the spent catalyst, the spent catalyst was quantitatively transferred to a polypropylene bottle containing 50 mL of 3 M hydrofluoric acid. The concentration of cobalt in solution was determined using atomic absorption spectrometry (AAS).

5.3. Result and Discussion

Solvent effects on the rate of TEOS uptake

The amount of the tetraethoxysilane adsorbed on the surface of Co_3O_4 was obtained using SEM/EDX. The molar ratio of silicon to cobalt $\left(\frac{Si}{Co}\right)$ increases with increasing exposure time seemingly plateauing after long exposure time (see *Fig. 5-1*). The rate of TEOS-uptake on the sample modified in dry n-hexane seems to accelerate for the first three hours before reaching virtual equilibrium after ca. 4 hours with the $\left(\frac{Si}{Co}\right)$ mole ratio about 63 mmol Si/mol Co. The TEOS-uptake is faster for the sample modified in ethanol (to which some water was added) than for the sample modified in dry n-hexane. Furthermore, the amount of tetraethoxysilane taken up after long exposure time seems to have increased and after an exposure time of 4 hours the Si/Co ratio was ca 75 mmol/mol. This may be ascribed due to the presence of water, which may facilitate hydrolysis of TEOS. For modifying cobalt oxide nanocubes in ethanol/water/glyoxylic acid or ethanol/water/ammonia solvent-mixture, the rate of uptake of tetraethoxysilane on the

surface of Co_3O_4 nanocubes is further enhanced. The sample treated with tetraethoxysilane in ethanol/water/ammonia mixture reaches a virtual equilibrium after 1.7 hours at a molar ratio of $\left(\frac{Si}{Co}\right)$ of ca. 80 mmol/mol while the sample contacted with tetraethoxysilane in ethanol/water/glyoxylic acid mixture seems to equilibrate already after 1 hour with a $\left(\frac{Si}{Co}\right)$ mole ratio of about 91 mmol/mol.

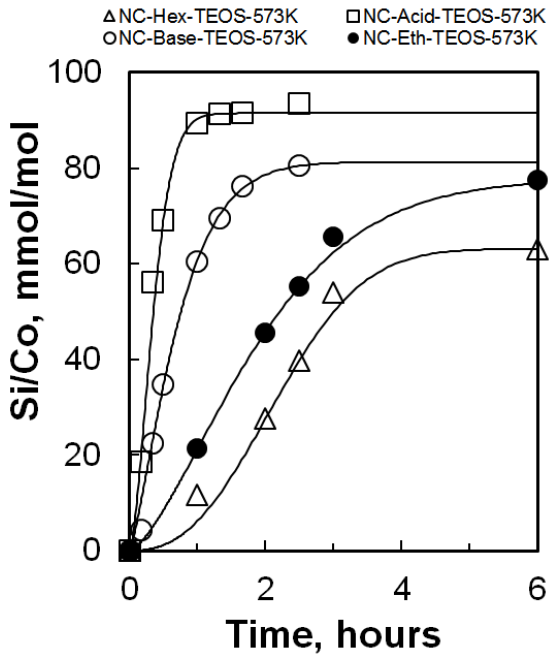

Figure 5-1: Uptake of tetraethoxysilane uptake by Co_3O_4 nano-cubes in various solvent mixture as a function of the time for $[TEOS]_{initial}$ = 6.3 mM (samples calcined at 573 K)

The formation of structures on the surface Co_3O_4-nanocubes (as alluded to in Chapter 4, neso-silicates may be formed in this process) may be modelled as a Johnson-Mehl-Avrami-Kolmogorov [18,19] growth process with an empirical rate of uptake:

$$\left(\frac{Si}{Co}\right) = \left(\frac{Si}{Co}\right)_{equi} . \left(1 - e^{\left(\frac{-t}{\tau}\right)^m}\right) \quad \text{..... Equation 5-1}$$

Where $\left(\frac{Si}{Co}\right)$ is the silicon to cobalt ratio at a particular time t, $\left(\frac{Si}{Co}\right)_{equi}$ is the equilibrium silicon to cobalt ratio, $\boldsymbol{\tau}$ is the time constant of the nucleation process and **m** is the dimensionality of the growth process[18,19]. The specific values of $\boldsymbol{\tau}$ is governed by the rate of constant and the number of nuclei. The best fits are obtained with the parameters shown in *Table 5-2.*

Table 5-2: Modelling the uptake of tetraethoxysilane in different solvent mixtures using the generic Johnson-Mehl-Avrami-Kolmogorov model[18,19]

Solvent	n-hexane	Ethanol/H_2O	ethanol/H_2O + glyoxylic acid	ethanol/H_2O + NH_3
M	2.47 ± 0.59	1.47 ± 0.31	1.64 ± 0.23	1.32 ± 0.31
τ, hours	2.50 ± 0.98	1.23 ± 0.32	0.41 ± 0.09	0.82 ± 0.21
$\left(\frac{Si}{Co}\right)_{equi}$, $\frac{mmol}{mol}$、	63.1 ± 9.6	77.6 ± 4.4	91.5 ± 4.6	81.3 ± 8.2
R^2	0.9988	0.9998	0.9906	0.9956

The $\left(\frac{Si}{Co}\right)_{equi}$ ratio is influenced by solvent and increases in order from n-hexane, ethanol/water, ammonia hydrolysis in ethanol/water to acid catalyzed hydrolysis in ethanol/water. It may be proposed that the $\left(\frac{Si}{Co}\right)_{equi}$ ratio is low when the modification is performed in n-hexane, (water-free environment) because of the low degree of de-ethoxylation in the absence of water resulting in steric hindrance in the adsorption of the bulky tetraethoxysilane on Co_3O_4. On the on other hand, when the modification is performed in a hydrolyzing environment, tetraethoxysilane is partially de-ethoxylated through the hydrolysis process[15,20]. The de-ethoxylation process in presence of water results in silanol species which are less bulky and as such have less steric hinderance and hence can adsorb easily on the surface. The difference in the total uptake of the samples prepared under hydrolyzing atmosphere may thus be related to the rate of production of the Si-OH. And increase in the concentration of silanols may increase the rate of their deposition on the surface of Co_3O_4.

It has been discussed in chapter 4 that the deposited silica oligomers may result in two dimensional thin layers over Co_3O_4 or 3 dimensional islands on the surface. The dimensionality of the growing entity, e.g. silica oligomers, can be obtained from the obtained values of **m**, which was determined to be 2.47 ± 0.59, 1.47 ± 0.31, 1.64 ± 0.23 and 1.32 ± 0.31 for the sample treated with tetraethoxysilane in n-hexane, ethanol/water mixture, mixture containing ethanol/water/glyoxylic acid and mixture containing ethanol/water/ammonia respectively. This implies growth in 2-3 dimensions when modifying in dry n-hexane. The parameter **m** for the samples hydrolysed in water containing solutions (in the

presence/absence of an acid or base) seems to indicate growth of one dimensional (rod-like shape) entities which start growing into two dimensions[19].

The obtained time constant, $\boldsymbol{\tau}$, for the growth of silica on the surface of Co_3O_4 nanocubes in n-hexane, ethanol/water mixture, mixture containing ethanol/water/glyoxylic acid and mixture containing ethanol/water and glyoxylic acid are 2.51 ± 0.93, 1.23 ± 0.10, 0.41±0.09 and 0.82 ± 0.21 hours, respectively. From the inverse relationship of τ and number of nuclei as well as the rate constant of the growth process, a decreasing order of the value of τ when different solvent mixtures are used may imply an increase in the number of silica nuclei or an increased rate of particle growth or a coeffect of both. Indeed, from *Figure 5-1,* it can be deduced that the rate of tetraethoxysilane uptake is higher in the presence of water and adding acid or base accelerates the process and the acid seems to be more effective than base. A similar order in the total amount of tetraethoxysilane taken up after long exposure time seems to have increased and may indicate the difference in the number of silica nuclei per unit volume in the system. An increased number of nuclei may result be the reason of increase the amount of tetraethoxysilane taken up after long exposure time when hydrolysis is used. The concentration of silica nuclei decreases in the order from sample NC-Acid-TEOS, NC-Base-TEOS, NC-Eth-TEOS to NC-Hex-TEOS.

Fourier transform infrared spectroscopy was used to investigate the nature of interaction between Co_3O_4 nanocubes and the modifying silica on the surface of the model catalyst after calcination at 573 K. *Fig. 5-2* shows the FTIR spectra of (un)modified Co_3O_4 in the region 525-700 cm^{-1}. All the samples show absorption bands at 550 cm^{-1} and 658 cm^{-1}. The band at 550 cm^{-1} is ascribed to the vibration of the Co-O stretch while the latter can be ascribed to the stretch vibration of the Co (III)-O bond in the Co_3O_4 lattice[21]. A side band appear at 659 cm^{-1} upon modification. This absorption band can been attributed to the bending modes of the Co-O-Si bonds reported by Yin *et al.*[22] for Co/SiO_2 core-shell structures reduced in hydrogen at 973 K . It may be difficult to recognize this absorption band as it intersects with the absorption bands due to Co (III)-O stretch in the Co_3O_4 lattice occurring at 658 cm^{-1} [21]. This band is more intense on sample modified in the presence of acid, suggesting that the modification in acid results more in the formation of surface cobalt silicates compared to modification in other solvents.

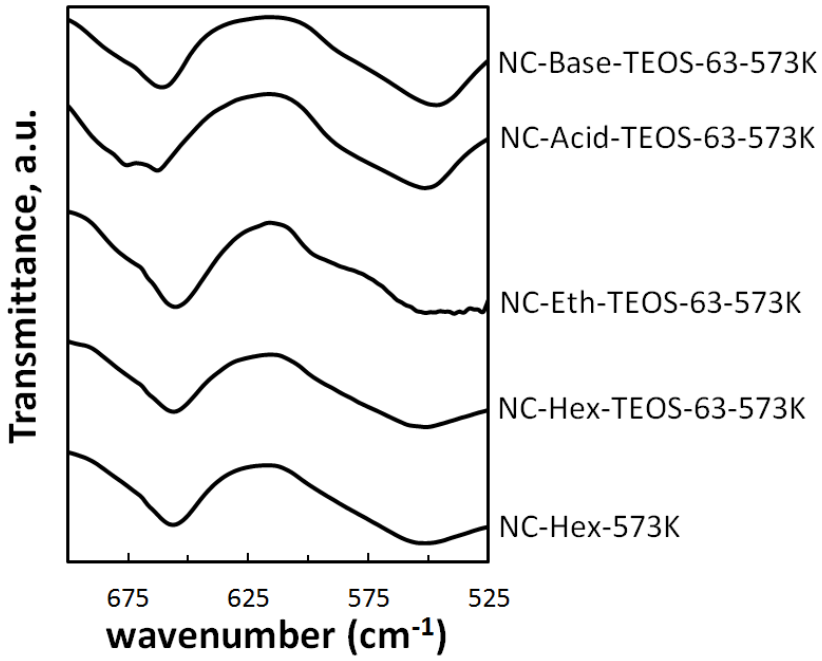

Figure 5-2: FTIR-spectra of unmodified Co_3O_4 nanocubes and Co_3O_4 nanocubes modified by contacting with solutions of tetraethoxysilane in different solvents (525 cm^{-1}-700 cm^{-1}: T_{cal} = 573 K)

Additional absorption bands are observed in the region of 700-1200 cm^{-1} (see *Fig. 5-3*). In this region, ammonia would be expected to show a sharp absorption bands due to the N-H vibrations[23] at 968 cm^{-1}. These absorption bands are not present in the infrared spectrum of sample NC-Base-TEOS-63-573K indicating that ammonia is not present on the surface of the Co_3O_4 nanocubes modified by TEOS in the presence of ammonia. Similarly, a sharp intense characteristic absorption band due glyoxylic acid at 1110 cm^{-1} is not present on the surface of Co_3O_4 nanocubes modified by TEOS in the presence of glyoxylic acid[24]. Ammonia and glyoxylic acid should have been removed during both the washing step and the subsequent calcination at 573 K.

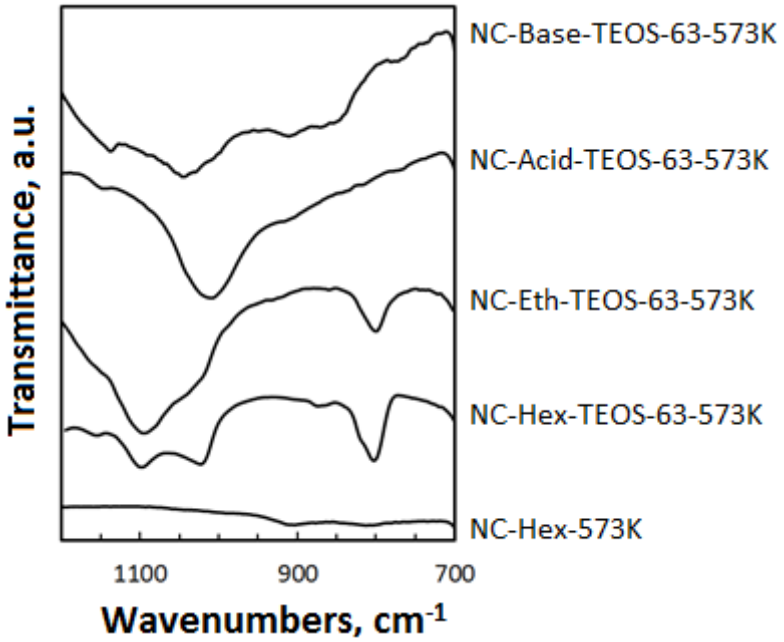

Figure 5-3: FTIR-spectra of unmodified Co_3O_4 nanocubes and Co_3O_4 nanocubes modified by contacting with solutions of tetraethoxysilane in different solvents (700 cm^{-1}-1200 cm^{-1}: T_{cal} = 573 K)

The most intense absorption bands due to the modification process after calcination at 573 K appear at 800 cm^{-1}, 1020 cm^{-1} and 1100 cm^{-1}. As described in Chapter 4, these peaks can be ascribed to the presence of extraneous silica in the modified samples. The band at 800 cm^{-1} can be attributed to the in-plane Si-O-Si bending vibration[22]. The band at 1020 cm^{-1} has been attributed to Co-O-Si vibration[25,26], but may also be attributed to the presence of oligomeric silicate species[27,28]. The simultaneous occurrence of the absorption band at 1020 cm^{-1} and the absorption band at 800 cm^{-1} may indicate that the band at 1020 cm^{-1} is more likely to be attributed to oligomeric silicate species[28] than Co-O-Si vibrations. The band at 1100 cm^{-1} is characteristic of the asymmetric stretching of the Si-O-Si of amorphous SiO_4 tetrahedra[27,29]. The bands at 800 cm^{-1} and 1100 cm^{-1} due to the presence of silica are most intense for samples NC-Hex-TEOS-63-573K, NC-Eth-TEOS-63-573K and NC-Base-TEOS-63-573K. This may be an indication that when the modification is performed in the n-hexane or ethanol/water mixture with or without a base catalyst followed by calcination at 573 K facilitates the formation of silica on the surface of Co_3O_4 nanocubes. The modification in the presence of glyoxylic acid, sample NC-Acid-TEOS-63-573K, shows an intense absorption band at 1020 cm^{-1}. Due to the absence of the strong bands at 800 cm^{-1} and 1100 cm^{-1} on this spectrum of this sample, the band at 1020 cm^{-1} can be assigned to Co-O-Si vibrations[26] suggesting that the modification of Co_3O_4 with tetraethoxysilane in the presence of glyoxylic acid facilitates the formation of surface cobalt silicates. The base of the band at 1020 cm^{-1} for sample NC-Acid-TEOS-63-573K is broad and stretches

from 1100 cm^{-1} to 700 cm^{-1} and therefore the existence of the Si-O-Si vibrations due to oligomeric silicates species cannot be completely excluded[28].

The formation of Co-O-Si bonds can occur either through the condensation reaction between tetraethoxysilane and the surface Co_3O_4 hydroxyl groups or during the calcination stage. To determine at which stage these bonds may have been formed, the infrared spectra of un-calcined modified samples were compared to those of modified samples calcined at 573 K (see *Fig 5-4*). In the presence of dry solvent (n-hexane), the alcohol condensation may be thought to be the dominant chemical reactions resulting in monodentate Co-O-Si species as observed in the adsorption of dimethyl-diethoxysilane on silica[30] and similar to those identified in the analogous iron-silica species[31]. This may result in tetraethoxysilane being not complete de-ethoxylated during the exposure of Co_3O_4 nanocubes to a solution containing tetraethoxysilane. The formation of silica on the surface of Co_3O_4 nanocubes for the sample NC-Hex-TEOS-63-573K is thus more likely to occur during the calcination step.

In fact, the infrared spectra of the un-calcined sample modified in n-hexane shows an absorption band at 1160 cm^{-1} and 1235 cm^{-1} which can be ascribed to the C-H rocking and wagging of the CH_3 in tetraethoxysilane respectively (see *Fig. 5-4).* These absorption bands disappear with a concurrent appearance of broad absorption band from 1100 cm^{-1} and 800 cm^{-1} attributed to the asymmetric stretching of the Si-O-Si of amorphous SiO_4 tetrahedra[27,29] and the in-plane Si-O-Si bending vibration[22] when calcined at 573 K indicating the formation of silica (see Fig. 5-3). A shoulder at 1020 cm^{-1} due to the Co-O-Si vibration[25,26] is also observed. This indicates that the interaction of silica and cobalt is induced by calcination for the sample modified in n-hexane. The presence of tetraethoxysilane which is not fully de-ethoxylated on the sample modified in n-hexane and not yet calcined may further be attested by the additional band ascribed to the asymmetric bending and asymmetric stretch vibration of the C-H bonds (CH_2, CH_3 of tetraethoxysilane) observed at 2900-3000 cm^{-1} (see *Fig. 5-4(right)*).

Conversely, the infrared spectra of the un-calcined sample modified under the hydrolysis conditions both in the presence or absence of acid/base (NC-Eth-TEOS-63, NC-Acid-TEOS-63, NC-Base-TEOS-53) do not shows any absorption band at 1160 cm^{-1} and 1235 cm^{-1} which can be ascribed to the C-H rocking , wagging of the CH_3 in tetraethoxysilane respectively and at 2900-3000 cm^{-1} ascribed to the asymmetric bending and asymmetric stretch vibration of the C-H bonds (CH_2, CH_3 of

tetraethoxysilane) (see *Fig. 5-4).* The absence of these absorption bands may suggest the hydrolysis process de-ethoxylates tetraethoxysilane molecules. However, additional broad bands, on these un-calcined samples are observed in the region 700 cm^{-1} – 1300 cm^{-1}. These bands are of the same pattern observed for the calcined samples in *Figure 5-3.* The most intense absorption bands due to the modification process under hydrolyzing environment appear at 800 cm^{-1}, 1020 cm^{-1} and 1100 cm^{-1}. Calcination of these samples at 573 K does not alter the spectra before and after calcination, leading to the conclusion that calcination does not affect the monitored species.

In this region (700 cm^{-1} – 1300 cm^{-1}), ammonia would be expected to show a sharp absorption bands due to the N-H vibrations[23] at 968 cm^{-1}. These absorption bands are not present in the infrared spectrum of sample NC-Base-TEOS-63-573K indicating that ammonia is not present on the surface of the Co_3O_4 nanocubes modified by TEOS in the presence of ammonia. Similarly, a sharp intense characteristic absorption band due glyoxylic acid at 1110 cm^{-1} is not present on the surface of Co_3O_4 nanocubes modified by tetraethoxysilane in the presence of glyoxylic acid[24]. Ammonia and glyoxylic acid should have been removed during the washing step.

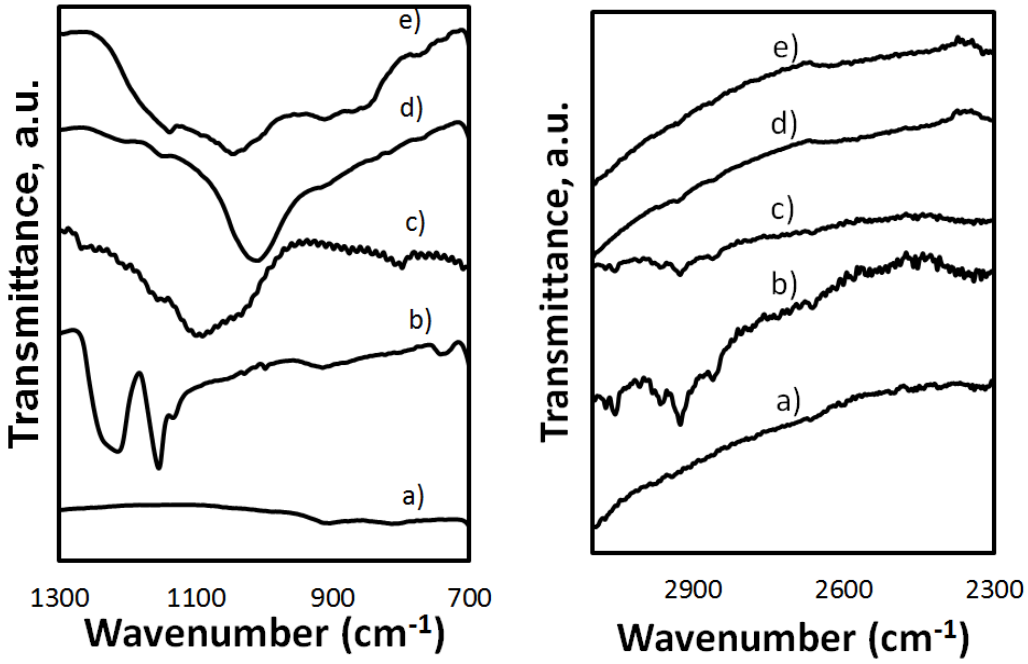

Figure 5-4: Infrared spectra of un-calcined; a) unmodified and samples modified with tetraethoxysilane in b) n-hexane c) water/ethanol mixture d) water/ethanol/glyoxylic acid and d) water/ethanol mixture/ammonia mixture with a silica loading of 63 mmol/mol (Si/Co) in the range of 700-1300 cm^{-1} (left) and in the range of 2300-3100 cm^{-1} (Right)

The introduction of foreign material on a catalyst surface may alter the electronic properties of the catalyst surface. X-ray photoemission spectroscopy was used to determine any change in

the electron binding energy of silica on the surface of Co_3O_4 nanocubes. The photo-emission characteristics of Co 2p of the samples are shown in *Fig. 5-6.* The photoemission features of the unmodified sample show a distinctive photoemission characteristic of Co 2p of pure Co_3O_4 (bottom spectrum) with spin-orbit peaks at ~780.01 eV and ~795.97 eV ascribed to Co $2p_{3/2}$ and Co $2p_{1/2}$, respectively. The modification of Co_3O_4 nanocubes with tetraethoxysilane in n-hexane results in a shift in binding energy of the Co $2p^{3/2}$ peak towards higher binding energies by +0.1 eV. A similar positive shift of +0.3 eV is observed when modification process is carried out in ethanol-water-ammonia mixture. Modifying cobalt(II,III) oxide nanocubes with tetraethoxysilane in a mixture of ethanol-water-glyoxylic acid resulted in a smaller shift of only +0.4 eV. The positive shift may indicate that electron density moves from cobalt towards silicon. The difference in the magnitude of the shift may be attributed to the difference in the interaction of surface cobalt with silica. For instance, de-ethoxylation is limited when TEOS adsorption on Co_3O_4 is performed in n-hexane thus increasing the chances of physisorption. As such the shift in the Co 2p binding energy for this sample may be due to electrostatic interaction of silica and surface cobalt. Similarly, modification under the hydrolysis conditions both in the presence or absence of acid/base results in the initial step may involve de-ethoxylation of TEOS, increasing the chances of formation of either Si-O-Si or Co-O-Si bonds. As described by the FTIR results, the modification in the presence of base seems to yield more Si-O-Si bonds, whereas the modification in the presence of glyoxylic acid seems to yield more Co-O-Si. This may further describe the difference in the magnitude in the shift of the Co 2p binding energy. A shift in the binding energy of the Co $2p^{3/2}$ may be induced by the formation of contact zones (Co-O-Si) , hence a major shift in the binding energy of the Co $2p^{3/2}$ for the sample NC-Acid-TEOS-63-573K may indicate that the modification process in the presence of glyoxylic acid results more into the formation of surface cobalt silicates.

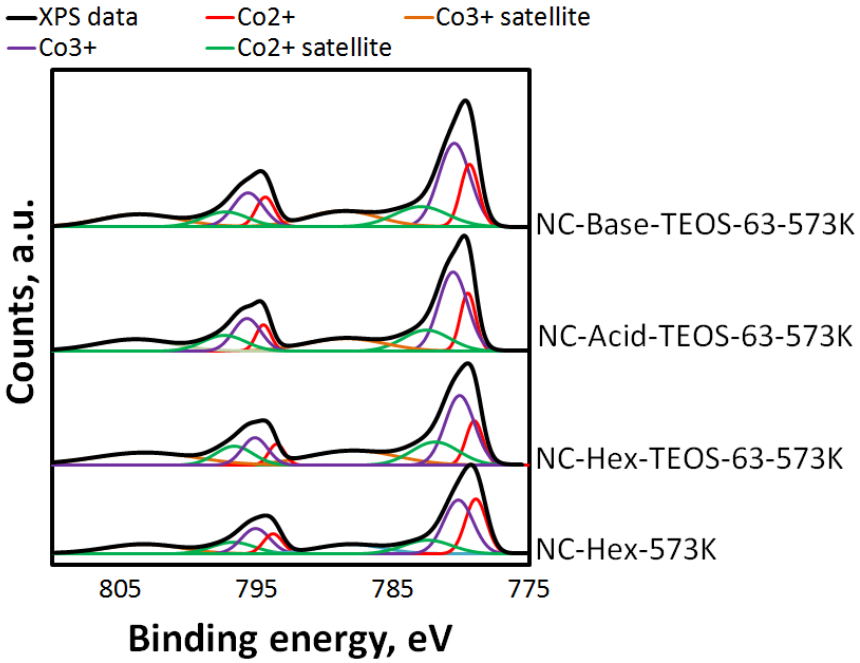

Figure 5-5: X-ray photoemission spectra of Co 2p of unmodified Co_3O_4-nanocubes and Co_3O_4 nanocubes modified with 63 mmol Si/mol by exposing nano-cubes to solutions of tetraethoxysilane in different solvent and subsequently calcined at 573 K

The catalytically active phase in the cobalt-based Fischer-Tropsch catalyst is metallic cobalt[32]. The precursor to the metallic phase is usually the oxidic phase, which needs to be reduced to yield the catalytically active phase. The amount of metallic phase present after activation relative to the initial amount of the oxide present (i.e. degree of reduction) is dependent on the reducibility of the oxide at a specific temperature. Reducibility is usually affected by the extent of the interaction between the active metal and the oxide support[7].

The reduction behaviour is often studied using temperature programmed reduction (TPR). The reduction of unsupported Co_3O_4 occurs via a consecutive two-step reduction process involving the reduction of Co_3O_4 to CoO followed by the reduction of CoO to metallic cobalt[33]. Temperature programmed reduction has previously been employed to extricate the formation and effects of metal-support interactions in cobalt-based catalysts[25,34] . Distortions in the classical temperature programmed reduction profile of Co_3O_4 have been reported for Co_3O_4 dispersed on a supports [25,34,35]. Previous studies[36–38] brought a perception that Co_3O_4 chemically bonded to silica will be more difficult to reduce than unsupported Co_3O_4. Moreover, new peaks may be observed at elevated reduction temperature (873 K-1073 K).

The temperature programmed reduction profiles of the model catalysts are shown in *Figure 5-6.* All model catalysts are completely reduced after being heated in 5% H_2/Ar up to 1223 K as determined from the total hydrogen consumption (*see Table 5-3*). The reduction profiles are normalised with respect to mass of the sample. The quantity of hydrogen consumed was determined integrating the peak area and relating it to the number of H_2 moles by multiplying by the calibration factor as described in *Chapter 4*.

A typical two-stepped reduction process is observed for the reduction of Co_3O_4 nano-cubes[7,34,39] with the first peak reaching a maximum at 580 K and the second peak occurring at 700 K. The first reduction step is fitted to a two-dimensional nucleation model according to Avrami-Erofeev model[18,19], whereas the subsequent reduction steps is thought to be best described according to a uni-molecular decay model[40]. The newly developed high temperature peak due to the interaction of Co_3O_4 with silica was best fitted using unimolecular decay model. It should be noted that a two-step process for Co_3O_4 → CoO → Co would theoretically require the first reduction peak to be 3 times smaller than the second reduction peak from the stoichiometry of reduction shown by chemical *Equation 5-2* and *Equation 5-3*. However, after deconvolution of the peaks, by fitting the whole TPR profile to these two models, the amount of hydrogen required for reduction of the first reduction step, typically assigned to the reduction of Co_3O_4 to CoO, is 4 times smaller than the amount of hydrogen required for the second reduction step. This suggests a slightly more complex reduction mechanism for Co_3O_4-nanocubes. The reason for this distortion in the peak ratios can arise from the crystallite size. The reduction of relatively large (ca. 24 nm), well-crystalline Co_3O_4 nanocubes may involve only reduction of cobalt in the near surface region[41], while the consecutive reduction involves a direct reduction of the bulk directly to metallic Co. In fact, highly crystalline Co_3O_4 has been reported to undergo a direct single reduction step from Co_3O_4 to Co[42].

$$\boldsymbol{Co_3O_4 + H_2 \rightarrow 3CoO + H_2O} \quad \text{.....Equation 5-2}$$

$$\boldsymbol{3CoO + 3H_2 \rightarrow 3Co + 3H_2O} \quad \text{..... Equation 5-3}$$

The peak maxima in the TPR-profiles of the modified model catalysts shifts to higher reduction temperature in comparison to the peak maxima obtained for the Co_3O_4 nano-cubes indication that the reduction process in retarded by the modification process (see *Table 5-2*). This shift is a clear

indication that Co_3O_4 is interacting strongly with the silica substrate either chemically, i.e. bonding to the surface which may affect activation energy, or physically, i.e. hindering access of hydrogen to the surface and hence altering the pre-exponential factor. An additional shoulder ascribed to reduction of cobalt interacting strongly with silica[39,43] appears at temperatures around 800 K. It should however be noted that, although this shoulder is attributed to the presence of surface silicate, the reduction temperature is not high enough to attribute it to the presence of stoichiometric Co_2SiO_4 synthesized and characterized as described in *Chapter 4*. Retardation of a part of the reduction process implies that the presence of silica on the surface of Co_3O_4 hinders the reduction of ionic cobalt suggesting that the silica is chemically bonded to Co_3O_4.

The amount of hydrogen required for the respective reduction steps for the (modified) samples NC-Hex-573K, NC-Hex-TEOS-63-573K, NC-Eth-TEOS-63-573K, NC-Acid-TEOS-63-573K and NC-Base-TEOS-63-573K, are shown in *Table 5-3.* The relative amount of hydrogen consumed for the high temperature reduction peak, which is tentatively ascribed to the reduction of cobalt in surface silicates), amounts to 1.1% of the total amount of hydrogen consumed for Co_3O_4 modified with TEOS in n-hexane. This corresponds to 1 mol of H_2 consumed relative to 4 mol of Si within the sample. This may imply tetraethoxysilane is mainly bonded through silica oligomers. The modification of Co_3O_4 with tetraethoxysilane in either ethanol/water mixture or ethanol/water/base results in an increase in the relative amount of hydrogen consumed for these species reducing at a high temperature to 2.3% and 2.9% of the total amount of hydrogen consumed respectively. This corresponds to 1 mol of H_2 consumed relative to ca. 2 mol of TEOS taken up by the sample indicating a substantial amount of silica present as oligomers in these samples. The largest amount of hydrogen used for the reduction of these difficult to reduce species is observed for the sample, which was modified with tetraethoxysilane in a water/ethanol/glyoxylic acid mixture (5.3% of the total amount of hydrogen consumed, which corresponds to 1 mol of H_2 consumed relative to 1 mol of Si in the sample). The relative amount of hydrogen consumed corresponds to the formation of surface silicates bonded as a monodentate on the surface. Hence, it may be concluded that the use of acid in the modification process reduces the formation of silica oligomers.

The kinetic parameters (activation energy, E_a, and the respective pre-exponential factors, A) for the reduction of Co_3O_4 were evaluated by fitting the whole temperature programmed reduction

profile to the to a two-dimensional nucleation model according to Avrami-Erofeev model[18,19] (for the first reduction peak) and a uni-molecular decay model[40] (for the subsequent reduction steps). The activation energy for the 1st reduction step in the reduction of Co_3O_4 nanocubes assuming the two-dimensional nucleation model was determined to be 34±3 kJ/mol ($A = 10^{0.7\pm0.4}$ s^{-1}), whereas the activation energy for the 2nd reduction step assuming a uni-molecular decay model was determined to be 127±21 kJ/mol ($A = 10^{7.2\pm1.5}$ s^{-1}) (*see Table 5-3*).

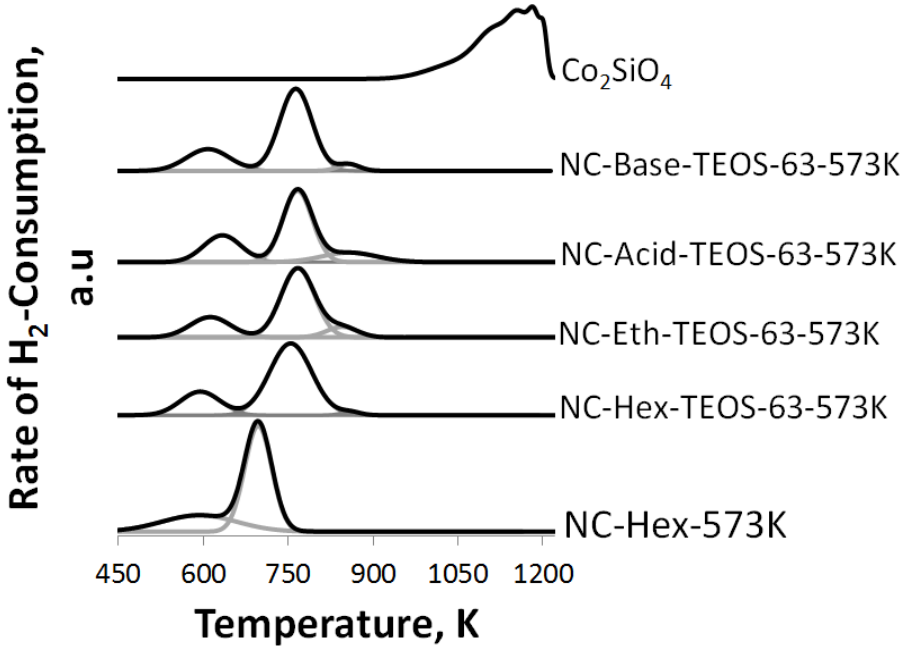

Figure 5-6: Temperature programmed reduction (TPR) profiles of Co_3O_4-nanocubes, and the nanocubes modified by exposing Co_3O_4 nanocubes to TEOS in dry n-hexane (Cat-HEX-TEOS-573K), solution of ethanol and water (Cat-Eth-TEOS-63-573K) , solution of ethanol and water containing glyoxylic acid (Cat-Acid-TEOS-63-573K) and solution of ethanol and water containing ammonia (Cat-Base-TEOS-573K) (ca. 30 mg of sample diluted with 1g of β-SiC; heating rate 10 K/min; 5% H_2 in Ar; grey lines: fit of consecutive two-dimensional nucleation model process and uni-molecular decay processes)

The hydrogen consumption peaks in the temperature programmed reduction profiles of Co_3O_4-nanocubes modified in different solvent/solvent mixtures were also fitted to a two-dimensional nucleation model according to Avrami-Erofeev[18,40] followed by a uni-molecular decay for both the second reduction step and the reduction step tentatively ascribed to reduction of the strongly bound cobalt. Upon modification, the activation required for reduction of Co_3O_4 nanocubes increases differently depending on the solvent used (*See Table 5-3)*. This increase in activation energy explains the shift towards higher reduction temperatures upon addition of tetraethoxysilane to the Co_3O_4 nanocubes. For all samples, both the activation energy for the

nucleus formation and the pre-exponential factor for tetraethoxysilane-modified samples are higher than that for the unmodified Co_3O_4 nanocubes. This would result in a compensation effect on the rate constant of the first reduction step.

However, for the uni-molecular decay of CoO → Co, the activation energy for the reduction process is higher for the tetraethoxysilane-modified samples relative to the unmodified sample while the pre-exponential factor, A, for this reduction step does not seem to vary upon modification in different solvents. Therefore, the delay in the reduction process of CoO → Co is due to an increase in the activation energy but not any changes in the pre-exponential factor. The activation energy for uni-molecular decay for the high temperature reduction peak (i.e. peak ascribed to the reduction of surface silicate) is lower than that of the preceding uni-molecular decay of CoO → Co. This does not seem consistent with previous results where the activation energy for the reduction of cobalt-support was higher than that of the preceding uni-molecular decay of CoO → Co[7]. This may tentatively suggest that the surface cobalt silicates may have been form during the reduction process.

Table 5-3: Hydrogen consumption during temperature programmed reduction of the samples and the derived kinetic parameters from the profile assuming that the first step follows a two dimensional nucleation mechanism, and the other reduction processes occur via a uni-molecular decay

Sample ID	Degree of reduction[a], α, %	Peak number	T_{max} K	H_2-consumption (mol-H_2/mol-Co)	Ea, kJ/mol	A s^{-1}
Cat-Hex-573K	88	1	580	0.26	34±3	$10^{0.7\pm0.4}$
		2	700	1.07	127±21	$10^{7.2\pm1.5}$
Cat-Hex-TEOS-63-573K	82	1	623	0.30	57 ± 11	$10^{1.6\pm0.9}$
		2	798	1.07	195 ± 34	$10^{8.6\pm2.6}$
		3	890	0.05	93 ± 25	$10^{3.5\pm1.4}$
Cat-Eth-TEOS-63-573K	83	1	625	0.23	61 ± 8	$10^{1.9\pm1.1}$
		2	777	1.05	177 ± 29	$10^{7.9\pm3.4}$
		3	855	0.06	87 ± 11	$10^{4.1\pm0.4}$
Cat-Acid-TEOS-63-573K	80	1	646	0.29	55 ± 9	$10^{2.2\pm1.1}$
		2	773	0.99	188 ± 49	$10^{6.8\pm2.7}$
		3	874	0.07	103 ± 15	$10^{2.6\pm0.9}$
Cat-Base-TEOS-63-573K	85	1	620	0.29	66 ± 13	$10^{1.2\pm0.8}$
		2	775	1.02	201 ± 45	$10^{7.1\pm1.8}$
		3	866	0.04	92 ± 8	$10^{4.2\pm1.6}$

[a] Degree of reduction determined after reducing the catalysts at 623 K for 16 hours with hydrogen

Figure 5.7 shows the hydrogen uptake of the reduced samples supported on β-SiC (10 wt-%) as a function of the hydrogen pressure. The total amount of chemisorbed hydrogen normalized with respect to the amount of cobalt in the catalyst seems to be slightly suppressed on the reduced samples after modification with tetraethoxysilane (TEOS) (see also Table 5-3). The total amount of hydrogen adsorbed by cobalt may be indirectly related to the degree of reduction of the cobalt precursor oxide (Co_3O_4 nanocubes) to metallic cobalt. The degree of reduction of the model catalysts were determine and shown in *Table 5-3*. It can be further noted that the hydrogen uptake on the sample modified with TEOS in a mixture of ethanol/water/glyoxylic acid seems to be more suppressed than the samples modified with TEOS in either n-hexane or ethanol/water (even in the presence of a base).

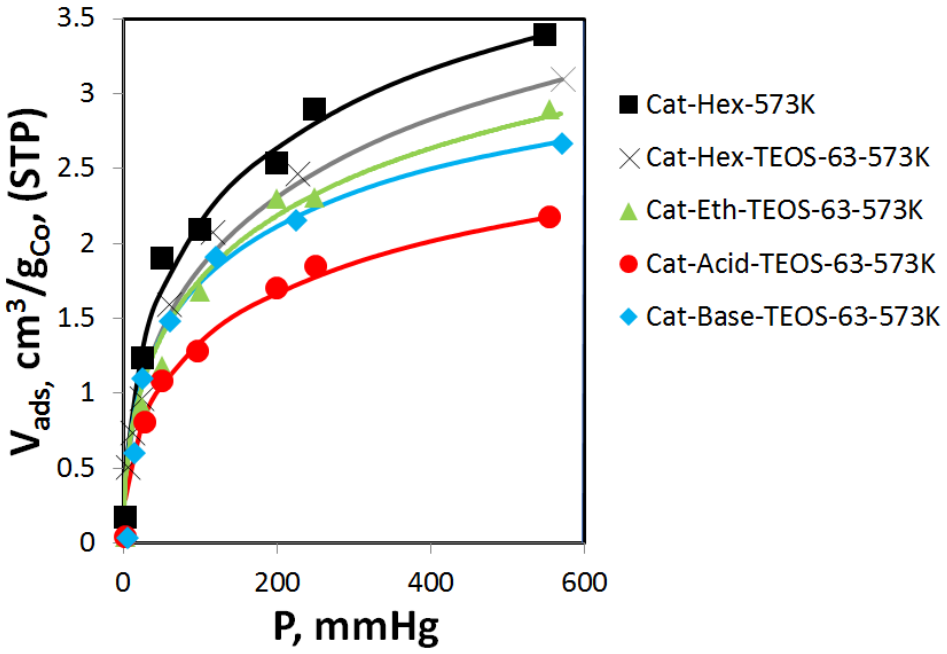

Figure 5-7: Hydrogen uptake on fresh catalyst samples calcined at 573 K and reduced at 623 K for 16 hours with H_2; Solid lines represent fit of the hydrogen uptake data to a Langmuir isotherm

The H_2 uptake on the surface of the reduced Co_3O_4 can be best described using the Langmuir isotherm assuming dissociative adsorption of hydrogen. A decrease in the total amount of chemisorbed hydrogen onto the surface of Co_3O_4 nanocubes upon modification indicates a decrease in the amount of available metal surface area after reduction of the Co_3O_4 nanocubes at 623 K for 16 hours (see *Table 5-4*). This difference in the total H_2 chemisorption may suggest the silicate islands interacts at different extents with Co_3O_4. The unmodified samples seem to indicate a dispersion of ca. 3%. A complete surface cobalt coverage would be obtained at a Si

loading of 30 mmol/mol if each tetraethoxysilane molecule occupies a single cobalt site. Thus, a tetraethoxysilane loading of about 63 mmol/mol $\left(\frac{Si}{Co}\right)$, would be expected to completely cover the surface cobalt since the $\left(\frac{Si}{Co_{Surface}}\right)$ ratio is 2:1. This may result in a complete suppression of H_2 uptake on the surface. However, a complete suppression in H_2 chemisorption is not achieved indicating Si did not cover of surface cobalt atoms. The amount of surface cobalt covered by silane molecules $(Co_{Covered})$ can be estimated from the amount hydrogen adsorbed on the unmodified sample and the amount of hydrogen adsorbed on the modified sample. The $\left(\frac{Si}{Co_{Covered}}\right)$ ratio may give an idea of how the silane adsorbs onto the surface of cobalt (see Table 7-5). When modified with tetraethoxysilane in n-hexane, the $\left(\frac{Si}{Co_{Covered}}\right)$ ratio varies from 6.8 to 29. However, a sample with a homogeneous dispersion of tetraethoxysilane only forming a monolayer without cross-linkage with a dispersion of ca. 3% would result in the $\left(\frac{Si}{Co_{Covered}}\right)$ of 2, suggesting 2 tetraethoxysilane molecule per atom of cobalt. The $\left(\frac{Si}{Co_{Covered}}\right)$ was 29 mol/mol when the modification was done in n-hexane (NC-Hex-TEOS-63-573K) and decreases to when the modification in hydrolysing environment (NC-Eth-TEOS-53 573 K = 20 mol/mol; NC-Base-TEOS-63-573K) with the modification in the presence of glyoxylic acid (NC-Acid-TEOS-63-573K) having the smallest $\left(\frac{Si}{Co_{Covered}}\right)$ ratio 6.8. The relatively high uptake of tetraethoxysilane points towards the formation of oligomers on the surface[27]. This may further indicate that with tetraethoxysilane in n-hexane, ethanol/water mixture and in the presence of a base, relatively larger clumps of silica are formed on relatively small amount of cobalt whereas the tetraethoxysilane modification in the presence of glyoxylic acid seem to cover more of the surface cobalt.

The spent catalyst was passivated and recovered, after which the hydrogen uptake on the re-reduced spent catalyst was determined (*see Table 5-4*). The hydrogen uptake on the re-reduced, spent catalyst does not change much. The measured uptake corresponds to a dispersion of 2-3.1% implying metal particle sizes between 14 and 20 nm. This would indicate minimal sintering/particle break-up upon catalyst activation and Fischer-Tropsch synthesis thus a change in the metal surface area cannot account for the difference in the activity.

Table 5-4: The amount of hydrogen taken up to form a monolayer on the catalyst reduced at 623 K for 16 hours (and the spent catalyst) and the amount of CO desorbed as per TPD analysis (total amount of CO dosed= 0.18 mmol/g_{Co})

Catalyst ID	Hydrogen uptake cm^3 H_2 (STP)/g_{Co}		Dispersion, %	
	Fresh catalyst	Spent catalyst	Fresh catalyst	Spent catalyst
Cat-Hex-573K	5.8±0.4	6.1±0.0	3.1	3.2
Cat-Hex-TEOS-63-573K	5.4±1.7	5.6± 0.8	2.8	2.9
Cat-Eth-TEOS-63-573K	5.2±0.6	5.5± 0.7	2.7	2.9
Cat-Acid-TEOS-63-573K	4.0± 0.1	3.6 ± 0.9	2.1	1.8
Cat-Base-TEOS-63-573K	5.0 ± 0.9	4.9 ± 0.6	2.6	2.5

Temperature programmed desorption of CO was used to characterize the chemisorption properties of reduced Co_3O_4 after modification with tetraethoxysilane in different solvents and calcination at 573 K (see *Fig. 5-8*)**.** This study was performed on supported catalysts. The CO-TPD profiles were fitted with a set of Gaussian curves. However, using Gaussian functions to deconvolute the TPD-spectra may not be very accurate when applied in the desorption process as the desorption process itself is a complex process. The desorption profiles of the model catalysts show two strong features with peak maxima at ca. 730 K and above 1000 K and weaker features at ca. 830K and 940 K. The multiple peaks shows that CO is adsorbed differently on the surface of cobalt suggesting a possibility of many different adsorption sites[44]. It should be noted that these desorption peaks occur at relatively high temperatures compared to the previously recorded desorption temperatures of CO from a cobalt surface[44,45]. This shift to higher temperatures may be not be very dissimilar to shift observed by Zagli and Falconer[46] attributed to the re-adsorption of desorbed CO. It should be noted, that the amount of catalyst loaded into the reactor for this temperature programmed desorption experiments was high to obtain a good signal-to-noise ratio, which would have resulted in an increase the likelihood of CO re-adsorption. The desorption peaks may originate from either the desorption of CO from dissimilar binding state or because of a coverage-dependent desorption. The peak at 730 K may be ascribed to the desorption of weakly bound CO which adsorbs associatively and those at 800 K and above are ascribed to the strongly bound CO which chemisorb dissociatively.

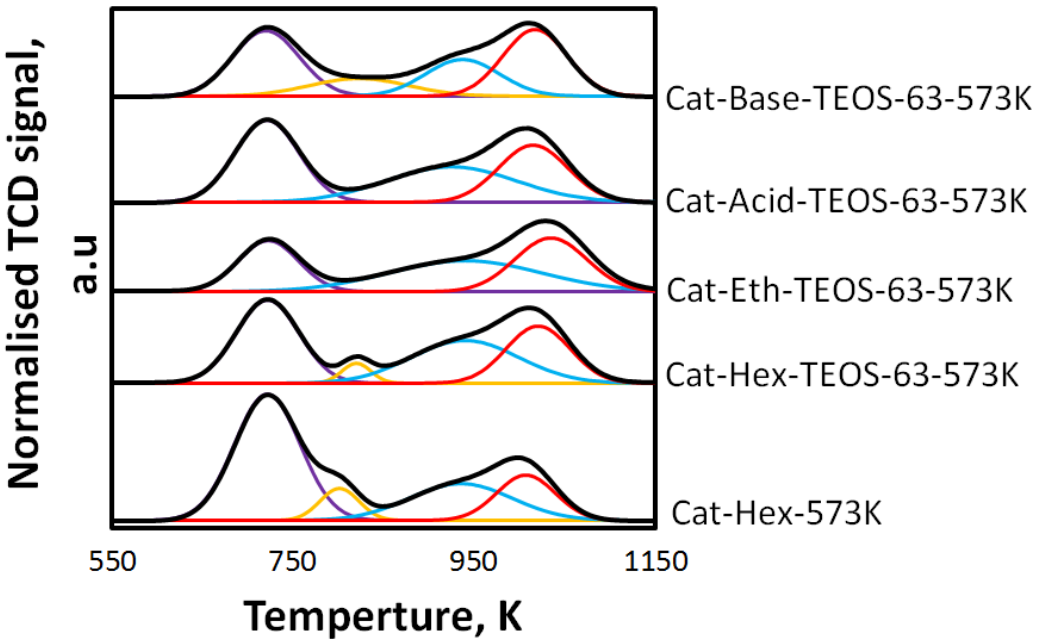

Figure 5-8: Temperature programmed desorption of CO from the unmodified catalyst and the catalyst modified by exposing Co_3O_4 nanocubes to TEOS in dry n-hexane (Cat-HEX-TEOS-573K), solution of ethanol and water (Cat-Eth-TEOS-63-573K) , solution of ethanol and water containing glyoxylic acid (Cat-Acid-TEOS-63-573K) and solution of ethanol and water containing ammonia (Cat-Base-TEOS-573K) (all catalyst supported on β-SiC (10 wt-%); heating rate 10 K/min; T_{red} = 623 K for 16 hours using 5% H_2 in Ar).

The total amount of CO adsorbed on the surface of the reduced, supported (modified) catalyst decreases by about a 20% in comparison to the unmodified, reduced, supported catalyst (*see also Table 5-4).* This indicates that the silica on the surface either blocks the adsorption sites or the electronic properties of cobalt are modified such that CO adsorption is hindered in a way. The temperature programmed desorption profiles of CO on the reduced samples change upon modification of the Co_3O_4 nanocubes with TEOS and new desorption peaks are seen to develop with the reduction of others (see *Fig. 5-8*)**.** This may suggest that new adsorption sites for CO are formed due to the interaction with silica. The ratio of the amount of CO desorbed attributed to the first desorption peak (associatively adsorbed CO) and amount of CO adsorbed attributed to the high temperature desorption peaks (dissociatively adsorbed CO) (see *Table 5-3)* is 1.05 for the unmodified Co_3O_4 catalyst. The ratio of the areas decreases drastically upon modification and the ratios become, 0.61, 0.54, 0.62 and 0.50 for catalysts, CAT-Hex-TEOS-63-573 K, CAT-Eth-TEOS-63-573K, CAT-Acid-TEOS-63-573K, and CAT-Base-TEOS-63-573 K. CO dissociation is thought to occur at higher temperatures after some CO has desorbed. A lower ratio of the

amount of CO desorbed at low temperature relative to the amount of CO desorbed at high temperature could imply a more facile dissociation of CO during the desorption process. It is thus implied that the modification of Co_3O_4 with TEOS enhances CO dissociation on the finally reduced catalyst.

Table 5-5: Relative amount of CO desorbed as molecularly adsorbed CO versus dissociatively adsorbed CO for samples dosed 15 times with 0.012 mmol CO/g_{Co} per dose

Catalyst ID	Amount of CO desorbed mmol CO (STP)/g_{Co}					Ratio of Peaks (A/B)
	Total	Peak A	Peak B			
		Peak 1 ~720 K	Peak 2 ~830K	Peak 3 ~940K	Peak 4 >1000K	
Cat-Hex-573K	0.179	0.093	0.014	0.043	0.029	1.08
Cat-Hex-TEOS-63-573K	0.156	0.059	0.006	0.051	0.040	0.61
Cat-Eth-TEOS-63-573K	0.158	0.052	-	0.069	0.057	0.54
Cat-Acid-TEOS-63-573K	0.147	0.056	-	0.049	0.042	0.62
Cat-Base-TEOS-63-573K	0.150	0.050	0.020	0.031	0.049	0.50

The effects of method of preparation of the catalyst Cat-Hex-573K, Cat-Eth-TEOS-63-573K, Cat-Acid-TEOS-63-573K and Cat-Base-TEOS-63-573K on the activity and selectivity in the Fischer-Tropsch synthesis was studied at a constant level of CO-conversion of ca. 15% (20 bar, 493 K), H_2/CO ratio = 2). This was achieved by adjusting the space velocity. i.e. tuning the inlet flow rate of synthesis gas (see *Table 5-4*). The process seems to reach steady stead after a time of about 12-16 hours on line for all catalysts (see *Fig. 5.9*) and the catalyst activity remains constant for over 44 hours on stream. The presence of the silica on the surface Co_3O_4 nanocubes increases the rate of CO consumption in order from Cat-Hex-573K, Cat-Hex-TEOS-63-573K, Cat-Eth-TEOS-63-573K, Cat-Base-TEOS-63-573K and Cat-Acid-TEOS-63-573K. it may be anticipated that the catalytic activity of the modified samples would be reduced in comparison to the unmodified catalyst (Cat-Hex-573K) because of the reduced surface area upon modification. Nevertheless, the activity of the modified catalysts is drastically improved, suggesting the reactivity of the cobalt surface has been enhance by the modification.

The modification of Co_3O_4 with this silica increases the turnover frequency of Co_3O_4 from 0.02 s^{-1} to 0.20-0.66 s^{-1} of the silica modified catalysts (see *Table 5-4*). Although, the correlation of the catalyst

properties (i.e. surface area) and the catalytic performance may seem to be contradictory, this may indicate that the reactivity of the exposed surface was altered upon modification with tetraethoxysilane. This improvement in performance might be ascribed to an alternative reaction pathway for CO-dissociation due to the presence of the silica structures. The rate of CO conversion in Fischer-Tropsch synthesis depends primarily on the rate of dissociation of CO on the surface of a catalyst[47,48]. Due to their low degree of polymerization, silica surface species on the surface of cobalt may possess a relatively high amount of Si-OH terminations. The interaction of such hydroxyl groups at the interface between the silicate island and cobalt may lower the activation barrier for CO-dissociation analogue to the hydrogen assisted CO-dissociation mechanism proposed by Ojeda *et al*.[48]. Theoretical results obtained a Co(111) surface modified with an alumina ligand containing with hydroxyl groups[47] also indicated that hydroxyl groups may accelerate CO dissociation. In fact, it has been shown in many instances that the modification in the CO dissociation barrier is usually result in enhanced catalytic activity for the CO hydrogenation[47,49]. A similar analogy may be used to substantiate the hypothesis that the hydroxyl groups attached to the silica in proximity to the catalytically active, metallic cobalt may interact with CO adsorbed on cobalt surface. Besides the possible interaction of the Si-OH species with CO, any electronic modification on surface cobalt atoms may alter the adsorption properties of CO and thus the rate of CO hydrogenation as well as the selectivity in this reaction. On the other hand, considering the relationship between degree of reduction, chemisorption properties and the catalytic performance, it should be expected that with reduced degree of reduction (*see Table 5-4*), and total adsorbate capacity, the catalyst performance be reduced.

Methane selectivity is a function of conversion. Thus, when the catalysts are tested at same conversion, methane selectivity may be expected to be similar. The selectivity to methane remains almost constant for all catalyst over a period of 44 hours (see *Fig. 5-9: right*). The methane selectivity for the unmodified catalyst (Co_3O_4) is 9.9%. Upon modification with tetraethoxysilane, Cat-Hex-TEOS-63-473K shows 8.6 % selectivity to methane whilst the selectivity towards methane increased for the catalyst Cat-Eth-TEOS-63-473K, Cat-Acid-TEOS-63-473K, and Cat-Base-TEOS-63-473K to 10.1%, 12.4% and 13.3% respectively. This indicates that the modification reduces the methane selectivity. This decrease in methane content can be attributed to the improved rate of CO dissociation. The increased rate of CO dissociation may consequently lead to increased coverage of the cobalt surface with C_1 species which in turn reduces the hydrogen to CO ratio on the surface of

cobalt with a limited hydrogen thus increasing the probability of chain growth[41,50,51]. This may also explain the observed increase in chain growth probability.

The major products of the Fischer-Tropsch synthesis over cobalt catalysts are olefins and paraffins[52]. The effects of method of preparation of the modified cobalt catalysts on the selectivity to olefins was investigated based on C_{2-5} fractions of the chromatograms (see *Fig. 5-10*). The olefin content obtained over the modified catalysts in the C_{2-5} fraction is always lower than the olefin content in the same carbon number range over the unmodified Co_3O_4 indicating that the modification of Co_3O_4 nanocubes with tetraethoxysilane facilitates the formation of paraffins over olefins in the C_{2-5} fractions. This may similarly be attributed to the enhance rate of CO dissociation which may lead to increased paraffin content.

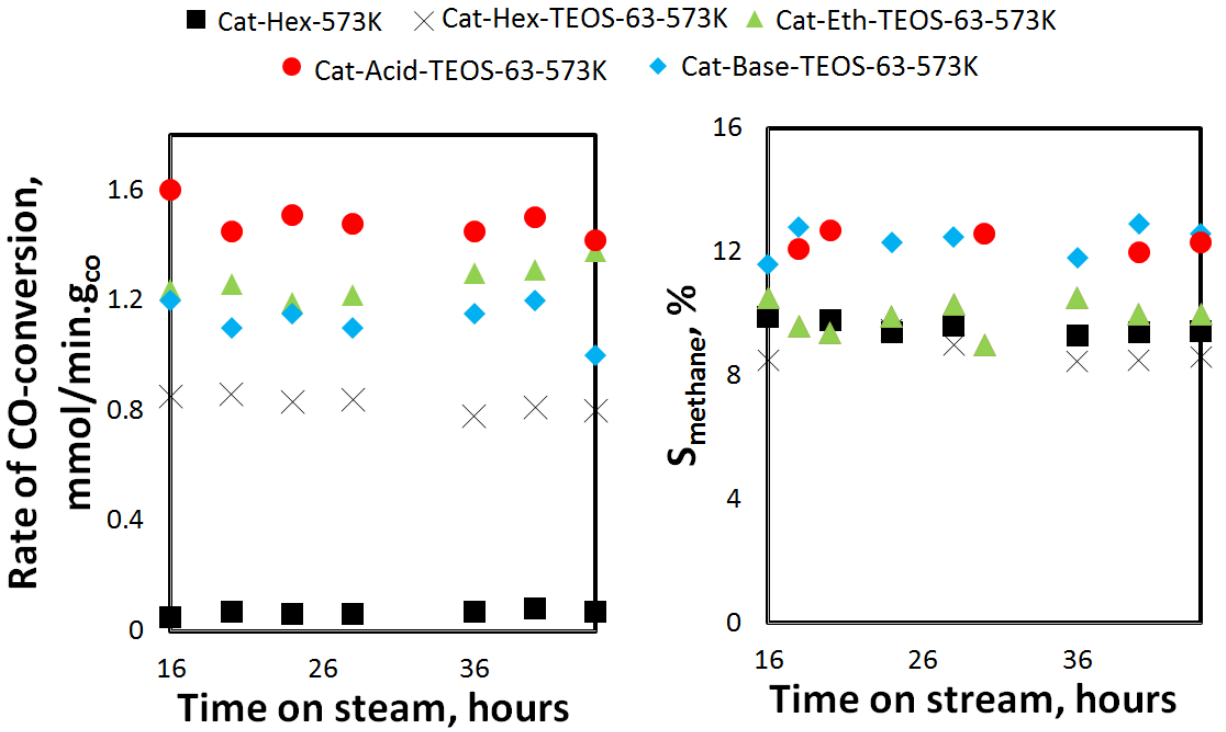

Figure 5-9: Effects of modifying Co_3O_4 with tetraethoxysilane in various solvent on the activity in Tropsch synthesis (20 bar, 493 K, H_2:CO = 2). on the Left: CO conversion as a function of time on stream and on the Right: methane selectivity as a function of time on stream

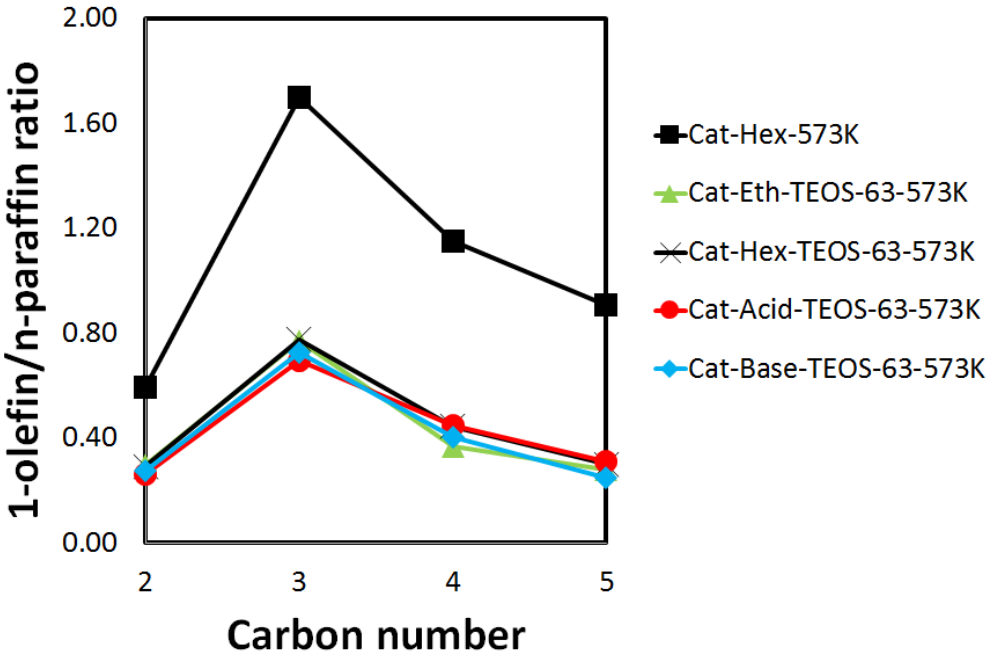

Figure 5-10: Ratio of 1-olefin/n-paraffin in the Fischer-Tropsch product as a function of chain length (in the region C_2 - C_5) after 44 hours on stream for the different model catalyst

Table 5-6: Comparison of activity, methane selectivity at ~15% CO conversion

Catalyst ID	**X_{CO}[a], %**	**$F_{CO,0}/W$, mmol/ ($s \cdot g_{Co}$)**	**TOF[b] s^{-1}**	**S_{CH4} C-%**
Cat-Hex	15.1	0.005	0.00101	9.9
Cat-Hex-TEOS-63-573K	14.6	0.103	0.0322	8.6
Cat-Eth-TEOS-63-573K	14.7	0.131	0.0423	10.4
Cat-Acid-TEOS-63-573K	15.9	0.155	0.0689	12.4
Cat-Base-TEOS-63-573K	14.4	0.140	0.0567	12.6

[a] Activity after 44 hrs on stream;

[b] turnover-frequency based on a cobalt dispersion from H_2 chemisorption before or after the Fischer-Tropsch synthesis:

5.4. Conclusions

In this chapter, the effectiveness of deposition method was investigated by varying solvent and using solvent mixtures containing a base (NH_3) or an acid (glyoxylic acid) on the modification of Co_3O_4 nanocubes with of tetraethoxysilane. Modification of Co_3O_4 nanocubes with tetraethoxysilane in n-hexane may occur through alcohol condensation, resulting in

tetraethoxysilane surface species with are not completely de-ethoxylated. De-ethoxylation can be effectuated by calcination at 573 K. This is confirmed by the disappearance of the C-H absorption bands from tetraethoxysilane in the infrared spectrum of sample NC-Hex-TEOS-63-573K. De-ethoxylation results in the formation of silica which in turn interact intimately with cobalt. Modification in a hydrolysing environment de-ethoxylates tetraethoxysilane even without calcination yielding silica oligomers on the particles. The modification of Co_3O_4 nanocubes with small amounts of tetraethoxysilane yields, besides silicate oligomers around the particles, to attachment of silicate species to the Co_3O_4 nano-particle as indicated by FTIR. The attachment varies with a solvent mixture used and more attachments are obtained when the modification is performed in a hydrolysing environment; particularly in the presence of glyoxylic acid.

The presence of the small amount silicate species of the surface of Co_3O_4 increases the turnover frequency and alters the selectivity in the Fischer-Tropsch synthesis. While the silicon loading of the model catalyst is the same, the catalytic activity of the sample modified in the presence of glyoxylic acid is high relative to the other catalysts. This may be related to the increased Co-O-Si attachments of this catalyst.

5.5. References

1 G. Schwab, *Adv. Catal.*, 1978, **27**, 1–22.

2 J. Liu, S. Zhang, Y. Zhou, V. Fung, L. Nguyen, D. E. Jiang, W. Shen, J. Fan and F. F. Tao, *ACS Catal.*, 2016, **6**, 4218–4228.

3 K. Hayek, M. Fuchs, B. Klotzer, W. Reichl and G. Rupprechter, *Top. Catal.*, 2000, **13**, 55–66.

4 A. Ostroverkh, V. Joha, P. Kús, S. Romana and V. Matolin, *Langmuir*, 2016, **32**, 6297–6309.

5 Y. Yang, J. Evans, J. A. Rodriguez, G. M. White and P. Liu, *Phys. Chem. Chem. Phys.*, 2010, **12**, 9909–9917.

6 C. H. Mejia, T. W. van Deelen and K. P. De Jong, *Nat. Commun.*, 2018, **9**, 4459–4465.

7 A. P. Petersen, R. P. Forbes, S. Govender, P. J. Kooyman and E. van Steen, *Catal. Letters*, 2018, **148**, 1215–1227.

8 M. Cargnello, P. Fornasiero and M. J. Gorte, *Catal. Letters*, 2012, **142**, 1043–1048.

9 L. Guczi, K. Frey, A. Beck, G. Petõ, C. S. Daróczi, N. Kruse and S. Chenakin, *Appl. Catal. A*

Gen., 2005, **291**, 116–125.

10 L. Macheli, A. Roy, E. Carleschi, B. P. D. Doyle and E. van Steen, *Catal. Today*, , DOI:https://doi.org/10.1016/j.cattod.2018.10.

11 W. Stober and A. Fink, *J. Colloid Interface Sci.*, 1968, **26**, 62–69.

12 S. Bhakta, K. C. Dixit, I. Bist, K. A. Jalil, S. L. Suib and J. F. Rusling, *Mater. Res. Express*, 2017, **3**, 1–14.

13 M. T. Harris, R. R. Brunson and C. H. Byers, *J. Non. Cryst. Solids*, 1990, **121**, 397–403.

14 L. V. Ng and A. V McCormick, *J. Phys. Chem.*, 1996, **100**, 12517–12531.

15 K. Kamiya, T. Yoko and H. Suzuki, *J. Non. Cryst. Solids*, 1987, **93**, 407–414.

16 J. Feng and H. C. Zeng, *Chem. Mater.*, 2003, **15**, 2829–2835.

17 X. Liu, G. Qiu and X. Li, *Nanotechnology*, 2005, **16**, 3035–3040.

18 M. Avrami, *J. Chem. Phys.*, 1939, **7**, 1103–1112.

19 M. Avrami, *J. Chem. Phys.*, 1942, **9**, 177–184.

20 O. Malay, I. Yilgor and Y. Z. Menceloglu, *J. Sol-Gel Sci. Technol.*, 2013, **67**, 351–361.

21 O. A. Fouad, S. A. Makhlouf, G. A. M. Ali and A. Y. El-Sayed, *Mater. Chem. Phys.*, 2011, **128**, 70–76.

22 X. J. Yin, K. Peng, A. P. Hu, L. P. Zhou, J. H. Chen and Y. W. Du, *J. Alloys Compd.*, 2009, **479**, 372–375.

23 M. Preuss and F. Bechstedt, *Phys. Rev. B - Condens. Matter Mater. Phys.*, 2006, **73**, 1554131–1554138.

24 J. J. Nájera, C. J. Percival and A. B. Horn, *Phys. Chem. Chem. Phys.*, 2009, **11**, 9093–9103.

25 I. Puskas, T. H. Fleisch, J. B. Hall, B. L. Meyers and R. T. Roginski, *J. Catal.*, 1992, **134**, 615–628.

26 A. H. Kababji, B. Joseph and J. T. Wolan, *Catal. Letters*, 2009, **130**, 72–78.

27 D. G. Kurth and T. Bein, *Langmuir*, 1995, **11**, 3061–3067.

28 X. Yang, P. Roonasi and A. Holmgren, *J. Colloid Interface Sci.*, 2008, **328**, 41–47.

29 X. Huang and Z. Chen, *J. Cryst. Growth*, 2004, **271**, 287–293.

30 D. W. Sindorf and G. E. Maciel, *J. Am. Chem. Soc.*, 1983, **105**, 3767–3776.

31 R. P. Mogorosi, N. Fischer, M. Claeys and E. van Steen, *J. Catal.*, 2012, **289**, 140–150.

32 J. X. Liu, P. Wang, W. Xu and E. J. M. Hensen, *Engineering*, 2017, **3**, 467–476.

33 N. Fischer, M. Minnermann, M. Baeumer, E. van Steen and M. Claeys, *Catal. Letters*, 2012, **142**, 830–837.

34 E. van Steen, G. S. Sewell, R. a. Makhothe, C. Micklethwaite, H. Manstein, M. de Lange and C. T. O'Connor, *J. Catal.*, 1996, **229**, 220–229.

35 O. J. Olusola and M. Sudip, *J. Pet. Technol. Altern. Fuels*, 2016, **7**, 1–12.

36 H. Ming, in *Cobalt: Characteristics, compounds and applications*, ed. L. J. Vidmar, Nova Science Publishers, Inc., 2011, pp. 1–38.

37 H. Ming and B. G. Baker, *Appl. Catal. A, Gen.*, 1995, **123**, 23–36.

38 D. Barkhuizen, I. Mabaso, E. Viljoen, C. Welker, M. Claeys, E. van Steen and J. C. Q. Fletcher, *Adv. Mater.*, 2006, **78**, 1759–1769.

39 R. Xie, D. Li, B. Hou, J. Wang, L. Jia and Y. Sun, *CATCOM*, 2011, **12**, 589–592.

40 H. Y. Lin and Y. W. Chen, *Mater. Chem. Phys.*, 2004, **85**, 171–175.

41 L. Hu, K. Sun, Q. Peng, B. Xu and Y. Li, *Nano Res.*, 2010, **3**, 363–368.

42 P. Arnoldy and J. A. Moulijn, *J. Appl. Sci.*, 1985, **93**, 38–54.

43 M. P. Rosynek and C. A. Polansky, *Appl. Catal.*, 1991, **73**, 97–112.

44 B. Viswanathan, R. Gopalakrishnan and R. Vetrivel, *React. Kinet. Catal. Lett.*, 1982, **18**, 209–212.

45 W. Jiawei, J. Chen, Q. Guo, H. Su, D. Dai and X. Yang, 2017, **663**, 56–61.

46 E. Zagli and J. L. Falconer, *J. Catal.*, 1981, **69**, 1–8.

47 T. van Heerden and E. van Steen, *Faraday Discuss.*, 2017, **197**, 87–99.

48 M. Ojeda, F. Jose, P. Terreros, S. Rojas, T. Herranz and L. G. Fierro, *Langmuir*, 2006, **22**, 3131–3137.

49 M. A. Vannice, *J. Catal.*, 1977, **50**, 129–134.

50 V. P. Santos, T. A. Wezendonk, J. J. D. Jaén, A. I. Dugulan, M. A. Nasalevich, H. U. Islam, A. Chojecki, S. Sartipi, X. Sun, A. A. Hakeem, A. C. J. Koeken, M. Ruitenbeek, T. Davidian, G. R. Meima, G. Sankar, F. Kapteijn, M. Makkee and J. Gascon, *Nat. Commun.*, , DOI:10.1038/ncomms7451.

51 J. Yang, W. Ma, D. Chen, A. Holmen and B. H. Davis, *Appl. Catal. A Gen.*, 2014, **470**, 250–260.

52 R. A. van Santen, I. M. Ciobîcâ, E. van Steen and M. M. Ghouri, *Adv. Catal.*, 2011, **54**, 127–187.

6. **Metal-support interactions in SiO_2/Co inverse catalyst for Fischer-Tropsch synthesis: effects of calcination temperature during the modification**

The formation of cobalt silicate in the inverse SiO_2/Co systems during calcination step in the preparation of catalysts is not easy to follow using a single technique. However, using both infrared spectroscopy and temperature programmed reduction it can be shown that calcination temperature is a key factor in the formation of cobalt silicate. Low temperature calcination (573-773 K) results in the formation of cobalt strongly interacting with silica. However, increasing the temperature to 873 K seems to result in weaker interactions between cobalt and silica. Only high temperature calcination results in the formation of cobalt silicate (Co_2SiO_4).

6.1 Introduction

The current endeavours in energy and fuel technology require use of discrete metal nanoparticles dotted on a carrier. The carrier is usually oxidic materials of semiconductors such silica or carbon derived materials such as silicon carbide or carbon nanotubes. The role of the carrier is not only to increase the dispersion of the catalytically active element but also to increase the mechanical and thermal stability of the catalyst. However, metals and support may interact in a way in which a chemical bond is formed between the metal and the support.

The formation cobalt-silica compounds in the Co/SiO_2 based catalysts can be influenced by varying synthesis parameters such as cobalt precursors, silica precursors, solvents, pH or calcination atmosphere and temperature[1,2]. The effects of pH on the formation of cobalt silicate in cobalt-silica catalyst have been reported by Ming and Baker[2] from the perspective of varying reducibility of catalysts prepared from different pH. Reactions that involve water are also prone to catalyst deactivation due to formation of silicate compounds[3].

Although past research has shown the formation of cobalt silicate in the Co/SiO_2 catalyst systems,[3,4] the mechanisms for the formation of such cobalt-silica compounds remain not fully understood. It is important that such mechanisms are understood, since they may affect the catalytic activity and selectivity in the catalyzed reactions. It may be recalled that although a certain amount of cobalt silicate may be necessary for improved dispersion of cobalt on silica as described by Coulter and Sault[5], the formation of cobalt-silica compounds is undesired in the context of Fischer-Tropsch catalysis as it may result in loss of active metal due to their highly irreducible nature (cobalt silicate only reduces at temperatures above 800 K).

The current reported results show incongruity on the chemistry and stage at which cobalt silicate may form[1,3,5]. Kogelbauer *et al.*[3] reported that metallic cobalt is a requirement for formation of cobalt silicate. However, van Steen *et al.*[1] proposed that an intermediate cobalt silicate surface phase can be formed during the initial decomposition of the cobalt nitrate precursor during preparation or by a reaction between the aqueous cobalt complexes and surface silanol groups. Ernst *et al.*[6] attributed the formation of cobalt silicate during reduction to the reaction of unreduced CoO with silica to form high surface area cobalt orthosilicate. The

dynamic behaviour of cobalt-silica systems thus offers an inimitable prospect to tailor interactions on the Co-SiO_2 catalyst based on a unique catalytic prerequisite.

Calcination steps in the preparation of a catalyst play an important role in catalyst properties. Temperature programmed reduction studies by van Steen et al.[1] has shown that high temperature calcination may results in a formation of cobalt silicate surface species possibly via a solid state reaction of cobalt compounds and silica.

The modification of Co_3O_4 with small amounts of tetraethoxysilane may enhances the catalytic activity of cobalt in the Fischer-Tropsch synthesis (as discussed in chapter 4 and 5), but these samples were all calcined at relatively low temperature (473-573K). High temperature calcination of cobalt oxide and silica mixtures may yield cobalt orthosilicates. This chapter discusses the effects of calcination on the interaction of silica and Co_3O_4 nanocubes.

6.2 Experimental

Synthesis of Co_3O_4

Sample NC-Hex_TEOS-73-573 K prepared as described in chapter 5, used to test the effects of calcination of the interaction of silica and Co_3O_4. In the synthesis, Co_3O_4 nanocubes with an average size of 23.8 ± 4.5 nm (as determined using TEM) were synthesized using a hydrothermal oxidative precipitation method[7,8]. A solution containing 5.3 g $Co(NO_3)_2.6H_2O$ (20 mmol, Merck, >99.0 %) in 20.0 mL deionized water was added to a solution containing 1.8 g of NaOH (45 mmol) and 5.4 g sodium dodecylsulphate (20 mmol) in 180 mL deionized water at 368 K with an addition rate of 10 mL/min. Air was purged through the solution for 5 hours, after which the solid was recovered by centrifugation. The crystals were purified by multiple washing steps with a 1.0 M aqueous HCl-solution and distilled water. Residual chlorine present in the sample was shown to be removed after calcination at 473 K for 2 hours in a static oven.

Modification of Co_3O_4 nanoparticles with tetraethoxysilane

The obtained, calcined cobalt oxide was re-suspended in n-hexane yielding a suspension with a solid concentration of 1.4 g/L. The Co_3O_4-nanocubes were contacted with a solution of tetraethoxysilane in n-hexane (6.4 mM; 0.143 vol.-%) for a period of 5 hours. This will yield a Si/Co loading in the final sample of 63 mmol/mol as determined using SEM-EDX (see chapter 4).

After contacting the solid with the solution, the solid was recovered by centrifugation and washed 5 times with 50 mL with n-hexane. The samples were subsequently dried at 393 K for 2 hours. To investigate the effects of calcination on both the modified and the unmodified samples, the obtained material was heated in oxygen at different temperature in the range573 K-1173 K for 2 hours in a static oven. The samples were named NC-Hex-573K, NC-Hex-673K, NC-Hex-773K, NC-Hex-1173K for the unmodified Co_3O_4 nanocubes calcined at 473 K, 573 K, 673 K, 773 K and 1173 K respectively. The modified Co_3O_4 nanocubes were labelled NC-Hex- TEOS-63-573, NC-HexTEOS-63-673, NC-Hex-TEOS-63-773, NC-Hex-TEOS-63-873K, NC-Hex-TEOS-63-973K, and NC-Hex-TEOS-63-1173 for the Co_3O_4 nanocubes modified with tetraethoxysilane calcined at 573 K, 673 K, 773 K, 873 K, 973 K and 1173 K respectively.

Characterization

The phase structure of the model samples was determined using a Bruker AXS D8 Advance X-ray laboratory diffractometer operated at 40 kV and 40 mA utilizing a Co source (λ_{Co}-Kα = 0.178897 nm) and a VÅNTEC position-sensitive detector.

The presence of the modifying ligands on the cobalt oxide surface prior to reduction was analysed using an FTIR spectrometer (Nicolet 5700). The sample was prepared by diluting 1.0 mg of the model catalyst with 0.2 g of KBr and then pressed into pellets. A total of 32 scans were taken in the range between 400 and 4000 cm^{-1} for each sample after a background scan of KBr was taken in the transmission mode at the resolution of 8 cm^{-1}.

Temperature programmed reduction analysis was carried out in Micromeritics AutoChem2950 (Micromeritics Instrument Corp., USA) equipped with a thermal conductivity detector. The samples were prepared by diluting 30 mg ca. Co_3O_4 (modified with silica or unmodified) with 1.0 g SiC to ensure quasi-isothermal conditions throughout the bed. This was done by suspending the (modified) nanocubes in ethanol and adding SiC followed by drying. The SiC diluted samples were placed into a quartz reactor in the Micromeritics AutoChem2950. The samples were dried and degassed at 393K under 50 mL (NTP) /min argon for 1 hour to ensure complete removal of excess moisture and other contaminants. The temperature was decreased to 340 K followed by the change in gas composition to 5 % H_2/Ar (vol/vol) keeping the flow rate at 50 mL (NTP)/min.

The temperature was linearly increased from 340 K to 1173 K using a constant heating rate of 10 K/min.

6.3 Result and Discussion

A combination of temperature programmed reduction, and spectroscopic techniques such as infrared spectroscopy and x-ray diffraction can be used to obtain insight in the formation of metal-support compounds during the calcination of the inverse catalyst systems. To isolate calcination effects on the properties of Co_3O_4 nanocubes from the cobalt-silica interaction during calcination, unmodified Co_3O_4 nanocubes were calcined at different temperatures.

X-ray diffractometry (XRD) was used to determine the phases present in each phase after calcination. *Figure 6-1* shows the X-ray diffraction pattern of Co_3O_4 nanocubes calcined at different temperatures (573-1173 K). Co_3O_4 is XRD-pure with the only observed peaks for all the samples are characteristic diffraction lines of spinel Co_3O_4[9] using a Co-K_α source (Eva software, CCD). While it may be expected that high temperature calcination may result in auto-reduction of Co_3O_4 to CoO[10], the CoO phase is not observed in any of the X-ray diffraction patterns. There are two possible explanations for this: 1) this may be because calcination temperature at 1173 K is not high enough to cause the auto-reduction process or (more likely) 2) CoO may have formed and re-oxidised during the cooling stage from 1173 K in air to room temperature. The lattice parameter for all unmodified samples calcined at different temperatures was determined by fitting the X-ray diffraction pattern to be 0.809 nm using the (311) reflection.

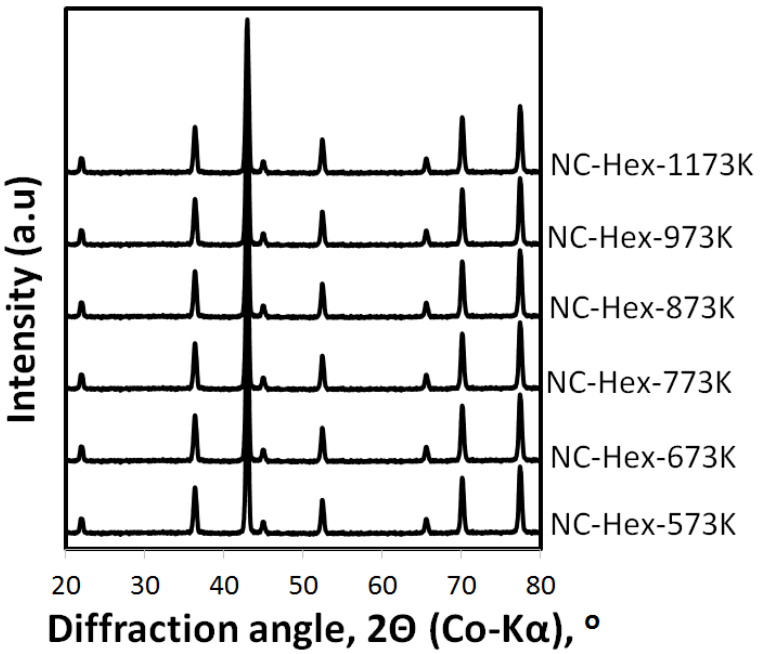

Figure 6-1: X-ray diffractogram of unmodified Co_3O_4 nanocubes samples calcined at 573-1173 K in a static oven and then cooled in the oven to room temperature

Upon modification, it may be expected that silica present of the surface of Co_3O_4 be observable on XRD. Attempts to confirm the presence of silica on the surface of Co_3O_4 using X-ray diffractrometry failed due to the either the amorphous nature and small amounts of silica (max. 4.5 wt.-%) present on the Co_3O_4 surface. The only phase observed on the XRD patterns was spinel Co_3O_4 (*see Fig. 6-2*) with a calculated lattice constant (from the (311) reflection) of 0.808 nm. When the sample is calcined at 1173 K, new diffraction lines attributed to cobalt silicate (α-Co_2SiO_4) are observed showing the existence of a mixture of Co_3O_4 and α-Co_2SiO_4 (*see Fig. 6-2*). The lattice constant for Co_2SiO_4 was determined to be: a = 0.478 nm, b = 1.03 nm and c = 0.6006 nm. The formation of cobalt silicate at high temperatures (1173 K) may be due to increased cobalt ion mobility at this temperature which may allow the diffusion of Si-ions into the Co-O matrix. Furthermore, when calcined at temperatures around 1173 K, Co_3O_4 in the sample may undergo auto-reduction from Co_3O_4 to CoO[10]. The reaction of CoO with SiO_2 may yield Co_2SiO_4[6]. The lack of formation of crystalline Co_2SiO_4 at lower temperatures may then be linked to the lack of CoO and cobalt ion mobility in the samples calcined at low temperature. Rietveld refinement points out that the composition of the Co_3O_4 phase is 97%-wt. while the Co_2SiO_4 phase constitute about 3 %-wt. For a sample modified with 63 mmol/mol (Si/Co), the theoretical weight composition of Co_2SiO_4 would be 6%-wt. This may indicate that not all the silica in the sample is transformed to Co_2SiO_4.

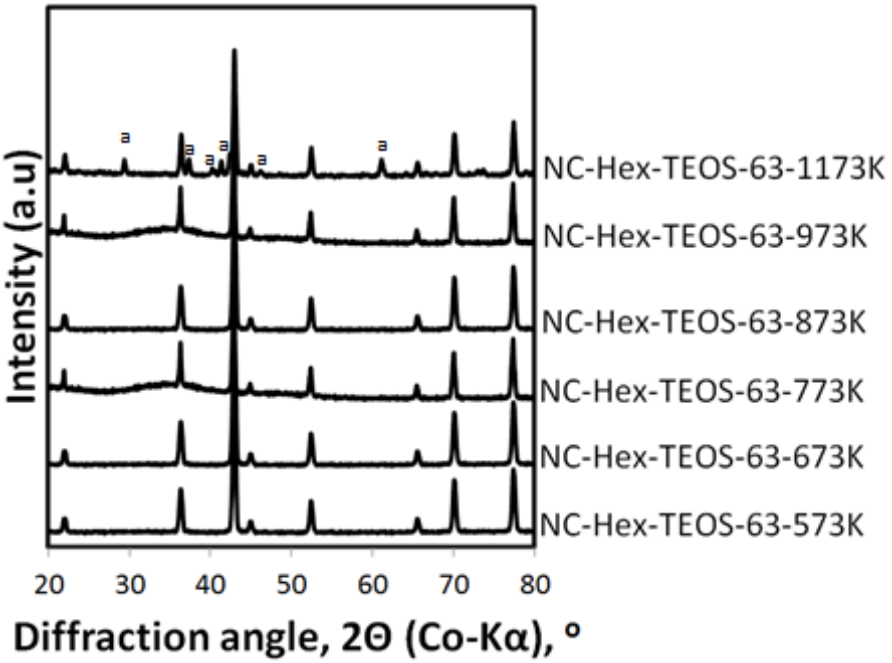

Figure 6-2: X-ray diffractogram of Co_3O_4 samples modified by contacting Co_3O_4 nanocubes with tetraethoxysilane and calcined at 573-1173 K (Diffraction lines marked with a are assigned to Co_2SiO_4 while the rest are assigned to Co_3O_4)

The crystallite sizes of all samples were determined using full width at half maxima of the (311) reflection using the Scherrer equation. Calcination of unmodified Co_3O_4 nanocubes at high temperature results in increase in the crystallite size from about 22 nm to 40 nm while calcination of tetraethoxysilane-modified Co_3O_4 nanocubes at similar temperature results in an increase in the crystallite size from about 22 nm to 31 nm (*see Fig. 6-3*). This indicates that higher temperature calcination of the samples results in sintering. However, tetraethoxysilane-modified samples sinter less than the unmodified sample, except when going to 1173 K, i.e. when forming bulk cobalt silicate. This may indicate that small amounts of silica, similar to small amounts of alumina[11], can reduce sintering to a greater extent.

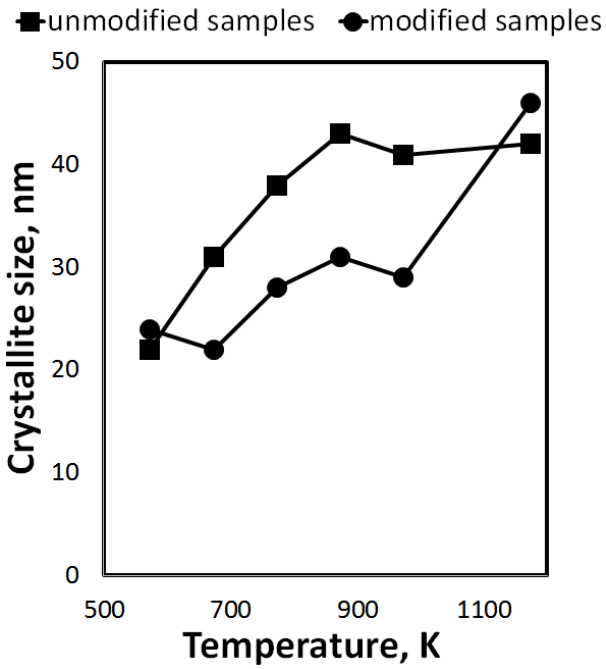

Figure 6-3: Effects of silica modification on Co_3O_4 nanocubes crystallite growth (sintering) during high temperature calcination

Transmission electron microscopy (TEM) was also used to confirm to study any visible changes in the morphology of the samples upon calcination. Transmission electron microscopy images of (modified) Co_3O_4 nanocubes calcined at 573 K and 1173 K are shown in *Figure 6-4.* Catalysts calcined at 573 K shows Co_3O_4 23.8 nm crystallites with a cubic shape. After calcination at 973 K, the crystallite size visibly increased to 44.2 nm, conforming to the X-ray diffraction results. During growth/sintering, the geometry of Co_3O_4 changes from well-defined cubes to irregular cubes of a larger crystallite size.

Calcination of modified samples at 573 K resulted in neither any visible change in terms of morphology nor even indications of amorphous silica phase. However, upon high temperature calcination, the shape of the modified sample again changed from well-defined nanocubes to irregular/truncated nanocubes. However, the crystallite size of the modified sample only increased to less than 30 nm. This is in conjunction with the-ray diffraction results which indicates that the modification process hinders sintering during high temperature calcination

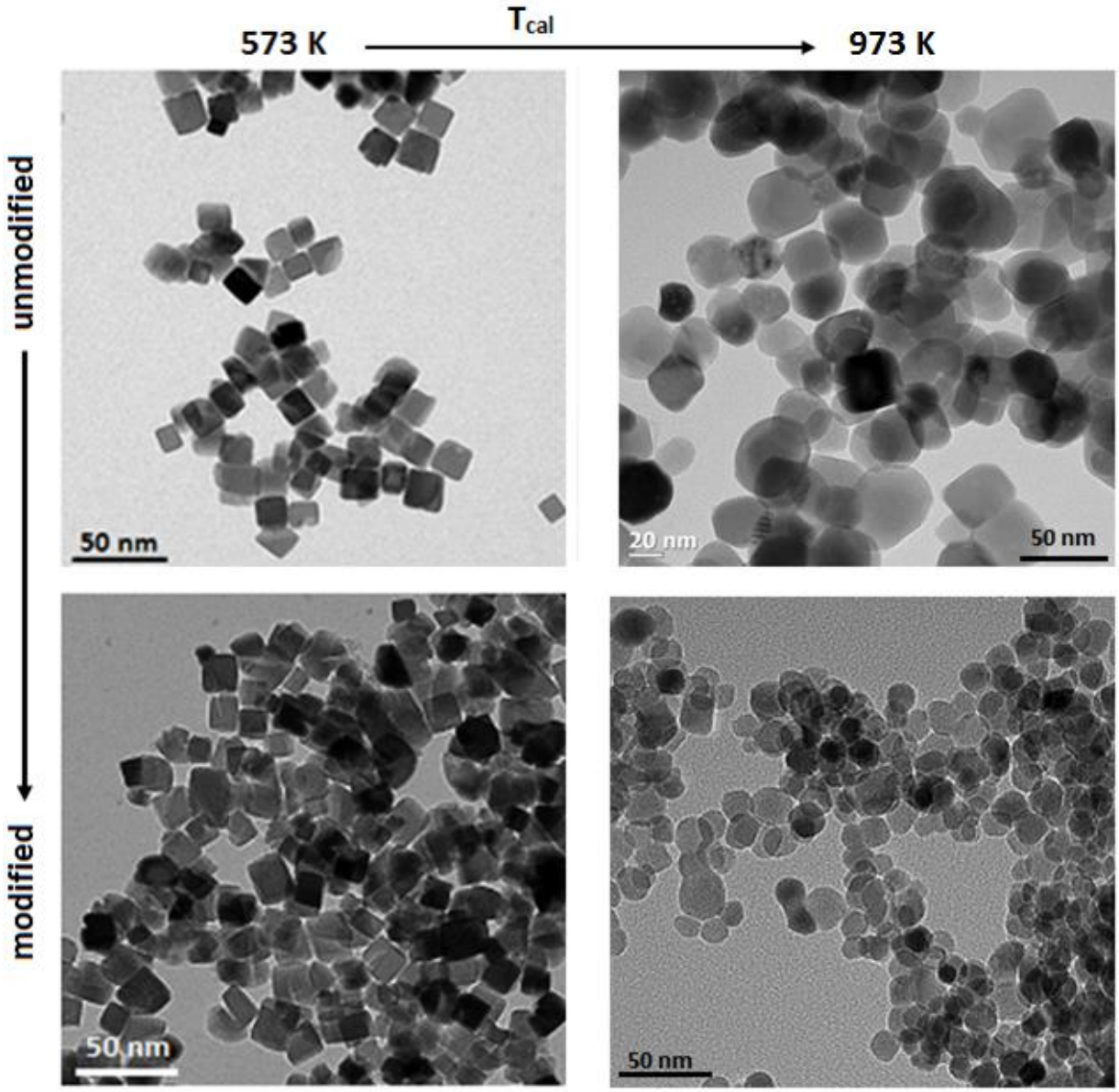

Figure 6-4: Modified Co_3O_4 nanocubes and Co_3O_4 modified with 63 mmol/mol tetraethoxysilane in n-hexane calcined at 573 K and 900 K in static oven

Fourier transform infrared spectroscopy poses a comparable view of how silica interacts with Co_3O_4 nanocubes during calcination. There is no difference in the FTIR-spectra of the unmodified samples up to a calcination temperature of 1173 K in the region 524-700 cm^{-1} (*see Fig. 6-5 (left)*). The spectra show two major absorption bands at 550 cm^{-1} and 658 cm^{-1}. The band at 550 cm^{-1} is ascribed to the vibration of the Co-O stretch while the latter can be ascribed to the stretch vibration of the Co (III)-O bond in the Co_3O_4 lattice[12]. Similarly, Fourier transform infrared spectroscopy was used to investigate the nature of interaction between Co_3O_4 nanocubes and the modifying silica on the surface of the model catalyst after calcination at 573-1173 K. *Figure 6-5 (right)* shows the FTIR spectra of modified Co_3O_4 calcined at different temperatures in the

region 525-700 cm^{-1}. All the samples show absorption bands at 550 cm^{-1} and 658 cm^{-1}. The band at 550 cm^{-1} is ascribed to the vibration of the Co-O stretch while the latter can be ascribed to the stretch vibration of the Co (III)-O bond in the Co_3O_4 lattice[12]. A side band appear at 670 cm^{-1} upon modification of the samples. This absorption band can been attributed to the bending modes of the Co-O-Si bonds as reported by Yin *et al*.[13] for Co/SiO_2 core-shell structures reduced in hydrogen at 973 K as described in *Chapter 4.*

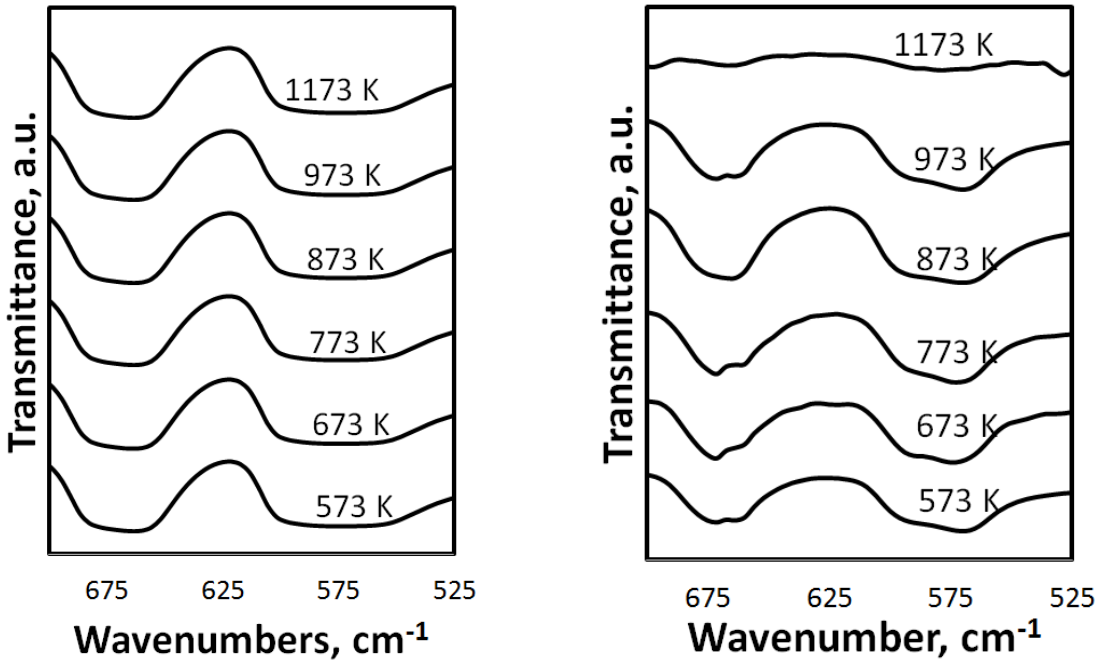

Figure 6-5: FTIR-spectra of Co_3O_4 nanocubes calcined at different temperatures from 573 – 1173 K in the range of 400-400 cm^{-1}

As describe previously (*Chapter 4*), modification of Co_3O_4 with tetraethoxysilane results in development of new absorption bands in the range of 700-1200 cm^{-1} (see *Fig. 6-6*). The samples modified and calcined at temperatures up to 773 K show these absorption bands at 800 cm^{-1}, 870 cm^{-1}, 1020 cm^{-1} and 1100 cm^{-1}. The band at 800 cm^{-1} may be attributed to the in-plane Si-O-Si bending vibration[13]. The band at 870 cm^{-1} may indicate the presence of monodentate Co-O-Si species as observed in the adsorption of dimethyldiethoxysilane on silica[14] and similar to those identified in the analogous iron-silica species[15]. The band at 1020 cm^{-1} has been attributed to Co-O-Si vibration[16,17], but may also be attributed to the presence of oligomeric silicate species[18,19]. The band at 1100 cm^{-1} is characteristic of the asymmetric stretching of the Si-O-Si of the amorphous SiO_4 tetrahedron[18,20]. The sample calcined at 873 K shows only new absorption bands at 800 and 1100 cm^{-1} attributable to plane Si-O bending vibration and the asymmetric stretching of the Si-O-Si of the amorphous SiO_4 tetrahedron[18,20] respectively, while the bands at 870 cm^{-1} and 1020 cm^{-1} attributable

to Co-O-Si asymmetric stretch vibrations disappeared. The disappearance of these bands is an indication that upon calcining the modified material at 873 K, Co_3O_4 and the surface silica species do not strongly interact.

New changes in the infrared spectrum are observed when the calcination temperature is further increased to 973 K and 1173 K. A set of additional absorption bands appears in the range between 900-940 cm^{-1}. Furthermore, the absorption band at 870 cm^{-1} reappears with high intensity. These bands have been ascribed to cobalt orthosilicate[21] and for sample calcined at 1173 K, these bands are comparable to bands observed for Co_2SiO_4 synthesized and characterized as described in *chapter 4*. The intensity of these bands is lower for the sample calcined at 973 K, which may be indicative the presence of Co_2SiO_4 or an intermediate phase between surface silicate and bulk cobalt silicate.

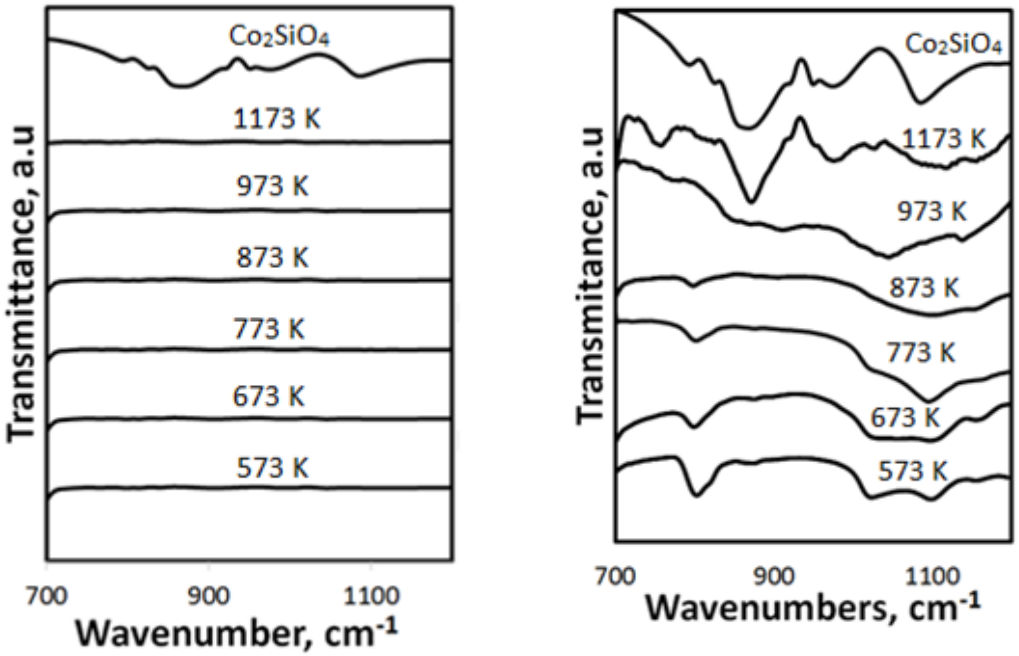

Figure 6-6: Infrared spectra of left: unmodified Co_3O_4 nanocubes calcined at different temperatures and right: Co_3O_4 nanocubes modified with tetraethoxysilane in n-hexane calcined at different temperatures (573 -1173 K) in the region between 700 and 1200 cm^{-1}.

The effect of calcination temperature on the reduction behavior of this materials was studied by using TPR. The total amount of hydrogen consumed in this experiment indicates that within the error of the experiment Co_3O_4-nanocubes are completely reduced at 750 K. The position of the peaks depends mostly on the synthesis method and pre-treatment conditions of the sample before the temperature programmed reduction is carried. The Co_3O_4 temperature programmed reduction profile shows two reduction peaks usually ascribed to a sequential reduction of Co_3O_4 to CoO

(succeeded by the reduction of CoO to Co)[1,2,11,22,23] (see *Fig. 6-7)*. The maximum for the first reduction peak for the unmodified Co_3O_4 nanocubes calcined at 573 K occurs at 530 K and the second peak maxima occurs at 700 K. The ratio of hydrogen consumption attributed to the two reduction peaks is 1:4, which is smaller than the required ratio of 1:3 for the sequential reduction of Co_3O_4 → CoO → Co. This may imply a more complex reduction process, when involving relatively large, well-crystalline Co_3O_4 nanocubes and the first reduction step may involve to some degree only surface reduction[24]. The first reduction peak was fitted to a two-dimensional nucleation model according to Avrami-Erofeev model[23], whereas the subsequent reduction processes is thought to be best described according to a unimolecular decay mode as described in Chapter 4. (the fitting parameters are given in *Table 6.2*).

Calcination of Co_3O_4 nanocubes at high temperatures retards both reduction steps. The reduction temperature for the two reduction processes has shifted to 623 K and 798 K respectively, for the sample calcined at 973 K. The reduction peak of Co_3O_4 nanocubes shifts to higher temperatures when calcination temperature is increased (see *Fig. 6-8*). A major increase in the reduction temperature is observed for the first reduction step as compared to the second reduction step. As a consequence, the two reduction peaks appear to merge, as observed after high temperature calcination of Co_3O_4 [2,11,25]. However, deconvolution of these peaks shows that the ratio of the hydrogen consumption attributable to each reduction step remains constant for the various calcination temperatures. This may indicate the reduction process remains a sequential process. The shift in the reduction peaks may be ascribed to increase in crystallite size upon increasing the calcination temperature as suggested by X-ray diffraction. As a consequence, the pre-exponential factor can be expected and was observed to decrease with increasing calcination temperature (see *Table 6-2)*. The activation energy does not seem to vary with calcination temperature. Hence, the shift of the reduction temperature of the first reduction step may be attributed to the change in the crystallite size. The pre-exponential factor for the unimolecular decay of CoO to metallic cobalt also decreases with increasing calcination temperature thus suggesting that calcination does not only

retard the reduction of Co_3O_4 to CoO, but also affects the succeeding reduction process of CoO → Co significantly.

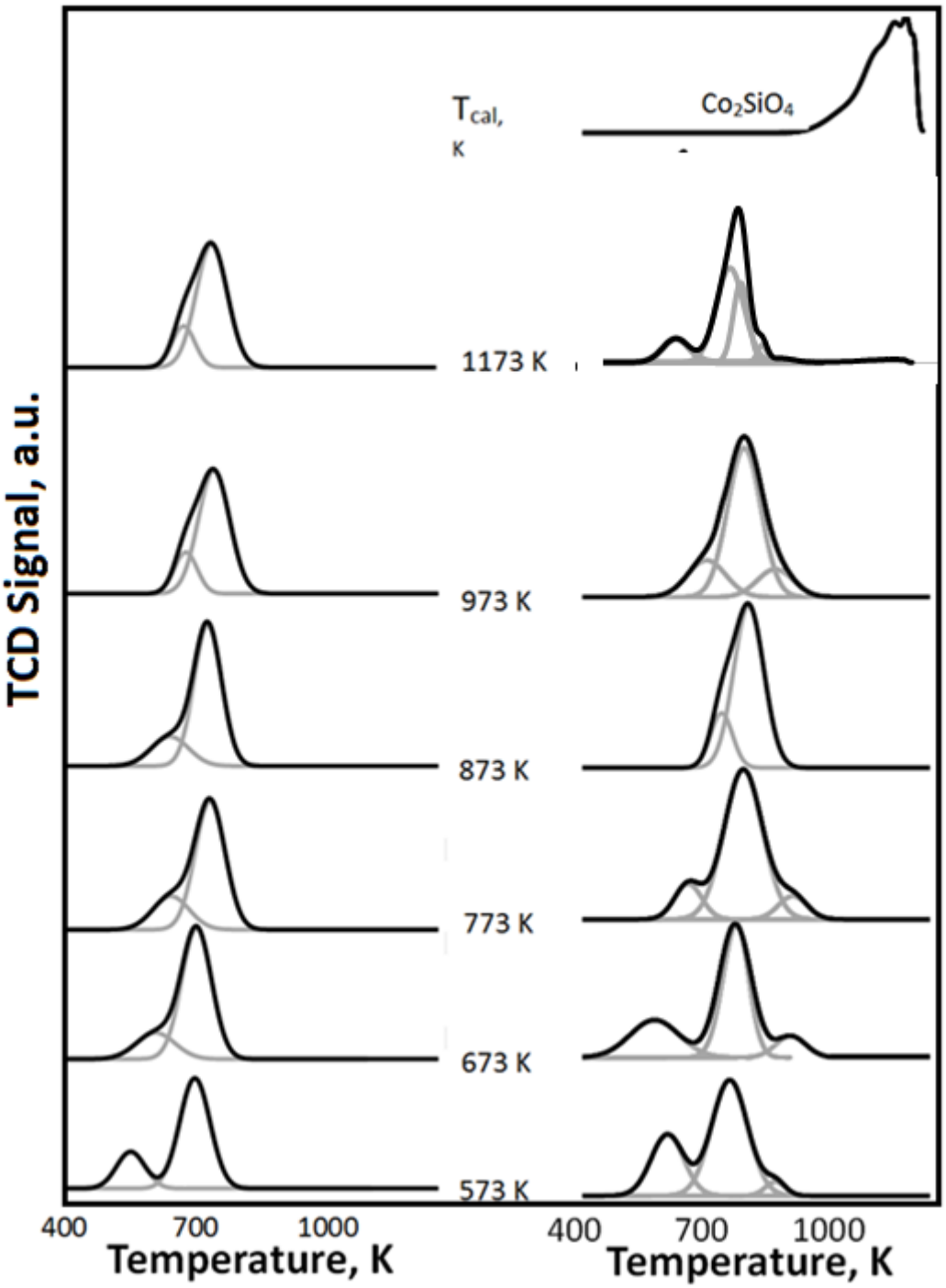

Figure 6-7: TPR profiles of unsupported materials of: Co_3O_4 nanocubes (left) and modified Co_3O_4 (Co/Si = 63 mmol/mol) (right) calcined at different temperatures (heating rate 10 K/min; 5% H_2 in Ar; grey lines: fit of consecutive two-dimensional nucleation model followed by a unimolecular decay for both the second and third reduction steps)

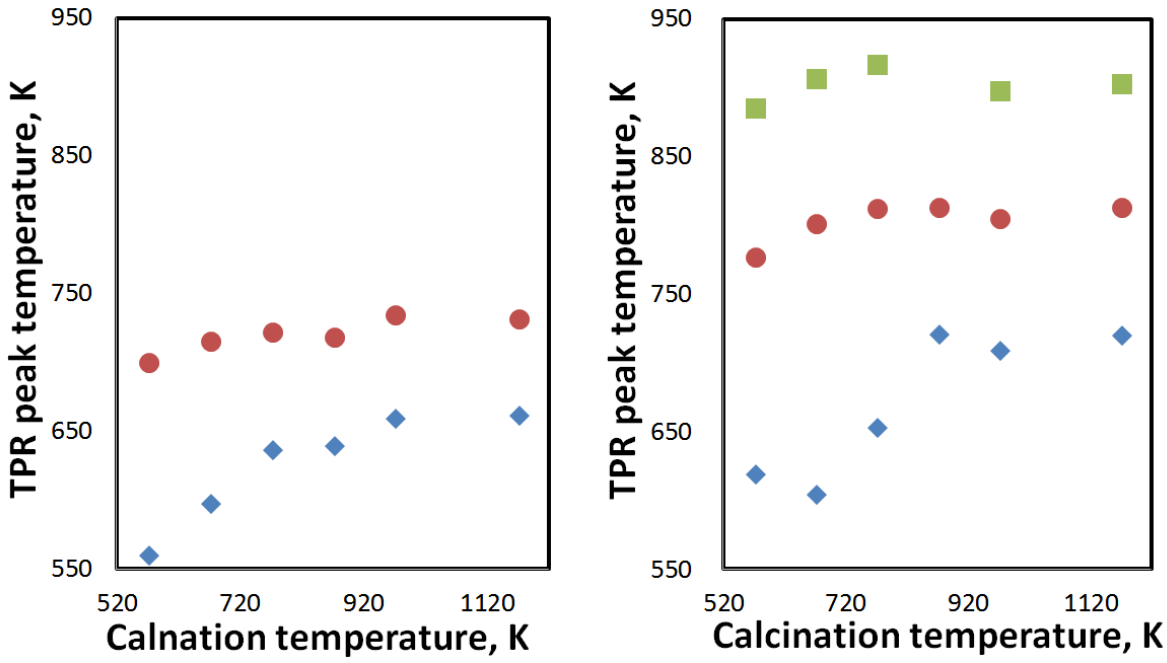

Figure 6-8: The observed peak maxima in the TPR-profile of the the unmodified Co_3O_4 nanocubes (left) and the TEOS-modified nanocubes (Si/Co=63 mmo/mol) right) as a function of the calcination temperature.

For supported catalysts, the rate of reduction is influenced significantly by metal-support interaction. Metal-support interaction are known to be more pronounce on smaller crystallites[26]. As such, for supported catalysts, the reducibility of metal oxides decreases with crystallite size[26]. The interaction of small quantities of silica and Co_3O_4 decreases the rate of reduction of both Co_3O_4 to CoO and that of CoO to metallic Co. This can be observed by comparing the reduction profiles of unmodified Co_3O_4 against a modified sample calcined at similar temperature (see *Fig. 6-7).* For instance, the reduction temperature for unmodified Co_3O_4 nanocubes calcined at 573 K occurs at 530 K and the second peak maxima occurs at 700 K and shift to 623 K and 798 K respectively, for the sample with a Si/Co-ratio of 63 mmol/mol calcined at 573 K (NC-Hex-TEOS-63-573K). Like unmodified samples, a major shift is observed for the first reduction peak and this results in merging of the first two reduction peaks (see *Fig. 6-7*). The ratio of hydrogen consumption attributed to the two reduction peaks remains ca. 1:4, even after modifying the Co_3O_4 nanocubes with TEOS.

It can be further observed that a high temperature shoulder starts appearing in the TPR-profiles of the Co_3O_4 nanocubes after exposure to solutions of tetraethoxysilane in n-hexane calcined at different temperatures except for the samples calcined at 873 K. As described in Chapter 4, this reduction peak has been attributed to the reduction of cobalt strongly interacting with a surface

silicate[1,22,27]. Upon increasing the calcination temperature, the peak due to the reduction of surface silicates also shifts towards higher reduction temperatures. This was again attributed to a decrease in the pre-exponential factor for this reduction process as a consequence of the growth of the particles. However, while the activation energy for the reduction of Co_3O_4 nanocubes remains approximately the same, the activation energy for the reduction of modified samples increases with increasing calcination temperature. Thus, a decrease in the rate of reduction cannot solely be ascribed to the sintering process but may also be attributed to an increase in the activation energy. It should be noted that this reduction process (due to strongly interacting cobalt and silica) seems to be absent for the sample calcined at 873 K (NC-Hex-TEOS-63-873K). The absence of this reduction peak for this sample, NC-Hex-TEOS-63-873K, may indicate the absence of any hard to reduce surface cobalt oxide. This may be linked to the mobility of Si-OH species present on the surface of the Co_3O_4 , which may facilitate the cleavage of Co-O-Si bonds resulting in the formation of Si-O-Si[12] as illustrated:

$$\mathrm{Co-O-Si\ +\ Si-OH\ =\ Co-OH\ +\ Si-O-Si}$$
$$\mathrm{2Co-OH \rightarrow\ Co-O-Co\ +\ H_2O}$$

Increasing the temperature further (>873 K), may then allow diffusion of Si into the Co-O matrix and start the formation of bulk-like cobalt silicates. This could explain the re-appearance of the high temperature peak at little somewhat higher calcination temperature. The re-appearance of this peak is coupled with the appearance of new reduction peaks observed around 1100 K for the sample calcined at 973 K (see *Fig. 6-7*), which might be attributed to the reduction of non-stoichiometric cobalt silicates (NC-Hex-TEOS-63-973K). In fact, the modified sample calcined at 1173 K (NC-Hex-TEOS-63-1173K) results in a reduction peaks resembling that of Co_2SiO_4 appearing above 1100 K. Calcination of Co_3O_4 nanocubes at high temperatures can results in auto-reduction of Co_3O_4 to CoO[10]. The reaction of CoO with SiO_2 may yield Co_2SiO_4[1]. As such, the formation of Co_2SiO_4, can only be related to the mobility of cobalt ions that allows diffusion of Si ion in the matrix of Co-O.

However, both temperature-programmed reduction and X-ray diffraction did not sure any presence of CoO in the system. It was thought that this could probably be due to the re-oxidation of CoO during the cooling process in flow of synthetic air to room temperature. As such, an unmodified and a modified sample were calcined at 1173 K for two hours in synthetic air flowing at 10 mL/min. To avoid re-oxidation during the cooling down process, the samples were cooled in argon till room temperature. The temperature-programmed reduction profiles of these samples (calcined at 1173 K

and cooled in argon) show that calcination at 1173 K results in the formation of CoO (see *Fig. 6-9*). The temperature programmed reduction profile of the unmodified sample shows a single reduction peak at 569 K with a hydrogen consumption of 0.93 mol H_2 per mol of cobalt (close to the theoretical H_2 consumption). The reduction peak is very sharp indicating that after the initiation of Co nucleation the reduction process happens faster, and this may be related to the amorphous nature of the resulting CoO after the auto-reduction. Similarly, a modified sample calcined at 1173 K and cooled in argon shows a reduction peak a peak attributable to the reduction of CoO at 616 K. Deconvolution of the peak shows a tail which could be related to strongly interacting CoO with silica. For the modified sample, a peak due to the reduction of Co_2SiO_4 is observed. This further substantiate the idea that Co_2SiO_4 may have been formed through the reaction of CoO with silica at 1173 K.

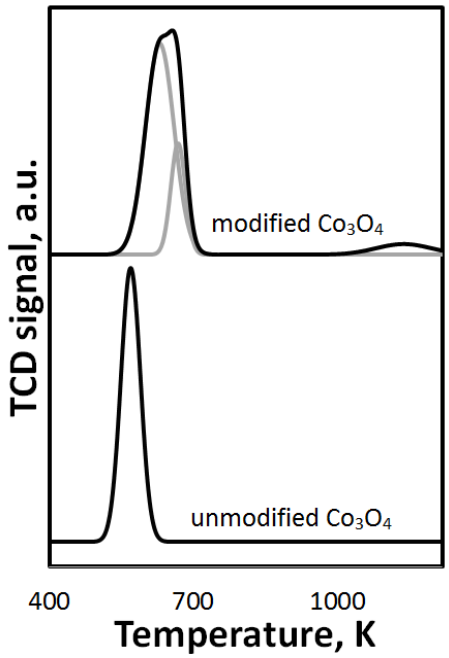

Figure 6-9: TPR profiles of unsupported materials of: Co_3O_4 nanocubes (E_a = 34±4 KJ/mol; A = $10^{4.3\pm0.2}$ s^{-1}) and modified Co_3O_4(Si/Co = 63 mmol/mol) calcined at 1173 K (E_a = 43±3 KJ/mol; A = $10^{3.8\pm0.1}$) and cooled in argon (heating rate 10 K/min; 5% H_2 in Ar; grey lines: fit of a unimolecular decay)

The kinetic parameters for the reduction process were determined by fitting the whole temperature programmed reduction profile. With increasing calcination temperature, the activation energy required for the reduction of these hard-to-reduce species increases (see *Table 6-2).* This therefore explains the shift towards higher reduction temperatures upon modifying the Co_3O_4 nanocubes with tetraethoxysilane. The pre-exponential factor, A, for this reduction step does not seem to vary upon increasing the calcination temperature for the modified samples. This implies that the reduction

process of Co_3O_4 is retarded due to an increase in the activation energy but hardly any changes in the pre-exponential factor. The change in the observed activation energy suggests a change in the bonding of the silicate species to the nanocubes. It is accepted that reducibility of a supported oxides is a function of the metal-support bond strength and hence activation energy. As such, modification of bond strength between silica and Co_3O_4 by heat treatments can affect the kinetics of the reduction process. The pre-exponential factor for the high temperature peak corresponding to the reduction of strongly interacting cobalt with silica also remains constant upon increasing the calcination temperature. However, the activation energy increases suggesting the Co-O bond strength has been enhanced by the presence of silica. The unaffected pre-exponential of the modified samples during calcination may similarly suggest, indirectly, that the crystallites size does not change. In fact, crystallite size seems to be unaffected by calcination temperature when the samples are modified. This suggest the small quantities of silica, drastically reduces sintering during high temperature calcination.

Table 6-1: Hydrogen consumption during temperature programmed reduction of the samples and the derived kinetic parameters from the profile assuming that the first step follows a two dimensional nucleation mechanism, and the other reduction processes occur via a uni-molecular decay

T_{cal}, K	Peak	Unmodified sample			Modified samples		
		H_2-consumption (mol-H_2/mol-Co)	Ea, kJ/mol	A, S^{-1}	H_2-consumption (mol-H_2/mol-Co)	Ea, kJ/mol	A, S^{-1}
573	1	0.261	34±3	$10^{0.7\pm0.4}$	0.292	57 ± 11	$10^{2.6\pm0.9}$
	2	1.069	127±21	$10^{7.2\pm1.5}$	1.023	195 ± 34	$10^{11.6\pm2.6}$
	3	-	-	-	0.015	93 ± 25	$10^{3.5\pm1.4}$
673	1	0.267	43±17	$10^{0.4\pm0.1}$	0.288	72± 17	$10^{1.6\pm0.8}$
	2	1.063	113±32	$10^{4.1\pm0.8}$	1.03	203 ± 13	$10^{8.6\pm2.1}$
	3	-	-	-	0.020	95 ± 12	$10^{2.5\pm0.9}$
773	1	0.257	29 ± 7	$10^{0.1\pm00}$	0.259	82± 8	$10^{1.9\pm1.1}$
	2	1.073	154 ± 27	$10^{3.7\pm1.3}$	1.043	215 ± 29	$10^{7.9\pm1.4}$
	3	-	-	-	0.031	122± 21	$10^{4.1\pm2.0}$
873	1	0.255	37 ± 9	$10^{0.13\pm0.04}$	0.272	88 ± 12	$10^{1.1\pm0.7}$
	2	1.078	133 ± 29	$10^{3.6\pm0.8}$	1.029	117± 13	$10^{7.3\pm1.8}$
973	1	0.249	41 ± 12	$10^{0.2\pm0.1}$	0.260	105±6	$10^{2..0\pm0.5}$
	2	1.082	149 ± 23	$10^{2.9\pm0.5}$	0.995	144±13	$10^{6.0\pm1.7}$
	3	-	-	-	0.072	133± 24	$10^{3.7\pm0.9}$
1173	1	0.260	49 ± 17	$10^{0.09\pm0.0}$	0.241	101±13	$10^{2.1\pm0.9}$
	2	1.073	146 ±9	$10^{3.0\pm0.7}$	0.949	125±6	$10^{8.2.1\pm1.5}$
	3	-	-	-	0.125	156 ± 24	$10^{7.3\pm3.1}$

6.4 Conclusions

The effects of calcination on the interaction of cobalt and silica in the Co/SiO_2 inverse catalysts prepared by modifying Co_3O_4 nanocubes with small amounts of tetraethoxysilane followed by calcination was explored. The formation of cobalt-silica compound characterized by high temperature reduction peaks, is dependent of temperature of calcination. Calcination of the modified Co_3O_4 nanocubes at temperatures below 773 K result in the formation hard-to reduce cobalt silica compound. Calcination at 773 -873 K is thought to results in weaker interactions between cobalt and silica. Higher temperature calcination (> 973 K) results in the formation of even more hard-to-reduce cobalt silicate with a stoichiometric Co_2SiO_4 phase being formed when calcination is done at 1173 K. The formation of the cobalt silicates at this temperature may be ascribed to the increase ion mobility of cobalt ions at 1173 K that allows diffusion of Si-ions into the Co-O matrix.

Calcination of Co_3O_4 nanocubes at higher temperature retards its reduction to cobalt. This retardation may be ascribed to sintering of Co_3O_4 nanocubes during calcination at high temperatures and can be observed from the changes in the pre-exponential factor. The presence of small quantities of silica reduce sintering to a greater extent. However, the rate of reduction is still greatly decrease due to the increased activation energy of reduction upon modification. This implies that the reducibility of Co_3O_4 is a function of cobalt-silica bond strength. The presence of silica in small quantities, thus, reduce the rate of reduction by increasing the activation energy.

6.5 References

1 E. van Steen, G. S. Sewell, R. a. Makhothe, C. Micklethwaite, H. Manstein, M. de Lange and C. T. O'Connor, *J. Catal.*, 1996, **229**, 220–229.

2 H. Ming and B. G. Baker, *Appl. Catal. A, Gen.*, 1995, **123**, 23–36.

3 A. Kogelbauer, J. C. Weber and J. G. Goodwin, *Catal. Letters*, 1995, **34**, 259–267.

4 G. Ortega-Zarzosa, C. Araujo-Andrade, M. E. Compean-Jasso, J. R. Martinez and F. Ruiz, *J. Sol-Gel Sci. Technol.*, 2002, **24**, 23–29.

5 K. E. Coulter and A. G. Sault, *J. Catal.*, 1995, 154, 56–64.

6 B. Ernst, S. Libs, P. Chaumette and A. Kiennemann, *Appl. Catal. A Gen.*, 1999, **186**, 145–

168.

7 J. Feng and H. C. Zeng, *Chem. Mater.*, 2003, **15**, 2829–2835.

8 X. Liu, G. Qiu and X. Li, *Nanotechnology*, 2005, **16**, 3035–3040.

9 R. Xie, C. Wang, L. Xia, H. Wang, T. Zhao and Y. Sun, *Catal. Letters*, 2014, **144**, 516–523.

10 G. S. Sewell, E. van Steen and C. T. O'Connor, *Catal. Letters*, 1996, **37**, 255–260.

11 A. P. Petersen, R. P. Forbes, S. Govender, P. J. Kooyman and E. van Steen, *Catal. Letters*, 2018, **148**, 1215–1227.

12 O. A. Fouad, S. A. Makhlouf, G. A. M. Ali and A. Y. El-Sayed, *Mater. Chem. Phys.*, 2011, **128**, 70–76.

13 X. J. Yin, K. Peng, A. P. Hu, L. P. Zhou, J. H. Chen and Y. W. Du, *J. Alloys Compd.*, 2009, **479**, 372–375.

14 D. W. Sindorf and G. E. Maciel, *J. Am. Chem. Soc.*, 1983, **105**, 3767–3776.

15 R. P. Mogorosi, N. Fischer, M. Claeys and E. van Steen, *J. Catal.*, 2012, **289**, 140–150.

16 I. Puskas, T. H. Fleisch, J. B. Hall, B. L. Meyers and R. T. Roginski, *J. Catal.*, 1992, **134**, 615–628.

17 A. H. Kababji, B. Joseph and J. T. Wolan, *Catal. Letters*, 2009, **130**, 72–78.

18 D. G. Kurth and T. Bein, *Langmuir*, 1995, **11**, 3061–3067.

19 X. Yang, P. Roonasi and A. Holmgren, *J. Colloid Interface Sci.*, 2008, **328**, 41–47.

20 X. Huang and Z. Chen, *J. Cryst. Growth*, 2004, **271**, 287–293.

21 S.-J. Jong and S. Cheng, *Appl. Catal. A Gen.*, 1995, **126**, 51–66.

22 M. P. Rosynek and C. A. Polansky, *Appl. Catal.*, 1991, **73**, 97–112.

23 H. Y. Lin and Y. W. Chen, *Mater. Chem. Phys.*, 2004, **85**, 171–175.

24 L. Hu, K. Sun, Q. Peng, B. Xu and Y. Li, *Nano Res.*, 2010, **3**, 363–368.

25 H. Ming, in *Cobalt: Characteristics, compounds and applications*, ed. L. J. Vidmar, Nova Science Publishers, Inc., 2011, pp. 1–38.

26 W. Wan, X. Nie, M. J. Janik, C. Song and X. Guo, *J. Phys. Chem. C*, 2018, **122**, 17895–17916.

27 R. Xie, D. Li, B. Hou, J. Wang, L. Jia and Y. Sun, *CATCOM*, 2011, **12**, 589–592.

7. Metal-support interactions in SiO_2/Co inverse catalyst for Fischer-Tropsch synthesis: understanding the ligand effects by using different silane ligands during the modification process

Cobalt oxide has been modified with tetraethoxysilane, triphenyl ethoxysilane and trimethyl chlorosilane by contacting cobalt oxide with these silanes in n-hexane. The presence of this material on the surface of cobalt has been confirmed using FTIR after reduction in H_2 at 573 K. Triphenyl ethoxysilane and trimethyl chlorosilane facilitates the formation of a mixture of hcp and fcc cobalt during the reduction process while cobalt oxide modified with tetraethoxysilane results in the formation of fcc cobalt only. The modification process alters the CO adsorption properties of the catalytically active material. CO-TPD studies show that upon modification, the amount of dissociatively adsorbed CO increases and this in turn alters the rate of CO conversion and methane selectivity in Fischer-Tropsch synthesis.

7.1 Introduction

The hydrogenation of CO in the Fischer-Tropsch synthesis requires adsorption of CO onto the surface of a catalytically active metal (e.g. cobalt). The adsorption of CO may occur either on the surface of the catalytically active metal or at the interface between the metal and the support. Previous studies have shown that the adsorption properties of gases on metals relies on the type of support onto which the catalytically active metal has been dispersed[1–3]. Vannice and colleagues[1,4,5] showed that the heat of adsorption of CO on metals can vary depending on the type of support. The change in heats of adsorption was originally attributed to metal-support interaction effects occurring due to the electron exchange between platinum and the support materials at the interface[6].

The influence of metal-oxide interfaces in catalysis predominantly hinges from the alteration in the electronic properties of the catalytically active metal[7]. For supported catalysts, the interaction of the metal and the support may result in electron transfer to the metal from the support or vice versa. This electron transfer may change the electronic configuration of the surface atoms. This electronic influence may not be restricted to the surface atom to which the ligand/support binds but may further alter atoms that are surrounding the ligand-blocked site. The change in the electronic properties can alter the heats of adsorption of the reactants and hence influence the chemical reaction rate[5].

Metal-support interactions have been thought to be detrimental in the context of catalysis as they suppress the adsorption capacity of adsorbate. However, today, the interaction of the support and the catalytically active metal can be used to tune the final properties of the catalyst guiding into the required selectivity. For instance, the role of metal-oxide interface has been observed in various catalyzed chemical processes such oxygen reduction reactions[8], oxidation of alcohols[9], hydrogenation[10] reaction, water-gas shift reaction[11,12] and Fischer-Tropsch synthesis[13]. In the case of Fischer-Tropsch, Co_3O_4 nanocubes were modified with tetraethoxysilane and the rate of CO conversion was drastically altered by the presence of the silica islands on the cobalt surface[13].

Temperature programmed desorption has often been employed to study the desorption of adsorbates from catalytic surfaces. The technique can be employed to define the nature of adsorption sites on the catalyst surface as well as to the nature of adsorption (e.g. associative

or dissociative adsorption)[14]. CO-temperature programmed desorption has also been used to study metal-support interactions. The chemical promotional effect occurring due to surface creeping of the support onto metallic cobalt crystallites were ideated from the use of temperature programmed desorption[15]. The use of temperature programmed desorption on the metal-support effects is not limited to creeping effects of the support: it has also been applied to study the electronic effects by varying the support material on a catalytically active metal[16]. In this study we discuss the use of temperature programmed desorption to disentangle the metal-ligand interface effect in cobalt-based catalysts. Here, cobalt (oxide) is modified with silane ligands with the aim to have Co-O-Si bridges mimicking the formation of ligand effect in Co/SiO_2 systems.

7.2 Experimental

Synthesis of cobalt nanoparticles

Cobalt nanoparticles (22-28 nm) were synthesized by a decomposition of a cobalt carbonyl $[Co(CO)_8]$[17]. In the synthesis, 1.08 g $Co(CO)_8$, oleic acid (0.5 mL) and dioctylamine (5.0 mL) were dissolved in dichlorobenzene (60 mL) at 333 K. Upon complete dissolution of $[Co(CO)_8]$, the temperature was increased to 453 K at a rate of 10 K/min to initiate the decomposition of the carbonyl precursor. The temperature was held at 453 K for 15 min. After the formation of a grey precipitate, the obtained hot solution was contacted with absolute ethanol (50 mL). The precipitate was washed several 5 times with absolute ethanol (200 mL). The powder was recovered by evaporating ethanol from the powder in open air in a fume-hood overnight.

Modification of the nanoparticles with silanes

The as-synthesized cobalt particles were re-dispersed in n-hexane yielding a suspension with a solid concentration of 1.4 g/L at room temperature. Silanes (tetraethoxysilane - TEOS, triphenyl ethoxysilane – TPES, or trimethyl chlorosilane - TMCS) were added to n-hexane solution and the final suspension had an initial concentration of silane of 5.51 mM. After contacting the solid with the stirred solution (300rpm), the solid was recovered by centrifugation and washed 5 times each with 50 mL of n-hexane and was dried by evaporation the solvent in open air. To obtain the deposition of a similar quantity of silanes $\left(\frac{Si}{Co}\right)_{targeted}$ = 28 mmol/mol) the contact time was varied. The obtained nanoparticles were named NP-Hex, NP-Hex-TEOS, NP-Hex-TPES

and NP-Hex-TMCS for the unmodified nanoparticles, samples contacted with TEOS, TPES and TMCS in n-hexane respectively.

Catalyst preparation

After washing, the obtained (un)modified nanoparticles were supported on to β-SiC microspheres (SiCAT, $d_{particle}$= 100 µm, S_{BET} = 25 m^2/g, V_{pore} = 0.30 cm^3 /g) by sonicating 0.1 g of the (modified) oxide together with 0.9 g of β-SiC microspheres in a 50 mL chloroform for 1 hour. The solvent was subsequently dried off at room temperature. The supported material was subsequently washed with acetone and the acetone was evaporated by leaving the sample in a fume-hood for 4 hours. The supported catalysts were named Cat-NP-573K, Cat-NP-TEOS-28-573K, Cat-NP-TPES-28-573K, Cat-NP-TMCS-28-573K for the unmodified nanoparticles and nanoparticles modified with tetraethoxysilane, triphenyl ethoxysilane or trimethyl chlorosilane respectively.

Characterization

The morphology of the samples was studied with a JEM200CX (JEOL, JAPAN) transmission electron microscope (TEM) operating at 120kV. The phase structure of the unsupported model catalysts was determined using a Bruker AXS D8 Advance X-ray laboratory diffractometer operated at 40 kV and 40 mA utilizing a Co source ($\lambda_{Co\text{-}K\alpha}$ = 0.178897 nm) and a VÅNTEC position-sensitive detector.

The silicon loading of the reduced sampled was determined using energy dispersive X-ray analysis (EDX) on a scanning electron microscope (LEO S444 SEM) equipped with a Four Quadrant Back Scatter Detector and an energy dispersive Fissons Kevex X-ray spectrometer.

FTIR spectrometer (Nicolet 5700) was used to determine if the modifying agent ($\left(\frac{Si}{Co}\right)$ ~ ca. 28 mmol/mol) remained on the surface of cobalt after reduction. The obtained (un)modified nanoparticles were reduced with hydrogen at 573 K for 8 hours. After reduction, the sample temperature was decreased to room temperature in helium gas. The reduced unsupported (modified) sample was immediately transferred to a glove box and prepared by immediately diluting 1.0 mg of the samples with 0.2 g of KBr and then pressed into translucent pellets. A total

of 32 scans were taken in the range of 400 – 4000 cm^{-1} for each reduced sample. For each sample after a background scan of KBr was taken in the transmission mode at the resolution of 8 cm^{-1}.

The reduction behaviour of the supported catalysts was studied using temperature programmed reduction (TPR) performed on an AutoChem2950 (Micromeritics Instrument Corp., USA). The sample (ca. 0.1 g) was degassed at 393 K under argon flow (50 mL (NTP)/min) for 1 hr. The temperature was subsequently decreased to 340 K followed by the change in gas composition to 5 vol-% H_2/Ar keeping the flow rate at 50 mL (NTP)/min. The temperature was linearly increased from 340 K to 1173 K at 10 K/min.

The degree of reduction of the catalyst was determined for all samples reducing the catalyst at 573 K for 8 hours, succeeded by cooling in argon. Temperature programmed reduction of the reduced samples by ramping the temperature by 10 K/min in a gas mixture of 5% H_2 in argon. The degree of reduction was computed from the relative hydrogen consumption of the reduced catalyst to that required for complete reduction of CoO.

Temperature programmed desorption of CO was performed in a 1 cm I.D. quartz reactor in an AutoChem2929 (Micrometics Instrument Corp., USA). For the TPD experiments, the loading of the catalysts was 10 wt.-% of cobalt oxide on β-SiC. The catalyst was crushed into a fine powder and loaded in to the quartz reactor. The catalysts were subsequently reduced under H_2 atmosphere (40 mL(NTP)/min) at 573 K for 16 hours (heating ramp of 10 K/min). The system was subsequently cooled down to 383 K in helium. Subsequently CO was injected into the helium flow (50 mL (NTP)/min (15 times with 0.012 mmol CO/g_{Co} per dose). The temperature of the system was then increased using a linear ramp of 10 K/min to 1223 K in a flow of helium (50 mL/min) monitoring the change in the thermal conductivity of the effluent using a TCD.

The dispersion of cobalt in the catalysts deposited on β-SiC was determined using H_2 chemisorption. This was performed on a Micromeritics ASAP 2020 using the static volumetric method. The sample holder was loaded with 0.5 g of sample sandwiched between two layers of glass wool. The sample holder was degassed at 383 K overnight to remove any adsorbed moisture. The catalyst was reduced *in situ* for 8 hours at 573 K with hydrogen. Following the

reduction, hydrogen was removed from the system using helium as a purge gas prior to evacuation. The H_2-chemisorption was conducted at 398 K.

Fischer-Tropsch synthesis

Fischer-Tropsch synthesis was carried out in a fixed bed reactor system. The model catalysts (0.1g modified or unmodified cobalt oxide/0.9g C) was diluted with silicon carbide ($d_{particle}$ = 200-500μm) and loaded into the isothermal zone of the reactor. Catalyst activation was carried out through hydrogen reduction (40 mL (NTP/min) at 1 bar and 473 K (heating rate: 5 K/min) for 16 hours. After catalyst activation, the catalyst is cooled down to 493 K in argon. Fischer-Tropsch synthesis was carried out at 493 K, 20 bar, $(H_2:CO)_{inlet}$=2 and $F_{CO,0}/W$ = 5.56 mmol/(min·g_{Co}) for 44 hours.

7.3 Result and discussion

The use of colloidal chemistry methods for the synthesis of cobalt nanoparticles may produce well dispersed particles with ease of size measurement alleviating the problem of correlating of the morphology of the finally obtained cobalt nanoparticles with any changes in catalytic performance. Cobalt-based nanoparticles were synthesized through thermal decomposition of cobalt carbonyl. The obtained nanoparticles are uniform both in shape and in size (see *Fig. 7.1*). Both the uniform shape and the narrow size distribution allows the use of these nanoparticles as a model for studying metal-support interaction in catalysis. The crystallite size distribution was determined from transmission electron microscopy with a minimum of 300 counted crystallites. The crystallite size distribution was modelled as a unimodal log-normal distribution. The synthesized particles attained a uniform icosahedron shape with the particle size of 26.1±4.3 nm (μ = 3.2588; σ = 0.079) (see *Fig. 7-1).*

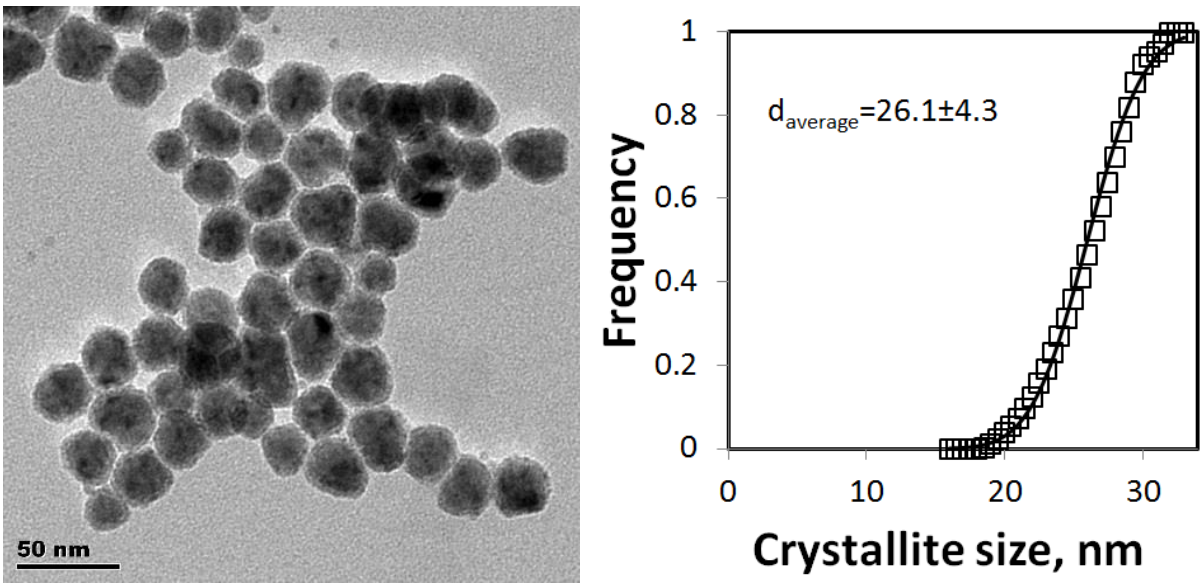

Figure 7-1: **C**obalt nano-crystallites obtained using decomposition of cobalt carbonyl[17] (left) and their cumulative size distribution (right) modelled as a log-normal distribution (μ = 3.2588; σ = 0.079)

Ex situ powder x-ray diffraction analysis shows that the synthesized particles are present as Co(II)O (see *Fig. 7-2*). There are no traces of either metallic cobalt or Co_3O_4. This may indicate that although synthesis method targets the synthesis of cobalt nanoparticles, exposure of the metal of the nanoparticles to oxygen during drying process may have resulted in the oxidation of the nanoparticle to CoO phase. However, the exposure seems not enough to result in complete oxidation to Co_3O_4. The crystallite domain from the Rietveld refinement of the XRD pattern (using TOPAS 4.1, Bruker AXS) in the as-synthesized particles is 13.6 nm. This is significantly less than the size obtained from transmission electron microscopy (TEM) indicating that each particle on the TEM micrograph may represent multiple crystalline domains.

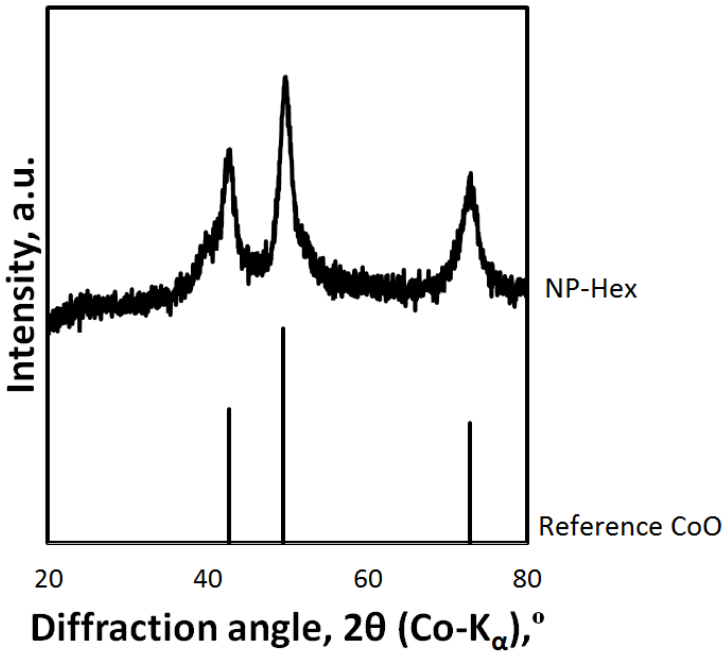

Figure 7-2: X-ray diffractogram of unreduced unmodified samples

The cobalt oxide nanoparticles were contacted with solutions of n-hexane containing the different silanes. The silicon uptake as a function of time was monitored using SEM/EDX by measuring the amount of silane on the samples relative to cobalt after a certain time interval. The $\left(\frac{Si}{Co}\right)$ molar ratio was plotted as a function of exposure time (see *Fig. 7-3*). The rate of uptake increases initially and reaches a virtual equilibrium after 4 hours with the $\left(\frac{Si}{Co}\right)$ mole ratio about 28 mmol/mol for the sample modified with 5.51 mM TEOS in n-hexane. The virtual equilibrium $\left(\frac{Si}{Co}\right)$ for the sample exposed to a solution containing 5.51 mM of triphenyl ethoxysilane in n-hexane, is 28.4 mmol/mol, which is attained after 10 hours. When the modification process is completed after exposing the cobalt nanoparticles to a solution containing 5.51 mM of trimethylchlorosilane in n-hexane, the virtual equilibrium $\left(\frac{Si}{Co}\right)$ ratio becomes 39 mmol/mol after 0.5 hours (*see Table 7-1*). This is an indication that the rate of uptake is fastest when the modification is performed with trimethyl chlorosilane and slowest when the modification is performed with triphenyl-ethoxysilane.

The uptake can be similarly modelled as a Johnson-Mehl-Avrami'Kologomirov[18,19] growth process described in the previous chapters with an empirical rate of uptake:

$$\left(\frac{Si}{Co}\right) = \left(\frac{Si}{Co}\right)_{equi} \cdot \left(1 - e^{\left(\frac{-t}{\tau}\right)^m}\right)$$

The obtained values of **m** are 2.3 ± 0.4, 1.7 ± 0.5 and 1.4 ± 0.2 for the samples modified with tetraethoxysilane, triphenyl ethoxysilane and trimethyl chlorosilane respectively (*see Table 7-1*). The values of **m,** suggest that the adsorbed particles on for sample modified tetraethoxysilane may have grown into 2 dimensional silica surface species growing from layers into 3D shapes whereas for the samples modified with triphenyl ethoxysilane and trimethyl chlorosilane are more similar to one dimensional structures[19]. The values of τ are 2.3 ± 0.1, 1.6 ± 0.6, 3.7 ± 0.8 hours for the samples modified with tetraethoxysilane, triphenyl ethoxysilane and trimethyl chlorosilane respectively. The value of τ is inversely related to the number of nuclei of the growing particles and the rate constant. Therefore, from the values of τ, it may be conjectured that the rate constant for the adsorption of trimethyl chlorosilane is higher, followed by that of tetraethoxysilane. On the other hand, the smaller value of τ for samples modified with trimethyl chlorosilane may indicate that there are many more silane nuclei adsorbed on the surface of cobalt compared to the number of silica nuclei adsorbed on the surface cobalt when the modification is done with tetraethoxysilane and triphenyl ethoxysilane.

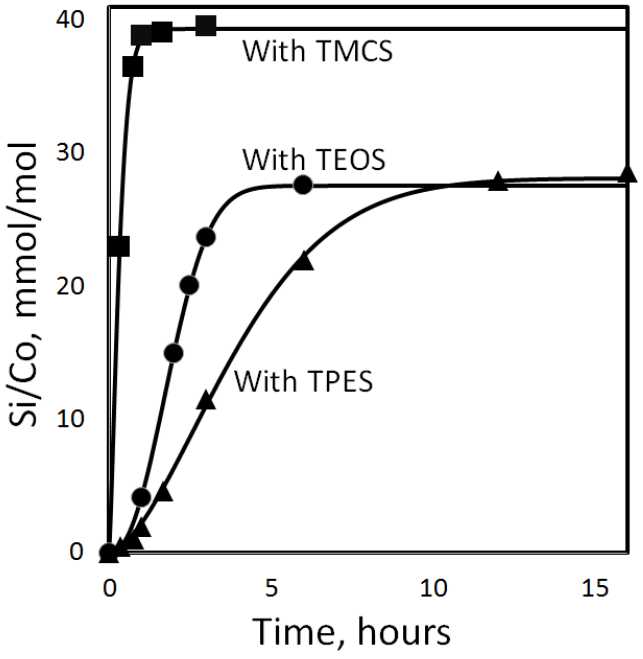

Figure 7-3: Silane uptake by cobalt oxide in dry n-hexane as a function of time for $[TEOS]_{initial}$ = 5.51 mM, $[TMCS]_{initial}$ = 5.51 mM $[TPES]_{initial}$ = 5.51 mM)

Table 7-1: Conditions for contacting cobalt nano-particles with solutions of silane in n-hexane (solid concentration 1.4 g/L) at room temperature to obtain maximum silane loading.

Catalyst ID	$[silane]_{initial}$, mM	Contact time, hours	$\left(\frac{Si}{Co}\right)$ ratio, mmol/mol	Dimensionality	Time constant, hours
NP-Hex-TEOS	5.51	5	28.7	2.3 ± 0.4	2.3 ± 0.1
Co-Hex-TPES	5.51	10	28.8	1.7 ± 0.5	1.6 ± 0.6
Co-Hex-TMCS	5.52	3	39.8	1.4 ± 0.2	3.7 ± 0.8

To obtain same silicon loading on the cobalt surface, the initial concentrations of the respective silanes and contact time were varied. The initial concentrations of the silane and the respective contact time recorded to obtain the individual silane loading are shown in *Table 7-2*. The targeted $\left(\frac{Si}{Co}\right)$ ratio on all samples was 28 mmol/mol, although the actual silane loading on the samples as determined using SEM/EDX varied slightly and the obtained $\left(\frac{Si}{Co}\right)$ ratio was 31.4 mmol/mol, 33.5 and 28.2 mmol/mol $\left(\frac{Si}{Co}\right)$ for the material NP-Hex-TEOS, NP-Hex-TEPS, and NP-Hex-TMCS respectively (the samples were named NP-Hex-TEOS-28, NP-Hex-TEPS-28, and NP-Hex-TMCS). It is clear from the contact times that the rate of silane uptake depends on the structure of the silane used. The rate of silane uptake is slowest for triphenyl ethoxysilane and is the quickest for trimethyl chlorosilane. The difference originates from the variation in the reactivity of each silane. Trimethyl chlorosilane is highly reactive due to its nucleophilic nature and thus its uptake on the hydroxylated cobalt oxide surface (as indicated by the infrared absorption bands of the unmodified nanoparticles at around 3400 cm^{-1}) is rapid (*see Fig 7-3*). On the other hand, triphenyl ethoxysilane is a bulky and relatively unreactive molecule and as such its rate of uptake on the surface of cobalt is relatively slow compared to both tetraethoxysilane and trimethyl chlorosilane.

Table 7-2: Conditions for contacting cobalt nano-particles with solutions of silane in n-hexane (solid concentration 1.4 g/L) at room temperature to obtain specified loadings of silicon to cobalt ratios as determined by SEM-EDX (target Si/Co ratio = 30 mmol/mol)

Catalyst ID	$[silane]_{initial}$, mM	$[silane]_{final}$, mM	Contact time, hours	$\left(\frac{Si}{Co}\right)$ ratio, mmol/mol
NP-Hex-TEOS	5.51	4.96	2.5	31.4
Co-Hex-TPES	5.51	4.93	10	33.5
Co-Hex-TMCS	5.52	5.01	1	28.2

Upon modification, there is no observable change for both the particle size and the morphology (see *Fig. 7-3*). The average diameter for the particles remains ca. 26 nm. The average crystallite size fitted to a log-normal distribution of unmodified cobalt oxide (NP-Hex) is 26.1 ± 4.3 (μ = 3.2588; σ = 0.079) while that modified with tetraethoxysilane, triphenyl ethoxysilane and trimethylchlorosilane are 26.7 ± 3.6 nm, (μ = 3.2843; σ = 0.071), 27.1±2.7 (μ = 3.2972; σ = 0.061) and 27.4 ± 4.2 (μ = 3.3070; σ = 0.075) respectively. Thus, the average crystallite size remains the same upon modification.

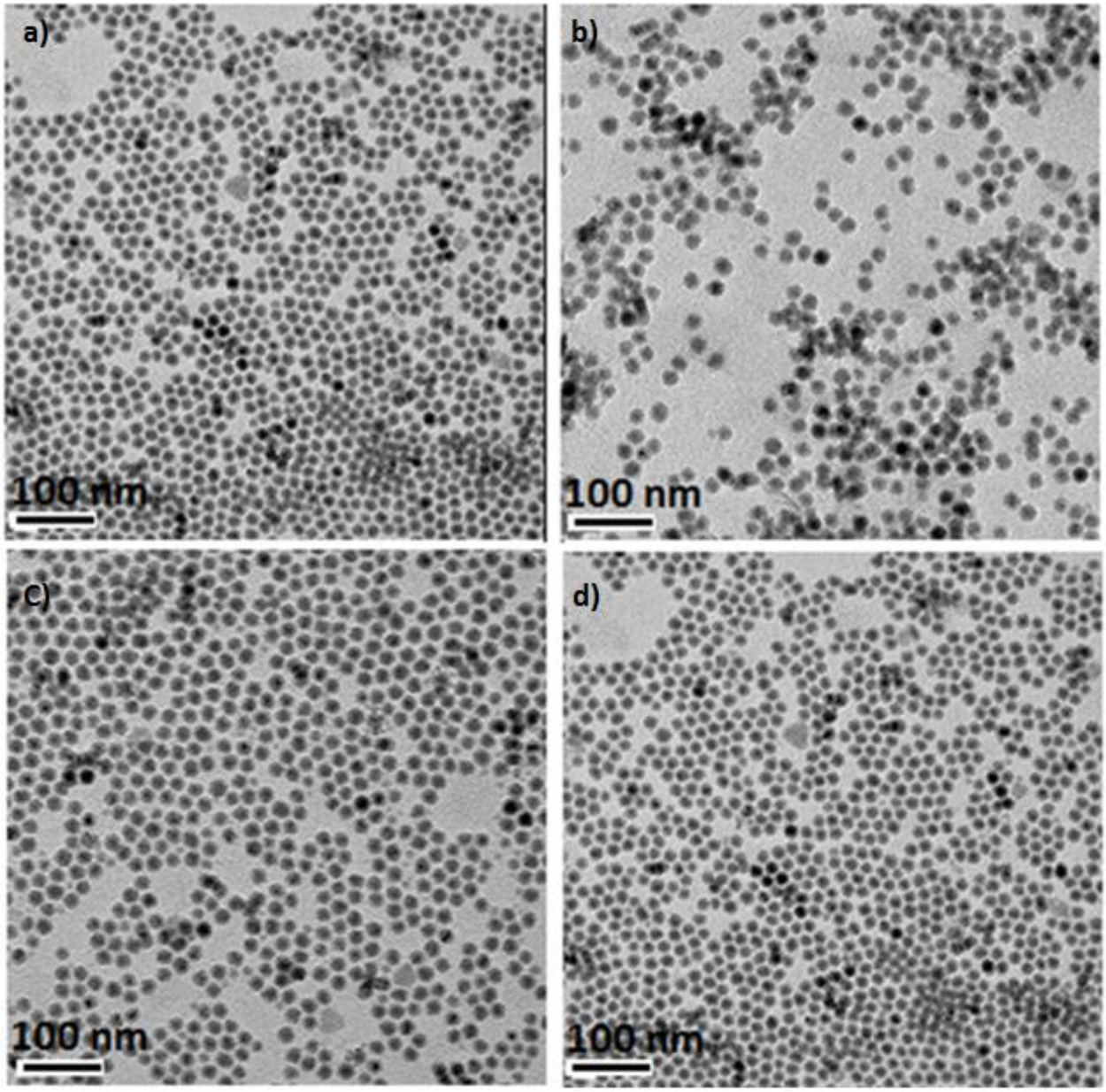

Figure 7-4: TEM images of: a) cobalt nano-crystallites obtained using decomposition of $Co_2(CO)_8$ (26.1 ± 2.3 nm) b) cobalt nano-crystallites obtained using decomposition of $Co_2(CO)_8$ modified with TEOS (26.7 ± 3.6 nm, μ = 3.2843; σ = 0.071), c) modified with TPES (27.1±2.7, μ = 3.2972; σ = 0.061) and d) modified with TMCS (27.4 ± 4.2, μ = 3.3070; σ = 0.075)

Ex situ XRD analysis shows that the synthesized particles are present as Co(II)O (see *Fig. 7-4*). The crystallite domain from the Rietveld refinement of the XRD pattern (using TOPAS 4.1, Bruker AXS) in the as-synthesized particles is 13.6 nm. The crystallite size obtained from XRD is significantly less that the particle size obtained from TEM suggesting that each TEM particle represents multiple crystalline domains. The X-ray diffractogram does not show any additional

X-ray diffraction lines for the modified samples. The samples only contain less than 4-wt.-% of the silanes and this may be too low for detection in the XRD. Moreover, the silanes may not form any crystalline layer that can diffract X-rays as they are expected to be well-dispersed over the cobalt surface.

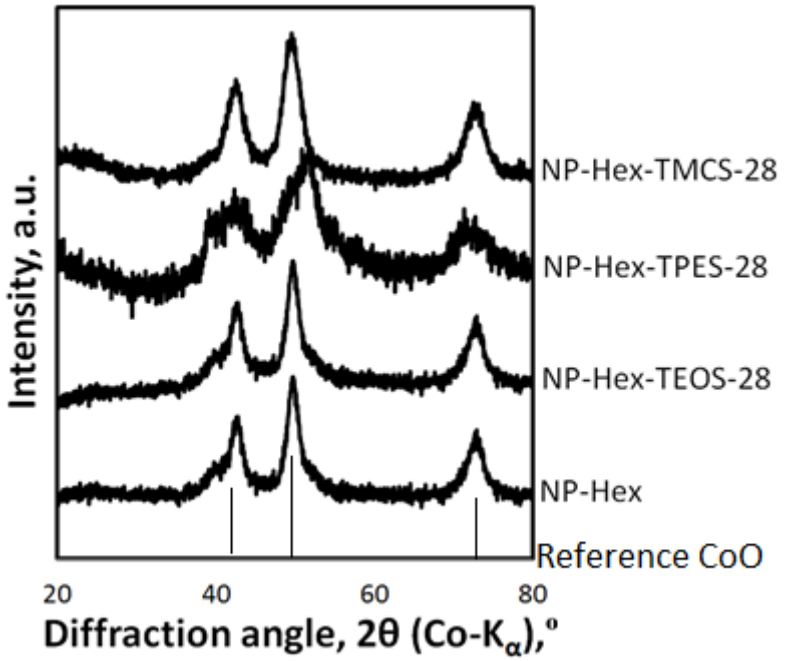

Figure 7-5: X-ray diffractogram of unreduced (modified) samples

Upon reduction with H_2 at 573 K for 8 hours, both unmodified cobalt oxide and cobalt nanoparticles modified with tetraethoxysilane were reduced to metallic (fcc) cobalt (see *Fig. 7-6*). While cobalt oxide modified with triphenyl ethoxysilane or trimethyl chlorosilane were reduced to a mixture of fcc and hcp cobalt. This indicates that while the silanes do not affect the phase structure of the oxide itself (i.e. modification does not facilitate oxidation or reduction), they have a greater influence on the resulting phase of cobalt during the reduction process. Rietveld refinement points out that the composition of the metallic (fcc) cobalt phase is 60%-wt. while the metallic (hcp) cobalt phase constitute about 40 %-wt.

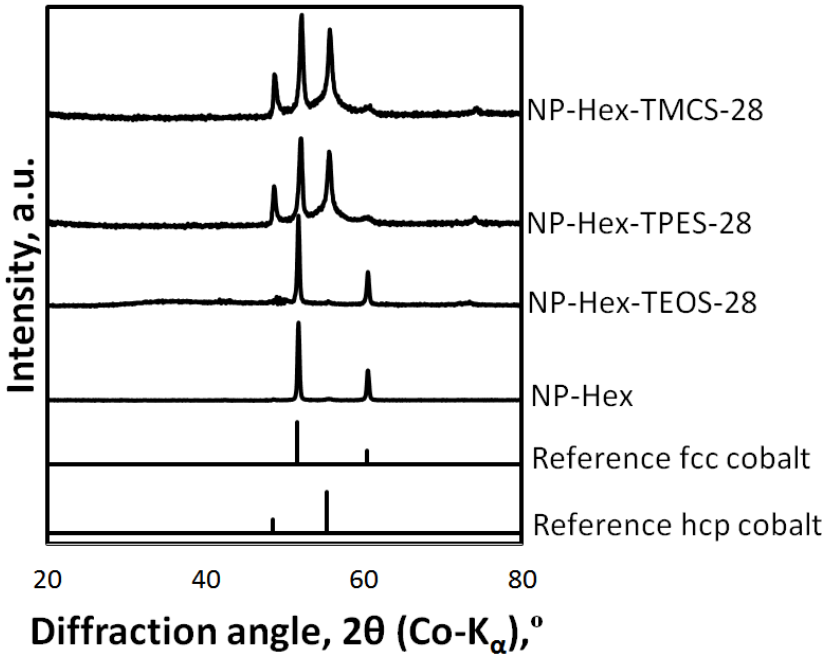

Figure 7-6: X-ray diffractogram of (modified) samples reduced at 573 K with H_2 for 8 hours

An insight about the modification process can be obtained further by characterizing the samples using infrared spectroscopy. The infrared spectrum of the reduced unmodified samples shows bands in three different regions i.e. absorption bands at 1628 cm^{-1}, 2940 cm^{-1} and 3380 cm^{-1} (see *Fig. 7-7*). The absorption bands at 1628 cm^{-1} and 3380 cm^{-1} are ascribed to the surface O-H bending and stretching vibrations[20,21] respectively while the bands at 2940 cm^{-1} may be due to the wagging, twisting and stretching frequencies of the alkyl groups from the organic solvents used.

The infrared spectra of a reduced sample modified with tetraethoxysilane, shows additional absorption bands at 460 $cm^{-1,}$ 800 cm^{-1} and 1100 cm^{-1}. These bands are characteristic for the presence of extraneous silica in the modified samples. The band at 800 cm^{-1} can be attributed to the in-plane Si-O-Si bending vibration[22]. The band at 460 $cm^{-1,}$ and 1100 cm^{-1} are typical band observed due to the asymmetric stretching of the Si-O-Si of the amorphous SiO_4 tetrahedron [23,24]. The base of the band at 1100 cm^{-1} for sample modified with tetraethoxysilane is broad and stretches from 11300 cm^{-1} to 900 cm^{-1} and therefore the existence of the Co-O-Si vibrations[25–27] which occurs at 1020 cm^{-1} cannot be completely excluded.

The relative intensity of the absorption bands at 2940 cm^{-1} due to the C-H vibration ethoxy groups of the tetraethoxysilane seems to be low for this sample after reduction. This may

indicate that the reduction process facilitates the de-ethoxylation process. The band at 1020 cm^{-1} may indicate the occurrence of Co-O-Si vibration, although the same band has been attributed to the presence of oligomeric silicate species[23,27].

The samples modified with trimethyl chlorosilane and triphenyl ethoxysilane both show intense and broad band peaking at 1020 cm^{-1}. These new absorption bands do not correspond to any bands in the pure silanes (see *Fig. 7-7*). This band does not correspond to any absorption bands in the pure silanes (trimethyl chlorosilane and triphenyl ethoxysilane). From the analogy that these types of silanes are monodentate ligands, this bands may be ascribed to the vibrations due to the Co-O-Si rather than the presence of Si-O-Si oligomers most especially because the samples are not calcined. This bond may be formed through the reaction of silanes with the surface hydroxyl of the cobalt surface releasing hydrogen chloride gas upon modifying with trimethyl chlorosilane or ethanol upon modifying with triphenyl ethoxy silane respectively. Additional absorption bands at 1170 and 1250 cm^{-1} for the sample modified with trimethyl chlorosilane and triphenyl ethoxysilane are ascribed to the stretch vibrations due to the Si-C group. The relative intensity of the absorption bands due to the wagging, twisting and stretching frequencies of the alkyl groups is higher and maybe an indication that trimethyl silyl species are present on the surface even after the reduction process.

Similar behaviour is observed when the modification is done using triphenyl ethoxysilane. However, the sample modified with triphenyl ethoxysilane show extra absorption bands at 1400-1450 cm^{-1} which can be ascribed to the presence of phenyl groups. This further indicates that the reduction process does not decompose the phenyl groups of the silanes. It is thus presumed at this stage that tetraethoxysilane is decomposed during the reduction process and may result in silica surface species while alkylated monodentate silanes (trimethyl chlorosilane and triphenyl ethoxysilane) remain intact even after reduction at 573 K.

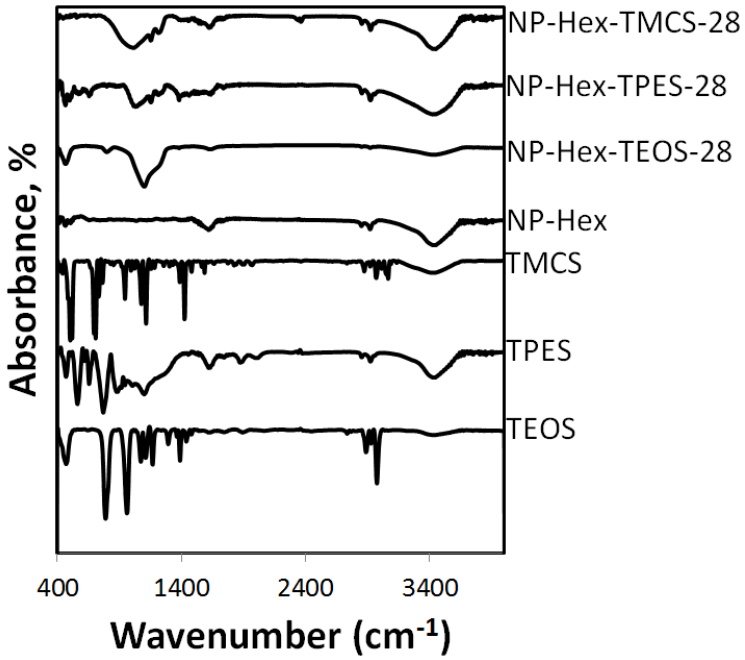

Figure 7-7: FTIR-spectra of the respective silanes and the reduced (modified) cobalt nanoparticles modified by exposure to solutions of silanes in n-hexane and the in the range of 700-4000 cm^{-1}

Surface electronic properties of catalytically active material can be altered by the presence foreign materials in their proximity. This may result in change of oxidation states or a mere electron redistribution on the surface of the metal. Cobalt in cobalt oxide in contact to electron withdrawing species is expected to a shift of the binding energies of the Co 2p photoemission lines to higher energies while electron donating groups are expected to shift the binding energy of the Co 2p to lower values. Surface electronic properties of (un)modified cobalt oxide was determined using X-ray photo-emission spectroscopy. *Figure 7-8* shows characteristic photoemission characteristic of the model catalyst samples. The photoemission peaks of the unmodified cobalt oxide resemble that of a Co 2p of pure CoO (bottom spectrum) with spin-orbit peaks at 778.57 eV and 794.42 eV being ascribed to Co $2p^{3/2}$ and Co $2p^{1/2}$ respectively. The ratio of the Co $2p^{3/2}$ to Co $2p^{1/2}$ is about 2. The two satellites peaks which are usually due to the presence of Co^{2+} are observed at 782.9 eV and 800.02 eV. The intensity of the satellite peaks in this spectrum relative to the main peaks agrees with previous work which shows a proportionality between the intensity of the 2+ component and the satellite structure for a CoO sample[28]. There are no new Co 2p photoemission peaks confirming that the samples remain as CoO even after modification. However, the introduction of silanes results in a shift in the binding energies of the Co 2p photoemission peaks.

The modification of cobalt nanoparticles with TEOS, the binding energy shifts to higher binding energy by 1.07 eV suggesting a reduction of the electron density on cobalt. This indicates that the electron density goes from cobalt to silica. When trimethyl chlorosilane is introduced on the cobalt nanoparticles, the Co $2p1^{/2}$ and Co $2p^{3/2}$ photoemission peaks shifts to lower binding energies by about 0.48 eV *(see Table 7-3)*; also the introduction of triphenyl ethoxysilane results in a shift to lower binding energies by 0.54 eV is observed. The downshift implies an increase in the electron density on cobalt. The difference in the shift suggests that electron donation from the silicon species is slightly stronger in the case of triphenyl ligand compared to trimethyl ligand, possibly due to the resonance effect. The resonance ability of the phenyl-groups may serve as an electron donating agent. This effect can account for the observed difference in the extent of the shift in the binding energy of the Co 2p photoemission peaks modified with triphenyl ligand and trimethyl ligand respectively.

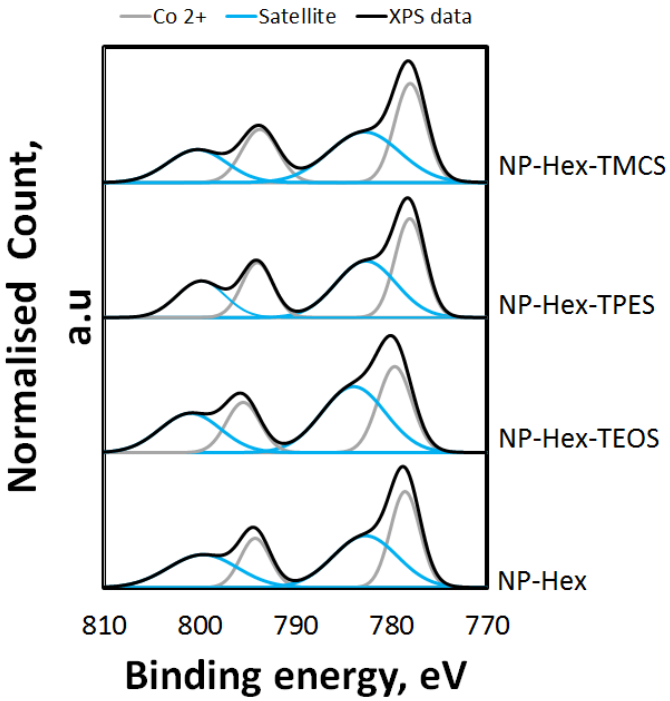

Figure 7-8: Co 2p photoemission features for the unreduced modified samples dried in open air in a fume-hood for 4 hours

Obviously, the photoemission profile of the Si 2p indicates the silanes were present on the samples. It may be expected that a shift in the Si 2p photoemission occurs in the opposite direction as opposed to the shift in the Co 2p peak if indeed the electron density moves across

silica and cobalt boundary. *Figure 7-10* shows the Si 2p XPS features of the modified samples. The Si peak of the samples is referenced against as-synthesised Stöber silica spheres (see Chapter 4 for synthesis method and characterization). The Si 2p photoemission peaks of the reference Stöber silica spheres is characterized by two convoluted peaks that are ascribed to SiO_2 (108.21 eV) and Si-O suboxides (107.23 eV). The ratio of the Si 2p photoemission peak attributed to SiO_2 and the Si 2p photoemission attributed to the Si-O suboxides is 4. The Si 2p photoemission peaks for the sample modified with tetraethoxysilane resembles that of reference silica, but the ratio of the peak ascribed to the Si 2p of SiO_2 (Si^{4+}) to that of the Si-O suboxide decreases drastically to 0.95. This indicates a significant increase in the relative quantity of suboxide. This may be ascribed to the difference in the structure of the silica islands on the surface of cobalt and the amorphous silica used as a reference. Furthermore, as expected a shift to the lower binding energy by 0.9 eV is observed in the Si 2p peak of the sample modified with tetraethoxysilane. This may confirm that electron density goes towards Si atoms from the cobalt atom.

The photoemission peaks of the samples modified with trimethyl chlorosilane and triphenyl ethoxysilane show quite a different Si 2p photoemission features. For these samples the observed photoemission line may be ascribed to the presence of Si-R at around 104.5 eV where R is of the methyl groups and 103.5 eV where R is of the phenyl groups). This may confirm that phenyl groups shift more electrons towards silicon than methyl groups and the difference can be attributed to the resonance effect of the electrons in the phenyl ring. In addition to this peak is a photoemission peak at 107 eV ascribed to Si-O of the suboxides. The maximum for the suboxide is shifted in the same direction as the binding energy of Co 2p (i.e. shifting towards lower binding energies). This may indicate an increase in the electron density on the silicon. This unexpected shift may be due to the electron density due to electron density moving from the highly electron rich alkyl groups to the Si atom, thus causing a shift to lower binding energy.

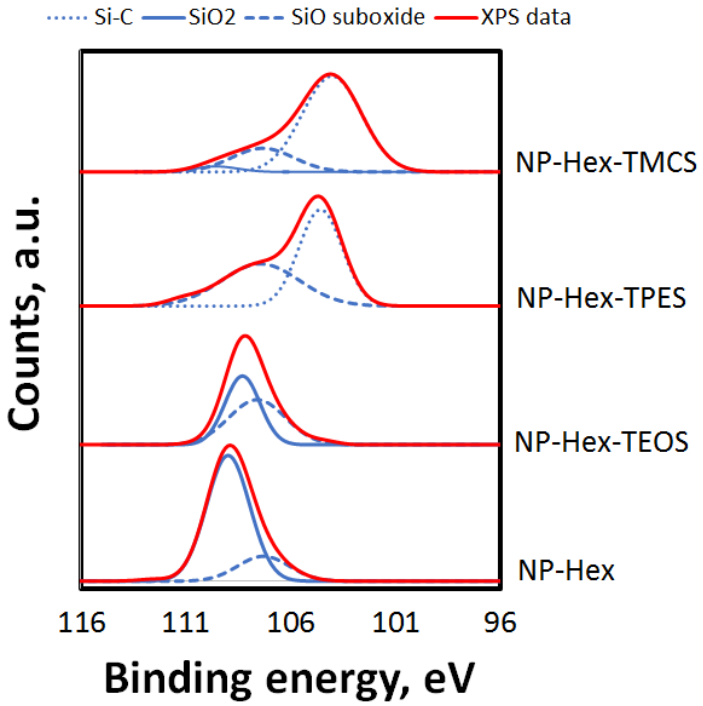

Figure 7-9: Si 2p photoemission features for the model samples

Table 7-3: XPS binding energies of Co 2p and Si 2p

Sample ID	Binding energy, eV				
	Co $2p^{1/2}$	Co $2p^{3/2}$	Si 2p (SiO_2)	Si 2p (Si-O)	Si 2p (Si-C)
NP-Hex	794.42	778.57	-	-	-
NP-Hex-TEOS	793.90	778.03	107.59	106.37	-
NP-Hex-TPES	794.01	779.64	-	106.83	103.52
NP-Hex-TMCS	794.23	778.08	-	106.93	104.55
SiO_2	-	-	108.48	107.23	-

The effect of the modification on reducibility of the catalyst was characterized using temperature-programmed reduction. *Figure 7-11* shows the TPR profiles of the (modified) CoO catalyst. The reduction of cobalt nanoparticles occurs in single reduction step with a peak maximum at 568 K. The single reduction step is usually ascribed to the reduction of CoO to

metallic cobalt. This reduction process is thought to be best described according to a uni-molecular decay model[29]. A shift is observed in the position of this main reduction peak to 577 K, 585 K and 583 K is observed when the material has been modified by adsorption of tetraethoxysilane, triphenyl ethoxysilane and trimethyl chlorosilane respectively. This shift in the peaks may be similar to the peak shift observed for cobalt oxide chemically bound to silica[30]. Furthermore, a second reduction peak (which is best fitted using uni-molecular decay) starts to appear at high temperatures. The appearance of a high temperature reduction peak may imply the presence of cobalt species in the sample which are more difficult to reduce. Such compounds may have been formed upon a chemical interaction between the silanes and the cobalt surface.

The TPR-profiles were deconvoluted accordingly by fitting the whole TPR profile to the uni-molecular model.

Upon modification with the silanes, the activation energy for the reduction of CoO nanoparticles assuming the unimolecular decay model was determined to be 45±6 kJ/mol (A = $10^{3.6\pm0.4}$ s^{-1}) (*see Table 7-3*). For the sample modified tetraethoxysilane, (28 mmol/mol), the activation energy for increased to 59±8 kJ/mol (A = $10^{3.1\pm0.3}$ s^{-1}) implying that the presence of silicon in the sample retards the reduction of Co_3O_4 to CoO. The consecutive uni-molecular decay of the hard-to-reduce cobalt oxides due to interaction with silanes has an activation energy of to metallic cobalt is also retarded and an activation energy of 74±11 kJ/mol (A = $10^{4.1\pm0.1}$ s^{-1}) was determined. Similarly, the activation energy of reduction also increases when the modification is done with triphenyl ethoxysilane and trimethyl chlorosilane. The change in the observed activation energy strongly suggests that silanes are bonded to the surface of cobalt, since it hinders the reduction of ionic cobalt in these materials.

Table 7-4: Kinetic parameter for the reduction of silane modified supported CoO

$\left(\frac{Si}{Co}\right)$ *ratio*,	Activation energy, kJ/mol		A, (s^{-1})		R^2,[a]	
mmol/mol	Peak 1	Peak 2	Peak 1	Peak 2	Peak1	Peak2
NP-Hex	45± 6	-	$10^{3.6\pm0.4}$	-	0.98	0.99
NP-Hex-TEOS-28	59 ± 8	74±11	$10^{3.1\pm0.3}$	$10^{4.1\pm0.1}$	0.99	0.99
NP-Hex-TPES-28	45 ± 15	77±9	$10^{3.4\pm0.8}$	$10^{.23\pm0.3}$	0.99	0.99
NP-Hex-TMCS-28	52 ± 9	81±6	$10^{2.1\pm0.1}$	$10^{.1.1\pm0.1}$	0.97	0.98

[a] Coefficient of regression obtained by fitting the TRP profiles to the respective reduction models

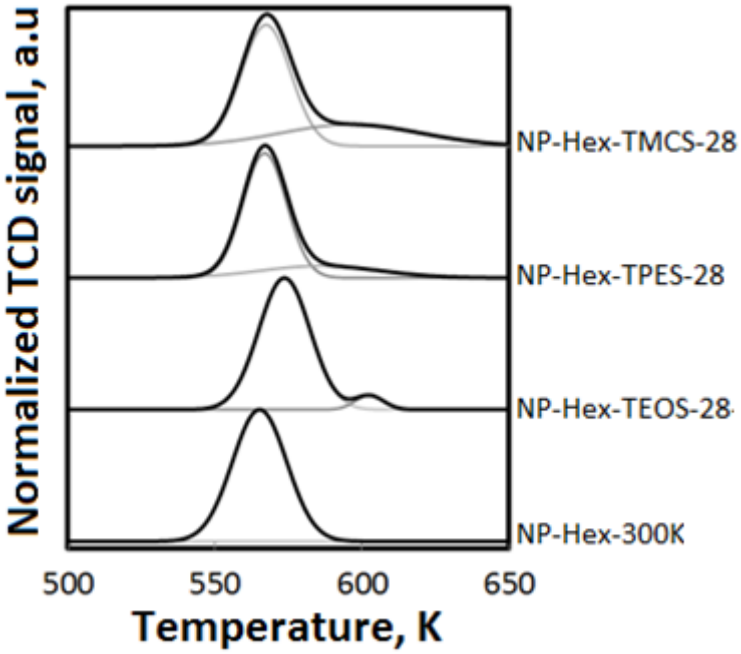

Figure 7-10: TPR profile of the unreduced model catalyst

The nature of the reduction peak due to strongly interacting cobalt oxide, differs from ligand to ligand. When modified with tetraethoxysilane the peak is not broad. However, the peak becomes very broad when modifying cobalt nanoparticles with either triphenyl ethoxysilane or trimethyl chlorosilane. This may be attributed to the high activation energy for the reduction of the cobalt species reduced at the high temperatures when modified with alkylated ligands than when using tetraethoxysilane.

The total hydrogen consumed in each profile was computed by integrating the area under the graph. From the computed hydrogen consumptions, all the catalysts are completely reduced after 650 K. *Table 7-4* summarises the hydrogen consumption of the catalyst with respect to the individual peaks. A 100% reduction is achieved at 620 K when the sample is modified with tetraethoxysilane. The total amount of H_2 is 1 mol H/mol of Co, i.e. the theoretical amount for the reduction of CoO. This indicates that the only species being reduced in the system is CoO. For the sample modified with akylated samples, the total hydrogen consumed surpasses the expected hydrogen consumption (by 9% for the sample modified with triphenyl ethoxysilane and 12 % for the sample modified by trimethyl chlorosilane). In fact, for the sample treated with triphenyl ethoxysilane, the amount of excess hydrogen consumed is consistent with the amount of phenyl groups. A sample containing 33.5 mmol Si/mol Co contains 0.1 mol of the phenyl

groups per mol of Co. The phenylated silane may be hydrogenated following the equation below:

$$-Si(Ph)_3 + 3H_2 \rightarrow -SiH_3 + 3(Ph\text{-}H)$$

By stoichiometry, 0.1 mol of H_2 per mol/mol Co will be consumed. This corresponds to 10 % excess H_2. This is not dissimilar to the measured 9 % excess hydrogen consumption. The 12 % excess H_2 consumption for the sample modified with trimethyl chlorosilane can be attributed to a similar effect.

Table 7-5: Relative amount of hydrogen consumption during temperature programmed reduction

	Expected stoichiometric amount of H_2 consumed (mol H_2/mol Co)	Actual amount of H_2 consumed (mol H_2/mol Co)
NP-Hex	1	1
NP-Hex-TEOS	1	1
NP-Hex-TPES	1	1.09
NP-Hex-TMCS	1	1.12

The active phase of the cobalt-based catalyst for the Fischer-Tropsch synthesis is metallic cobalt [39]. Hence, the reduction from cobalt oxide to the metallic phase is a pre-requisite. The activation process is usually performed in hydrogen at a constant temperature for a certain time. In the current study, (modified) cobalt oxide (CoO) catalysts were activated in hydrogen at 573 K for 8 hours. The activity of the catalyst may be affected by the degree of reduction of cobalt oxide to metallic cobalt at this isothermal activation. It was thus important to determine the effects modification on the degree of reduction of the catalysts. The degree of reduction of the catalyst was determined for CoO and the modified samples by reducing the catalyst at 573 K, followed by cooling in argon. The reduced samples were subsequently reduced in a temperature programmed manner by ramping the temperature by 10 K/min in a gas mixture of 5% H_2 in argon up to 1K. The degree of reduction was computed from the relative hydrogen consumption of the reduced catalyst to that required for complete reduction of CoO. *Table 7-5* summaries

the degree of reduction of the respective catalyst. The degree of reduction of the unmodified catalyst is only slightly reduced by the modification process indicating that that the interaction of cobalt with the silanes is strong enough to suppress the reduction of cobalt oxide to metallic cobalt at 573 K.

Table 7-6: Degree of reduction of the supported model catalysts after 8-hours reduction at 573 K

Catalyst ID	Degree of reduction, %
NP-Hex	95
NP-Hex-TEOS	92
NP-Hex-TPES	90
NP-Hex-TMCS	87

The modification process reduces the metal dispersion of the supported nanoparticles both on the fresh and spent catalyst (*see Table 7-6*). H_2 chemisorption was used to determine the effects of silane modification on the dispersion of the supported (modified) cobalt nanoparticles. The H_2 chemisorption on the surface of the reduced samples can be best described using the Langmuir isotherm for a dissociative adsorption. When silanes are introduced on the surface of cobalt, the total amount of H_2 adsorbed per gram of material decreases slightly (*Table 7-5*). The largest drop in the H_2 adsorption capacity is observed when the sample is modified with triphenyl ethoxysilane followed by trimethyl chlorosilane and tetraethoxysilane. The unmodified samples seem to indicate a dispersion of ca. 3%. A silane loading of about 30 mmol/mol $\left(\frac{Si}{Co}\right)$, would be expected to completely cover the surface cobalt if the $\frac{(Si)}{(Co_{Surface})}$ ratio is 1:1. This may result in a complete suppression of H_2 uptake on the surface. However, a complete suppression in H_2 chemisorption is not achieved indicating that the $\left(\frac{Si}{Co_{Surface}}\right)$ ratio is not 1:1. The amount of surface cobalt covered by silane molecules $(Co_{Covered})$ can be estimated from the amount hydrogen adsorbed on the unmodified sample and the amount of hydrogen adsorbed on the modified sample. The $\left(\frac{Si}{Co_{Covered}}\right)$ ratio may give an idea of how the silane adsorbs onto the surface of cobalt (see Table 7-5). When modified with tetraethoxysilane, the $\left(\frac{Si}{Co_{Surface}}\right)$ ratio is about 20 mol/mol. This ratio decreases drastically to

3.6 and 4.2 when the modification is done with triphenyl ethoxysilane and trimethyl chlorosilane respectively. This may indicate that with tetraethoxysilane, larger clumps of silica are formed on relatively small amount of cobalt whereas the triphenyl ethoxysilane and trimethyl chlorosilane seem to cover more of the surface cobalt. Fischer-Tropsch synthesis does not seem to cause any sintering or particle breakdown as the dispersion of cobalt does not seem to change during the Fischer-Tropsch synthesis.

Table 7-7: The amount of hydrogen taken up to form a monolayer on the catalyst reduced at 473 K for 8 hours, and metal loading of the spent catalyst

Catalyst ID	V_m, $cm^3(H_2, STP)/g_{Co}$		$\left(\frac{Si}{Co_{Surface}}\right)$, mol/mol		Metal loading of spent catalyst, %
	Fresh catalyst	Spent catalyst	Fresh catalyst	Spent catalyst	
NP-Hex	6.21±0.17	6.13±0.12	0	0	7.2
NP-Hex-TEOS	5.92±0.98	5.88±0.23	20	22	7.5
NP-Hex-TPES	4.43±0.44	4.550±0.53	3.6	3.2	7.3
NP-Hex-TMCS	4.98±0.38	4.89±0.31	4.2	4.3	7.0

The strength of adsorption of CO from the model catalysts was investigated using CO-TPD. CO programmed thermal desorption curves of unmodified cobalt show two distinct desorption peaks located 640-750 K and at 950-1100 K for all the supported catalysts after dosing CO during the adsorption stage (see *Fig. 7-12*). The double peaks shows that CO is adsorbed differently on the surface of cobalt suggesting a possibility of minimum of two different adsorption sites[31]. It should be noted that these desorption peaks occur at relatively high temperatures compared to the previously recorded desorption temperatures of CO from a cobalt surface[31]. This shift to higher temperatures may be not be very dissimilar to shift observed by Zagli and Falconer[32] attributed to the re-adsorption of desorbed CO. It should be noted, that the amount of catalyst loaded into the reactor for this temperature programmed desorption experiments is high, which will increase the likelihood of CO re-adsorption.

The desorption peaks may originate from either the desorption of CO from dissimilar binding state or because of a coverage-dependent desorption. The first desorption peak occurring in the temperature range of 640-750 K relates to the CO which is not strongly adsorbed (i.e. molecularly adsorbed) compared to the CO which is strongly adsorbed resulting in the seconds

desorption peak usually ascribed to the CO adsorbing in a dissociative manner. This has been verified using labelled isotopic exchange experiments which are dependent on the recombination and desorption of dissociated carbon monoxide molecule[33,34]. The dissociation of CO may also be confirmed by following the formation of CO_2 in the system. The formation of CO_2 may result from a recombination reaction involving oxygen atoms from a dissociatively adsorbed CO with adsorbed CO or surface C species.

Upon modification cobalt nanoparticles with silanes, the total amount of CO adsorbed is decreased by about 16% - 27 % (see *Table 7-6)*. A decrease in the total amount of CO adsorbed on the surface of cobalt indicates that the presence of silane hinders the adsorption of CO. This may be related to the reduction in the available surface area for adsorption. The presence of silane on the surface of cobalt may block some adsorption sites and hence a decrease in the total absorption capacity of cobalt. The decrease in the CO adsorption capacity is consistent with the decrease in the H_2. However, while it may be expected that the ratio of CO adsorbed to H_2 required to form a monolayer is 1:0.5. the obtained ratio is about 1:1 indicating that less CO is adsorbed than expected. This may be ascribed to the lateral interactions occurring between the CO molecules upon adsorption.

Furthermore, the temperature programmed desorption profile changes with the development of new desorption peaks while others disappear. This suggests that the cobalt-ligand interface may result in the formation of new adsorption sites for CO on the surface or alternatively facilitates CO dissociation upon desorption. Moreover, the ratio of the low temperature CO desorption peaks (650 K - 750 K) to that of the high temperature desorption peak (800 K - 1100 K) is altered. For the unmodified sample, the low temperature desorption peak accounts for 0.10 mmol of CO and the high temperature desorption peak accounts for 0.08 mmol CO (ratio =1.25) (see *Table 7-6*). Upon modification a change in the ratios of the desorption peaks is observed. When cobalt oxide is modified with tetraethoxysilane, the ratio of the CO attributed to the low temperature desorption peak to that of high temperature desorption becomes 0.5. A similar effect is observed when cobalt is modified with alkyl group containing silanes. The ratio of molecularly adsorbed CO to dissociatively adsorbed CO is 0.29 and 0.44 for trimethyl chlorosilane and triphenyl ethoxysilane modified cobalt respectively. This may be an indication

that the presence of the silanes on the surface of cobalt facilitates the dissociation of CO upon adsorption.

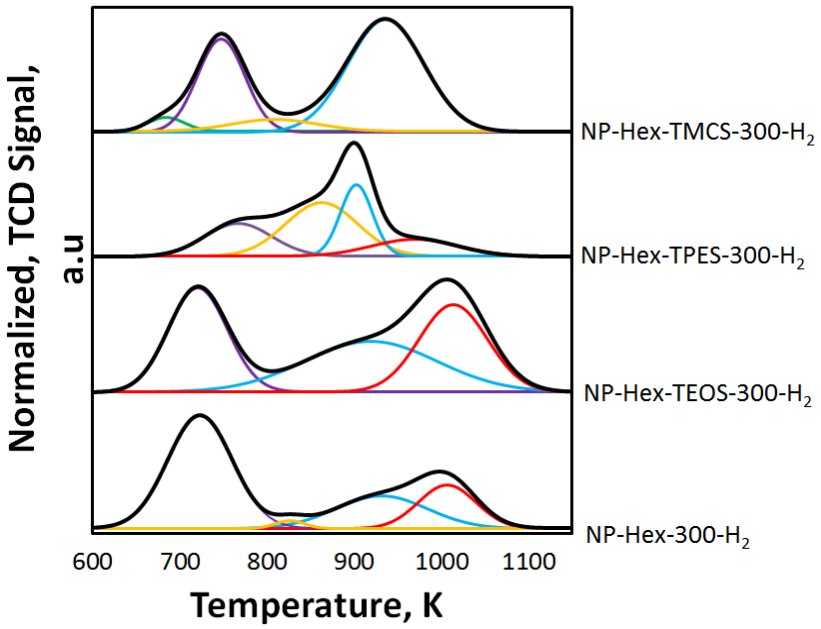

Figure 7-11: CO-TPD profiles of the modified supported catalysts reduced at 573 K, for 8 hours in hydrogen

CO tends to withdraw electrons upon adsorbing on cobalt surface as electron rich surfaces as electron rich surfaces donate more electrons to the CO 2π obirtals[35]. Therefore, electron donating ligands (e.g. triphenyl ethoxysilane, trimethyl chlorosilane) attached to the surface of cobalt may be expected to weaken the C=O bond thus facilitating the dissociation of CO. if the dissociation takes place at the adsorption temperature, a larger amount of dissociated CO would result in a reduced uptake. This may explain why modification of cobalt with electron donor silanes yields a larger fraction of dissociatively adsorbed CO. On that note, electron withdrawing ligands (e.g. tetraethoxysilane) attached to the surface of cobalt may be expected to strengthen the Co=C bond. It may be expected that since electron density goes from the surface cobalt atom to silica, when cobalt is modified with tetraethoxysilane as indicated by XPS, the C=O bond be strengthened, retarding the rate of C=O dissociation. However, from the CO temperature programmed desorption results, the ratio of the amount of dissociatively adsorbed CO to that of molecularly adsorbed CO is increasing when cobalt is modified with electron withdrawing silica. This suggest an alternative mechanism for the dissociation of CO and precludes the opinion that CO dissociation is facilitated only through electron enrichment of cobalt surface. This may alternatively suggest that the silica islands, through the hydroxyl groups, may interact

directly with CO in a way that may reduce the CO dissociation barrier in a way similar to the suggested route for hydrogen assisted CO dissociation on terrace sites[36]. A similar effect by the hydroxyl groups has been shown for presence of hydroxyl groups on the alumina ligand on a cobalt surface[37].

An attempt to deconvolute the CO-TPD peaks was made using Gaussian distribution. It is can been seen that after deconvolution, for the unmodified sample, the high temperature desorption may result from a possibility of three convolved desorption peaks having maxima at 830 K, 900 K and 1000 K (*see Table 7-7*). These desorption peaks may originate from the desorption of dissociatively adsorbed CO from dissimilar binding state. Using Gaussian functions to deconvolute the TPD-spectra may not be very accurate when applied in the desorption process as the desorption process itself is a complex process. Upon modification, a change in the ratio on the individual convolved high temperature peaks also changes thus resulting in a shift in the overall peak. From these shifts, information on the strengths of the Co-C bond could be derived. These shifts to lower temperatures may suggest that the Co-C band has been weakened whereas shifts to higher temperatures may indicate a stronger Co-C. When modified with tetraethoxysilane, the high temperature peak comprises only of two peaks that desorb at 900 K (minor peak) and 1000 K (major peak).

When modified with triphenyl ethoxysilane, the high temperature desorption peak comprises mainly on the peak at 830 K and 900 K and the peak at 1000 K, seems to vanish. Modification with trimethyl chlorosilane results only in CO desorbed at 900 K. This difference in the ratios of dissociatively adsorbed CO implies that although all silanes seem to facilitate the dissociation of CO, the adsorption strength may differ as well. A shift of the high temperature desorption peak during tetraethoxysilane modification to relatively low temperatures desorption peaks observed for the modification with trimethyl chlorosilane and triphenyl ethoxysilane may suggest that trimethyl chlorosilane and triphenyl ethoxysilane decreases the adsorption strength of dissociatively adsorbed CO.

Table 7-8: Relative amount of CO desorbed as molecularly adsorbed CO versus dissociatively adsorbed CO for samples dosed 15 times with 0.012 mmol CO/g_{Co} per dose

Catalyst ID	amount of CO desorbed (mmol/g_{Co})					Ratio Peak A/Peak B
	Total	Peak A	Peak B			
		Peak 1 (700 K)	Peak 2 (830 K)	Peak 3 (900 K)	Peak 4 (1000 K)	
NP-Hex	0.18	0.10	0.005	0.041	0.034	1.25
NP-Hex-TEOS	0.15	0.06	-	0.043	0.047	0.67
NP-Hex-TPES	0.13	0.03	0.045	0.035	0.020	0.30
NP-Hex-TMCS	0.14	0.05	-	0.09	-	0.55

Fischer-Tropsch synthesis

The supported catalysts were activated in hydrogen at 573 K for 16 hours. The reduced unmodified catalyst was used as a control experiment with a conversion of 2% ca. after 44 hours on stream at 493 K, 20 bar, $(H_2/CO)_{inlet}$ = 2 and $F_{CO,0}/W$ = 5.56 mmol/(min·g_{Co}). The catalytic activity of all catalysts remains constant over the 44 hours (see *Fig. 7-13)*. At approximately similar silicon loading, the catalytic activity is enhanced by the modification albeit at different extents (see *Table 7-7*). There are different factors that must be taken into account to describe the change in catalytic activity. These factors include differences in phase structure, degree of reduction, difference in exposed surface area of the active metal and change in electronic properties. The degree of reduction decreases upon modifying cobalt nanoparticles with the respective silane, albeit only to a small extent.

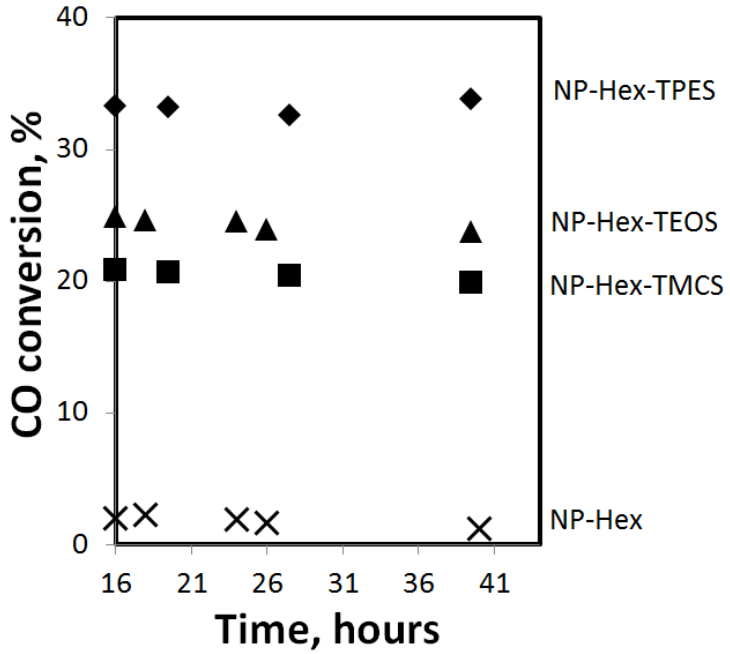

Figure 7-12: Conversion of CO as a function of time on stream for the model catalysts

Phase structure of the catalytically active also play an important role in catalysis. Metallic hcp cobalt has been previously reported to be catalytically more active that fcc cobalt[39] since the CO dissociation barrier (tested in absence of H_2) is lower on hcp cobalt surface compared to the dissociation barrier over fcc[38,39]. The improved catalytic activity of cobalt nanoparticles upon modification with triphenyl ethoxysilane and trimethyl ethoxysilane may be (partially) attributed to the formation of hcp cobalt. However, the increase in the rate of CO dissociation for the catalyst modified with tetraethoxysilane results in an fcc cobalt phase.

The catalytic activity may also be changed by particle breakdown or sintering under reaction conditions. Based on hydrogen uptake analysis of the spent catalyst (*see Table 7-6*), the metal dispersion of the (modified) catalyst does not vary after the Fischer-Tropsch synthesis indicating minimal sintering or particle break down. However, the modification process reduces the amount of surface cobalt. It may then, be expected that a decrease in the available surface area due to the attachment on ligands may supress the catalytic activity. Instead, the catalytic activity is rather enhanced indicating a beneficial effect of modifying the cobalt oxide surface with silane. This indicates that the effect is chemical in nature. It has been postulated that the presence of the ligand affects the metal-adsorbate interactions thus enhance some specific reaction pathways.

It may be expected that the change in electronic properties suggested by XPS, may alter the catalytic activity in CO hydrogenation (Fischer-Tropsch synthesis) and the selectivity. Electron donor ligands (e.g. triphenyl ethoxysilane, trimethyl chlorosilane) attached to the surface of cobalt may be expected to weaken the C=O bond thus facilitating the dissociation of CO. This has been suggested by the CO temperature programmed desorption data, where the ratio of the amount of dissociatively adsorbed CO increases drastically relative to the amount of associatively adsorbed CO increases upon modification with triphenyl ethoxysilane and trimethyl chlorosilane respectively. This increase in the proportion of the amount of dissociatively adsorbed CO may account for the increased rate of CO hydrogenation for the modified samples.

While the change in the rate of CO hydrogenation is a function of the rate of CO dissociation, rate of CO conversion in the Fischer-Tropsch synthesis is also governed by the rate of oxygen removal from the surface of cobalt surfaces[40]. Alkyl groups (e.g. methyl and phenyls) are hydrophobic in nature. The presence of this species on the cobalt catalyst system may impede the water formed during the Fischer-Tropsch synthesis from re-adsorbing on to the cobalt active sites and this may lead to an increased rate in the Fischer-Tropsch synthesis[36].

A change in electronic properties may not only change the rate of CO conversion but also the product selectivity as evidenced by e.g. olefin to paraffin selectivity. Olefins form a major fraction of the C_{2-5} fraction of the Fischer-Tropsch synthesis[41]. Olefins are nucleophilic in nature as the have unsaturated C=C bonds which are electron-sufficient. It may be anticipated that olefins may desorb quickly from electron rich surface, due to the repulsive force created between two electron-rich surfaces[42]. Furthermore, the rate of secondary hydrogenation may not be very high as olefins are not expected to re-adsorb on electron rich surfaces. As such, it can be expected that modification of a cobalt surface with electron donating ligands (triphenyl ethoxysilane and trimethyl chlorosilane) could result in a higher selectivity towards olefins. The effect of modification of cobalt with silane on the formation of olefins was investigated in the C_{2-5} fractions (see *Fig. 7-14*). The olefin/paraffin ratio is relatively low for the sample modified with tetraethoxysilane. It may be argued that this is associated with a decrease in the electron density of the cobalt surface upon modification with tetraethoxysilane. An electron-deficient

cobalt surface may favour secondary hydrogenation of primarily formed olefins as it readily re-adsorbs olefins[43]. Furthermore, this type of surface has been reported to favour the dissociation of hydrogen[44]. However, this was concluded on H_2 chemisorption results in the absence of CO[44]. On the other hand, the olefin/paraffin ratio of the samples modified with electron donor ligands (triphenyl ethoxysilane and trimethyl ethoxysilane) remains unchanged.

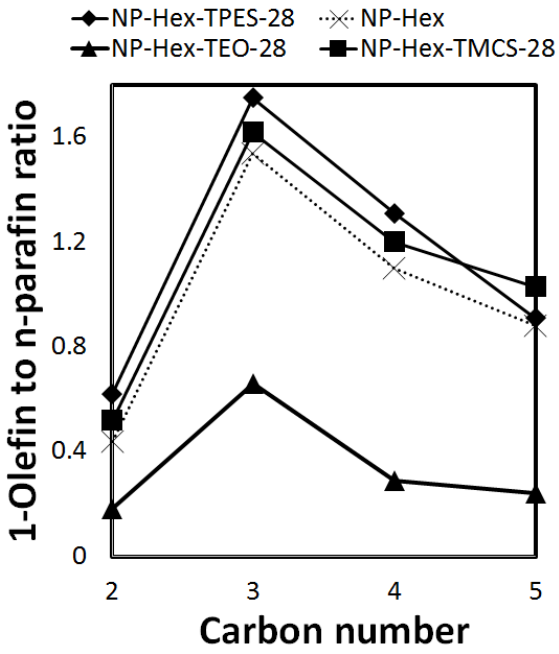

Figure 7-13: Ratio of 1-olefin/n-paraffin in the Fischer-Tropsch product as a function of chain length (in the region C_2 - C_5) after 44 hours on stream for the different model catalyst

Olefin selectivity is a function of conversion[45–47], as such the overall change in olefin selectivity cannot be decidedly assigned to the ligand effect. The change in olefin selectivity for the sample modified with tetraethoxysilane is accompanied by a change in both methane selectivity and chain growth probability in the range C_{3-8} (see *Table 7-7*). This decrease in methane content can be attributed to the improved rate of CO dissociation. The increased rate of CO dissociation may consequently lead to increased coverage of the cobalt surface with C_1 species which in turn reduces the hydrogen to CO ratio on the surface of cobalt with a limited hydrogen thus increasing the probability of chain growth[48–50]. This may also explain the observed increase in chain growth probability. However, the modification with the other silanes does not show a strong dependency on the olefin content on conversion, but a strong influence on the methane selectivity; methane selectivity is increased drastically and goes along with a decrease in chain growth probability of the C_{3-8} fractions. While increase in the coverage of cobalt surface with C_1 surface species may reduce methane selectivity, the increase in methane selectivity for the

samples modified with triphenyl ethoxysilane and trimethyl chlorosilane cannot be attributed a decrease in the coverage of cobalt with the monomeric species because the overall conversion of CO is increased suggesting more of the CO may have been converted to the monomeric species per time. At high surface coverage of cobalt surface with C_1 monomeric species, any available hydrogen is consumed in the hydrogenative desorption resulting in more methane[50].

The ultimate length of the chain may not only be a function of surface coverage by the C_1 monomers but may also be governed by the rate of chain growth relative to the rate of termination. The rate of termination is known to decrease with increasing metal-carbon bond strength[51] and the selectivity towards either paraffins or olefins is controlled by the rate of C-H formation versus the rate of termination. The observed decrease in the selectivity towards longer chains for these sample may therefore imply that the modification process has reduced the Co-C bond strength as it is suggested by the CO TPD result. The observed shifts in the dissociative CO desorption peak from the temperature programmed desorption data to relatively low temperatures.

Table 7-9: Activity and selectivity of reduced CoO particles modified by exposure to solutions of silanes in hexane in the Fischer-Tropsch synthesis (reduction in H_2, T_{red} = 573K, t_{red} = 16 hrs; Fischer-Tropsch synthesis: T = 493K, p = 20 bar, $F_{CO,0}/W$ = 0.09 mmol/(g_{Co}·s), $(H_2/CO)_{inlet}$ = 2)

Catalyst ID	X_{CO}[a], %	S_{CH4}, %	Chain growth probability, α
NP-Hex	2.4	13.4	0.66
NP-Hex-TEOS	25.5	10.4	0.72
NP-Hex-TPES	31.4	29.6	0.58
NP-Hex-TMCS-	22.3	28.7	0.60

7.4 Conclusions

The ligand effects of metal-support interaction in the Fischer-Tropsch synthesis has been studied by contacting the cobalt oxide (CoO) with silane ligands. The modification of cobalt with silane ligands was aimed to mimic the formation of metal-support interaction of the Co/SiO_2 systems. The modification of the CoO nanoparticle with TEOS may result in the formation of

silica islands on the surface of cobalt as observed upon the modification of Co_3O_4 with TEOS and result in an enhanced activity as evidenced in Chapter 4. The presence of the silanes on the surface increase the rate of CO-conversion. Tetraethoxysilane modified samples show a decrease in the methane selectivity and an increase in the chain growth probability albeit the comparison is at different conversions.

Modification of cobalt with triphenyl ethoxysilane and trimethyl chlorosilane results with an electron-rich cobalt surface. This weakens the C=O bond and thus facilitates the CO dissociation. This may explain the observed increased rate of CO-conversion. Moreover, electron-rich cobalt surface may facilitate a quicker desorption of products and this may explain the reduced chain growth probability and increase olefin content when cobalt is modified with alkylated ligands.

7.5 References

1 M. A. Vannice and P. Chou, in *Metal Support Interactions*, ed. R. Baker, 1986, pp. 76–88.

2 S. J. Tauster, S. C. Fung and R. L. Garten, *J. Am. Chem. Soc.*, 1978, **100**, 170–175.

3 S. J. Tauster, *J. Catal.*, 1978, **55**, 29–35.

4 M. A. Vannice, *J. Catal.*, 1977, **50**, 129–134.

5 M. A. Vannice, L. C. Hasselbring and B. Sen, *J. Chem. Phys.*, 1985, **89**, 2972–2973.

6 S. J. Tauster, S. C. Fung, R. T. K. Baker and J. A. Horsley, *Science*, 1981, **211**, 1121–1125.

7 R. P. Mogorosi, N. Fischer, M. Claeys and E. van Steen, *J. Catal.*, 2012, **289**, 140–150.

8 Q. Jia, S. Ghoshal, J. Li, W. Liang, G. Meng, H. Che, S. Zhang and S. Mukerjee, *J. Am. Chem. Soc.*, 2017, **139**, 7893–7903.

9 G. Zhao, F. Yang, Z. Chen, Q. Liu, Y. Ji, Y. Zhang, Z. Niu, J. Mao, X. Bao, P. Hu and Y. Li, *Nat. Commun.*, 2017, **8**, 1–8.

10 C. Xu, G. Chen, Y. Zhao, P. Liu, X. Duan, L. Gu, G. Fu, Y. Yuan and N. Zheng, *Nat. Commun.*, 2018, **9**, 3367.

11 S. Aranifard, S. C. Ammal and A. Heyden, *J. Catal.*, 2014, **309**, 314–324.

12 K. Mudiyanselage, S. D. Senanayake, L. Feria, S. Kundu, A. E. Baber, J. Graciani, A. B. Vidal, S. Agnoli, J. Evans, R. Chang, S. Axnanda, Z. Liu, J. F. Sanz, P. Liu, J. A. Rodriguez and D. J. Stacchiola, *Angew. Chemie Int. Ed.*, 2013, **52**, 5101–5105.

13 L. Macheli, A. Roy, E. Carleschi, B. P. D. Doyle and E. van Steen, *Catal. Today*, , DOI:https://doi.org/10.1016/j.cattod.2018.10.

14 P. I. Lee, J. A. Schwarz and J. C. Heydweiller, *Chem. Eng. Sci.*, 1985, **40**, 509–519.

15 T. Wang, Y. Ding, J. Xiong, L. Yan, H. Zhu, Y. Lu and L. Lin, *Catal. Letters*, 2006, **107**, 47–52.

16 S. Shaikhutdinov, R. Meyer, C. Lemire and H. J. Freund, *Catal. Letters*, 2003, **86**, 211–219.

17 Y. Bao, W. An, C. H. Turner and K. M. Krishnan, *Langmuir*, 2010, **26**, 478–483.

18 M. Avrami, *J. Chem. Phys.*, 1939, **7**, 1103–1112.

19 M. Avrami, *J. Chem. Phys.*, 1942, **9**, 177–184.

20 V. K. Patel, J. R. Saurav, K. Gangopadhyay, S. Gangopadhyay and S. Bhattacharya, *RSC Adv.*, 2015, **5**, 21471–21479.

21 S. A. Makhlouf, Z. H. Bakr, K. I. Aly and M. S. Moustafa, *Superlattices Microstruct.*, 2013, **64**, 107–117.

22 X. J. Yin, K. Peng, A. P. Hu, L. P. Zhou, J. H. Chen and Y. W. Du, *J. Alloys Compd.*, 2009, **479**, 372–375.

23 D. G. Kurth and T. Bein, *Langmuir*, 1995, **11**, 3061–3067.

24 X. Huang and Z. Chen, *J. Cryst. Growth*, 2004, **271**, 287–293.

25 I. Puskas, T. H. Fleisch, J. B. Hall, B. L. Meyers and R. T. Roginski, *J. Catal.*, 1992, **134**, 615–628.

26 A. H. Kababji, B. Joseph and J. T. Wolan, *Catal. Letters*, 2009, **130**, 72–78.

27 X. Yang, P. Roonasi and A. Holmgren, *J. Colloid Interface Sci.*, 2008, **328**, 41–47.

28 T. J. Chuang, C. R. Brundle and D. W. Rice, *Surf. Sci.*, 1976, **59**, 413–429.

29 H. Y. Lin and Y. W. Chen, *Mater. Chem. Phys.*, 2004, **85**, 171–175.

30 H. Ming, in *Cobalt: Characteristics, compounds and applications*, ed. L. J. Vidmar, Nova Science Publishers, Inc., 2011, pp. 1–38.

31 B. Viswanathan, R. Gopalakrishnan and R. Vetrivel, *React. Kinet. Catal. Lett.*, 1982, **18**, 209–212.

32 E. Zagli and J. L. Falconer, *J. Catal.*, 1981, **69**, 1–8.

33 T. Zubkov, G. A. Morgan, J. T. Yates, O. Kuhlert, M. Lisowski, R. Schillinger, D. Fick and H. . Jansch, *Surf. Sci.*, 2003, **526**, 57–71.

34 T. Zubkov, G. A. Morgan and J. T. Yates, *Chem. Phys. Lett.*, 2002, **362**, 181–184.

35 G. Chen, C. Xu, X. Huang, J. Ye, L. Gu, G. Li, Z. Tang, B. Wu, H. Yang, Z. Zhao, Z. Zhou, G. Fu and N. Zheng, *Nat. Mater.*, 2016, **15**, 564–569.

36 M. Ojeda, F. Jose, P. Terreros, S. Rojas, T. Herranz and L. G. Fierro, *Langmuir*, 2006, **22**, 3131–3137.

37 T. van Heerden and E. van Steen, *Faraday Discuss.*, 2017, **197**, 87–99.

38 M. Sadeqzadeh, H. Karaca, O. V. Safonova, P. Fongarland, S. Chambrey, P. Roussel, A. Griboval-Constant, M. Lacroix, D. Curulla-Ferré, F. Luck and A. Y. Khodakov, *Catal. Today*, 2011, **164**, 62–67.

39 D. I. Enache, B. Rebours, M. Roy-Auberger and R. Revel, *J. Catal.*, 2002, **205**, 346–353.

40 E. Iglesia, S. L. Soled and R. a Fiato, *J. Catal.*, 1992, **137**, 212–224.

41 R. A. van Santen, I. M. Ciobîcâ, E. van Steen and M. M. Ghouri, *Adv. Catal.*, 2011, **54**, 127–187.

42 C. L. Bianchi and V. Ragaini, *journall Catal. Catal.*, 1997, **168**, 70–74.

43 T. Bhatelia, C. Li, Y. Sun, P. Hazewinkel, N. Burke and V. Sage, *Fuel Process. Technol.*, 2014, **125**, 277–289.

44 M. E. Dry, T. Shingles, L. J. Boshoff and G. J. Oosthuizen, *J. Catal.*, 1969, **15**, 190–199.

45 D. B. Bukur, Z. Pan, W. Ma, G. Jacobs and B. H. Davis, *Catal. Letters*, 2012, **142**, 1382–1387.

46 E. van Steen, M. Claeys, K. P. Möller and D. Nabaho, *Appl. Catal. A Gen.*, 2018, **549**, 51–59.

47 W. Ma, G. Jacobs, Y. Ji, T. Bhatelia, D. B. Bukur, S. Khalid and B. H. Davis, *Top. Catal.*, 2011, **54**, 757–767.

48 L. Hu, K. Sun, Q. Peng, B. Xu and Y. Li, *Nano Res.*, 2010, **3**, 363–368.

49 V. P. Santos, T. A. Wezendonk, J. J. D. Jaén, A. I. Dugulan, M. A. Nasalevich, H. U. Islam, A. Chojecki, S. Sartipi, X. Sun, A. A. Hakeem, A. C. J. Koeken, M. Ruitenbeek, T. Davidian, G. R. Meima, G. Sankar, F. Kapteijn, M. Makkee and J. Gascon, *Nat. Commun.*, , DOI:10.1038/ncomms7451.

50 J. Yang, W. Ma, D. Chen, A. Holmen and B. H. Davis, *Appl. Catal. A Gen.*, 2014, **470**, 250–260.

51 R. A. van Santen, A. De Koster and T. Koerts, *Catal. Letters*, 1990, **7**, 1–14.

8. **Concluding remarks**

8.1. Overview

Metal-support interaction play a crucial role in heterogeneous catalysis as recent results have shown that metal-support interactions in the supported metal catalysts have a weighty effect on the catalytic activity and selectivity[1–3]. For instance, it is long-familiar that the CO adsorption strength is altered due to strong metal-support interactions, and this will affect the performance of the catalytically active metal, e.g. cobalt, in the CO hydrogenation. This therefore highlights the need for model systems aimed to understand and manipulate metal-support interactions in these catalytic systems.

The conventional approaches utilized to understand the effects of metal-support interactions (e.g. changing of supports) constitutes other support characteristics such as porosity, which may affect the performance of the catalyst. Model systems have been developed to separate such effects from the exclusive view changes brought about by metal-support interactions at the metal-support interface. Progress in the synthesis of nano-materials allows now targeted synthesis of inverse model systems[4] aiding the understanding of metal-support interactions. This thesis focused on the modification of cobalt oxide nano-crystals with silane compounds (Tetraethoxysilane, triphenyl ethoxysilane or trimethyl chlorosilane), characterized and tested for their activity in Fischer-Tropsch synthesis. The adsorption/impregnation of these compounds on cobalt oxide results in the formation of nano-sized islands on these nano-particles[5]. The presence of these silanes retards the reduction of cobalt oxide to metallic cobalt and affects the activity of these materials in the Fischer-Tropsch synthesis.

Tuning metal-support interactions by varying silica loading

Co_3O_4 nanocubes were synthesized using an oxidative hydrothermal precipitation[6] of cobalt oxide from a nitrate salt. The obtained Co_3O_4 nanocubes were contacted with tetraethoxysilane in different solvent succeeded by drying and calcining. Tetraethoxysilane is taken up by Co_3O_4 during contact. During preparation, tetraethoxysilane is de-ethoxylated into silica mostly likely during the calcination step and may result into neso or island silicate.

The presence of silica on the surface of Co_3O_4 nanocubes was qualitatively confirmed using infrared spectroscopy and quantitatively using energy dispersive X-ray spectroscopy (EDX). Absorption bands due to the vibrations of the Si-O-Si at 800 cm^{-1} and 1100 cm^{-1} have been

confirmed when Co_3O_4 is modified with tetraethoxysilane confirming that silica is present on the surface of cobalt oxide. A new absorption band also exist at 1020 cm^{-1}. This absorption band has been ascribed to the vibrations due to Co-O-Si bonds vibration [7,8]. Different silica loading on the surface of Co_3O_4 was achieved by using different initial concentrations of tetraethoxysilane in n-hexane during preparation. The relative intensity of these absorption bands increases with increasing silica content on the samples and remain intact after high temperature reduction.

The presence of silica on the surface of Co_3O_4 does not affect the phase structure or morphology of cobalt oxide but impedes the reduction of cobalt oxide to metallic cobalt. This is related to the increase in the activation energy required for the reduction process. With increasing silica content, the activation energy required for the reduction process increases indicating that silica interacts more strongly with Co_3O_4 when the silica content is increased.

When tested under industrially relevant conditions for the performance in the Fischer-Tropsch synthesis, the reduced supported modified Co_3O_4 catalyst show an improved catalytic activity. It is observed that the cobalt yield time yield increases with increasing silica loading up to more than 7-fold. The increase in activity does not seem to correlate with a change in the resulting metal surface area. The presence of silica on the surface of Co_3O_4 nanocubes reduces the available surface area for chemisorption and this may be because surface silica blocks some adsorption sites. However, there is no evidence for particle breakdown/growth during the Fischer-Tropsch synthesis both on the unmodified and tetraethoxysilane modified Co_3O_4 nanocubes. This may explain the steady activity of the catalyst over 44 hours on stream.

Formation of cobalt silicate during calcination

During calcination of the samples silica and cobalt may interact in a way that can result into the formation of irreducible cobalt silicate. Infrared spectroscopy and X-ray diffraction have been further used as tools to investigate the effects of heat treatments on the formation of metal-support interaction. When calcined at low temperatures, (573 K) the intensity of the bands ascribable to Co-O-Si is high, suggesting that the interaction between cobalt and silica is stronger. This band ceases at calcination temperature of 873 K, indicating that cobalt oxide and silica only interact weakly. A further, increase in the calcination temperature to 1173 K results into the formation of a mixture of cobalt oxide and Co_2SiO_4. Temperature programmed

reduction indicates that calcination of unmodified Co_3O_4 results in delay in the reduction process of Co_3O_4 with hydrogen. This delay is correlated to the change in crystallite size of Co_3O_4 nanocubes which increases with increase in calcination temperature. The change in crystallite size may alter the rate of hydrogen activation and the rate of formation of Co nuclei which are linked to the pre-exponential factor. However, for modified samples the delay is due to the increase in the activation energy which depends on the Co-O-Si bond strength as the silica seems to hinder the sintering process.

Tuning metal-support interactions using different solvents/solvent mixtures

The adsorption of tetraethoxysilane on a hydroxylated surface, such as the surface of Co_3O_4– nanocubes (as visualized by an absorption band at 3380 cm^{-1} in the FTIR spectrum of calcined Co_3O_4 nanocubes[9]) may proceed by an alcohol producing condensation[10,11] yielding chemically bonded surface silicate species. This process may be facilitated by hydrolysis of tetraethoxysilane during the modification process. Infrared spectroscopy can be further used to disentangle the effects of method of modification on the formation of metal-support interactions. Co_3O_4 was contacted with tetraethoxysilane in different solvent mixtures. The infrared spectra of a sample modified in a n-hexane, shows the absorption bands due to physiosorbed tetraethoxysilane. These bands, however, vanish upon calcination at 573 K with the development of the bands ascribed to Si-O-Si and Co-O-Si vibrations. When modified in solvent mixtures containing ethanol/water/ (acid or base), the absorption bands due to the adsorption of ethoxylated tetraethoxysilane species are not observed suggesting that tetraethoxysilane is rather de-ethoxylated during the hydrolysis process. The difference in the infrared spectra of the samples modified in the presence of acid and base arises in the relative intensities of the absorption band attributable to the Co-O-Si vibrations at 1020 cm^{-1}. The comparative intensity, of this absorption band is high when the modification is performed in the presence of glyoxylic acid and lower for a sample modified in the presence of ammonia is lower. This may indicate that the acid-based hydrolysis leads to a stronger interaction of cobalt oxide with silica compared to both base catalysed hydrolysis. This effect can be confirmed using temperature programmed reduction showing that the intensity of the Co-O-Si peak can be corelated to the quantity of hydrogen consumed by the reduction of cobalt oxide interacting strongly with silica. The difference in the interaction leads to the difference in the catalytic activity of the samples. Modification in the presence of acid (glyoxylic acid) lead to higher

activity. This can be correlated to the increased number of Co-O-Si bridges suggested by both infrared and temperature programmed reduction.

Tuning the selectivity using different ligands

Electronic properties of cobalt oxide can be modified by the presence of the silane ligands. Depending on the nature of the silane, electrons can be withdrawn from or donated to cobalt atoms to which the silane is bonded. Cobalt oxide (CoO) was synthesized via cobalt carbonyl decomposition. The obtained cobalt oxide was contacted with electron withdrawing tetraethoxysilane and electron donating silanes (triphenyl ethoxysilane and trimethyl chlorosilane), by contacting the cobalt oxide with the silanes in n-hexane. The presence of this material changes the electronic properties of cobalt as indicated by X-ray photoemission. The change in the electronic properties drastically affect the adsorption properties of CO on the surface of cobalt and as such selectivity in the Fischer-Tropsch. The rate of CO conversion is increased by both electron donor and electron withdrawing groups. This indicates that the modification offers different routes for the dissociation of CO. However, the selectivity varies drastically and may be an indication that the Co-C bond strength may be difference in each case.

8.2. Reference

1 S. J. Tauster, *J. Catal.*, 1978, **55**, 29–35.

2 M. A. Vannice, L. C. Hasselbring and B. Sen, *J. Chem. Phys.*, 1985, **89**, 2972–2973.

3 R. P. Mogorosi, N. Fischer, M. Claeys and E. van Steen, *J. Catal.*, 2012, **289**, 140–150.

4 M. Cargnello, P. Fornasiero and M. J. Gorte, *Catal. Letters*, 2012, **142**, 1043–1048.

5 A. P. Petersen, R. P. Forbes, S. Govender, P. J. Kooyman and E. van Steen, *Catal. Letters*, 2018, **148**, 1215–1227.

6 X. Xiao, X. Liu, H. Zhao, D. Chen, F. Liu, J. Xiang, Z. Hu and Y. Li, *Adv. Mater.*, 2012, **24**, 5762–5766.

7 I. Puskas, T. H. Fleisch, J. B. Hall, B. L. Meyers and R. T. Roginski, *J. Catal.*, 1992, **134**, 615–628.

8 A. H. Kababji, B. Joseph and J. T. Wolan, *Catal. Letters*, 2009, **130**, 72–78.

9 R. Xu and H. C. Zeng, *Langmuir*, 2004, **20**, 9780–90.

10 L. L. Tedder, G. Lu and J. E. Crowell, *J. Appl. Phys.*, 1991, **69**, 7037–7049.

11 J. J. Brinker and G. Scherer, *Sol-Gel Science: The Physics and Chemistry of Sol-Gel*

Processing, Academia Press, Inc., New York, 1990.

Appendix A: supplementary experimental data

A-1: H_2-TPR analysis

H_2 TPR was calibrated by reducing 30 mg of silver oxide (Ag_2O) with 5% hydrogen in argon at a flow rate of 50 mL(NTP)/min upon heating from 323 K to 773 K at a constant heating rate of 10 K/min. Relative errors are typically ±1.2 % for TPR as determined from the repeated calibration data. A calibration factor ($f_{TPR,i}$) was determined from the area under the graph of TCD signal vs Temperature and was determined to be 6.1±0.8. The relative amount of hydrogen consumed for the model catalysts was determined from the respective peaks. The area of a peak is related to the hydrogen in the gas mixture by the calibration factor ($f_{TPR,i}$) as shown:

$$\dot{n}_{H_2,consumed} = f_{TPR,i} \cdot A_i$$

A-2: CO TPD analysis

CO TPD was calibrated by manually injecting a known volume (1 mL, 2 mL and 5 mL) of 5 % CO in helium. A calibration factor ($f_{TPR,CO}$) was determined from the area under the graph of TCD signal vs time and was determined to be 0.84±0.03. The relative amount of CO adsorbed during the pulsing step can be determined by integrating area of TCD signal VS time. Figure A-2 shows the CO pulse adsorption of catalyst NC-Hex-TEOS-63-573K after activation at 623 K for 16 hours. Adsorbed CO seem to desorb and re-adsorb during the pulsing stage.

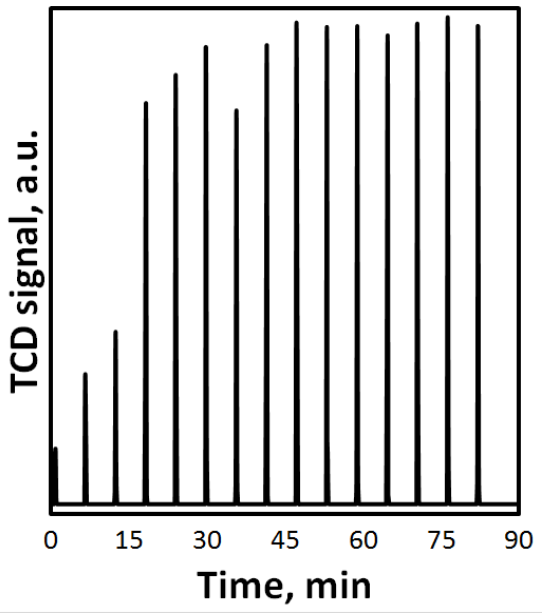

Figure A-1: CO pulse adsorption of catalyst NC-Hex-TEOS-63-573K after activation at 623 K for 16 hours

A-3: AAS analysis

Atomic absorption spectrometer was calibrated by measuring the absorbance of three solutions of know concentrations (25 mg/L, 30 mg/L and 50 mg/L) and plotting a graph of absorbance versus absorbance (*see Fig. A-2*). A straight-line graph with linear regression of 0.9999 was obtained. The graph was then used to determine the cobalt loading from the corresponding absorbances.

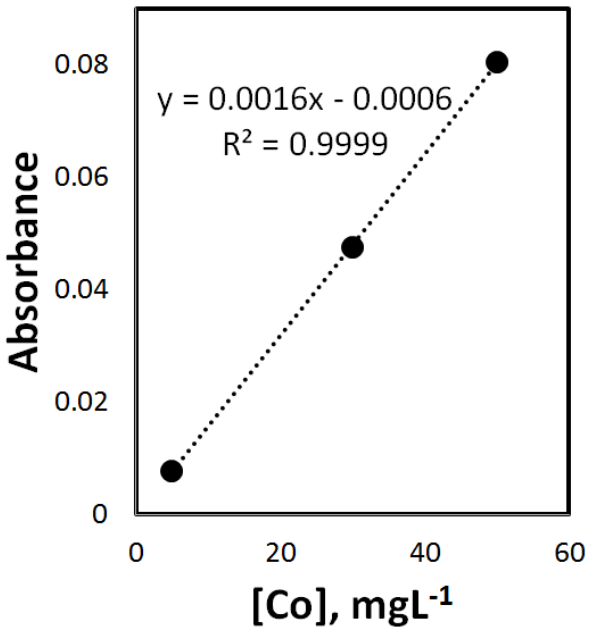

Figure A-2: An AAS calibration graph for the determination of Cobalt loading on the spent catalyst.

A-4: Sample EDX Pattern

SEM EDX was used to determine the silane loading on cobalt by computing the $\frac{Si}{Co}$ ratio. An EDS pattern for sample NC-Hex-TEOS-63-573K is shown in *Figure A-3.* The sample contains silicon, cobalt and oxygen atoms.

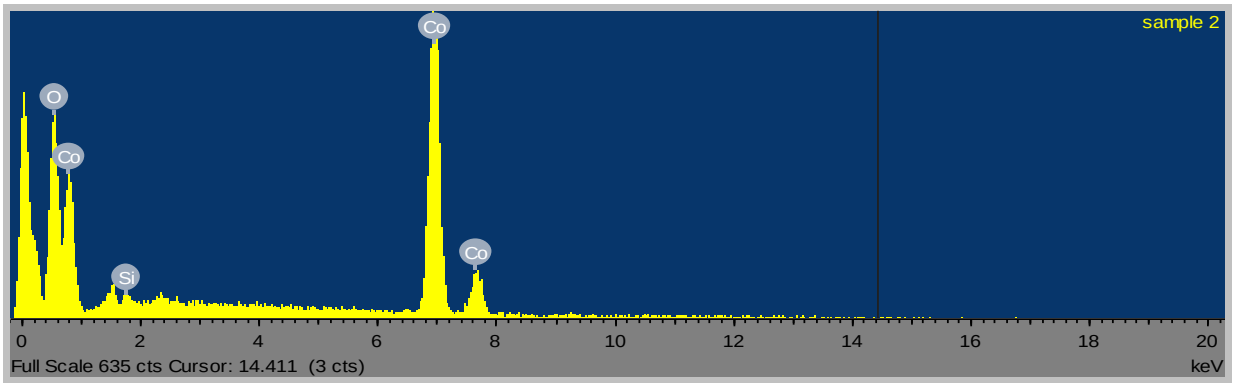

Figure A-3: EDX patterns of sample NC-Hex-TEOS-63-573 K

Appendix B: Fischer-Tropsch synthesis

B-1: the reactor system

Fischer-Tropsch synthesis was used as a reaction to test the effects of metal-support interaction on the performance of the catalyst. The synthesis was performed in a fixed-bed reactor system shown in *Figure B-1.* All catalyst (1.0 g of 10-wt.% cobalt oxide on SilC) were tested 493 K for performance in the Fischer-Tropsch synthesis for 44 hours after reduction with H_2 (10 mL/min) at a constant temperature (623 K for Co_3O_4 nanocube and 573 K for CoO)

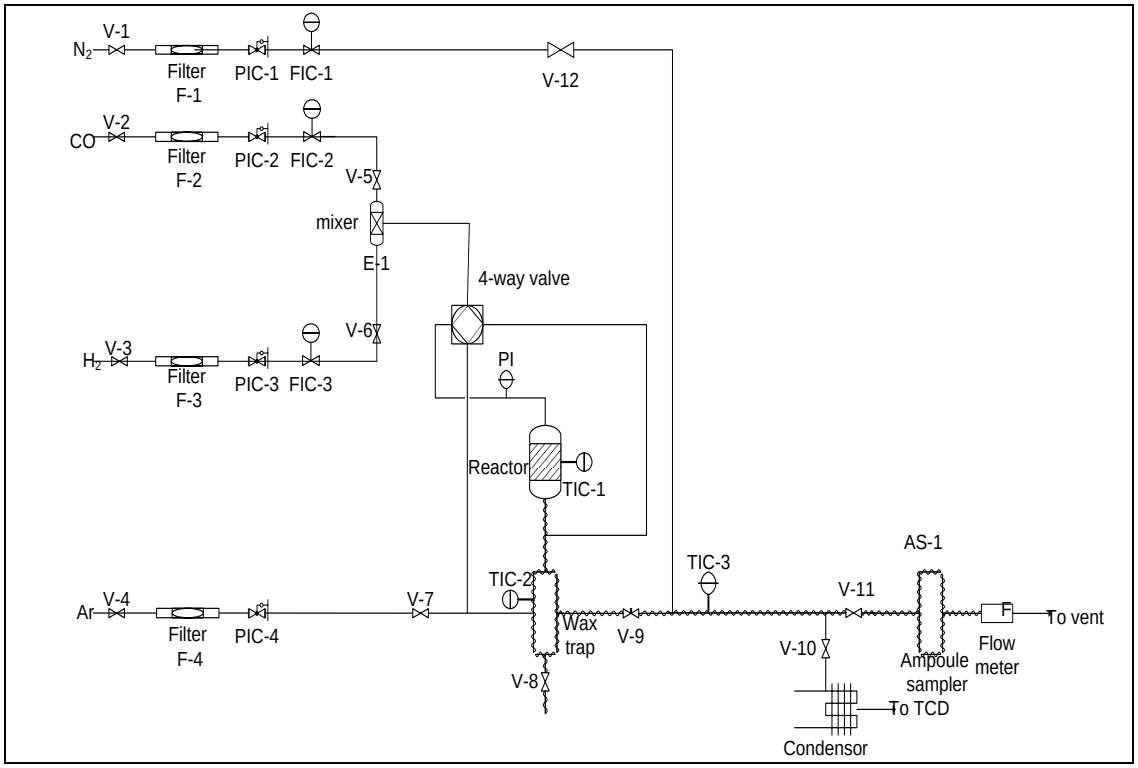

Figure B-1: Flow diagram for a Fixed bed reactor system for Fischer-Tropsch synthesis (V-1-12: flow control valves; FIC-1-4: flow indicator controllers; AS-1: Ampoule Sampler, TIC: temperature indicator controller)

B-2: Loading the reactor

A fixed bed reactor was loaded with 1.0 g of catalyst containing 10-wt.% cobalt oxide supported on β-SiCmicrospheres (SiCAT, $d_{particle}$=100 µm). The catalyst was diluted further with 2.0 g of SiC mesh ($d_{particle}$= 200-250 µm) using ethanol to make a homogeneous slurry which was

subsequently dried at 343 K and loaded into the fixed bed reactor. Additional SiC mesh (10.0 g) was added for the purpose of heat distribution across the reactor

B-3: Sampling

On-line sampling

On-line sampling was carried on a GC-TCD (Varian 4900) equipped with three columns that are connected three different channels with different detectors for analysis of inorganic gases (H_2, N_2, CO, CH_4 and CO_2). Nitrogen was used as an internal standard for the on-line analysis. The operating conditions and the gases detected in each column are given in *Table B-1.*

Table B-1: Sampling condition of the micro GC equipped with a TCD

	Channel 1	Channel 2	Channel 3
Gases analysed	CO, N_2, CH_4, Ar	CH_4, CO_2	H_2
Column temperature (K)	353	353	353
Carrier gas	H_2	He	Ar
Inlet gas pressure (kPa)	150	100	150
Injection time (ms)	120	120	120
Injector temperature (K)	313	313	313
Back flush time (s)	160		160
Sampling time (s)	180	180	180
Columns	20m, Molecular Sieve 5A	10m, Porapak Q	10 m, Molecular Sieve 5A

A calibration gas mixture with a known composition of hydrogen, nitrogen, carbon monoxide, methane and argon (*see Table B1*) was used to calibrate the online gas chromatography TCD. The peak areas obtained from the TCD analysis were then used to calculate the relative calibration factors normalized for nitrogen, f_{TCD}, for each species (*see Table B-2*). Relative standard deviation (repeatability of this analysis technique) are typically *±0.3* % for TCD as determined from the repeated calibration data

Table B-2. Determination of calibration factor for the TCD-GC

	Ar	N_2	CH_4	CO	H_2
Run 1	461.3	304.6	489.5	805.5	32580
Run 2	475.9	317.6	521.3	825.6	32567
Run 3	475	316.7	520.7	824.3	32516
Run 4	476.7	317.9	522.8	827.6	32578
Run 5	477.8	318.5	523.6	828.7	32509
Average	**476.8**	**317.5**	**522.6**	**825.8**	**32567**
STDEV	**1.5**	**1.0**	**1.6**	**1.5**	**16.5**
% DEV	**0.3**	**0.3**	**0.3**	**0.2**	**0.1**
Ai/AN2	**1.5**	**1**	**1.6**	**2.6**	**102.6**
fi	**1.21**	**1**	**0.59**	**0.69**	**13.5**

Sample TCD-GC chromatogram taken online using unmodified Co_3O_4 catalyst is shown in *Figure 9.3.* The chromatogram shows the argon peak eluting at 0.79 minutes, nitrogen peak at 0.97 minutes and the CO peak at 1.67 minutes. The methane peak could not be identified by the TCD-GC and hence methane was analysed with FID-GC with the rest of the organic compounds

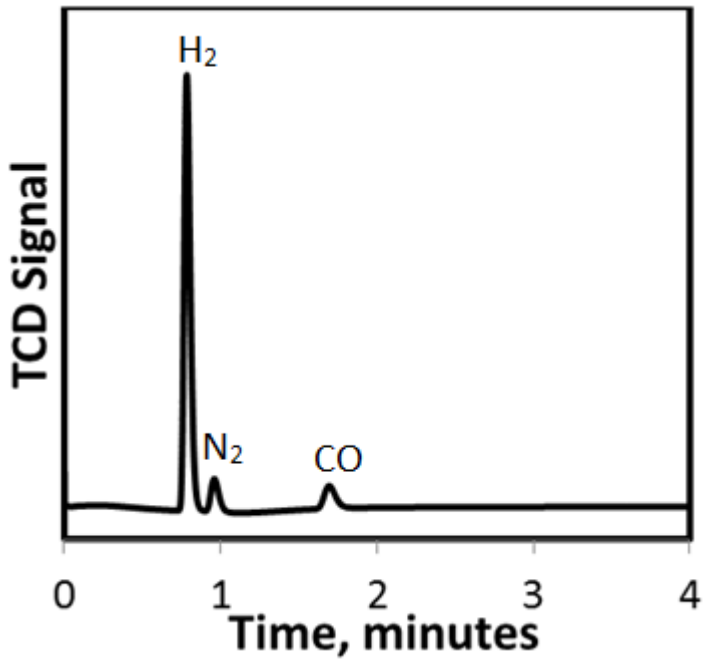

Figure B-2: Sample TCD-GC chromatogram taken online using unmodified Co_3O_4 catalyst.

Off-line sampling

Off-line analysis was carried on a GC-FID (Varian 3400) for analysis of organic gases. Cyclohexane was used as an internal standard for the off-line analysis. The operating conditions and the gases detected in each column are given in *Table E-1.* Sampling was done by inserting the capillary

end of an evacuated ampoule though the septum into the heated product stream at the sampling point consequently breaking the capillary (ampule) inside the ampule sampler. The product vapor was sucked into the previously evacuated chamber of the ampoule. The ampoule was then sealed off using a butane flame and taken for gas chromatograph (Varian 3400) coupled with flame ionization detector (FID). Conditions of the gas chromatographic analyses are given in *TableBE-3.*

Table B-3: Sampling condition of the micro GC equipped with a TCD

Detector	Flame ionisation detector (FID), T=523K
Column	Column RTx-1 (Restek)
	Fused silica capillary column, 60 m x 0.25 mm
	Stationary phase: 0.5µm dimethyl siloxane (crosslinked)
Carrier gas	Hydrogen
Introduction gas	Nitrogen
Column head pressure	2.9 bar (absolute)
Injector	Split injector, T=523K
	Split ratio 1:20
Temperature program	Initial T = 218K 1.5 min, isothermal
	At 20K/min to 273 K, 0 min isothermal
	At 14K/min to 373K, 0 min isothemal
	At 16K/min to 553K, 23 min isothermal

B-4 Unloading the reactor

After the Fischer-Tropsch synthesis, the spent catalyst was passivated by flowing CO_2 (20 mL/min (NTP)) 2 hours at room temperature. The catalyst was removed by first removing the 10.0 g of the SiC that was on top of the catalyst bed initially added for the even heat distribution in the reactor. The catalyst was then recovered by separating from the silicon carbide using a 150 µm sieve.

Appendix C: Sample calculations

C-1: Calculating the dispersion using hydrogen chemisorption

The hydrogen volume required for monolayer coverage on the sample was determined from the linearized Langmuir isotherms. The dispersion D, of the Co was computed from *Equation C-1*:

$$\boldsymbol{D = \frac{S*Ar*V_m}{M*L}} \qquad \text{..... Equation C-1}$$

Where S is stoichiometric factor between hydrogen and cobalt, Ar is the atomic weight of cobalt, V_m is the monolayer volume of the hydrogen adsorbed (usually reported as cm^3/g of total catalyst) M is the total mass of the catalyst and L is the weight percentage of Co in the catalyst determined from atomic absorption spectrometry.

C-2: Calculating the final concentration of TEOS

The total quantity of cobalt oxide used in the modification process is 0.5 g in 350 mL n-hexane, 0.1 g of which is withdrawn from the mother liquor per sampling. A sample contacting 63 mmol/mol (Si/Co), NC-Hex-TEOS-63-573K, has 1.2 mmol of cobalt:

$$n_{Co} = \frac{0.1\ g * 3}{241 \frac{g}{mol}} = 1.2\ mmol$$

For a sample containing 63 mmol/mol (Si/Co), the amount of TEOS adsorbed can therefore be determined from the ration as;

$$n_{ads} = 0.063 * 1.2\ mmol = 72\ \mu mol\ of\ TEOS$$

which is equivalent to a concentration of 205µM. The final concentration can then be calculated from the difference between the initial and adsorbed concentration;

$$C_{final} = 6.0\ mM - 0.205 mM = 5.795\ mM$$